VNIVERSITAT DE VALÈNCIA

Topics in Physics Beyond the Standard Model

PhD Thesis

Andrea Caputo

IFIC - Universitat de València - CSIC
Departamento de Física Teórica
Programa de Doctorado en Física

Under the supervision of

Pilar Hernandez Gamazo

Valencia, Julio 2020

Pilar Hernández Gamazo, catedrática del Departamento de Física Teórica de la Universidad de Valencia,

Certifica:

Que la presente memoria, "Topics in physics Beyond The Standard Model" ,ha sido realizada bajo su dirección en el Instituto de Física Corpuscular, centro mixto de la Universidad de Valencia y del CSIC, por Andrea Caputo, y constituye su Tesis para optar al grado de Doctor en Ciencias Físicas.

Y para que así conste, en cumplimiento de la legislación vigente, presenta en el Departamento de Física Teórica de la Universidad de Valencia la referida Tesis Doctoral, y firman el presente certificado.

Valencia, Julio 2020

Pilar Hernández Gamazo

List of Publications

This PhD thesis is based on the following publications:

- *The seesaw path to leptonic CP violation* [1]
  Caputo, A. and Hernandez, P. and Kekic, M. and Lopez-Pavon, J. and Salvado, J.
  Eur. Phys. J. **C77** (2017) no.4, 258, [1611.05000].

- *The seesaw portal in testable models of neutrino masses* [2]
  Caputo, A. and Hernandez,P. and Lopez-Pavon, J. and Salvado, J.
  JHEP **1706** (2017) 112, [1704.08721].

- *Looking for Axion Dark Matter in Dwarf Spheroidals* [3]
  Caputo, A. and Garay, C. P and Witte, S.J.
  Phys.Rev. D **98** (2018) no.8, 083024, [1805.08780].

- *Leptogenesis from oscillations and dark matter* [4]
  Caputo, A. and Hernandez, P. and Rius, N.
  Eur.Phys.J. C **79** (2019) no.7, 574, [1807.03309].

- *Detecting the Stimulated Decay of Axions at Radio Frequencies* [5]
  Caputo, A. and Regis, M. and Taoso, M. and Witte, S. J.
  JCAP **1903** (2019) 027, [1811.08436].

- *Searching for Sterile Neutrino with X-ray Intensity Mapping* [6]
  Caputo, A. and Regis, M. and Taoso, M.
  Phys.Lett. B **100** (2019) no.11, 116007, [1911.09120].

- *Minimal flavor violation in the see-saw portal* [7]
  Barducci, D. and Bertuzzo, E. and Caputo, A. and Hernandez, P.
  JHEP **06** (2020) n.185, [2003.08391].

The following are additional papers I worked on during my PhD but which slightly esulate from the main topics of my PhD research and are therefore not included as chapters. They are quoted as ordinary references when necessary.

- *Constraints on millicharged dark matter and axionlike particles from timing of radio waves* [8]
  Caputo, A. and Sberna, L. and Frias, M. and Blas, D. and Pani, P. and Shao, L. and Yan, W.
  Phys.Rev. D **100** (2019) no.6, 063515, [1902.02695].

- *Sub-MeV Dark Matter and the Goldstone Modes of Superfluid Helium* [9]
  Caputo, A. and Esposito, A. and Polosa, A.
  Phys.Rev. D **100** (2019) no.11, 116007, [1907.10635].

- *Dark Matter, Dark Photon and Superfluid He-4 from Effective Field Theory* [10]
  Caputo, A. and Esposito, A. and Geoffray, E. and Polosa, A. and Sun, S.
  Phys.Lett. B **100** (2019) no.11, 116007, [1911.04511].

- *Binary pulsars as probes of a Galactic dark matter disk* [11]
  Caputo, A. and Zavala, J.F and Blas, D.
  Phys. Dark Univ. **10** (2018) 1-11, [1709.03991].

- *Cosmic implications of a low-scale solution to the axion domain wall problem* [12]
  Caputo, A. and Reig, M.
  Phys. Rev. **D100** (2018) no.6, 063530, [1905.13116].

- *Radiative Axion Inflation* [13]
  Caputo, A.
  Phys. Lett. **B797** (2019) 134824, [1902.02666].

- *No chiral light bending by clumps of axion-like particles* [14]
  Blas, D. and Caputo, A. and Ivanov, M. and Sberna, L.
  Phys. Dark Univ. **27** (2019) 100428, [1910.06128].

- *Gravitational-wave detection and parameter estimation for accreting black-hole binaries and their electromagnetic counterpart* [15]

Caputo, A. and Sberna, L. and Toubiana, A. and Babak, S. and Barausse, E. and Marsat, S. and Pani, P.
Phys. Dark Univ. **27** (2020) 100428, [2001.03620].

- *Dark Photon Oscillations in Our Inhomogeneous Universe* [16]
  Caputo, A. and Liu, H. and Mishra-Sharma, S. and Ruderman, J.T.
  [2002.05165].

- *Modeling Dark Photon Oscillations in Our Inhomogeneous Universe* [17]
  Caputo, A. and Liu, H. and Mishra-Sharma, S. and Ruderman, J.T.
  [2004.06733].

- *Revisiting longitudinal plasmon-axion conversion in external magnetic fields* [18]
  Caputo, A. and Millar, A. and Vitagliano, E.
  [2005.00078].

- *Axion helioscopes as solar magnetometers* [19]
  O'Hare, C.A.J. and Caputo, A. and Millar, A. and Vitagliano, E.
  [2006.10415].

- *Exploring New Physics with O(keV) Electron Recoils in Direct Detection Experiments* [20]
  Bloch, I. M. and Caputo, A. and Essig, R. and Redigolo, D. and Sholapurkar, M. and Volansky, T.
  [2006.14521].

Preface

In this doctoral thesis we have focused on different phenomenological and theoretical aspects of physics beyond the Standard Model. In particular, we studied very well motivated extensions of the standard model which can explain light neutrino masses with the presence of heavy neutral leptons. We focused on the collider phenomenology of these models as well as on theoretical aspects related to their flavor symmetries. On the more cosmological side, we investigated minimal models that can explain neutrino masses, the matter-antimatter asymmetry as well as dark matter. Moreover, we also dedicated some effort to propose new direct and indirect searches for dark matter.

This thesis is organized as follows: in the introductory Chapter 1 we provide a brief overview of the Standard Model. Then, In Chapter 2, we discuss some of the open problems in the Standard Model, highlighting in particular the original contributions presented in this thesis.

El Chapter 3 consiste en un resumen detallado en español de los objetivos, motivación, metodología, resultados y conclusiones de esta tesis.

Finally we present the original articles that consitute the body of this thesis. All papers have been maintained in their original published form. This implies there will be a certain amount of repetition between them and possibly sometimes different notations are used, however Chapter 2 provides the necessary introductory material and context to help reading each article as an independent entity.

Acknowledgements

I cannot guarantee these acknowledgements will be original nor very well written, but for sure they will be sincere because I really feel super lucky to have many people I should thank.

First of all, I want to thank my supervisor Pilar, who guided me into the world of physics, with passion and patience. One of the thing I admire more about Pilar is her curiosity and witness to learn always new things. I remember an entire week spent together studying Primordial Black Holes, a subject new for both of us, after attending a related seminar. I also thank her for all the help outside physics (better not to talk about my experience with my first house in Geneva..) and for being the best supervisor I could have wished, leaving me the freedom to do whatever I liked most, especially when I become independent and more interested to astro stuff.

Then, I want to thank Diego Blas, who has been a second supervisor for me since our first chat at CERN when I was the mascot of the theory group. I was very lucky meeting you Diego, I think this changed my path quite a bit, in a way I like a lot!

I am also very grateful to Antonello, who took me under his wing to have a lot of fun with dark matter, and especially to Angelo, from whom I learnt a lot and with whom is a real pleasure to work. I hope we will continue for a long time!

I thank a lot Paolo, who gave me the opportunity to work on topics related to General Relativity, that I love, with enormous patience, allowing me to learn an enormous amount of new amazing things (and thanks for sharing your Mathematica Notebooks!).

I am also very happy to thank Marco, for giving me the possibility to learn an astonishing amount of physics about dark matter and astroparticle, always having time for me, since the very beginning when we started checking some silly Mathematica bugs in my code when I was trying to reproduce his work about PBHs.

I thank Sam, who is an amazing scientist and a good friend, who offered me the possibility to work with him and learn from him a lot, with our first project about axion decay, when I was a little bit stuck with other projects.

A lot of people asked me how it has been possible to have so many papers during my Ph.D., the truth is that I have been very lucky, always having terrific collaborators. It is then a real pleasure to thanks Marija, Jordi and Jacobo, with whom I did my first papers (and thank you Jacobo for paying my last year!), as well as Nuria and Carlos. Then I want to thank the fantastic NYU crew, Hongwan, Josh and Sid, who taught me a lot, and with whom I still have so many other things to do. I thank Enrico and Alex, for all the work together, as well as Jesus, for the patience when we were trying to find dark matter with pulsars, and Misha. I thank Daniele and Enrico (Bertuzzo) for all the fun and cross-checks in our last work. I really thank also Marco R. in Turin, as well as Edoardo, for all the nights spent discussing crackpot physics, and Alex for all the hours spent cross-checking computations and Mathematica notebooks.

I thank Mario, friend and collaborator, who gave me the possibility to learn about domain walls and other cool stuff, in a project which was a lot of fun and of which I am very proud of.

I thank Diego Redigolo, for being not only a fantastic phyisicist, but another mentor for me, with always a lot of useful suggestions and time to do physics together (and thanks for having invited me to TAU for a seminar! that changed my career). I thank Itay, Mukul, Rouven and Tomer for the crazyness of our last ambulance chasing, as well as Ciaran, for a super interesting paper which anticipated somehow the hot period after XENON1T excess.

I thank all the group of friends and collaborators here in Valencia: Victor, who has become a good friend as we are very similar, Fernando, my office mate since the very beginning, Hector, although he still sucks at soccer, Stefan, who runs too much for my taste, and then Olga, Dani, Sergio, Andrea, Pablo, Miguel Folgado, Miguel Escudero,as well as Valentina, who has been a good friend in these years and who now has the money to invite me back in the future!

I met so many people during these 4 years, it is very difficult to remember and mention now everyone, but I still want to thank a lot Thomas, for his hospitality at KIT (they have been very beautiful three months!), as well as Oliver, Andreas, Alvaro and Elisa in Karlsruhe, Lam and Alberto for having me at Columbia, Marc and Emanuele for hosting me at JHU, as well as all the fantastic group there, especially Jose Luis, who gave me the possibility to learn about line intensity mapping. Then I want to thank Alfredo, who

inspired me a lot during many hours spent at CERN discussing physics and drinking coffee in the common room, Marco Nardecchia, Guillermo, Carlos, Georg, Javi, Luca. I also want to thank Elena, Michelle and Nanie, who were so kind to me when I was at CERN my first year of Ph.D. I thank all the friends I met during school, conferences, seminars and research periods abroad, in particular the GGI crew ("where are you ?! I am lost"), Josh F., Alessandro, Francesco, Gabriel, Aditya, Jiaxin, NicolÃš, Andrea, Davide, Giuseppe and Bernardo, who has become my friend although I have stolen his desk at CERN.

I really thank Laura, who has been always a friend I could count on, as well as my partner in crime for many works already, and I bet many others to come.

I thank all my lifelong friends Roberto, Gianni, Leda, Franco, Giuseppe, Luca, Devid, Cesare, Bri, who will be always home for me.

I really thank all my family, in particular my dad and my mum, who allowed me to study and always gave me all I needed to do it, as well as my brother, the most gentle person I know. I love you.

Finally, I want to thank my love. No, no, I am not talking about Juventus. I am talking about the person with whom I have shared until now 10 years of my life. We grew up together and suffered many things together. I thank you for supporting me and enduring me, I thank you to be as you are, I couldn't wish anything more.

Contents

Chapter 1

The Standard Model

The Standard Model (SM) [21, 22, 23, 24, 25, 26] of particle physics is a beautiful and extremely well-verified theory. Indeed its successes are countless and some of its predictions, as the anomalous magnetic moment of the electrons, have been tested to one part in 10^{10}(!). Nevertheless, and lucky enough for my Ph.D., there are still some missing pieces, puzzles that remain unexplained within the SM and most likely imply the existence of new physics beyond the SM (BSM).

1.1 The rules of the game

In the language of Quantum Field Theory (QFT) the basic laws of Nature are encoded in the action S, that is to say in integral over spacetime of the Lagrangian density $\mathcal{L}$

$$S = \int d^4x \mathcal{L}[\phi_i(x), \partial_\mu \phi_i(x)], \tag{1.1}$$

where the index i runs from 1 to the number of fields in the theory. A free quantum field, $\phi(x)$, creates or annihilates particles at a given point of spacetime x; each type of particle has an associated quantum field. In general, the Lagrangian needs to satisfy some properties:

- it is a function of the fields and their derivatives at point x
- it is local: does not contain terms with fields at different points
- it is real
- it is invariant under spacetime translations and Lorentz transformations

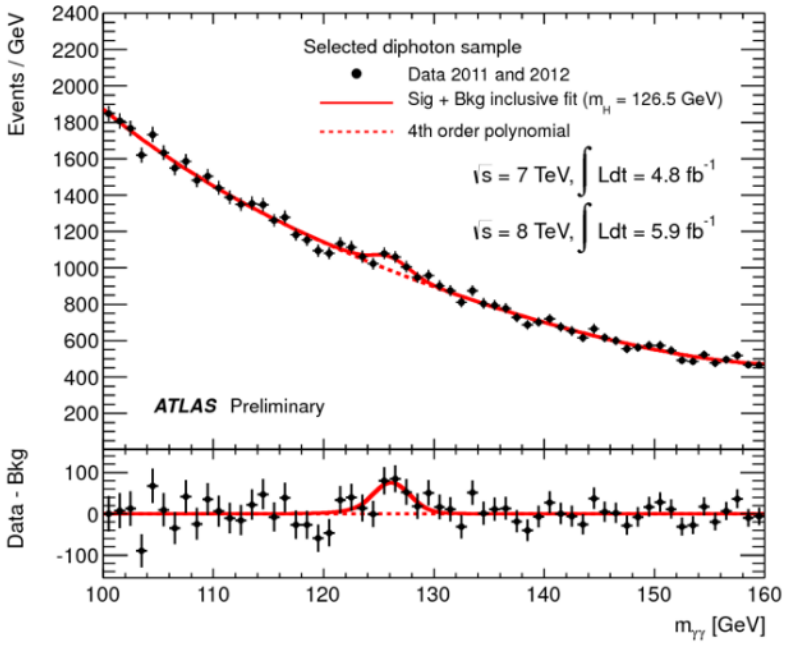

Figure 1.1: The invariant mass from pairs of photons selected in the Higgs to $\gamma\gamma$ analysis, as shown at the seminar at CERN on 4 July 2012. The excess of events over the background prediction around 125 GeV is consistent with predictions for the Standard Model Higgs boson.

Fields should have well-defined transformation properties under Lorentz transformations. In particular, elementary particles fall into three categories: scalars or spin-zero fields, fermions or spin-1/2 fields and vector bosons or spin-one fields. [1]

An important class of symmetries that we observe in Nature are related to rephasing invariance, that is the Lagrangian is invariant under a change of phase of the fields. This change can be *global* if it is the same in all space-time points, ie. for a $U(1)$ symmetry:

$$\phi(x) \to e^{i\alpha}\phi(x), \tag{1.2}$$

or *gauge* if it is independent in each space-time point:

$$\phi(x) \to e^{i\alpha(x)}\phi(x). \tag{1.3}$$

[1] Actually, the last point is a curious one; if you look around you, the world does not seem to be Lorentz invariant. For example, even the chair you are sitting on while reading this thesis is breaking Lorentz! In particular, it breaks boosts, as there is a preferred reference frame that is the one in which the chair is at rest. Actually, it also breaks rotational invariance. There is no time to elaborate on this problem, the interested reader can read [27, 28, 29, 30] to have a clue of what is happening (a small hint: the theory needs to be Lorentz invariant, not the ground state).

In the presence of several fields, $\phi_a(x)$, $a = 1, ..., N$, more general transformations are possible. In particular that corresponding to a unitary rotation of the fields:

$$\phi_a(x) = U(x)_{ab}\phi_b(x), \quad U \in SU(N), \tag{1.4}$$

is an $SU(N)$ gauge transformation.

Gauge symmetries imply the existence of a special type of massless vector fields, one for each symmetry generator, that mediate forces: the famous gauge bosons. Electromagnetism, the weak and the strong force are all the result of gauge symmetries. The gauge principle is therefore a unifying principle of all forces of Nature, except maybe gravity.

Coming back to the building blocks of a general Lagrangian in QFT, one needs to impose other two requirements:

- Naturalness: every term not forbidden by symmetry should be added to $\mathcal{L}$
- Renormalizability: a Lagrangian to be renormalizable contains only terms up to dimension four in the fields and their derivatives [31, 32]

The request of renormalizability is not a mere artifact to get rid of infinities as traditionally assumed. Renormalizability has been a criterion that defined a certain type of universality in our theories, which otherwise would be essentially arbitrary: it is a property of those special theories where the physics at long distances does not depend on the microscopic details.

So, to build a model one should provide the symmetry group, the matter content in the form of a number of matter fields, with well-defined transformation properties under the symmetry group, and the properties of the quantum vacuum state. When the vacuum is not invariant under the symmetry transformation we say that the symmetry is spontaneously broken. In the case of a global symmetry, the Goldstone theorem establishes that massless bosons should appear in the spectrum, one corresponding to each of the broken generators of the symmetry group. For gauge symmetries, no Goldstone bosons appear in the spectrum, but instead the corresponding gauge bosons become massive. This is the famous Higgs mechanism [21, 22, 26].

The Standard Model (SM) is the most general theory according to the previous requirements that describe the interaction of a series of particles and is invariant under the gauge symmetry group

$$G_{SM} = SU(3)_C \times SU(2)_L \times U(1)_Y, \tag{1.5}$$

$(1,2)_{-\frac{1}{2}}$	$(3,2)_{-\frac{1}{6}}$	$(1,1)_{-1}$	$(3,1)_{-\frac{2}{3}}$	$(3,1)_{-\frac{1}{3}}$
$\begin{pmatrix}\nu_e \\ e\end{pmatrix}_L$	$\begin{pmatrix}u^i \\ d^i\end{pmatrix}_L$	e_R	u_R^i	d_R^i
$\begin{pmatrix}\nu_\mu \\ \mu\end{pmatrix}_L$	$\begin{pmatrix}c^i \\ s^i\end{pmatrix}_L$	μ_R	c_R^i	s_R^i
$\begin{pmatrix}\nu_\tau \\ \tau\end{pmatrix}_L$	$\begin{pmatrix}t^i \\ b^i\end{pmatrix}_L$	τ_R	t_R^i	b_R^i

Table 1.1: Fermionic matter content of the Standard Model: $(d_{SU(3)}, d_{SU(2)})_Y$. Different rows are the different generations and the two sides of the table correspond to left L, and right R chiral fields. The i index refers to color. Spin indices are not shown.

where C stands for the color group, L indicates that this symmetry only affects the left-handed chiral fermion fields and Y is the hypercharge. All matter fields transform as irreducible representations of this group. For the non-abelian factors, we denote the corresponding representation by its dimension, while the hypercharge is just a number. So we use the notation

$$(d_{SU(3)_C}, d_{SU(2)_L})_Y, \tag{1.6}$$

to fully characterize the representation.

The fermionic matter content of the SM is summarized in Table 1.1. The three rows represent the three generations or families of quarks and leptons, while the left and right sides contain the left and right chiral components of the fermionic fields

$$\frac{1 \pm \gamma_5}{2} f_{R,L} = \pm f_{R,L}. \tag{1.7}$$

Left and right chiral components in the limit of vanishing mass are in one-to-one correspondence to helicity components. Parity relates the two, therefore the SM is a chiral theory that breaks parity in a maximal way: parity partners carry different gauge charges.

In the following we will often use a more compact notation where we refer to all the elements in a column by a unique symbol that carries a family index, i:

$$Q_{L,i}(3,2)_{1/6},\ U_{R,i}(3,1)_{2/3}\ D_{R,i}(3,1)_{-1/3}, \tag{1.8}$$

and

$$L_{L,i}(1,2)_{-1/2}, E_{R,i}(1,1)_{-1}. \tag{1.9}$$

The gauge symmetries imply the existence of a number of gauge bosons, one per symmetry group generator. The number of generators for a $SU(N)$

group is N^2-1, and therefore we have eight gluons for the $SU(3)_C$ group, three weak vector bosons for the $SU(2)_L$ and one hypercharge vector boson for $U(1)_Y$, this corresponds to the following representations:

$$G_a^\mu(8,1)_0, \quad W_a^\mu(1,3)_0, \quad B^\mu(1,1)_0. \tag{1.10}$$

These are the mediators of the color, weak and hypercharge forces.

The last essential ingredient of the SM is a unique scalar field, the famous Higgs field

$$\phi(1,2)_{1/2}. \tag{1.11}$$

With all these matter and gauge fields, the most general renormalizable Lagrangian complying with the required symmetries is of the form:

$$\mathcal{L} = \mathcal{L}_{\text{kin}} + \mathcal{L}_{\text{Yukawa}} + \mathcal{L}_\phi + \mathcal{L}_\psi, \tag{1.12}$$

$\mathcal{L}_{\text{kin}}$ describes the free propagation of the fields as well as their gauge interactions. It is simply written as

$$\begin{aligned} \mathcal{L}_{\text{kin}} &= -\frac{1}{4}G_{a\mu\nu}G_a^{\mu\nu} - \frac{1}{4}W_{a\mu\nu}W_a^{\mu\nu} - \frac{1}{4}B_{\mu\nu}B^{\mu\nu} + \frac{1}{2}D^\mu\phi^\dagger D_\mu\phi \\ &+ \sum_{f=Q_L,L_L,U_R,D_R,E_R} i\bar{f}\gamma^\mu D_\mu f \end{aligned} \tag{1.13}$$

where the field strengths:

$$\begin{aligned} G_a^{\mu\nu} &= \partial^\mu G_a^\nu - \partial^\nu G_a^\mu - g_s f_{abc} G_b^\mu G_c^\nu, \\ W_a^{\mu\nu} &= \partial^\mu W_a^\nu - \partial^\nu W_a^\mu - g\epsilon_{abc} W_b^\mu W_c^\nu, \\ B^{\mu\nu} &= \partial^\mu B^\nu - \partial^\nu B^\mu, \end{aligned} \tag{1.14}$$

where f_{abc} and ϵ_{abc} are the structure constants and g_s and g are the coupling constants of the non-abelian gauge groups $SU(3)_C$ and $SU(2)_L$. Defining also the covariant derivatives are then

$$\begin{aligned} D^\mu Q_L &= \partial^\mu Q_L + ig_s G_a^\mu \lambda_a Q_L + igW_b^\mu T_b Q_L + ig' B^\mu Y_Q Q_L, \\ D^\mu U_R &= \partial^\mu U_R + ig_s G_a^\mu \lambda_a U_R + ig' B^\mu Y_U U_R, \\ D^\mu D_R &= \partial^\mu D_R + ig_s G_a^\mu \lambda_a D_R + ig' B^\mu Y_D D_R, \\ D^\mu L_L &= \partial^\mu L_L + igW_b^\mu T_b L_L + ig' B^\mu Y_L L_L, \\ D^\mu E_R &= \partial^\mu E_R + ig' B^\mu Y_E E_R, \\ D^\mu \phi &= \partial^\mu \phi + igW_b^\mu T_b \phi + \frac{i}{2} g' B^\mu \phi \end{aligned} \tag{1.15}$$

where $\lambda_a, a = 1-8$ are the generators of the color group (Gell-Mann matrices), the $T_b, b = 1-3$'s are the generators for $SU(2)_L$ (Pauli matrices)

and Y_f are the hypercharges. g' is the gauge coupling associated to hypercharge. An important observation is that all these terms do not mix families, the family index in the kinetic terms for the fermions is summed. This implies in particular that these interactions have a large global symmetry group. We can perform unitary and global rotations of the all the generations within each of the fields, Q_L, L_L, U_R, D_R, E_R independently and the kinetic Lagrangian will remain invariant.

$$G_{\text{kin}} = U(3)_{Q_L} \times U(3)_{L_L} \times U(3)_{U_R} \times U(3)_{D_R} \times U(3)_{E_R}. \tag{1.16}$$

Going back to Eq. 1.12, the $\mathcal{L}_\psi$ indicates generic mass terms for the fermions of the theory. There are no mass terms for the fermions in the SM. In fact, a Dirac mass term of the type

$$m_D = m_D \bar{\psi}_L \psi_R, \tag{1.17}$$

is impossible, as it does not preserve gauge symmetry. Moreover a Majorana mass term

$$m_M = m_M \bar{\psi}^c_R \psi_R, \tag{1.18}$$

is also forbidden as it breaks at least the hypercharge-$U(1)_Y$ symmetry. Therefore $\mathcal{L}_\psi = 0$.

The Yukawa part of the Lagrangian reads

$$-\mathcal{L}_{\text{Yukawa}} = Y^d_{ij} \bar{Q}_{Li} \phi D_{Rj} + Y^u_{ij} \bar{Q}_{Li} i\sigma_2 \phi^\dagger U_{Rj} + Y^e_{ij} \bar{L}_{Li} \phi E_{Rj} + h.c., \tag{1.19}$$

where i, j are family indices and therefore the couplings Y's are general 3×3 matrices, which are called Yukawa's matrices. This part of the Lagrangian is a crucial one

- in general it mixes families or generations and violates CP
- it gives fermions masses after spontaneous symmetry breaking

Finally, the last ingredient is the scalar potential. Its most general form is:

$$\mathcal{L}_\phi = -\mu^2 \phi^\dagger \phi - \lambda (\phi^\dagger \phi)^2. \tag{1.20}$$

If λ is negative, then we are in trouble as the potential will be unbounded from below. If instead $\lambda > 0$ and $\mu^2 > 0$, then the potential energy as a minimum at $\phi = 0$. Finally, if $\lambda > 0$ but $\mu^2 < 0$ then the potential energy has a minimum away from $\phi = 0$, at

$$|\phi| = \mu/\sqrt{\lambda} \equiv \frac{v}{\sqrt{2}}. \tag{1.21}$$

In the quantum theory, this value at the classical minimum is the vacuum expectation value:

$$\langle 0|\phi|0\rangle = \frac{v}{\sqrt{2}}. \tag{1.22}$$

Using the gauge freedom, we can make a choice for the direction of the vacuum state, for example

$$\langle \phi \rangle = \begin{pmatrix} 0 \\ v/\sqrt{2} \end{pmatrix}, \tag{1.23}$$

which is obviously not invariant under the $SU(2)_L \times U(1)_Y$ transformations. As a result, the gauge symmetry is spontaneously broken to

$$G_{SM} \to SU(3)_C \times U(1)_{em}, \quad \Big(Q_{em} = T_3 + Y\Big), \tag{1.24}$$

corresponding to the color and electromagnetic forces, while the gauge fields corresponding to the three broken generators get a mass

$$W_\mu^\pm = \frac{1}{\sqrt{2}}\Big(W_\mu^1 \mp i W_\mu^2\Big), \tag{1.25}$$

$$Z_\mu^0 = \frac{1}{\sqrt{g^2 + g'^2}}(g W_\mu^3 - g' B_\mu). \tag{1.26}$$

The fourth vector field, orthogonal to Z,

$$A_\mu = \frac{1}{\sqrt{g^2 + g'^2}}(g' W_\mu^3 + g B_\mu), \tag{1.27}$$

remains massless: this is the photon.

The spontaneous symmetry breaking mechanism is an essential feature of the SM since it is the mechanism of mass generation. All the massive particles in the SM, except the Higgs itself, get their masses from this vacuum expectation value. This can be easily seen by considering perturbations around the true vacuum:

$$\phi = \begin{pmatrix} 0 \\ v/\sqrt{2} \end{pmatrix} + \tilde{\phi}, \tag{1.28}$$

the Yukawa Lagrangian becomes :

$$\mathcal{L}_{\text{Yukawa}} = Y_{ij}^d \frac{v}{\sqrt{2}} \bar{d}_{Li} d_{Rj} + Y_{ij}^u \frac{v}{\sqrt{2}} \bar{u}_{Li} u_{Rj} + Y_{ij}^e \frac{v}{\sqrt{2}} \bar{l}_{Li} e_{Rj} + h.c. + ... \tag{1.29}$$

These are Dirac mass terms for the Dirac fields:

$$u = u_L + u_R, \;\; d = d_L + d_R, \;\; l = l_L + e_R. \tag{1.30}$$

with mass matrices:

$$m_{ij}^f = \frac{v}{\sqrt{2}} Y_{ij}^f. \tag{1.31}$$

There is no mass term for neutrinos however, and therefore neutrinos are massless in the SM.

1.2 Global symmetries and parameter counting

As we have seen, in the absence of Yukawa matrices, the SM has a very large global symmetry, namely

$$G_{\rm kin} = U(3)^5 = SU(3)_q^3 \times SU(3)_l^2 \times U(1)^5, \tag{1.32}$$

where

$$\begin{aligned} S(3)_q^3 &= SU(3)_Q \times SU(3)_U \times SU(3)_D, & (1.33)\\ S(3)_l^2 &= SU(3)_L \times SU(3)_E, & (1.34)\\ U(1)^5 &= U(1)_B \times U(1)_L \times U(1)_Y \times U(1)_{PQ} \times U(1)_E. & (1.35) \end{aligned}$$

Of the five abelian $U(1)$ charges one can be identified with the baryon number (B), one with the global hypercharge (Y), one with the lepton number (L), one with the PQ symmetry (that we will discuss in later chapters) and the last one with a global rotation of the field E_R.

The Yukawa interactions break the global symmetry (while preserving, of course, the gauged hypercharge). Let us see this with an example. Consider the leptonic Yukawa term

$$Y^e_{ij} \bar{L}_{Li} \phi E_{Rj}. \tag{1.36}$$

If we set $Y^e = 0$, we do unitary rotations of the three generations in L and E, that is to say, the theory enjoys the large global symmetry of the kinetic terms $U(3)_E \times U(3)_L$. When we introduce the Yukawa term, the symmetry is reduced to a $U(1)^3$. Then, one can use the broken generators of $U(3)_E \times U(3)_L$ to rotate conveniently the Yukawa matrix Y^e (of course, for definition, the unbroken generators will not affect the direction of the Yukawa matrix). For example, one can rotate it to a real diagonal matrix, which will be proportional to the lepton masses. This example makes also clear that not all the parameters of the theory are physical. Indeed the Yukawa matrix Y^e is a complex, 3×3 matrix, which then has 9 complex parameters, or 18 real (9 moduli and 9 phases). However, we should then subtract parameters in the broken subgroup, as we can use them to remove unphysical parameters and orient the matrix in a convenient direction in the generation space. In the case of the breaking $U(3)_E \times U(3)_L \to U(1)^3$ we can reduce by 15 parameters, which implies we have three physical parameters, that are identified with the lepton masses in the mass basis. As a general rule one has

$$\begin{aligned} \#physical\ \ params = \#Yukawa\ params - \#Flavor\ group\ params + \\ + \#exact\ symmetry\ group\ params \end{aligned} \tag{1.37}$$

where in the case above the exact symmetry group is given by the accidental symmetry $U(1)_e \times U(1)_\mu \times U(1)_\tau$.

The same reasoning can be applied to the Yukawa matrices Y^u, Y^d in the quark sector. There are 36 total real parameters between these two matrices. The flavor symmetry from the kinetic terms is $U(3)^3$, which gives a total of 27 generators. In fact a unitary matrix $U(N)$ has $1/2N(N+1)$ phases and $1/2N(N-1)$ moduli. So in our case $U(3)^3$ gives $3 \times 6 = 18$ phases and $3 \times 3 = 9$ moduli. Then, the Yukawa's matrices preserve baryon number $U(1)_B$, so that our counting rule Eq. 1.37 gives

$$26 - 27 + 1 = 10 \tag{1.38}$$

parameters, which are six quark masses, three mixing angles and one phase.

This is pretty much what happens in quantum mechanics with the Zeeman effect. In the absence of any external field, the hydrogen system enjoys an $SO(3)$ rotational symmetry with degenerate states. However, when an external magnetic field is introduced, the symmetry is broken $SO(3) \to SO(2)$, with the system invariant only under rotation in the plane perpendicular to the magnetic field. There are two broken generators in this case, which can be used to rotate a generic field configuration $\mathbf{B} = B_x\hat{x} + B_y\hat{y} + B_z\hat{z}$ so that $B_x = B_y = 0$. These are unphysical parameters and there is only one physical parameter B_z, which is the magnitude of the magnetic field in this new coordinate system.

Proceeding in this way one can count the parameters of the SM theory, which are in total 18 [33]. There are 3 couplings in the kinetic term g_s, g, g' (which determine the strength of the three forces), two parameters associated with the Higgs potential μ, λ and finally 13 parameters from the Yukawa sector. Three of the latter are the lepton masses, while ten comes from the quark Yukawa sector. Indeed we have two Yukawa matrices in this sector, for a total of 36 real parameters (two complex 3×3 matrices). However, the pattern of symmetry breaking tells us that there are 26 broken generators, which are the number of parameters in the three 3×3 unitary matrices = 27, minus the phase of the preserved baryon number $27 - 1 = 26$. Actually, the large number of parameters is certainly one of the less appealing features of the SM.

Weinberg himself wrote in his fundamental work "[the theory] has too many arbitrary features for [its] predictions to be taken very seriously".

1.3 Family mixing

We have seen in the previous sections that the mass matrices are related to the Yukawa matrices and the Higgs vev

$$m^q_{ij} = \frac{v}{\sqrt{2}} Y^q_{ij}. \tag{1.39}$$

In general, these matrices are not diagonal and, as we saw, contain unphysical parameters. To remove these parameters, one goes to the mass basis. So one diagonalizes the mass matrix, performing a bi-unitary transformation, that is to say, a unitary transformation acting on the left field and another unitary transformation acting on the right ones. The diagonal mass (indicated with a hat) then reads

$$\hat{m}^q_{ij} = (V^q_L)_{ik} m^q_{kl} (V^{q\dagger}_R)_{lj}. \tag{1.40}$$

Of course, when we diagonalize the mass matrix we rotate the chiral fields via the unitary matrices $V_{L,R}$

$$q^i_L = (V^q_L)_{ij} q'^j_L, \tag{1.41}$$
$$q^i_R = (V^q_R)_{ij} q'^j_R, \tag{1.42}$$

where the 'primes' indicate the fields in the mass basis. In this basis the Yukawa matrices are diagonal (as they are proportional to the mass matrices). Also, neutral currents are left unchanged because of the universality of the couplings of fermions of different families to the photon and the Z boson. However weak interactions mix up and down components, therefore in this new basis the coupling of the fermions to the $SU(2)_L$ gauge bosons $W^\pm_\mu \equiv \frac{1}{\sqrt{2}}(W^1_\mu + iW^2_\mu)$(coming from the covariant derivative) will be more complicated

$$\mathcal{L}_{Wqq} = \frac{g}{\sqrt{2}} \bar{u'}_L i\gamma_\mu (V_{uL} V^\dagger_{dL}) d'_L W^\mu. \tag{1.43}$$

Then one identifies the so-called CKM (Cabibbo- Kobayashi- Maskawa) matrix

$$V \equiv V_{uL} V^\dagger_{dL}, \tag{1.44}$$

which is unitary and is **not** diagonal, which means that the $SU(2)_L$ gauge bosons couple to quark mass eigenstates of different generations (flavor changing quark interactions). The CKM matrix has four physical parameters, three mixing angles and one complex phase. A useful parametrization is the Wolfenstein parametrization [34]

$$V = \begin{pmatrix} 1-\lambda^2/2 & \lambda & A\lambda^3(\rho - i\eta) \\ -\lambda & 1-\lambda^2/2 & A\lambda^2 \\ A\lambda^3(1-\rho-i\eta) & -A\lambda^2 & 1 \end{pmatrix} + \mathcal{O}(\lambda^4), \tag{1.45}$$

where λ, A, ρ are the three real mixing angle, while η is the only physical phase of the SM.

Note that the same reasoning can be applied to the leptons. However, as in the SM there are not right handed neutrinos, we have the freedom of redefine the two components of the left-handed doublets with the same unitary matrix, which then disappears from the theory. The result is a theory in which the lepton number is conserved in each generation.

1.4 CP violation: the symmetry between matter and antimatter

There are some important discrete symmetries beside gauge symmetries, namely: charge conjugation C, which exchanges particle and antiparticles, parity transformation P, which reverses the momentum of a particle without flipping its spin and time reversal T, which reverses the momentum of a particle and also flips its spin. Given a spinor ψ, the operation of charge conjugation acts as

$$C : \psi \to -i\gamma_2\psi^*. \tag{1.46}$$

One can also check, for example, that the vector $\bar{\psi}\gamma^\mu\psi$ is invariant under charge conjugation. Under parity instead one has that for Dirac spinors left- and right-handed spinors are exchanged and the transformation assumes the very simple form

$$P : \psi \to \gamma_0\psi. \tag{1.47}$$

Finally, the time reversal symmetry T is trickier as it cannot be implemented with a unitary operator, but rather requires an antilinear or antiunitary operator. In addition to reverse the momentum of a particle, T should also flip its spin; then it can be shown that the action of T on a Dirac fermion reads

$$T\psi(t, \mathbf{x}) \to \gamma_1\gamma_3\psi(-t, \mathbf{x}). \tag{1.48}$$

Any local Lorentz invariant field theory should actually preserve the combination of the three CPT. We also know that QCD and QED conserve both C and P separately, as well as their combination CP. Weak interactions make everything more interesting. In fact, electroweak theory breaks parity by construction, as it is a chiral theory, that is to say, it treats differently left- and right-handed fields. Actually, a chiral theory also violates charge conjugation [35, 36]. What about the combination of the two CP? In principle the theory may or may not violate CP, it depends on the undetermined parameters of the theory. How does this happen? It can be checked with

the transformations given above that CP-violation in the SM reduces to the presence of complex entries in the Yukawa matrices; if there is one, then the theory is CP-violating. In the case of the standard model the incriminated phase is the left-over phase of the CKM matrix in the quark sector δ_{CKM} [36]. A basis-independent way to quantify CP-violation is via the Jarlskog invariant [37]

$$Im[V_{ij}V_{kl}V_{il}^{*}V_{kj}^{*}], \tag{1.49}$$

where V is the CKM matrix. The remarkable thing is that it depends on all the physics mixing angle! If any of the mixing angles is zero, then there is no CP violation. It is then manifest one actually needs $N \geq 3$ flavors to have CP violation in the theory. For one and two families the CKM matrix can always be made real by suitable fermion rotations, this is not the case for three families or more. This is quite suspicious; to say it in the words of I. Rabi " who ordered this?".

1.4.1 Strong CP

There is a more subtle potential source of CP violation in the SM, which has its roots in the complex vacuum structure of $SU(3)$. In the Lagrangian of the SM there is a term allowed by symmetries

$$\mathcal{L}_{\text{strong CP}} = -\bar{\theta}\frac{g_s^2}{16\pi^2}G_{\mu\nu}^{a}\tilde{G}^{a\mu\nu}, \tag{1.50}$$

where $\tilde{G}_{a\mu\nu} = \frac{1}{2}\epsilon_{\mu\nu\rho\sigma}G^{a\rho\sigma}$. This term violates parity P, but preserves charge conjugation C, therefore breaks CP invariance. Interestingly enough this term can be written as a total derivative and would be normally dropped from the Lagrangian. However, in the case of non-abelian gauge theories there are field configurations that make boundary terms non trivial. Therefore, one has to keep this term in the Lagrangian and actually it also has important phenomenological implications. In fact, it contributes to the electric dipole moment of the neutron, which is a CP-violating quantity. However, measurements of the neutron electric dipole moment, d_n, has found no evidence for it [38, 39, 40], implying an upper bound on the adimensional coupling $\bar{\theta}$:

$$\bar{\theta} < 4 \times 10^{-10}. \tag{1.51}$$

The fact that $\bar{\theta}$ is so close to zero seems to require some extra explanation and this is known as the *strong CP problem*. An important point is that even if this coupling is zero, the violation of CP in the Yukawa Langrangian can generate an effective $\bar{\theta}$, which is however extremely tiny [41].

Finally, we stress that if CP was preserved in the SM, the laws of Nature would have been the same for matter and for antimatter, and the asymmetry

we observe in the Universe could have not been generated dynamically. On the other hand, the subtle breaking of CP in the SM is most probably not large enough to explain the Universe we see [42, 43]. We will come back to the issue of matter-antimatter asymmetry later in this thesis.

1.5 Hints for something more

The SM is a wonderful theory as it is, however many aspects are unsatisfactory and puzzling even at the fundamental level, as we already noticed in the previous sections. For example:

- Why are there three families? The number of fermion generation is completely arbitrary, still it has important consequences like CP violation;
- Why is parity broken? In a sense one would not expect space to be asymmetric!
- The large number of parameters as well as the arbitrariness of most of them challenge SM predictivity. There is for example no explanation to the large hierarchy in the pattern of quark and lepton masses as shown in Fig. 1.2. This is the problem S. Weinberg says he would like to solve (and he is thinking about it since 1972!);

All these points are already an indication that the SM may require some extra physics to be a complete theory. But there is compelling evidence that the theory described above is not complete. On the one hand it predicts massless neutrinos, while in the meantime we have measured tiny neutrino masses ! The second inconsistency comes when we analyse how the SM would behave at arbitrarily high energy. We briefly discuss both aspects.

1.6 Neutrinos: To be or not to be (massless)

"I have done a terrible thing: I have postulated a particle that cannot be detected", W. Pauli

One of the most important results in particle physics in recent times is the discovery of neutrino masses. This has been a major achievement over several decades of intense experimental research, an effort that was awarded the Nobel prize in 2002 to the pioneers of this research (Prof. R.Davis and Prof. M. Koshiba), and in 2015 to the most groundbreaking results obtained

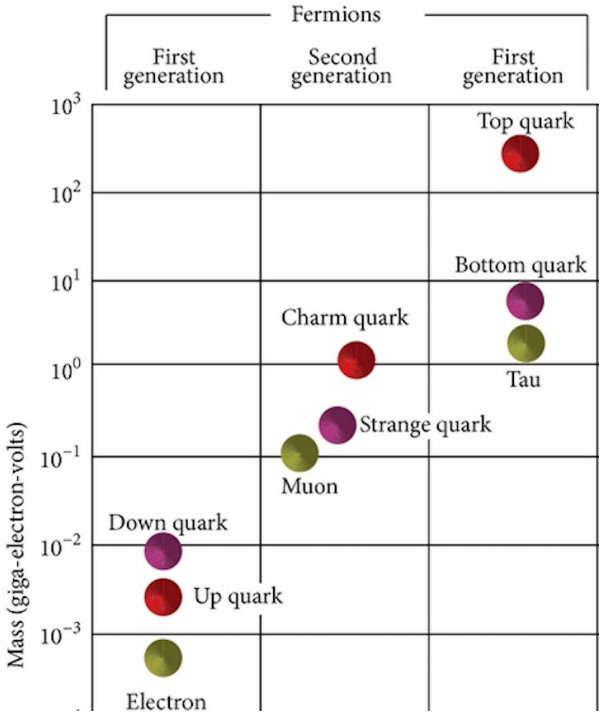

Figure 1.2: Masses of leptons and quarks of the SM in GeV .

by the experiments SuperKamiokande and SNO (Prof. Kajita and Prof. A. McDonald).

It is very easy to extend the SM to accomodate neutrino masses. One would just need to extend the SM by three right-handed neutrinos, ν_R, singlets under the three gauge groups, $(0,0)_0$, so that a Yukawa coupling can be writen also for neutrinos:

$$Y^{\nu}_{ij}\bar{L}_{Li}\phi\nu_{Rj} + h.c. \tag{1.52}$$

Spontaneous symmetry breaking leads to a neutrino mass matrix of the form:

$$m_\nu = Y_\nu \frac{v}{\sqrt{2}}, \tag{1.53}$$

in complete analogy with the remaining quarks and leptons. The neutrino mass matrix is a general matrix and therefore, as in the quark sector, leads to lepton mixing, as explained in sec. 1.3.

The neutrinos that couple to the leptons e, μ, τ denoted by $\nu_{e,\mu,\tau}$ or flavour neutrino states are a unitary combination of the neutrino mass eigenstates, $\nu_{1,2,3}$:

$$\begin{pmatrix}\nu_e\\ \nu_\mu\\ \nu_\tau\end{pmatrix} = U_{PMNS}(\theta_{12},\theta_{13},\theta_{23},\phi)\begin{pmatrix}\nu_1\\ \nu_2\\ \nu_3\end{pmatrix}. \tag{1.54}$$

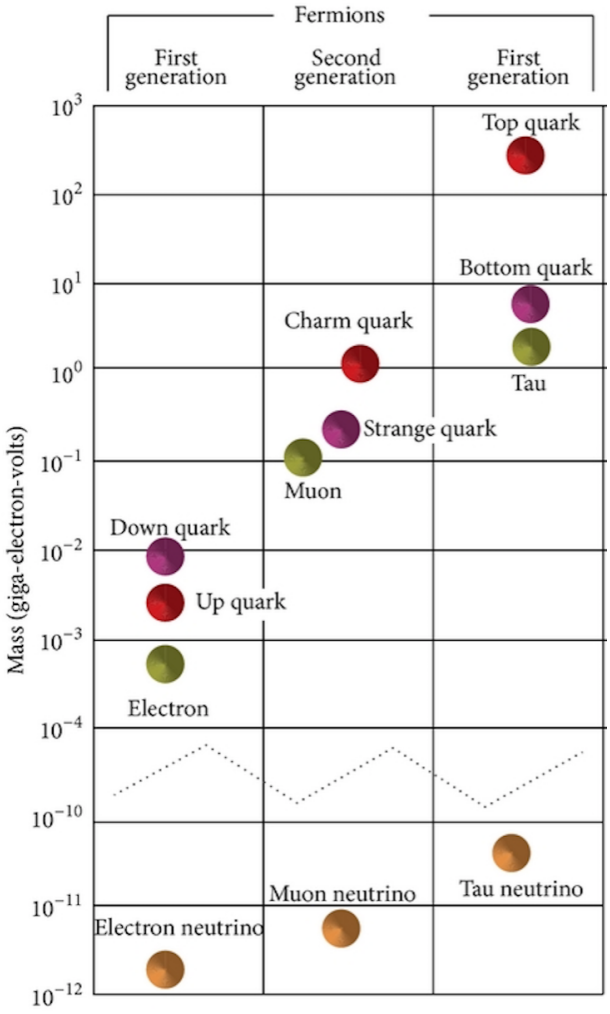

Figure 1.3: Masses of fermions in the SM including neutrinos.

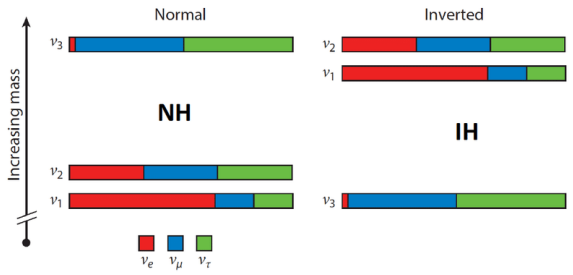

Figure 1.4: Normal and inverted ordering for the neutrinos mass spectrum.

The mixing matrix $U_{PMNS}(\theta_{12}, \theta_{13}, \theta_{23}, \delta)$ is the Pontecorvo-Maki-Nakagawa-Sakata(PMNS) mixing matrix, the leptonic analogous to the CKM one in the quark sector, and depends on three mixing angles and one CP violating phase, often refered to as Dirac phase. The conventional parametrization is

$$U_{\text{PMNS}} = \begin{pmatrix} 1 & 0 & 0 \\ 0 & c_{23} & s_{23} \\ 0 & -s_{23} & c_{23} \end{pmatrix} \begin{pmatrix} c_{13} & 0 & s_{13}e^{-i\delta} \\ 0 & 1 & 0 \\ -s_{13}e^{i\delta} & 0 & c_{13} \end{pmatrix} \begin{pmatrix} c_{12} & s_{12} & 0 \\ -s_{12} & c_{12} & 0 \\ 0 & 0 & 1 \end{pmatrix} \quad (1.55)$$

where $\theta_{ij} \in [0, \pi/2]$ and $\delta \in [0, 2\pi]$.

The tiny differences of neutrino masses have been measured thanks to the quantum interference phenomena of *neutrino oscillations*. Neutrinos are produced in a weak process in combination with an electron, muon or tau lepton, therefore they are created in a flavour state. However, neutrinos are so weakly interacting that they can maintain quantum coherence over macroscopic distances. The different mass eigenstates evolve in space-time independently picking up a phase that depends on the neutrino mass. Therefore, after the neutrino has traveled some distance, called baseline, the superposition of the mass eigenstates has been modified and if it is intercepted by a detector where the neutrino interacts by the inverse process, a different lepton flavour might be measured. The probability for an ultra-relativistic neutrino of momentum p, produced with a lepton of flavour α to be detected via a lepton with flavour β is a oscillatory function of the baseline given by:

$$P(\nu_\alpha \to \nu_\beta) = \sum_{ij} U^*_{\alpha i} U_{\beta i} U_{\alpha j} U^*_{\beta j} \exp\left(-i \frac{\Delta m^2_{ji} L}{2|p|} \right). \quad (1.56)$$

It is a superposition of waves with wavelengths depending on the neutrino mass square differences, $\Delta m^2_{ij} \equiv m^2_j - m^2_i$, and amplitudes depending on the elements of the mixing matrix, $U_{\alpha i}$.

Neutrino flavour transitions have been measured in a plethora of experiments, some using natural sources of neutrinos, solar and atmospheric,

others using neutrino beams produced in reactors or particle accelerators. All these measurements have provided a coherent picture that can be precisely explained in terms of the 3 neutrino mixing parameters: two mass differences and the PMNS mixing matrix [44, 45, 46]. Neutrino oscillations data have provided a precise determination of the neutrino mass square differences, but still cannot distinguish between the two possible ordering of the neutrino mass eigenstates, as shown in Fig. 3.1. The spectrum where the two most degenerate states are the lightest is the normal ordering or hierarchy (NH) while when they are the heaviest is the inverted one (IH). The mixing angles are also precisely measured although there remains the so-called octant degeneracy in the largest angle that is close to maximal, $\theta_{23} \simeq \pi/4$, but could differ from this value giving the same fit to data if is above or below maximal by the same amount. Finally, although there is a hint for $\delta \neq 0, \pi$ at 3σ, implying leptonic CP violation at this confidence level, this parameter is still very uncertain.

Best fit parameters [45]		
	Normal Ordering	Inverted Ordering
$\sin^2\theta_{12}$	$0.310^{+0.013}_{-0.012}$	$0.310^{+0.013}_{-0.012}$
θ_{12}	$33.82^{0.78}_{-0.76}$	$33.82^{0.78}_{-0.76}$
$\sin^2\theta_{23}$	$0.580^{+0.017}_{-0.021}$	$0.584^{+0.016}_{-0.020}$
θ_{23}	$49.6^{1.0}_{-1.2}$	$49.8^{+1.0}_{-1.1}$
$\sin^2\theta_{13}$	$0.02241^{+0.00065}_{-0.00065}$	$0.02264^{+0.00066}_{-0.00066}$
θ_{13}	$8.61^{0.13}_{-0.13}$	$8.65^{+0.13}_{-0.13}$
δ_{CP}	215^{40}_{29}	284^{+27}_{-29}
$\frac{\Delta m^2_{21}}{10^{-5}eV^2}$	$7.39^{0.21}_{-0.20}$	$7.39^{0.21}_{-0.20}$
$\frac{\Delta m^2_{3l}}{10^{-3}eV^2}$	$2.525^{0.033}_{-0.032}$	$-2.512^{0.034}_{-0.032}$

On the other hand, neutrino oscillations cannot measure the absolute neutrino masses, only mass differences. Neutrino masses on the other hand affect the kinematics of beta-decay and in particular they modify the shape of the end-point spectrum. The measurement of tritium beta decay has provided the most stringent upper bound of this type [47, 48]

$$m_{ee} < 2\text{eV}, \tag{1.57}$$

a measurement that is expected to be improved by an order of magnitude in the near future by the Katrin experiment [49].

Neutrino masses in the eV range can have an impact in cosmological observables. In particular, they can sizeably modify the perturbations in the cosmic microwave background (CMB) as well as the power spectrum of large scale structures. Presently the best limit on the sum of neutrino masses comes actually from cosmology, accordingly to the last Planck release [50]

$$\Sigma = \sum_i m_i < 0.12. \tag{1.58}$$

The minimal extension of the SM with massive neutrinos brings two additional problems to the model. Firstly, the flavour puzzle becomes more puzzling, with a huge gap between neutrino mass and the rest as shown in Fig. 1.3. Secondly, the mixing pattern of neutrinos and quarks looks fundamentally different with

$$V_{\rm CKM} \simeq \begin{pmatrix} 1 & 0 & 0 \\ 0 & 1 & 0 \\ 0 & 0 & 1 \end{pmatrix}, \tag{1.59}$$

while

$$U_{\rm PMNS} \simeq \begin{pmatrix} \sqrt{\frac{2}{3}} & \sqrt{\frac{1}{3}} & 0 \\ -\sqrt{\frac{1}{6}} & \sqrt{\frac{1}{3}} & \sqrt{\frac{1}{2}} \\ \sqrt{\frac{1}{6}} & -\sqrt{\frac{1}{3}} & \sqrt{\frac{1}{2}} \end{pmatrix}.$$

1.7 Landau poles, stability and all that

Imagine the SM is *the theory of everything*. This would imply that the model should describe physics at arbitrarily high energy scales. Would this be consistent? There are actually some fundamental problems if one does not introduce new degrees of freedom. It turns out that the hypercharge gauge coupling g' and the Higgs self-coupling, λ, present a Landau pole: that is, perturbation theory predicts that the coupling diverges at some high energy scale, $\Lambda_{\rm landau}$. An equivalent statement is that the SM is a *trivial theory*: in the absence of a cutoff, the value of the renormalized g_s and λ couplings is zero and therefore inconsistent with phenomenology. If we take the Landau pole scale as the scale where new physics should enter to make the theory consistent, we find that while the hypercharge gauge coupling diverges at scales much larger than the Planck scale, $M_{\rm Planck}$ (the scale where gravity should kick in), the Landau pole for the Higgs self-coupling depends very sensitively on the top quark mass, the Higgs mass and the strong coupling.

Another requirement for the consistency of the SM at high energy scales is the stability of the Higgs potential: $\lambda(\mu) > 0$ for all μ. Again, whether this is the case depends very sensitively on the same parameters. The measured parameters indicate that the SM is very close (2σ) to being fully consistent up to the $M_{\rm Planck}$ or the electroweak vacuum could become metastable at large scales $\Lambda \gtrsim 10^{10} GeV$ [51, 52, 53, 54, 55]. It is an intriguing feature of the SM that its Landau pole is beyond $M_{\rm Planck}$ and so close to the stability limit, since this involves a correlation between apparently free parameters of the model that could have taken any value (see Fig. 1.5 for a plot where the stability region and the region with $\Lambda_{Landau} < M_{\rm Planck}$ are identified).

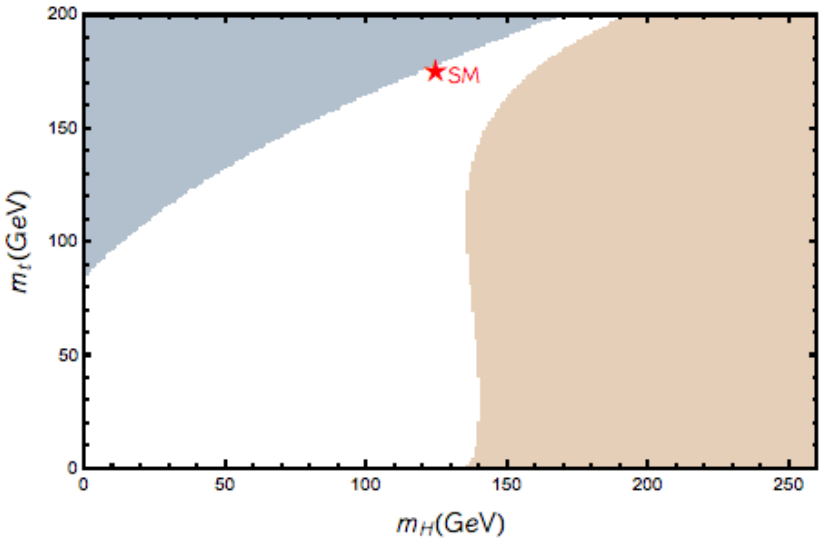

Figure 1.5: Regions where the stability condition and the condition $\Lambda_{Landau} < M_{\text{Planck}}$ are satisfied, plotted as a function of the Higgs and the top quark masses. The blue region indicates the portion of the parameter space of absolute instability; the light brown region corresponds to a region where perturbativity is lost before the Planck scale. The red star corresponds to the measured values of the SM, which lies in a meta-stable region [51].

Chapter 2

A walk beyond the SM

We concluded the previous chapter with multiple hints pointing to the fact that the SM cannot be the complete theory of nature. In the most conservative scenario, the theory needs to be modified at least when the Planck scale is reached. At this scale gravity should be quantized and this is of course not taken into account in the SM. The SM was not designed to deal with gravity, which is the fourth and weakest force in nature. A theory that aims to unify all four forces is called Quantum Gravity and might require a different framework than the one of quantum field theory. The value of the Planck scale is roughly $M_{\text{Planck}} \sim 10^{19}\text{GeV}$, while the electroweak scale (EW) lies around $v \sim \mathcal{O}(10^2)\text{GeV}$. There are almost 17 orders of magnitudes of difference between these two scales; it is therefore likely that new physics, with a characteristic scale Λ, appears in the gap between the EW and the Planck scales, $v < \Lambda < M_{Pl}$.

Let us suppose that a number of new particles, fields, with masses Λ lie in this range. This means that at high energy the complete theory (or UV completion) would be

$$\mathcal{L} = \mathcal{L}_{SM}[\phi] + \mathcal{L}_{BSM}[\phi, \Psi], \tag{2.1}$$

where $\mathcal{L}_{SM}[\phi]$ is the SM Lagrangian discussed in the previous chapter, ϕ representing all the fields of the SM, while $\mathcal{L}_{BSM}[\phi, \Psi]$ depends on the new physics at large scale and Ψ indicates collectively all the new degrees of freedom in the theory.

At low energies $E \ll \Lambda$, however, the theory should be well described by an *effective field theory* (EFT) where the new degrees of freedom do not appear, because they are too heavy to be produced at these energies. We say that it is then possible to 'integrate them out'. This will inevitably lead to a non-local theory, in which the effect of the heavy degrees of freedom is encoded in new non-local interactions of the SM fields. However, this

non-locality is only observable at energies $E \sim \Lambda$ and at the energies much smaller than this, one can write a set of local operators:

$$\mathcal{L} \simeq \mathcal{L}_{\text{SMEFT}} = \mathcal{L}'_{SM} + \sum_i \frac{c_i^5}{\Lambda} O_i^{(5)} + \sum_i \frac{c_i^6}{\Lambda^2} O_i^{(6)} + .., \tag{2.2}$$

where the O_i^d are gauge-invariant operators constructed out of the SM fields with dimension, d. The powers of Λ therefore match the dimensions of each term, so that the coefficients c_i are dimensionless. The precise value of these coefficients depends on the UV completion, but they are expected to be smaller than one if the couplings in the UV theory are perturbative [56, 57]. In principle, this is an infinite sum of local operators, but their contribution to any low-energy process becomes of $\mathcal{O}(\frac{E}{\Lambda})^{d-4}$. In practice, one can truncate the series at a given order or dimension, depending on the required accuracy. Note the presence of a prime in Eq. 2.2 for the SM Lagrangian. This refers to the fact that the SM parameters $\{g, g', g_s, \mu, \lambda, Y^f\}$ in $\mathcal{L}'_{SM}$ are different from the UV ones in the original high energy theory $\mathcal{L}_{SM}$, they get a finite renormalization depending on the scale Λ.

The philosophy of the effective field theory relies on the fact that different energy scales involve different interactions and at each scale we want to concentrate on the relevant physics. This happens also in many other situation in physics. Think, for example, about multipole expansion in electrodynamics. If the wavelengths we are interested to, λ, are much larger than the typical size of the systems, R, then we can mostly ignore the details of charge distribution and retain e.g only the dipole term in the expansion.

2.1 Vertigo: fear of high scales

The introduction of new physics at high scale actually highlights a crucial problem of the theory, which is usually called the hierarchy problem. As explained above the effect of the existence of new particles at scale Λ at low-energies is the renormalization of the SM parameters. Particularly problematic is the effect on the μ parameter of the Higgs potential, the Higgs mass, which is generically of the form:

$$\mu' - \mu = \frac{g^2}{(16\pi)^2}\Lambda^2, \tag{2.3}$$

where g is some generic coupling of the UV completed theory, $\mathcal{L}$.

Of course in the lab, for $E \ll \Lambda$, we measure the effective mass of the Higgs, μ' and not μ. However, if $\Lambda \gg 10$ TeV, this finite quantum correction

will be much larger than the mass itself $\delta\mu \gg \mu'$. This is the hierarchy problem, affecting elementary scalars, whose masses are quadratically sensitive to any mass scale of new physics.

This is not the case for fermions or gauge bosons, where the corrections are proportional to the masses themselves. The reason being chiral symmetry in the case of fermions and gauge symmetry in the case of gauge bosons, that are recovered in the massless limit. The hierarchy problem is a problem of scale separation, between the electroweak and any UV scale. Let me also stress that this is not a problem of consistency, but rather a problem of **naturalness** or fine-tuning.

An example of a natural theory is QCD. Think, for example, about the mass splitting between charged and neutral pions. Neutral and charged pions are degenerate due to isospin symmetry, which is broken by QED. If we compute the photon loop that generate mass corrections, in the pion effective theory we get

$$\delta m^2 \sim \frac{e^2}{16\pi^2}\Lambda^2, \tag{2.4}$$

which should be compared with the observed meson splittings

$$m^2_{\pi^\pm} - m^2_{\pi_0} \sim (35.5\text{MeV})^2. \tag{2.5}$$

So to explain the observed value, we expect the cut off to be around 850 MeV; in fact ρ mesons enter the game at 770 MeV, providing a cut off for the effective theory. Similar naturalness arguments were used by Gaillard and Lee to predict the charm-quark mass from the mass-splitting of neutral kaons.

The hierarchy problem inspired a lot of ideas in the past years and many theories have been developed trying to solve this problem, among others: technicolor theories, supersymmetry, composite Higgs theories and extra dimensions. In most cases, these solutions imply new physics not far beyond the TeV scale that can screen the higher new physics scale. For example in supersymmetric theories, the corrections of Eq. 2.4 is cancelled between the fermionic and bosonic degrees of freedom. Instead in composite Higgs theories, no fundamental scalars other than composite or goldstone bosons exist, and the scale Λ is dynamically generated, like the QCD confinement scale.

2.2 Data and problems, problems and data

Apart from these problems of theoretical nature, there are actually also data-driven problems that the SM has to face. We have already mentioned

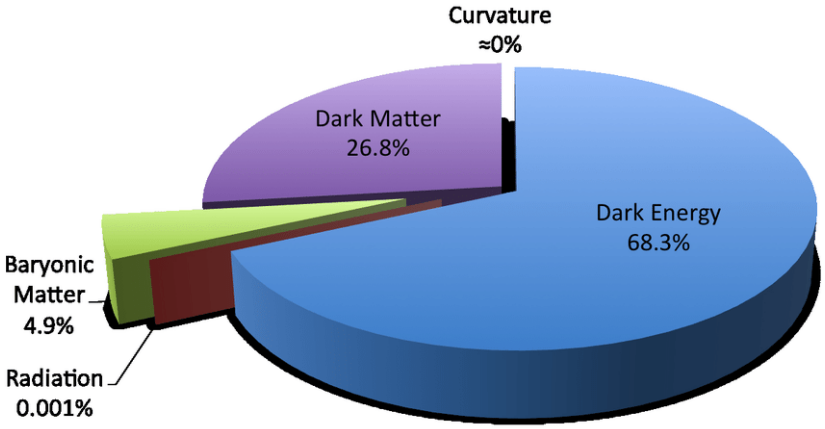

Figure 2.1: Composition of the Universe today. Most of it is in the form of dark components whose origin is unknown to us, namely dark energy and dark matter.

neutrino masses, that could be explained by a very minimal extension of the SM, but could also be the first hint of a new physics scale.

When we look at the universe at large scales, the SM fails to explain its structure. In fact, it cannot explain the main components of the energy density in the Universe, see Fig. 2.1. It cannot explain neither why there are baryons. According to the SM, the Big Bang should have created equal amounts of matter and antimatter in the early universe. However, if this was the case we would not be here as matter and antimatter would have annihilated long ago. Luckily enough everything we see from the smallest life forms on Earth to the largest stellar objects seems to be made almost entirely of matter, which implies that in the early instants of the Universe when the Universe was very hot, there was a tiny asymmetry of one extra particle of matter in 10^{10} over antimatter. This is the famous matter-antimatter asymmetry that cannot be explained by the SM [58, 59, 42, 43], but can be explained in the presence of new physics.

Moreover, the SM cannot explain the fact that there is 4-5 times more non-relativistic matter in the universe that is non-baryonic matter and that we have seen only via its gravitational interactions. This is the famous dark matter, whose nature is still a mystery. Many extensions of the SM have been proposed that can explain dark matter in terms of a new particle, relic from the Big Bang.

There are actually other interesting problems which the SM faces and that I will not discuss in this manuscript. For example, it is well known that the universe is actually expanding and is doing it with a positive acceleration. When the expansion of the universe was measured to accelerate, this was like looking at a bullet which comes back once discharged. In the

contest of general relativity this is due to a kind of energy, called "Dark Energy", which acts as anti-gravity and pull things apart faster and faster. The structure of the energy at large scales can be explained accurately if it has undergone an inflationary phase. The dynamics underlying inflation and the origin of dark energy remain a huge challege for fundamental physics.

2.3 New Physics and Neutrino Masses

Interestingly, in the tower of higher dimensional operators of the SMEFT there is a unique $d = 5$ operator of the form

$$O^{(5)} = \bar{L}_i \tilde{\phi} c_{ij}^{(5)} \phi^* L_j^c + h.c, \tag{2.6}$$

the famous Weinberg operator [60]. After spontaneous symmetry breaking, this term gives rise to a Majorana neutrino mass for the SM neutrinos:

$$\mathcal{L}^{(5)} \to \bar{\nu}_{Li} c_{ij}^{(5)} \frac{v^2}{2\Lambda} \nu_{Lj}^c + h.c, \tag{2.7}$$

$$m_\nu = c_{ij}^{(5)} \frac{v^2}{\Lambda}. \tag{2.8}$$

Neutrinos are Majorana particles in this case. There are two interesting observations:

- Generic new physics can generate neutrino masses
- The smallness of neutrino masses could be explained if it originates in a new physics scale, the larger the scale the smaller the neutrino mass: this is the famous seesaw mechanism [61, 62]

An open fundamental question in neutrino physics is whether such a scale exists and what new physics is to be found at that scale. Unfortunately the measurement of neutrino masses, cannot answer this question, because they only fix the combination

$$\frac{c_{ij}^{(5)}}{\Lambda} \leq 10^{-15} \text{GeV}^{-1} \left(\frac{m_\nu}{0.1\text{eV}} \right). \tag{2.9}$$

Since the adimensional coupling is not expected to be larger than one, this provides an upper bound for Λ:

$$\Lambda \geq 10^{15} \text{GeV} \left(\frac{m_\nu}{0.1\text{eV}} \right), \tag{2.10}$$

but the scale can be much smaller if the coupling is much smaller. What value for the coupling is natural or not depends on the UV theory.

This effective interaction implies that total lepton number is not a global symmetry of the theory. This has two important implications. The first is the existence of new physical CP phases, indeed the mixing matrix contains two additional physical phases [63, 64] in this case, that we usually denote ϕ_1, ϕ_2:

$$U_{\rm PMNS}^{\rm Majorana} = U_{\rm PMNS}(\theta_{12}, \theta_{13}, \theta_{23}, \delta) \begin{pmatrix} 1 & 0 & 0 \\ 0 & e^{i\phi_1} & 0 \\ 0 & 0 & e^{i\phi_2} \end{pmatrix}, \tag{2.11}$$

with $\phi_i \in [0, 2\pi]$.

The second is a model-independent prediction, a smoking gun signature for the nature of neutrinos, that is the neutrinoless double beta decay (provided Λ is larger than the momentum transfer in the process, $\sim$ 100MeV). Some isotopes can in fact decay through double beta decay

$$(A, Z) \to (A, Z+2) + 2e^- + 2\bar{\nu}_e. \tag{2.12}$$

If the neutrinos are Majorana particles, this process can actually happen without neutrinos in the final state, clearly violating Lepton number by 2 units. Such process will be sensitive to both Majorana phases and absolute mass through the effective $0\nu\beta\beta$ mass parameter

$$m_{\beta\beta} = \sum_i |U_{ei}^2 m_i|, \tag{2.13}$$

where m_i are the neutrino mass eigenstates. In Fig.2.2 we show the effective neutrino mass as a function of the lightest neutrino masse. The shaded regions are the predictions for NH and IH, obtained using the best fit oscillation data, the grey regions are experimentally excluded regions, and the blue band is the result of KamLand-Zen [65].

In the first part of this thesis we will consider the possibility that neutrino masses originate from a new physics scale, Λ, associated to the mass of new heavy particles which are not much heavier than the EW scale $\Lambda \sim v$, but for which the smallness of $c_{ij}^{(5)}$ can be understood as arising from small yukawa couplings of similar magnitude as that of the electron in the SM. We will consider in turn some phenomenological implications of the minimal model, where the only addition to the SM are heavy Majorana singlet neutrinos, the so-called Type I seesaw model, as well as a possible extension of the minimal model by additional new physics, $\Lambda_{NP} \gg v$.

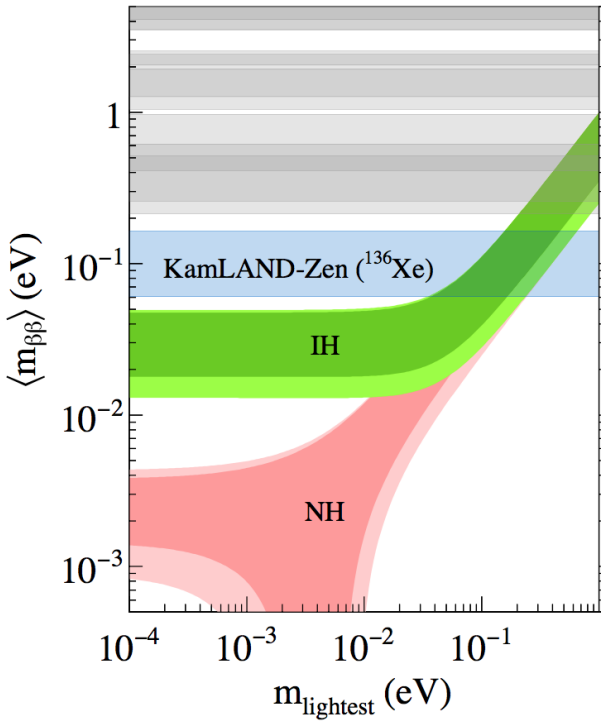

Figure 2.2: Effective neutrino mass as a function of the lightest neutrino mass. The shaded regions are the predictions for NH and IH based using the best fit oscillation data, the grey regions are exclusions from experiments, and blue band is the result of KamLand-Zen [65].

2.3.1 Type I seesaw model at low scales

In this minimal model with massive neutrinos, the SM is enlarged with additional (at least two) fermionic singlets, $N_R(1,1)_0$, and the most general Lagrangian is considered, which involves a lepton-number breaking Majorana mass term

$$\frac{1}{2}\bar{N}_R M_N N_R^c + \bar{L}_L Y_\nu \tilde{\phi} N_R + h.c, \tag{2.14}$$

where M_N is the Majorana mass and Y_ν a Yukawa matrix which couples the SM lepton doublets with the new degrees of freedom. So after electroweak symmetry breaking one is left with the mass term

$$\frac{1}{2}(\bar{\nu}_L^c \;\; \bar{N}_R) \begin{pmatrix} 0 & m_D \\ m_D^T & M_N \end{pmatrix} \begin{pmatrix} \nu_L \\ N_R^c \end{pmatrix} \equiv \frac{1}{2}\bar{N}^c M N, \tag{2.15}$$

where $m_D \equiv Y_\nu \frac{v}{\sqrt{2}}$ is the Dirac mass matrix and we defined $N \equiv (\nu_L, N_R^c)$, where N_R^c is the charged conjugate of the N_R field. Note that we did not include direct Majorana contributions to the mass of ν_L, such as, for example, that induced by Weinberg operator, because for the time being we are considering a complete renormalizable theory.

One then has to diagonalize the matrix M to go to the mass basis. In the simplest case of one family one has

$$\begin{pmatrix} \nu_L \\ N_R^c \end{pmatrix} = \begin{pmatrix} \cos\theta & \sin\theta \\ -\sin\theta & \cos\theta \end{pmatrix} \begin{pmatrix} \nu_1 \\ \nu_2 \end{pmatrix}, \tag{2.16}$$

where $\tan 2\theta = 2m_D/M_R$ and the eigenvalues are

$$m_{1,2} \simeq \frac{M_R}{2} \mp \left(\frac{M_R}{2} + \frac{m_D^2}{M_R}\right) \rightarrow m_1 \simeq \frac{m_D^2}{M_R},\; m_2 \simeq M_R, \tag{2.17}$$

This is the hearth of the see-saw mechanism: if $M_R \gg m_D$ then $m_1 \ll m_2 \simeq M_R$. Note that the complete mass matrix for three new heavy singlets is a 6×6, symmetric, complex matrix and the general result for the 3×3 light neutrino mass matrix is,

$$m_\nu = -\frac{v^2}{2} Y_\nu M_R^{-1} Y_\nu^T. \tag{2.18}$$

We could have analogously derived this result by matching to an effective theory where the heavy neutrino are integrated out, in which case we would have obtained the Weinberg interaction, so we can identify

$$\Lambda \sim M_R, \quad c^{(5)} \sim Y_\nu^2. \tag{2.19}$$

Besides the three light neutrinos, ν_i, this model predicts the existence of three heavy Majorana neutrinos, N_h, with a mass matrix given approximately by M_R. These new particles are also referred in the literature as heavy neutral leptons. Besides having three light massive neutrinos, this model has a rich phenomenology associated to these heavy states. The neutrino states that couple to the electron, muon and tau leptons are unitary combinations of *both* the light and heavy states, therefore the latter also couple to the $W^{\pm}, Z$, as dictated by the $U_{\alpha h}$ mixing submatrix:

$$\nu_\alpha = U_{\alpha i}\nu_i + U_{\alpha h}N_h, \quad \alpha = e, \mu, \tau. \tag{2.20}$$

A convenient and general parametrization of this heavy mixing matrix uses as inputs the PMNS mixing matrix and masses of the light neutrinos. This is the famous Casas-Ibarra parametrization:

$$U_{\alpha h} = iU_{PMNS}\sqrt{\text{diag}(m_\nu)}R^\dagger(z)\text{diag}(M_N)^{-1/2}, \tag{2.21}$$

where R is a general complex orthogonal 3×3 matrix, m_ν is the light neutrino mass matrix and M_N that of the heavy states.

As we discussed above, light neutrino masses cannot pin down the new mass scale M_R. When this model was first proposed, the scale was assumed to be very large, near its upper bound, since this was close to the scale of grand unification (GUT), where the three gauge couplings tend to unify. This requires $Y_\nu \sim \mathcal{O}(1)$. However, the quadratic dependence on the Yukawa implies that for a Yukawa of order of the electron one, $Y_\nu \sim Y_e \sim 10^{-6}$, the scale M_R could be around the EW scale. This would have have the advantage of avoiding the hierarchy problem.

In this thesis, we focused on the range $1GeV \lesssim M_R \lesssim 100$ GeV. This is a very appealing since the heavy neutrinos are light enough to be produced at hadron and lepton colliders.

2.3.2 The seesaw path to leptonic CP violation

In our first work [1] we studied the sensitivity of future lepton colliders as the FCC-ee and the fixed target experiment SHiP [66] to right handed neutrino with masses below M_Z. In particular, we studied for the first time the implications of the measurement of the mixing of the heavy states to electrons and muons as regards leptonic CP violation. We showed that the measurement of flavour ratios are sensitive probes of leptonic CP violation in the context of seesaw models.

We considered the most minimal model with just two singlets that leads to a spectrum with two light and two heavy neutrinos, while the lightest

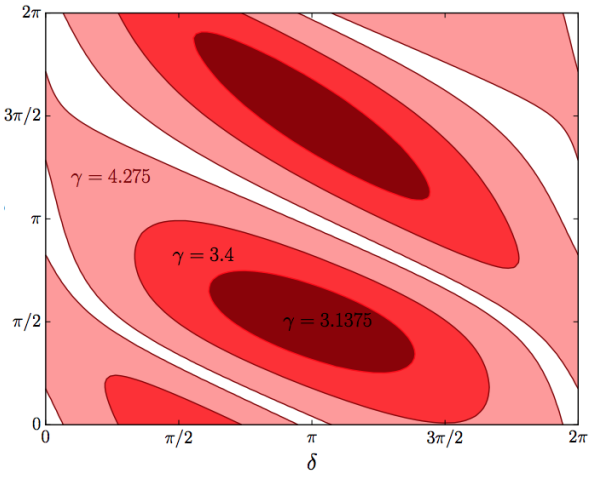

Figure 2.3: 5σ CP-violation SHiP discovery regions on the plane (θ, δ) in the case of normal ordering (NH) as studied in [1].

one remains massless. One can adapt the Casas-Ibarra parametrization to this case as

$$U_{\alpha h} = iU_{PMNS}\sqrt{m_\nu}P_{NO}R^\dagger(z)M_N^{-1/2}, \tag{2.22}$$

where $R(z)$ is a generic complex orthogonal 2×2 matrix which depends on the complex angle $z = \theta + i\gamma$, and where P_{NO} is a 3×2 matrix which depending on the mass ordering (NH, IH) is

$$P_{NH} = \begin{pmatrix} \mathbf{0} \\ I \end{pmatrix}, \; P_{IH} = \begin{pmatrix} I \\ \mathbf{0} \end{pmatrix}, \tag{2.23}$$

where I is the 2×2 identity matrix and $\mathbf{0} = (0, 0)$.

The SHIP experiment will look for heavy neutrinos produce from charmed and beauty meson decays [66]. On the other hand FCC-ee will produce sterile neutrinos from the decay of the Z boson produced from $e^+ - e^-$ collisions [67, 68]. The relevant production and decay channels for the right handed fields can be found in many references, for example in [69]. The relevant point for the present discussion is that the heavy field will decay into SM leptons through the mixing in Eq. 3.21. In particular, and crucially, the ratio of electron/muon mixings is largely determined by the PMNS matrix and not by the unknown complex angle z, nor the masses of the heavy states. In Fig. 2.4 we show the possible values of the flavour mixings for the normal and inverted ordering of the light neutrinos. The size of the regions depends on the unknown Majorana CP violating phases. While there is an ambitious experimental plan to measure the Dirac CP violating phase δ, it will be extremely difficult to measure Majorana phases. The indirect measurement we proposed achieves precisely this in the context of seesaw

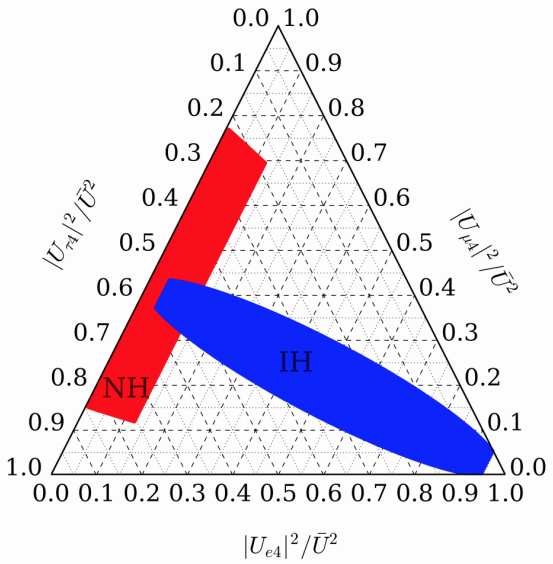

Figure 2.4: Ternary diagram for the normalized flavour mixings fixing the known oscillation parameters to their best fit values and varying the CP phases in the intereval $[0, 2\pi]$ for NH (red) and IH (blue). This figure is from [2], and has been later repeated in many other works.

models. More precisely, in [1] we quantified the CP discovery potential of these future experiments, and demonstrated that a $5\,\sigma$ CL discovery of leptonic CP violation would be possible in a very significant fraction of parameter space as shown in Fig. 2.3. Summarizing, finding neutral heavy leptons with the mixing pattern in the colored regions of Fig. 2.4 would be a convincing evidence that these heavy states are responsible for neutrino masses, and determination of the mixing with a error smaller than the size of the regions will provide a measurement of the leptonic CP violating phases. More details can be found in [1].

2.3.3 The seesaw portal in testable models of neutrino masses

The very beautiful prediction of Fig. 2.4 relies on the minimality of the model considered. One may wonder, for example, how some new physics would modify the predictions of the low-energy theory represented by the minimal model with the two singlet states only. We addressed this question in Ref. [2] where we extended the minimal seesaw model to consider implications of new physics at some higher energy scale, Λ. We parametrized the new physics in terms of a low-energy effective field theory, that differs from the usual one for the SM, that is the SMEFT, because it now must

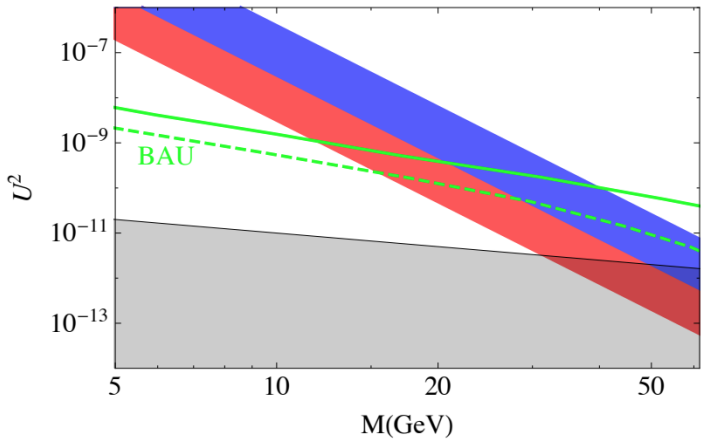

Figure 2.5: Regions on the mass-mixing plane M, U where LHC displaced track selection efficiency is above 10% in the inner tracker (IT, blue band) and muon chamber (MC, red band). The grey shaded region cannot explain the light neutrino masses and the green lines correspond to the upper limits of the 90%CL bayesian region for successful baryogenesis in the minimal model for NH (solid) and IH (dashed), taken from [74].

include the new singlet states N_R. Interestingly, there are two more $d = 5$ operators with respect to the SMEFT:

$$O_{NH} = \bar{N}_R^c N_R \phi^\dagger \phi, \tag{2.24}$$
$$O_{NB} = \bar{N}_R^c \sigma^{\mu\nu} N_R B_{\mu\nu}, \tag{2.25}$$
$$O_5^W = (\phi L)^T (\phi L). \tag{2.26}$$

The last is Weinberg's operator that only contains the SM fields, but the new ones, O_{NH} and O_{NB} are only there because there are new fermionic singlets in the theory (the seesaw states, N_R provide therefore a new portal to new physics). The EFT including singlets had been studied before in refs. [70, 71, 72, 73]. In our work however our focus was on the new production mechanism of the RH neutrinos in Higgs decays via O_{NH}. This opens a new search strategy at LHC. In particular, we investigated the LHC prospects for the detection of the Higgs decay into two sterile neutrinos which then decay via mixing producing spectacular and very clean signals with two displaced vertices. We studied this process in some detail and derived the limits shown in Fig. 2.5. Interestingly we found that an approximate lepton number symmetry could provide a natural hierarchy for the couplings of the three $d = 5$ operators, so the smallness of neutrino mass would not imply the inobservability of the O_{NH} interaction.

2.3.4 Minimal Flavour Violation in the seesaw portal

The effective theory including heavy singlet neutrinos that are responsible for neutrino masses has been baptized νSMEFT in our third work on this topic [7]. At a higher dimension, $d = 6$, many more new operators with respect to the SMEFT appear and one may wonder to what extent the assumption in the previous section concerning the decay of the heavy neutrinos via mixing is robust. In particular, whether the neutrinos decay promptly or are long lived depends strongly on the flavor structure of the theory and it is easy to arrange that the decay modes could be dominated by $d = 6$ operators and not by mixing. This would make it much more difficult to establish the connection between they new states and neutrino masses.

In Ref. [7] we studied νSMEFT up to $d = 6$ under the assumption of Minimal Flavor Violation. The Minimal Flavor Violation (MFV) paradigm [75, 76] provides a natural suppression of flavor changing neutral currents (FCNC) and lepton number violating (LNV) processes, in the context of generic new physics models, derived from a symmetry principle. It states in brief that all flavor and charge-parity violating interactions in the EFT should be linked to the ones of the renormalizable Lagrangian. In Ref. [7] we investigated for the first time the phenomenological implication of this assumption in the νSMEFT, studying how this affects the decay signatures of the heavy neutrinos, a property which is essential for experimental search strategies. This is shown in Fig. 2.6.

Our study also provided a hierarchy of relevance of the $d = 6$ operators, demonstrating that in this scenario, the dominant production channels for the heavy neutrinos at colliders are the Higgs decay studied in the previous section as well as dimension six operators with two RH neutrinos that preserve lepton number, $\mathcal{O}_{NX} = (\bar{N}_R \gamma^\mu N_R)(\bar{X}\gamma_\mu X)$ with $X = e, u, d, q, L, N$.

2.4 Dr.Jekyll and Mr.Hyde: aka matter antimatter asymmetry

Cosmic rays from the Sun indicates that it is composed of matter. Also the fact that Neil Armstrong did survive demonstrates that the Moon is made of matter. The survival of planets actually demonstrates that the solar system is made essentially of matter. While cosmic rays provide evidence of the existence of antimatter in the galaxy only at the 10^{-4} level, compatible with it being produced in astrophysics environments. On larger scales the

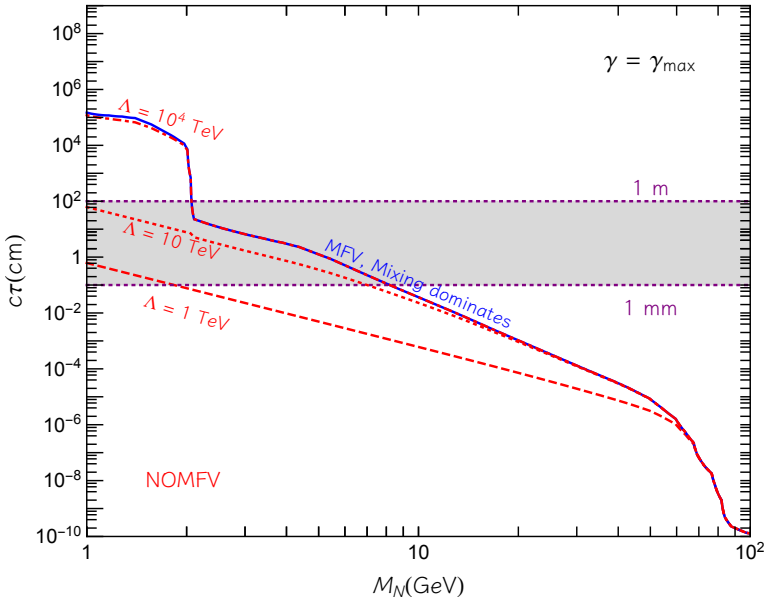

Figure 2.6: Proper decay length $c\tau$ of the sterile neutrinos as a function of their mass scale M_N for $\gamma = \gamma_{max}$ (maximum value allowed by experiments) and $\theta = 0$. The red lines show the results without assuming MFV for three different values of the new physics scale: $\Lambda = 1$ TeV (dashed line),$\Lambda = 10$ TeV (dotted line) and $\Lambda = 10^4$ TeV (dot-dashed line). The blue lines are instead drawn assuming MFV, with the decay rate driven by the mixing.

evidence is actually less stringent, nevertheless also at the level of cluster of galaxies there is evidence for the absence of large amounts of antimatter.

Therefore it really seems that there is an actual asymmetry between baryons and antibaryons in the Universe, which is quantified via the baryon to photon ratio $\eta \equiv n_B/n_\gamma = (5.7 - 6.7) \times 10^{-10}$ [77]. The tiny quark-antiquark asymmetry today would correspond to a super tiny asymmetry at early times ($t < 10^{-6}$s) [78]

$$\frac{n_q - n_{\bar{q}}}{n_q} \sim 3 \times 10^{-8}. \tag{2.27}$$

It seems then evident that we need a dynamical mechanism to generate this asymmetry, which is called Baryogenesis.

There are three basic ingredients necessary to generate a baryon asymmetry from a symmetric initial condition, the famous Sakharov conditions [79]:

- Baryon number violation: obviously there should be interactions that violate baryon number, otherwise there is no way to generate an asymmetry starting from a symmetric situation;
- C and CP violation: even in the presence of baryon number violating processes, both charge conjugation C and charge conjugation combined with parity CP, need to be violated. If this is not the case B-violating interactions will create an excess of baryon and antibaryons at the same rate, keeping the net baryon number to zero;
- Non-equilibrium condition: in thermal equilibrium the phase space density of baryon and antibaryons are identical, implying $n_b = n_{\bar{b}}$

Are these conditions satisfied in the SM?

In the SM baryon number is classically conserved. However, it is violated at the quantum level via the triangle anomaly as shown by 't Hooft [80]. This violation of B is never manifest in perturbation theory. It is associated with the vacuum structure of the spontaneously broken $SU(2)_L$ gauge theory and the transitions between different vacua of the theory. These transitions violate baryon number and lepton number by 3 units each, but with a very small tunneling amplitude

$$\mathcal{A} \sim 10^{-173} \tag{2.28}$$

However, Kumin, Rubakov and Shaposnikov realized that at high temperature such a process can actually be unsuppressed, as thermal energy makes it possible to hop over the barrier between vacua, instead of tunneling [81].

These transitions can then occur for temperature larger than $T \gtrsim 100$ GeV and are called sphalerons, a term which comes from ancient Greek and means 'ready to fall'. To be more precise, a sphaleron is a static, saddle point solution to the field equations. Notice that sphalerons processes rapidly decouple after electroweak phase transition; after that baryon and lepton number are conserved and no net charge can be generated.

These configurations provide the essential ingredient for two very well known model of Baryogenesis

- Electroweak Baryogenesis [82] where all Sakharov conditions are fullfilled in the process of sphalerons freeze out. However this model requires physics beyond the standard model to provide a first order electroweak phase transition [58, 59] and large enough CP violation [42, 43];
- Baryogenesis through Leptogenesis, where the asymmetry is generated initially in the lepton sector and then transferred to the baryon sector via sphaleron processes.

Leptogenesis is the most relevant scenario in the context of extenstions of the SM with massive neutrinos. In fact, and interestingly enough, the singlet N_R of the previous section, not only help to explain the light neutrino masses, but also provide new input to the Sakharov conditions.

The simplest and most studied scenario is one in which the sterile neutrinos are very heavy, typically with masses $M_N \gtrsim 10^8 - 10^9$GeV and decay out of equilibrium [83] to generate a lepton asymmetry, which is then converted to a baryon asymmetry through sphalerons. It is important to highlight that in this contest is crucial that the new Yukawa of the sterile neutrinos also provide the necessary source of CP violation.

A second, and more testable, scenario object of the present thesis involves instead the singlet states at the GeV scale and goes under the name of ARS mechanism, from the names of its first proponents Akhmedov-Rubakov-Smirnov [84, 85]. In this case the mechanism proceeds as follows. In the early Universe, before electroweak phase transition, the singlet neutrinos are produced in flavor eigenstates via their Yukawa couplings and then oscillate because they are, as we have seen, linear combinations of mass eigenstates. Since CP is not conserved, lepton number gets unevenly distributed between different flavours. If the temperature is high enough (larger than the mass scale of the right handed neutrinos) lepton number is globally conserved, however, and crucially, there can still be a flavoured lepton asymmetry, stored in different species. That is to say,

the initially created states (let's label them A, B and C) with lepton numbers $L_A = L_B = L_C = 0$ will evolve through oscillations into states with $L_A \neq 0, L_B \neq 0, L_C \neq 0$, but with still $L_A + L_B + L_C = 0$. Then, the sterile neutrinos communicate the lepton flavored asymmetry to ordinary neutrinos and charged leptons via Yukawa couplings. This asymmetry can be transferred to baryons at different rate for different flavors through sphalerons. For this mechanism to work it is essential that at least one of the sterile neutrinos does not equilibrate with the SM by the time of electroweak phase transition. Consequently the Yukawa coupling needs to be small enough to ensure this. Let us say that N_A has a large enough Yukawa coupling and comes to thermal equilibrium before the electroweak phase transition (t_{EW}). Then, let's say that N_B instead has a small Yukawa such that it does not equilibrate by t_{EW}. The third type N_C may or may not equilibrate, let us assume it does equilibrate. In this situation the ordinary lepton numbers L_A and L_C are communicated to ordinary leptons before t_{EW}, while L_B is not. Therefore $L_A + L_C$ transferred to the leptonic sector can then be transferred to the baryonic sector via sphalerons. Notice that it is crucial that one of the species does not equilibrate by t_{EW}, otherwise the lepton asymmetry transferred to the SM sector would vanish $L_A + L_B + L_C = 0$. We stress that for the mechanism to work at least two right handed neutrinos need to be involved, while the third one is auxiliary.

It is in my opinion quite astonishing that a model born to solve the problem of light neutrino masses can also address the question of the matter-antimatter asymmetry. It could be even more astonishing if extensions of the simplest model (consisting of at least two right handed neutrinos) can also tackle other puzzles of the SM. Indeed, given that the ARS model naturally explains both neutrino masses and matter antimatter asymmetry, it would be extremely beautiful to embed it, for example, in a larger model which tackles maybe the most important mystery of nature nowadays: dark matter. In Ref. [4] we considered motivated extensions of the ARS mechanism, and studied the conditions under which new physics does not spoil the overall picture, while providing a candidate for dark matter. We studied several possibilities, but the most appealing is the one where the accidental $B - L$ global symmetry of the SM is promoted to be a gauge symmetry. This automatically leads to the introduction of three singlet states, to avoid anomalies, which interestingly makes the type I seesaw model the minimal particle content compatible with this gauge symmetry. Of the three singlet states, the two heavier majorana fermions take part in the generation of the baryon asymmetry, while the lighest one in the keV range, is the dark matter. The production of the dark matter is not via mixing, but it is dominated by the B-L gauge boson decay. The correct DM abundance is

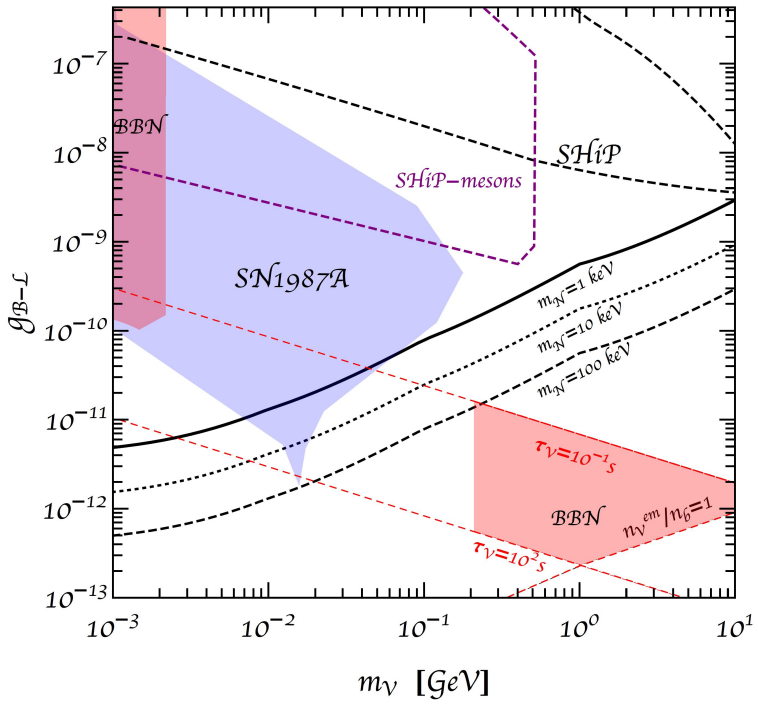

Figure 2.7: Shaded regions are presently excluded by supernova observations [86], BBN bounds estimated in [87]and the combined beam dump experiments from [88]. Unshaded regions represent the reach of SHIP from meson decay and bremsstrahlung searches [89]. The curves indicate the values of (g_{B-L}, m_V) where the lightest sterile neutrino N_1 can account for the whole dark matter for three values of the neutrino masses, $m_N = 1, 10, 100$keV in solid, dotted and dashed lines.

achieved for very small B-L gauge couplings, g_{B-L}, as shown in Fig. 2.7, via the mechanism of freeze-in (see next section for more details).

2.5 Dark Matter

Dark Matter (DM) is actually my favorite SM puzzle. It has been firmly established that almost 25% of the gravitating energy content of the universe is non-baryonic. We do not know the nature of this component nor how it interacts, but we know that it does not emit nor absorb light. Moreover it should be very weakly interacting with all the particles of the SM, because otherwise we would had already detected it!

DM induces a gravitational potential, a fact that has been established by a variety of observations at different scales. In particular we have evidence from galaxy rotation curves [90], gravitational lensing [91], and a variety of

kinematical measurements [92]. Also the observed temperature perturbations in the cosmic microwave background (CMB) point to a $\sim 26\%$ of the energy content of the Universe being in the form of non-baryonic matter.

There is a vast literature on DM and some very good reviews on the subject (see for example Ref. [93, 94, 95, 96] or the Ph.D. thesis [97]). In the following, I will briefly review the two main production mechanisms and enumerate some relevant candidates with their properties and possible detection strategies.

2.5.1 Dark Matter production

The most popular candidate for dark matter is an elusive massive particle that has remained as a relic of the Big Bang. There are two main mechanisms that can set the dark matter abundance in the universe:

- Freeze-out

This is the simplest and most common mechanism to fix the abundance of species in an expanding universe [78, 98, 99]. Imagine to have two particles A, B which interact in the early Universe, when the temperature is much larger than the two masses $T \gg m_{A,B}$. Let us assume that the two particles annihilate efficiently into each other and keep thermodynamical equilibrium. If they remain in thermal equilibrium when T drops below their masses, their abundance will be exponentially suppressed by the Boltzmann factor for a non-relativistic thermal distribution $n_{A,B} \propto e^{-m_{A,B}/T}$. This would be a disaster, as it means that essentially no massive particle can be left over as the Universe cools down. However, the Universe is expanding while cooling down. So at a certain point the interaction $AA \leftrightarrow BB$ becomes inefficient because the rate of the expansion of the Universe is faster than the rate of the considered interactions. Then the species under scrutiny are said to decouple and the abundance "freezes-out" at its value at the time at which the rate

$$n_A \langle \sigma v \rangle \sim H, \tag{2.29}$$

where n_A is the number density of the species A, $\langle \sigma v \rangle$ the thermally averaged cross section and H is the Hubble expansion rate. The particle A can be our dark matter candidate and the particle B a SM particle or any other particle belonging to the dark sector. The precise quantitative prediction of the freeze-out abundance involves the solution of Boltzmann equations, a set of differential equations that describe the evolution of the densities

for interacting species in an expanding background. The result for the relic abundance can be accurately approximated by

$$\Omega_A \equiv \frac{m_A n_{A,0}}{\rho_c} = \frac{T_0^3 (m_A/T)_{\rm fo}}{\rho_c M_{\rm Planck} \langle \sigma v \rangle_{\rm fo}}, \tag{2.30}$$

where the subscript 0 refers to quantities evaluated at the present time, "fo" to quantities evaluated at freeze-out, $M_{\rm Planck}$ is the Planck mass, and ρ_c the critical density of the universe [50]. Note that the relic abundance mainly depends on the cross section, rather than the mass. The latter in fact enters only via the ratio $(m_A/T)_{\rm fo}$, which is typically of order 20[78]. Actually this formula leads to an exciting coincidence: if one considers the correct observed relic abundance $\Omega_A = \Omega_{DM}$ and assume a typical electroweak interaction cross section, the DM particle mass turns out to be $m_A \simeq$ 100 GeV $-$ 1 TeV at or slightly above the EW scale. This is the so called WIMP miracle, where WIMP stands for Weakly Interacting Massive Particle. The interested reader can look at Ref. [100, 96] for details about specific WIMP models.

- Freeze-in

We have seen that in the freeze-out mechanism a particle starts in thermal equilibrium and then decouples when the interaction rate drops below the Hubble rate. In the freeze-in scenario, on the other hand, the particle never enters equilibrium and the initial relic abundance is negligible. Even if the interactions with the thermal bath are weak, the particle can still be produced and the correct relic abundance achieved [101, 102]. In contrast with the freeze-out case, the larger the coupling is, the larger the resulting abundance. One of the original results of this thesis, published in Ref. [4], is the study of a freeze-in scenario in the context of a minimal extension of the SM that can also explain neutrino masses and the baryon asymmetry. The non-equilibrium condition of the new states is mandatory to generate a baryon asymmetry. We explored the possibility that these new physics sectors could also explain dark matter, necessarily via freeze-in, while the prediction of the baryon asymmetry is preserved.

Recently, much interest has arisen regarding the possibility to explain dark matter with primordial black holes (PBH). These are quite peculiar dark matter candidates, as they are not "standard particles" but rather black holes formed primordially (as opposed to astrophysically from star collapse), as they must have been present before structures form to be a good dark matter candidate. PBHs have recently attracted a lot of attention at the dawn of the Gravitational Wave (GW) era. However, there are quite strong constraints on this scenario. For example, too light PBHs $M \lesssim 10^{-16} M_\odot$

would have already evaporated via Hawking-Bekenstein. Too massive PBH $M \gtrsim 10^2 M_\odot$ would accrete too much matter in the early universe and emit ionizing radiation, which is strongly constrained by CMB observations [103]. Furthermore in all the mass range between $10^{-11} - 10^2\ M_\odot$ there are a variety of constraints coming from different lensing sources [104, 105, 106, 107, 108]. For a recent review about all these constraints and many more see [109].

Many candidates have been proposed and the most popular ones are those naturally capable of resolving additional fundamental problems at the forefront of particle physics. This is the case for right-handed neutrinos at the keV scale and axions, which I have been investigating during my Ph.D. and I describe in the following.

2.5.2 Sterile Neutrino Dark Matter

We have seen that an extension of the SM with right-handed singlet fermions, or sterile neutrinos, nicely explains the light neutrino masses and the baryon asymmetry. While just two right-handed neutrinos at the GeV scale are needed in order to explain the measured neutrino mass differences and can account for the baryon asymmetry, the introduction of a third species is also appealing, as it could explain that the lightest neutrino is massive, and provide a DM candidate. Furthermore, in this case, the number of right-handed neutrinos is equal to the number of SM generations, as would be necessary for example in a left-right symmetric embedding of the SM at high energy scales [62]. This is why a sterile neutrino with a mass around the keV scale has attracted a lot of interest, since it could be a viable and appealing DM candidate [85, 110]. As we have seen, a sterile neutrino mixes with ordinary active neutrinos and can be produced in the early Universe through mixing, this is referred to as Dodelson-Widrow mechanism [111, 112, 113, 114], via resonantly enhanced oscillations in presence of a primordial lepton asymmetry [115] or through the decay of heavy particles [116, 117, 118, 119, 4]. In this thesis, in Ref. [4], we have explored a model with a new $U(1)_{B-L}$ gauge symmetry, where the presence of three sterile neutrinos is required for anomaly cancellation. We showed that in this model the two heavier Majorana fermions take part in the generation of the baryon asymmetry, while the lightest one, in the keV range, can be produced through freeze-in and explain the dark matter abundance. In this scenario the keV sterile neutrino can decay at loop level to a light neutrino and a photon $N_1 \to \nu_L \gamma$, with a peculiar signature given by an X-ray line at energy $M_{N_1}/2$, but with a rate that can be small enough to evade the strong X-ray constraints. We will comment more on this in 2.5.4.4, highlighting in particular the innovative contributions to the problem of Ref. [6].

2.5.3 Axion Dark Matter

Another good dark matter candidate that we have explored in this thesis is the axion, a pseudo Goldstone boson which inherently appears in the Peccei-Quinn solution to the strong CP problem. In Sec. 1.4 we have already introduced the strong CP problem. An elegant solution to this puzzle was formulated by Peccei and Quinn, with the so called Peccei-Quinn mechanism [120, 121]. The idea is very simple: one adds to the SM a new quark χ, with left and right-handed components in the fundamental representation of $SU(3)_c$. There is also a new complex scalar, σ. The new degrees of freedom: χ_L, χ_R and σ have charges $1/2$, $-1/2$ and 1 under a new global $U(1)$ symmetry, the Peccei-Quinn (PQ) symmetry, which allows the coupling:

$$\bar{\chi}_L \sigma \chi_R + h.c., \tag{2.31}$$

The PQ symmetry is spontaneously broken by the scalar potential and σ gets an expectation value, s, giving a mass to the new quarks, which needs to be heavy enough to evade experimental constraints on searches for coloured heavy quarks. The scalar σ can then be parametrized as

$$\sigma(x) = \frac{1}{\sqrt{2}}\Big(s + \eta(x)\Big)e^{ia(x)/s}. \tag{2.32}$$

The scalar potential is independent of the field $a(x)$. A chiral rotation makes it disappear from the term eq. (2.31). However, the chiral anomaly implies that it reappears in the action as

$$\delta S = \int d^4x \frac{a(x)}{s} \frac{g^2}{16\pi^2} \mathrm{Tr} G_{\mu\nu} \tilde{G}^{\mu\nu}, \tag{2.33}$$

shifting the $\bar{\theta}$ parameter, that is to say the latter becomes a dynamical variable

$$\frac{a(x)}{s} + \bar{\theta}, \tag{2.34}$$

rather than just a numerical parameter. Now the small observed value is just the vacuum expectation value of a field, we have found a dynamical reason for the smallness of a parameter, and as usual this was related to another secret symmetry of the theory. The field $a(x)$ is called the axion, the Goldstone boson of the PQ symmetry which then acquires a mass due to non-perturbative QCD effects.

If the mass of the axion is $\lesssim 20$ eV, one can check (evaluating its lifetime $\tau_a \propto 1/m_a^5$) that it is stable on cosmological timescales and can contribute substantially to the current fraction of energy density in the Universe stored in the form of dark matter. In recent years an increasing amount of attention has shifted toward searching for axion dark matter. Many of these searches,

although certainly not all, rely on the axion coupling to photons. Indeed the axion has a coupling of the type

$$\mathcal{L} \supset -\frac{1}{4} g_{a\gamma\gamma} a F_{\mu\nu} \tilde{F}^{\mu\nu} \tag{2.35}$$

where $F_{\mu\nu}$ is the electromagnetic field strength, $\tilde{F}^{\mu\nu}$ its dual and $g_{a\gamma\gamma}$ an effective axion-photon coupling. If the extra quarks are not charged under electromagnetism then this coupling could in principle vanish. However, all the axion must couple to quarks, either the ones of the SM or some other heavy species.

2.5.3.1 Axion vacuum misalignment

The main production mechanism for axions in the early Universe is called the vacuum misalignment mechanism [122, 123, 124], a largely model-independent, non thermal, production process.

One should consider the evolution of the axion field in an expanding universe, ignoring all the couplings with SM particles and considering only gravity. First of all we can write the Lagrangian as

$$\mathcal{L} = \frac{1}{2} \partial_\mu a \partial^\mu a - V(a), \tag{2.36}$$

where the potential $V(a)$ is generated by QCD non-perturbative effects and reads

$$V(a) = m_a^2 f_a^2 \left(1 - \cos\left(\frac{a}{f_a}\right)\right). \tag{2.37}$$

Note that the potential is a periodic function of the dimensionless combination $a/f_a \equiv \theta$. In Eq. 2.37 f_a is the axion decay constant, which is equal to sN, up to a model dependent QCD anomaly coefficient; m_a instead is the mass of the QCD axion

$$m_a \simeq m_\pi \frac{f_\pi}{f_a}, \tag{2.38}$$

where m_π, f_π are the pion mass and decay constant respectively. The Lagrangian in terms of the new adimensional field θ becomes

$$\mathcal{L} = f_a^2 \left(\frac{1}{2} \partial_\mu \theta \partial^\mu \theta - m_a^2 (1 - \cos\theta)\right). \tag{2.39}$$

The equation governing the dynamics of θ are then easily derived by the principle of minimal action and is

$$\ddot{\theta} + 3H\dot{\theta} - \frac{1}{a^2(t)} \nabla^2 \theta + \frac{dV}{d\theta} = 0, \tag{2.40}$$

where $a(t)$ is the scale factor of our expanding universe[1] and $H \equiv \frac{\dot{a}}{a}$ is the Hubble rate, which quantifies how fast is the expansion of the universe. Neglecting the spatial gradient (which is also equivalent to focus on the zero mode) and working for small θ

$$\ddot{\theta} + 3H\dot{\theta} + m_a^2\theta = 0, \tag{2.41}$$

where the axion mass is actually a time dependent quantity, as it varies with the temperature $m_a \equiv m_a(T)$. At high temperatures QCD is deconfined and the non-perturbative effects are strongly suppressed, and therefore one can neglect the axion mass and is left with the simple equation

$$\ddot{\theta} + 3H\dot{\theta} = 0, \tag{2.42}$$

which basically tells us that the axion field is frozen to its initial value θ_I. Later on, however, the axion mass term starts to dominate over the Hubble friction. This happens roughly when the two terms in the equation of motion become of the same order

$$3H(t_{osc}) = m_a(t_{osc}). \tag{2.43}$$

At this point the equation is the one of a damped oscillator with frequency m_a and the energy density can be shown to scale as $\rho_a \propto a^{-3}$. This is the same behavior as ordinary matter, and the reason why the axion turns out to be a good dark matter candidate. In particular the energy density can be written as

$$\rho_a(t) \propto \rho_a(t_{osc})\Big(a_{osc}/a(t)\Big)^3, \tag{2.44}$$

where $\rho_a(t_{osc})$ is the axion density at the time when it starts to oscillate, while a_{osc} is the scale factor at that time. Furthermore, up to the beginning of oscillation the axion field is approximately constant and takes the value θ_I (ie. misaligned with the true vacuum at zero). The energy density is then also approximately constant and given by

$$\rho(t_{osc}) \simeq \frac{1}{2} m_a(T_{osc})^2\theta_I^2. \tag{2.45}$$

The conclusion is neat and important: the energy density is fixed by the initial value of the axion vacuum misalignment and the mass. The precise expression for the relic density today depends on whether PQ symmetry is broken before or after inflation. After PQ symmetry breaking, the axion field can take some random value in the range $[-\pi, \pi]$ in causally disconnected regions of the universe. If the breaking happens before inflation

[1] The notation is a little bit unfortunate, as the axion field and the scale factor are indicated by the same letter. However, it should be clear from the contest when we refer to one or the other

(pre-inflationary scenario), one of these causal disconnected region will blow up becoming our whole visible universe: in this scenario the initial value of the axion field is everywhere the same and fixed to some random value. On the other hand, if PQ symmetry is broken after inflation (post-inflationary scenario), different patches of our universe will have different values of θ_I. In this case the initial angle entering the determination of dark matter relic abundance will be an averaged one: $\sqrt{\langle\theta_I^2\rangle} = \pi/\sqrt{3}$.

Axion DM is a fascinating and hot topic, the interested reader may want to look at some excellent reviews of the subject [125, 126].

2.5.4 Dark Matter Searches

Testing any of these dark matter hypothesis involves different strategies. Here I briefly discuss the different types of dark matter searches, focusing on my own contribution to the field.

2.5.4.1 Direct Searches

In direct searches, dark matter is searched by the final state of its possible interaction with a detector on Earth. Indeed as we live in a dark matter halo with a density estimated to be

$$\rho_{DM}^{local} \simeq 0.3\text{GeV/cm}^3, \tag{2.46}$$

some of these particles will pass through Earth with a certain rate. One can then build a large enough detector, capable of observing the scattering of a dark matter particle off the electrons or nucleons of the specific target material. The expected signal is of course extremely subtle and to minimize cosmic and radioactive backgrounds usually such detectors are located underground. The idea of direct detection was born in a paper written by the Field Medallist Edward Witten [127].

The basic physics can be identified by studying the kinematics of the scattering dark matter particle on a nucleus. Typically the nucleus can be considered at rest in these experiments (the thermal energy is very low compared to the mass of the particles in the material), while the dark matter particle is non-relativistic. Let us call the dark matter candidate χ; it will enter the detector with an energy and a momentum given by

$$E_i = \frac{|\vec{p}|^2}{2m_\chi}, \ \vec{p} = m_\chi \vec{v}, \tag{2.47}$$

and the final energy will be given instead by

$$E_f = \frac{(\vec{p} - \vec{q})^2}{2m_\chi} + \frac{\vec{q}^2}{2m_N}, \tag{2.48}$$

where m_N is the mass of the nucleus and $\vec{q}$ is the momentum transfer. The maximum momentum transfer and the corresponding maximum recoil energy will be

$$|\vec{q}|_{max} = 2\mu_{\chi N} v, \tag{2.49}$$

$$|E|_R^{max} = \frac{|\vec{q}|_{max}^2}{2m_N} = \frac{2m_\chi^2 v^2}{m_N}, \tag{2.50}$$

where v is the typical dark matter velocity and $\mu_{\chi N} \equiv \frac{m_\chi m_N}{m_\chi + m_N}$ is the reduced mass. The lower the mass, the lower the recoil energy, which will then be harder to detect. On the other hand, in recent years increasing attention has been given to the study of models of dark matter with masses below the GeV, whose search requires new ideas and detection techniques [128, 129, 130, 131, 132, 133, 134, 135, 136, 137, 138, 139, 140, 141, 142], for a review see e.g. [143, 144, 93]. In particular, the mass range between the keV and the GeV is usually referred to as *light-DM* range. A promising proposal to explore this range is that of employing superfluid 4-He [145, 146, 147, 148] detectors, whose properties are particularly amenable for the search of dark matter as light as the keV, via the detection of phonons, gapless excitations of the superfluid. In Ref. [9, 10] we studied the potential of detecting dark matter particles with masses as low as few keVs. A novel Effective Field Theory (EFT) approach was employed to model the interactions between dark matter and 4-He [149, 150].

2.5.4.2 Indirect searches

Indirect searches for DM are based on the observation of its effects in astrophysical and/or cosmological phenomena. The most employed strategy consists of looking for the radiation produced in DM annihilations or decay in different environments or epochs of the universe. In the case of decay the flux of radiation will be proportional to the number density of the dark matter source, while in the case of annihilation it will be proportional to the square of the number density.

In this thesis, I will present two original works on indirect detection focussed on probing both a keV sterile neutrino and axion dark matter particle, using radio observations and X-rays, that we briefly summarize in the following.

2.5.4.3 Detecting the Stimulated Decay of Axions at Radio Frequencies

In the recent years a huge effort has been dedicated to the search of axion dark matter. In most of the cases the detection technique relies on the axion-photon coupling $g_{a\gamma\gamma}$. Of particular importance here is the notion that one may be able to exploit the large number density of axions in astrophysical environments to indirectly infer their existence through the detection of low-energy photons. In fact, there have been various attempts to use radio telescopes to detect axion dark matter [151, 152, 153], most of which have focused on axion-photon resonant conversion. The difficulty with resonant searches is that they rely on a comprehensive understanding of highly uncertain astrophysical environments, such as neutron stars magnetosphere or extra-galactic magnetic fields [154]. In this thesis, in Refs. [3, 5], we studied the potential of searching instead for axion decay, a signal with much less astrophysical uncertainties. The rate of decay for an axion like particle, for which the effective coupling to photon and the mass are unrelated, is given by

$$\Gamma_{a\to\gamma\gamma} = \frac{m_a^3 g_{a\gamma\gamma}^2}{64\pi}. \tag{2.51}$$

Specifically we focused on radio searches, with particular attention to an important future mission, SKA [155]. Of course, looking at a given frequency corresponds to looking at a given axion mass: when decaying, an axion of mass m_a will produce two photons each with a frequency $\nu = m_a/4\pi$. Therefore, we calculated the flux of photons from the decay of axion dark matter in different environments and compared it with telescope sensitivities. We explored a variety of astrophysical objects such as dwarf spheroidal galaxies, the galactic center, as well as galaxy clusters. In particular we highlighted that for ALPs with masses below meV, the stimulated decay arising from the presence of ambient photons results in a large enhancement of the decay rate, especially in environments with large radio emission like the galactic center. Once the axion mass and the coupling to photons are fixed, the main uncertainty comes from the dark matter distribution in the structure under consideration. Indeed, the effect of stimulated emission can be well determined since the distribution of ambient photons can be confidently derived from continuum radio measurements. This is different from the possible signal coming from photon-axion conversion in strong magnetic fields around stars, which is potentially more promising but suffers from larger uncertainties associated with the poorly known astrophysics. In conclusion, we have showed that with near-future radio observations by SKA, it will be possible to increase sensitivity to the axion-photon coupling by nearly one order of magnitude with respect to the present constraints, as shown in Fig 2.8.

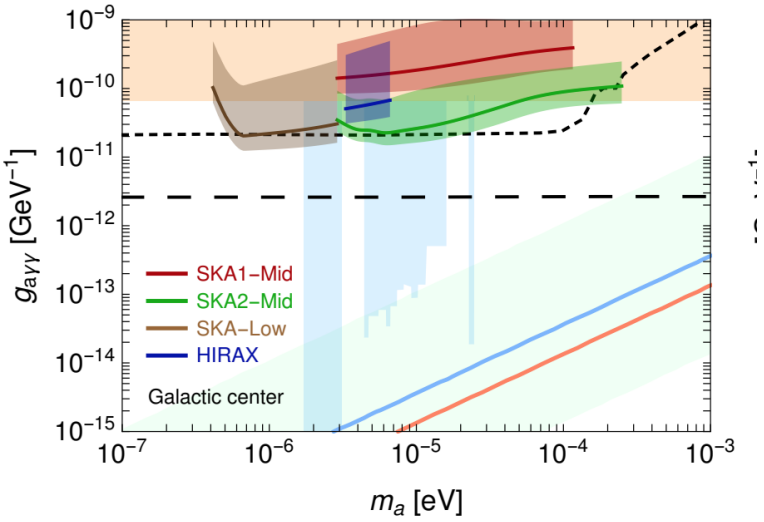

Figure 2.8: Projected sensitivities for the Galactic Center. The green, red and brown bands correspond to different phases and configurations of SKA [155]. The blue band corresponds instead to a different telescope, with a larger field of view, the interferometer HIRAX [156]. Results are displayed alongside current bounds from haloscopes [157, 158](light blue) and helioscopes [159](orange), projected bounds from ALPS-II [160] (black, short dashed) and IAXO [161, 162] (black, long dashed), and benchmark QCD axion models [163, 125](light green band, blue line, orange line).

2.5.4.4 Searching for Sterile Neutrino with X-ray Intensity Mapping

On a similar line, but regarding instead the keV sterile neutrino dark matter hypothesis, we explored in Ref. [6] a possible experimental technique to detect the X-ray radiation coming from the radiative decay of a sterile neutrinos ν_s. As we already stated, an important decay channel for a sterile neutrino is the radiative decay into a light active neutrino and a photon $N_1 \to \gamma\nu$, occurring with a rate [168, 169]:

$$\Gamma_S \equiv \Gamma_{\nu_s \to \nu\gamma} \sim (7.2\ 10^{29})^{-1} \left(\frac{\sin^2 2\theta}{10^{-8}}\right) \left(\frac{m_S}{1\,\mathrm{keV}}\right)^5 \mathrm{s}^{-1}, \tag{2.52}$$

where θ is the mixing angle between active and sterile neutrinos, and m_S is the mass of the latter. Therefore a smoking gun signature for sterile neutrino DM would be to detect a monoenergetic photon from the above process. The cosmological X-ray emission associated to this process is then composed by a collection of lines at different energies, corresponding to different redshifts. Constraints on the sterile-active neutrino mixing have been set from the non-observation of such decay line from different objects, including dwarf-spheroidal galaxies, clusters of galaxies, the Milky Way and the X-ray background (again see, e.g., reviews in Refs. [170, 164, 110] and references therein).

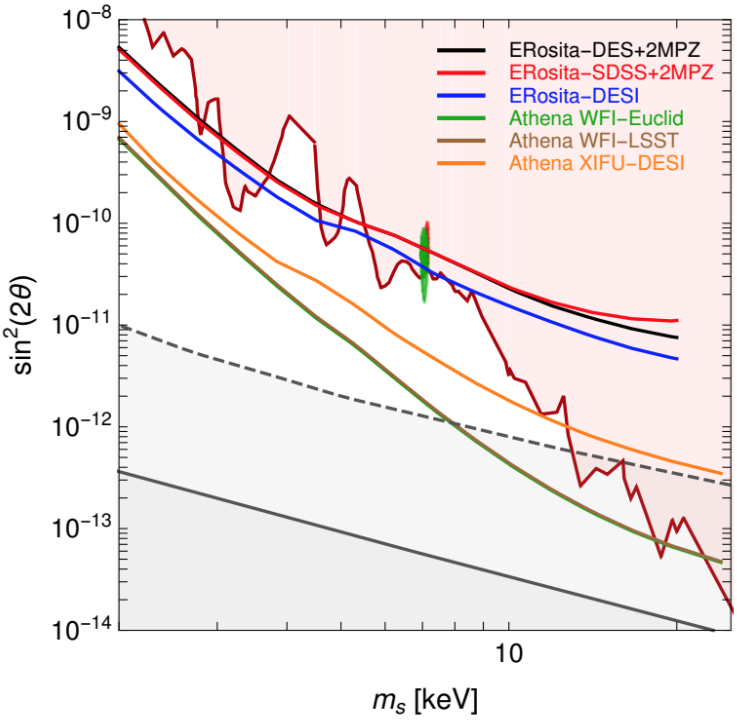

Figure 2.9: Projected 95% C.L. bounds for the different cross-correlation analyses from different catalogs. The plot presents the results in the sterile mixing vs mass plane. The light red region is excluded by current X-ray observations [164]. The red and green contours are the $2-\sigma$ regions for the 3.55 keV line excess respectively from the MOS stacked clusters [165] and M31 [166]. For the case of resonant production, the solid (dashed) gray line shows where sterile neutrino accounts for all the DM for a lepton asymmetry $L = 7 \cdot 10^{-5}$ ($L = 2.5 \cdot 10^{-3}$, the maximum value allowed by BBN [167]). Below these lines sterile neutrino is a subdominant DM component (for these choices of L and considering resonant production only).

In this thesis, Ref. [6], we used a different approach, following [171], we cross-correlated such emission lines with catalogs of galaxies tracing the dark matter distribution at different redshifts. The idea is simple: galaxies are good tracers of the dark matter density in the universe; at the same time the dark matter can emit light if it decays to photons (at different frequencies depending on its mass). Therefore it seems natural to look for correlation between these two quantities, an electromagnetic signal and the galaxy distribution. In Fig. 2.9 we show our discovery/constraints prospects for the sterile neutrino mixing angle θ. We performed a cross-correlation study in the X-ray band for the mission eROSITA [172], presently operating, and the next-generation X-ray telescope Athena [173]. We also combined each of the two with various galaxy catalogs [174, 175]. Details of the analysis can be found in Ref. [6].

Chapter 3

Resumen de Tesis

3.1 Introducción

El Modelo Estándar (SM) [21, 22, 23, 24, 25, 26] de partículas es una teoría hermosa y extensamente contrastada. De hecho, sus éxitos son innumerables y algunas de sus predicciones, como el momento magnético anómalo de los electrones, se han confirmado con una precisión de una parte en 10^{10} (!). Sin embargo, y por suerte para mi doctorado, todavía hay preguntas abiertas que no se explican dentro del SM y requieren probablemente una dinámica subyacente o nueva física más allá del SM (BSM).

Esta tesis explora, desde un punto de vista fenomenológico, algunas de las posibles extensiones del SM que permiten las preguntas abiertas en física fundamental:

- El origen de las masas de los neutrinos
- El origen de la asimetría entre materia y antimateria en el Universo
- El origen de la materia oscura

En este resumen, explicaremos brevemente estos tres problemas abiertos, así como las contribuciones originales planteadas en esta tesis para resolverlos, así como nuestras principales conclusiones.

3.1.1 Masas de los neutrinos

Uno de los resultados más importantes en tiempos recientes en física de partículas es el descubrimiento de las masas y mezclas de los neutrinos, tras

varias décadas de experimentos con neutrinos cósmicos y haces producidos en aceleradores. Este descubrimiento ha dado lugar al premio Nobel en 2002 a los pioneros en la detección de neutrinos cósmicos (Prof. R.Davis and Prof. M. Koshiba), y en 2015 a los experimentos que obtuvieron los primeros resultados concluyentes, SuperKamiokande y SNO (Prof. Kajita and Prof. A. McDonald).

Es fácil extender el SM para incorporar neutrinos masivos. Basta con hipotetizar la existencia de nuevos campos singletes, ν_{Ri}, es decir sin carga electrodébil ni fuerte, de forma que un acoplamiento del tipo Yukawa entre los campos: doblete leptónicos, Higgs y singlete es posible:

$$Y^{\nu}_{ij}\bar{L}_{Li}\phi\nu_{Rj} + h.c., \tag{3.1}$$

donde Y_ν es una matriz genérica que mezcla las generaciones of familias. La ruptura espontánea de simetría implica que este término contiene una masa de Dirac para los neutrinos de la forma:

$$m_\nu = Y_\nu \frac{v}{\sqrt{2}}, \tag{3.2}$$

en completa analogía con los quarks y los leptones cargados.

Los neutrinos que se acoplan a los leptones e, μ, τ y que denotamos por $\nu_{e,\mu,\tau}$ son los estados de sabor no son en general los estados con masa bien definida, $\nu_{1,2,3}$, sino una combinación unitaria de estos:

$$\begin{pmatrix}\nu_e\\ \nu_\mu\\ \nu_\tau\end{pmatrix} = U_{PMNS}(\theta_{12},\theta_{13},\theta_{23},\phi)\begin{pmatrix}\nu_1\\ \nu_2\\ \nu_3\end{pmatrix}. \tag{3.3}$$

La matriz de mezcla $U_{PMNS}(\theta_{12},\theta_{13},\theta_{23},\delta)$ es la famosa matriz de mezcla de Pontecorvo-Maki-Nakagawa-Sakata(PMNS), análoga a la matriz de CKM en el sector quark. Como esta última se puede parametrizar en términos de tres ángulos de mezcla, θ_{ij}, y una fase, δ, que puede implicar la violación de la simetría CP si es distinta de 0 o π. La parametrización convencional de la matriz PMNS es

$$U_{\rm PMNS} = \begin{pmatrix}1 & 0 & 0\\ 0 & c_{23} & s_{23}\\ 0 & -s_{23} & c_{23}\end{pmatrix}\begin{pmatrix}c_{13} & 0 & s_{13}e^{-i\delta}\\ 0 & 1 & 0\\ -s_{13}e^{i\delta} & 0 & c_{13}\end{pmatrix}\begin{pmatrix}c_{12} & s_{12} & 0\\ -s_{12} & c_{12} & 0\\ 0 & 0 & 1\end{pmatrix} \tag{3.4}$$

donde $\theta_{ij} \in [0, \pi/2]$ y $\delta \in [0, 2\pi]$.

Las diminutas diferencias de masas entre los neutrinos se han medido gracias al fenómento de interferencia cuántica denominado, *oscilación de neutrinos*. Los neutrinos producidos en un proceso electrodébil en combinación con un electrón, muón o leptón τ, son creados en estados de sabor.

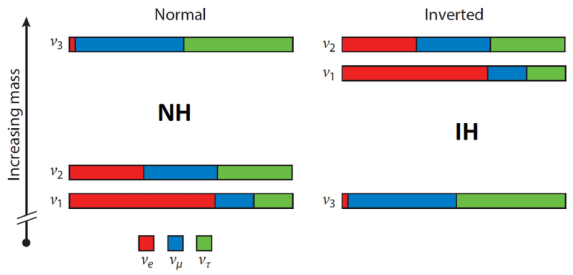

Figure 3.1: Normal and inverted ordering for the neutrinos mass spectrum.

Sin embargo, los neutrinos interaccionan tan débilmente que pueden mantener la coherencia cuántica en distancias de cientos de km. Los distintos estados de masa evolucionan en el espacio-tiempo de forma independiente con un factor de fase que depende de las masas de los neutrinos. Cuando este estado coherente alcanza el dectector a una cierta distancia, la superposición de estos estados de masa se ha visto modificada de forma que cuando el neutrino interacciona de nuevo a través de una interacción electrodébil, un sabor distinto del original puede ser observado. La probabilidad de que un neutrino ultrarelativista con momento p, producido en conjunción con un leptón de sabor α, sea detectado con sabor β viene dado por una función oscilatoria como función de la distancia entre la fuente y el detector:

$$P(\nu_\alpha \to \nu_\beta) = \sum_{ij} U^*_{\alpha i} U_{\beta i} U_{\alpha j} U^*_{\beta j} \exp\left(- i \frac{\Delta m^2_{ji} L}{2|p|} \right). \tag{3.5}$$

Es por tanto una superposición de ondas con longitud de onda determinada por las diferencias de masas de los neutrinos, $\Delta m^2_{ij} \equiv m^2_j - m^2_i$, y amplitudes que dependen de los elementos de matriz de la PMNS, $U_{\alpha i}$.

Estas transiciones de sabor de los neutrinos han sido medidas en varios experimentos, algunos que han empleado fuentes naturales de neutrinos como los provinientes del sol o de las capas altas de la atmósfera, así como en experimentos terrestres con haces de neutrinos de reactores nucleares y aceleradores de partículas. Todas estas medidas se pueden explicar en el contexto de la mezcla de tres neutrinos, en términos por tanto de dos diferencias de masas independientes y tres ángulos de mezcla. El resultado de análisis globales de datos en este contexto ha permitido obtener estos parámetros con gran precisión [44, 45, 46]:

Best fit parameters [45]		
	Normal Ordering	Inverted Ordering
$\sin^2\theta_{12}$	$0.310^{+0.013}_{-0.012}$	$0.310^{+0.013}_{-0.012}$
θ_{12}	$33.82^{0.78}_{-0.76}$	$33.82^{0.78}_{-0.76}$
$\sin^2\theta_{23}$	$0.580^{+0.017}_{-0.021}$	$0.584^{+0.016}_{-0.020}$
θ_{23}	$49.6^{1.0}_{-1.2}$	$49.8^{+1.0}_{-1.1}$
$\sin^2\theta_{13}$	$0.02241^{+0.00065}_{-0.00065}$	$0.02264^{+0.00066}_{-0.00066}$
θ_{13}	$8.61^{0.13}_{-0.13}$	$8.65^{+0.13}_{-0.13}$
δ_{CP}	215^{40}_{29}	284^{+27}_{-29}
$\frac{\Delta m^2_{21}}{10^{-5}eV^2}$	$7.39^{0.21}_{-0.20}$	$7.39^{0.21}_{-0.20}$
$\frac{\Delta m^2_{3l}}{10^{-3}eV^2}$	$2.525^{0.033}_{-0.032}$	$-2.512^{0.034}_{-0.032}$

Estos experimentos no nos han permitido aún determinar cual es el ordenamiento de estos estados, mostrado en la Fig. 3.1. Si los dos estados más degenerados son los más ligeros hablamos de un orden o jerarquía normal (NH) y si son los más pesados hablamos de un orden or jerarquía inverso (IH). Los ángulos de mezcla han sido medidos con gran precisión, aunque permanece una degeneración de octante para el ángulo más cercano a ser máximo, $\theta_{23} \simeq \pi/4$. Aunque existe un indicio a 3σ de que $\delta \neq 0, \pi$ y por tanto que habría una nueva violación de CP en el SM, este indicio ha de confirmarse con un mayor nivel de confianza.

Por otra parte, las oscilaciones de neutrinos no permiten medir la escala absoluta de masas, sólo miden diferencias. Los experimentos más sensibles a la masa de los neutrinos en el laboratorio son los que miden con precisión el espectro de la desintegración beta del tritio. El limite más preciso ha sido recientemente obtenido por el experimento Katrin [49]

$$m_{ee} < 1.1\text{eV}. \tag{3.6}$$

Masas de los neutrinos en el rango del eV pueden tener un impacto importante en la evolución del Universo. En particular las masas de los neutrinos pueden modificar de forma significativa las perturbaciones de la radiación de fondo de microondas (CMB) así como el espectro a gran escala. Actualmente estos observables cosmológicos, en particular los obtenidos por el experimento Planck [50], implican el límite:

$$\Sigma = \sum_i m_i < 0.12, \tag{3.7}$$

en el contexto de un modelo cosmológico estándar.

La extensión mínima del SM con neutrinos masivos aquí descrita plantea un SM aún más extraño. Si el mecanismo de generación de masa es el mismo que para los quarks y leptones cargados, por qué los neutrinos tienen

masas mucho más pequeñas (ver Fig. 1.3), lo cual equivale a una enorme jerarquía en los acoplamientos de Yukawa. Además el patrón de mezcla de familias en los quarks y leptones, codificado en las matrices CKM y PMNS, es radicalmente distinto.

En esta tesis estudiaremos extensiones del SM que permiten explicar estas jerarquías.

3.1.2 Dr.Jekyll y Mr.Hyde: aka asimetría materia-antimateria

El Universo que observamos está hecho esencialmente de materia. Los rayos cósmicos del Sol indican que está compuesto de materia. También el hecho de que Neil Armstrong sobreviviera a su paseo por la Luna implica que está hecha de materia. La supervivencia de los planetas en realidad demuestra que también el sistema solar está hecho esencialmente de materia. Los rayos cósmicos también proporcionan evidencia de la existencia de antimateria en la galaxia al nivel 10^{-4} compatible con ser producida en objetos astrofísicos. En escalas más grandes, las evidencias son en realidad menos estrictas, aunque también a la escala de los cúmulos de galaxias hay evidencia de la ausencia de grandes cantidades de antimateria.

Por lo tanto, realmente parece que hay una asimetría real entre bariones y antibariones en el Universo, que se cuantifica a través de la razón entre la densidad de bariones y la entropía $Y_B = n_B/s$. En el Universo temprano, sin embargo, la materia y la antimateria estaban casi en la misma proporción, por lo que el Y_B observado hoy implicaría una pequeñísima asimetría de [78]

$$\frac{n_q - n_{\bar{q}}}{n_q} \sim 3 \times 10^{-8}. \tag{3.8}$$

Parece entonces evidente que necesitamos una explicación dinámica y convincente para esto. La generación dinámica a partir de un estado simetríco original se denomina bariogénesis. Hay tres ingredientes básicos necesarios para generar una asimetría bariónica, planteados originalmente por Sakharov [79]:

- Violación del número bariónico: obviamente debería haber interacciones que violen el número bariónico, de lo contrario no hay forma de generar una asimetría a partir de una situación simétrica;
- Violación de C y CP: incluso en presencia de procesos de violación del número bariónico, tanto la conjugación de carga C como la conjugación de carga combinada con paridad CP deben violarse, de lo

contrario las interacciones que generan B crearían un exceso de bariones y antibariones a la misma velocidad, manteniendo el número neto nulo;

- Condición de no equilibrio: en el equilibrio térmico, la densidad de bariones y antibariones es idéntica ya que viene dada por la distribución de Fermi-Dirac lo que implica $n_b = n_{\bar{b}}$

Todas las condiciones de Sakharov se cumplen en el SM. La corriente asociada al número bariónico no está conservada a nivel cuántico. Es anómala. El número leptónico, L, también lo es y sólo la combinación $B - L$ es conservada. Es decir en el SM, se puede violar la conservación de número bariónico si se viola en la misma proporción la del número leptónico. El proceso de convertir bariones en leptones es sin embargo extremadamente raro e irrelevante en vacío, pero no así a alta temperatura. Kumin, Rubakov y Shaposnikov [81] probaron que estos procesos, llamados transiciones de esfalerones, son eficientes para $T \gtrsim 100$ GeV.

En este contexto dos ideas principales se han propuesto para la generación de la asimetría bariónica:

- Bariogénesis a la escala electrodébil [81, 82]. La asimetría se genera cuando las transiciones de violan $B + L$ salen del equilibrio en la transición de fase electrodébil. El SM sin embargo no da un resultado del orden de magnitud correcto porque la transición de fase no es de primer orden [58, 59] y porque la violación de CP del SM es demasiado pequeña [42, 43];
- Bariogénesis via leptogénesis, donde primero se genera una asimetría en un sector leptónico extendido, conectado posiblemente con las masas de los neutrinos, y es transferida a los bariones por los esfalerones a $T \gg 100$GeV

3.1.3 Materia Oscura

La materia oscura es mi rompecabezas favorito. De hecho, ahora es evidente que casi 25% del contenido del universo está hecho de materia que gravita pero no es bariónica. En realidad, no sabemos mucho de su naturaleza. Sabemos con certeza que no interactúa con la luz, es decir que no emite luz, ni la absorbe, y que además debe interactuar muy débilmente con el SM, porque de lo contrario la habríamos detectado.

Por otra parte, la evidencia de sus interacciones gravitacionales es múltiple y proviene de una diversidad de fuentes, a diferentes escalas. En particu-

lar, tenemos evidencias a partir de las curvas de rotación de galaxias. [90], de las lentes gravitacionales [91], y una variedad de medidas cinemáticas [92]. Además, las observaciones de CMB implican que $\sim 26\%$ del contenido de energía del Universo está en forma de materia oscura.

El candidato más popular a la materia oscura es una partícula masiva y con interacciones débiles o ultradébiles, que permanece inerte en el Universo, como rélica del Big Bang. Hay muy buenos resúmenes del estado del campo (ver, por ejemplo, Ref. [93, 94, 95, 96]). Entre los múltiples candidatos que se han estudiado, los más interesantes son aquellos naturalmente capaces de resolver otros problemas abiertos en la física de partíÂŋculas. Es el caso, por ejemplo, de los famosos WIMPs (partículas masivas débilmente interaccionantes) que podrían formar parte de modelos supersimétricos que expliquen la jerarquía entre la escala electrodébil y la escala de Planck. Otro ejemplo, serían los neutrinos singletes dextrógiros como los que permiten dar masa a los neutrinos, y quizá explicar la asimetría bariónica. Y un candidato de gran actualidad es el axión, que resulta de extensiones del SM que permiten entender porque las interacciones fuertes no violan CP de forma dramática a través del llamado término de violación fuerte de CP. Efectivamente el Lagrangiano del SM podría contener un término de la forma

$$\bar{\theta}\frac{g_3^2}{16\pi^2}G_{\mu\nu}\tilde{G}^{\mu\nu} \tag{3.9}$$

donde g_3 es la constante de acoplamiento de interacciones fuertes y $\tilde{G}_{\mu\nu} = \frac{1}{2}\epsilon_{\mu\nu\rho\sigma}G^{\rho\sigma}$ con $G_{\mu\nu} \equiv G^I_{\mu\nu}T^I$, y donde T^I son los generadores de $SU(3)$.

Este término viola la paridad P, pero conserva la conjugación de carga C, por lo tanto, rompe la simetría CP. Este término contribuye al momento dipolar eléctrico del neutrón, que se puede medir con muchísima precisión. No se ha encontrado evidencia de este momento dipolar, y ello se traduce en un límite superior en el parámetro adimensional $\bar{\theta}$

$$\bar{\theta} < 4 \times 10^{-10}. \tag{3.10}$$

El hecho de que este ángulo $\bar{\theta}$ sea tan pequeño parece requerir una explicación adicional y esto es lo que se denomina el problema de *strong CP*. Una solución elegante fue formulada por Peccei y Quinn. La idea es muy simple, uno añade al modelo estándar un nuevo quark χ, cuyas componentes levógiras y dextrógiras tienen cargas diferentes bajo una simetría global $U(1)_{PQ}$. Además un escalar σ permite escribir una interacción tipo Yukawa y al tomar un valor esperado en el vacio, s:

$$\sigma = \frac{1}{\sqrt{2}}\Big(s + \eta\Big)e^{ia/s}, \tag{3.11}$$

rompe espontáneamente la simetría de Peccei-Quinn dando lugar al campo al axión, $a(x)$, es decir el bosón de Goldstone asociado. Se puede demostrar

fácilmente que el axión se acopla a los gluones con un término de la forma

$$\delta S = \int dx^4 \frac{a(x)}{s} \frac{g^2}{16\pi^2} TrG_{\mu\nu}\tilde{G}^{\mu\nu}, \tag{3.12}$$

y por tanto $\bar{\theta}$ se convierte en una variable dinámica

$$\frac{a(x)}{s} + \bar{\theta}. \tag{3.13}$$

El pequeño valor observado es solo el valor esperado vacío, hemos encontrado una razón dinámica para la pequeñez de un parámetro, y además un candidato a materia oscura!

Efectivamene este término genera también una masa para el axión por efectos no perturbativos de QCD, inversamente proporcional a s. Si la masa del axión es $\lesssim 20$ eV, este bosón es estable en escalas de tiempo cosmológicas y puede contribuir sustancialmente a la fracción de materia en el Universo [122, 123, 124].

Todos los modelos de materia oscura mencionados son en principio testeables mediante búsquedas directas o indirectas. En las búsquedas directas, el objetivo es la observación de la señal inducida por la dispersión de una partícula de materia oscura en un detector. Este es el método más sensible a WIMPs para masas en el rango de los 100GeV o más allá. En los modelos de interés en esta tesis, los relacionados con neutrinos masivos y los de axiones, las búsquedas indirectas son más eficaces. Por ejemplo, la desintegración de un axión de materia oscura podría producir una señal observable en radio frecuencias. La desintegración de un neutrino estéril con una masa en el rango de los keV produce una señal en rayos X.

En esta tesis he estudiado por una parte las distintas posibilidades de explicar la materia oscura en modelos de neutrinos masivos, que además predicen la asimetría bariónica.

Además he hecho contribuciones novedosas a la posibilidad de detectar materia oscura en la forma de neutrinos masivos, mediante mapas de intensidad de rayos X, y la detección de la desintegración estimulada de axiones en radiofrecuencias.

3.2 Resultados y Conclusiones

3.2.1 Modelos de masas de neutrinos y la asimetría bariónica

En la primera parte de esta tesis, que incluye las publicaciones [1, 2, 7, 4] hemos explorado varios aspectos de modelos de masas de neutrinos que se originan en una escala de nueva física, asociada a la masa de nuevas partículas con masas alrededor de la escala electrodébil y más concretamente modelos con nuevos neutrinos de Majorana, singletes bajo la simetría gauge. En este contexto, la pequeñez de las masas de los neutrinos resulta de acoplamientos de Yukawa no menores que el del electrón, por lo que estos modelos no tienen jerarquías más pronunciadas que el SM, ni tampoco requieren tuneo fino de la masa del Higgs.

En la versión más mínima, se añaden al menos dos nuevos singletes fermiónicos, N_R. El Lagrangiano más general es el del SM con los términos extra:

$$\frac{1}{2}\bar{N}_R M_N N_R^c + \bar{L}_L Y_\nu \tilde{\phi} N_R + h.c, \tag{3.14}$$

donde M_N es una matriz de masa de Majorana 2×2 y Y_ν es una matriz 3×2 que acopla los dobletes leptónicos con los nuevos grados de libertad. La ruptura de la simetría electrodébil implica una matriz de masas:

$$\frac{1}{2}(\bar{\nu}_L^c \;\; \bar{N}_R) \begin{pmatrix} 0 & m_D \\ m_D^T & M_N \end{pmatrix} \begin{pmatrix} \nu_L \\ N_R^c \end{pmatrix} \equiv \frac{1}{2}\bar{N}^c M N, \tag{3.15}$$

donde $m_D \equiv Y_\nu \frac{v}{\sqrt{2}}$ y hemos definido $N \equiv (\nu_L, N_R^c)$, donde N_R^c es el conjugado de carga del N_R. No hay contracciones de Majorana para los ν_L porque ello violaría la simetría gauge en la teoría renormalizable.

Para una familia, la diagonalización de la matriz M lleva a:

$$\begin{pmatrix} \nu_L \\ N_R^c \end{pmatrix} = \begin{pmatrix} \cos\theta & \sin\theta \\ -\sin\theta & \cos\theta \end{pmatrix} \begin{pmatrix} \nu_1 \\ \nu_2 \end{pmatrix}, \tag{3.16}$$

donde $\tan 2\theta = 2m_D/M_R$ y los autovalores son

$$m_{1,2} \simeq \frac{M_R}{2} \mp \left(\frac{M_R}{2} + \frac{m_D^2}{M_R}\right) \rightarrow m_1 \simeq \frac{m_D^2}{M_R},\; m_2 \simeq M_R, \tag{3.17}$$

Esta es la esencia del mecanismo de seesaw: This is the hearth of the see-saw mechanism: si $M_R \gg m_D$ entonces $m_1 \ll m_2 \simeq M_R$.

El resultado general para la matriz de masas ligeras en el caso de 3 familias es

$$m_\nu = -\frac{v^2}{2} Y_\nu M_R^{-1} Y_\nu^T. \tag{3.18}$$

Además de los tres neutrinos ligeros, ν_i, este modelo predice la existencia de tres neutrinos pesados de Majorana, N_h, con una matriz de masas dada aproximadamente por M_R. Estas partículas son conocidas en la literatura también como leptones neutros pesados y dan lugar a una rica fenomenología. Los estados que se acoplan por las corrientes cargadas al electrón, muón y τ son combinaciones unitarias tanto de los neutrinos ligeros como de los pesados. Por tanto los neutrinos pesados se acoplan al $W^{\pm}, Z$, con una acoplamiento controlado por la submatriz $U_{\alpha h}$.

$$\nu_\alpha = U_{\alpha i}\nu_i + U_{\alpha h}N_h, \quad \alpha = e, \mu, \tau. \tag{3.19}$$

Una parametrización conveniente y completamente general es la de Casas-Ibarra, que usa como parámetros los elementos de la matriz PMNS y las masas de los neutrinos ligeros, que son medibles:

$$U_{\alpha h} = iU_{PMNS}\sqrt{\text{diag}(m_\nu)}R^\dagger(z)\text{diag}(M_N)^{-1/2}, \tag{3.20}$$

donde R es una matriz ortogonal compleja genérica, m_ν es la matriz diagonal de los neutrinos ligeros y M_N la de los pesados.

En esta tesis nos hemos enfocado en valores de las masas de los neutrinos pesados en el rango $1GeV \lesssim M_R \lesssim 100$ GeV, que por tanto son lo suficientemente ligeros como para ser producidos en colisionadores.

3.2.1.1 La ruta *seesaw* hacia la violación CP

En nuestra primera publicación [1] estudiamos la sensitividad de futuros colisionadores leptónicos como el FCC-ee y los futuros experimentos de blanco fijo, SHiP, a estas nuevas partículas. En particular hicimos el primer estudio de las implicaciones de la medida de la razón entre las mezclas a electrón y a muón para la determinación indirecta de la violación de CP en la matriz de mezcla U_{PMNS}, en particular a las fases de Majorana. Demostramos que estos observables son muy sensibles a estas fases.

En particular consideramos el modelo más mínimo con dos singletes que da lugar a un espectro con dos neutrinos ligeros (el más ligero) sería sin masa, y dos peados casi degenerados. Adaptamos la parametrización de Casas-Ibarra a este modelo:

$$U_{\alpha h} = iU_{PMNS}\sqrt{m_\nu}P_{NO}R^\dagger(z)M_N^{-1/2}, \tag{3.21}$$

donde $R(z)$ es 2×2 que depende de un ángulo complejo, $z = \theta + i\gamma$. P_{NO} es 3×2 y dependiendo del espectro neutrinos ligeros (NH, IH) tiene la forma:

$$P_{NH} = \begin{pmatrix}\mathbf{0}\\ I\end{pmatrix}, \; P_{IH} = \begin{pmatrix}I\\ \mathbf{0}\end{pmatrix}, \tag{3.22}$$

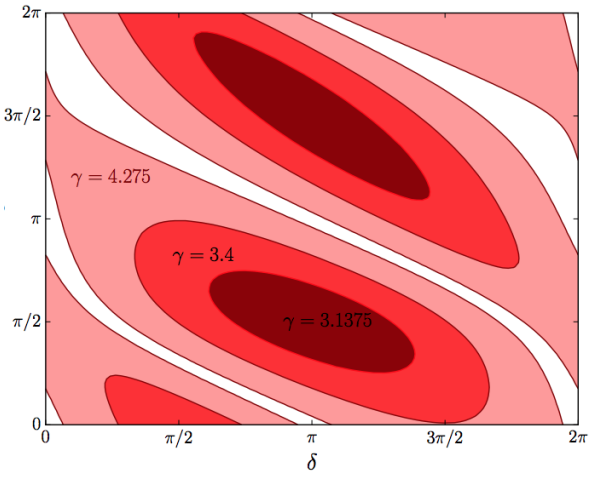

Figure 3.2: Regiones donde se puede descubrir violación de CP a 5σ CL en el plano (θ, δ) en el caso de NH [1].

donde I es la matriz identidad 2×2 y $\mathbf{0} = (0, 0)$.

El experimento SHIP puede detectar estos neutrinos pesados en la desintegración de mesones D y B [66]. Por otra parte, el FCC-ee es un colisionador e^+e^- con una energía en centro de masas de la masa del Z y puede detectar los neutrinos pesados en la desintegración del Z [67, 68]. La En Fig. 3.3) mostramos los valores posibles de los mixings para el espectro ordenado normal e invertido de los neutrinos ligeros. La anchura de las regiones depende de las fases de Majorana en la matriz PMNS. Aunque existe un ambicioso programa experimental para medir la fase de CP, δ, medir las fases de Majorana es mucho más dificil. La medida indirecta propuesta en este trabajo permitiría un descubrimiento de violación de CP a 5σ de nivel de confianza en una fracción muy significativa del espacio de parámetros, como demuestra la Fig. 3.2. La conclusión de este trabajo es que el descubrimiento de los mediadores de las masas de los neutrinos, y su patrón de mezcla acorde con las regiones de la Fig. 3.3 constituiría una evidencia muy fuerte de que estos estados son responsables de las masas de los neutrinos. La determinación de las mezclas con una precisión mejor que la anchura de esas regiones permitiría determinar las fases de violación de CP. Más detalles pueden consultarse en el artículo [1].

3.2.1.2 El portal *seesaw* en modelos testables de masas de neutrinos

La predicción mostrada en la Fig. 3.3 depende hasta cierto punto del hecho de que el modelo considerado es mínimo. En la segunda publicación,

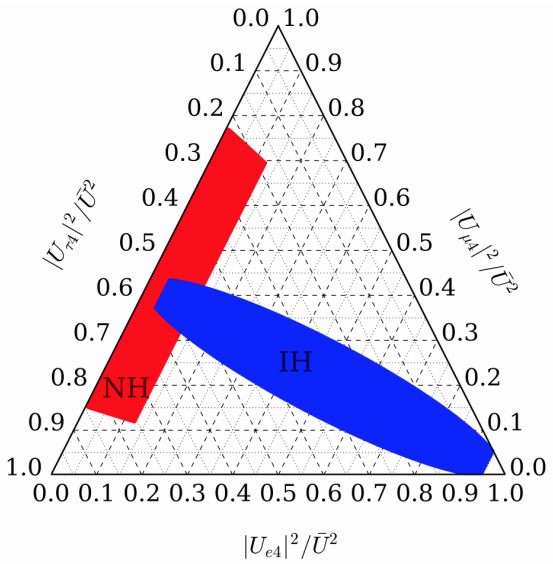

Figure 3.3: Diagrama ternario para los elementos de la matriz de mezcla, asumiendo los parámetros de la matriz PMNS dados por los ajustes globales y variando las fases de violación de CP en el rango $[0, 2\pi]$ para NH (red) y IH (blue). Esta figura es de la Ref. [2], y ha sido posteriormente usada en muchos trabajos posteriores por otros grupos.

Ref. [2], tratamos de cuantificar en que medida esta predicción sería robusta en el contexto de modelos más complejos con nueva física adicional a los singletes del modelo mínimo. Para contestar esta pregunta asumimos la presencia de nueva física a una escala, Λ, lo suficientemente separada de la escala electrodébil. En esta situación es posible parametrizar la nueva física en términos de una teoría efectiva que difiere de la estándar en el SM, es decir el SMEFT, porque incluye además los singletes pesados, N_R. En este caso, hay dos operadores de dimensión 5 con respecto al SMEFT:

$$O_{NH} = \bar{N}_R^c N_R \phi^\dagger \phi, \tag{3.23}$$

$$O_{NB} = \bar{N}_R^c \sigma^{\mu\nu} N_R B_{\mu\nu}, \tag{3.24}$$

$$O_5^W = (\phi L)^T (\phi L). \tag{3.25}$$

El último es el famoso operador de Weinberg que sólo contiene campos del SM, pero los nuevos, O_{NH} and O_{NB}, incluyen además los singletes. Esta teoría efectiva ha sido estudiada en la literatura previa en los artículos Refs. [70, 71, 72, 73]. En nuestro trabajo sin embargo, nos focalizamos en el nuevo mecanismo de producción de los neutrinos pesados en las desintegraciones del Higgs mediadas por el operador O_{NH}. Es de gran interés dado que abre una nueva estrategia de búsqueda de estos estados en el LHC. En particular, investigamos el potencial del LHC para la detección del decay del Higgs en dos neutrinos pesados que a su vez se desintegran mediante la mezcla con los ligeros, produciendo señales espectaculares de dos vértices

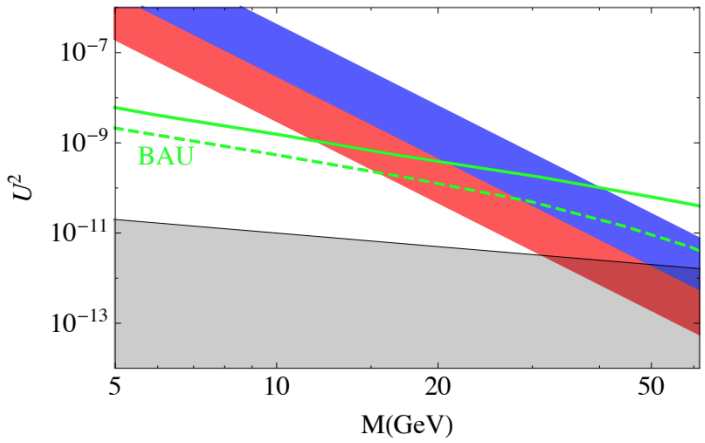

Figure 3.4: Regiones en el plano masa-mezcla M, U donde la eficiencia de selección de trazas desplazadas en el LHC supera el 10% en el detector interno de trazas (IT, banda azúl) y en la cámara de muones (MC, banda roja). La zona gris no puede explicar las masas de los neutrinos mientras que las lineas verdes corresponden a los límites al 90% CL para la predicción correcta de la simetría bariónica en este modelo para NH (linea continua) e IH (linea discontinua) de acuerdo a Ref. [74].

desplazados. Estudiamos este proceso en detalle y derivamos los límites de la Fig. 3.4. Encontramos además que una simetría leptónica aproximada podría explicar la jerarquía entre los distintos coeficientes de los operadores de $d = 5$, de forma que la pequeñez de las masas de los neutrinos serían compatibles con un coeficiente lo suficientemente grande del operador O_{NH} para observar esta rara desintegración del Higgs.

3.2.1.3 Violación Mínima de Sabor en el seesaw portal

La teoría efectiva que incluye singletes pesados responsables de las masas de los neutrinos ha sido bautizada como νSMEFT en nuestro tercer trabajo sobre este tema [7]. Cuando nos vamos a la siguiente dimensión, $d = 6$, muchos operadores nuevos aparecen con respecto al SMEFT. En este contexto, no está claro que las predicciones del estudio anterior permanezca, en particular la asunción de que la desintegración de los neutrinos pesados está dominada por la mezcla con los ligeros. En particular, el que los neutrinos pesados sean de vida media larga o no depende fuertemente de la estructura de sabor de los coeficientes de los operadores de $d = 6$. Si la desintegración fuera mediada por operadores de $d = 6$, la correlación con las masas de los neutrinos ligeros sería mucho menor.

En nuestra publicación, Ref. [7], estudiamos la νSMEFT hasta $d = 6$ bajo la hipótesis de violación mínima de sabor (MFV). Este paradigma

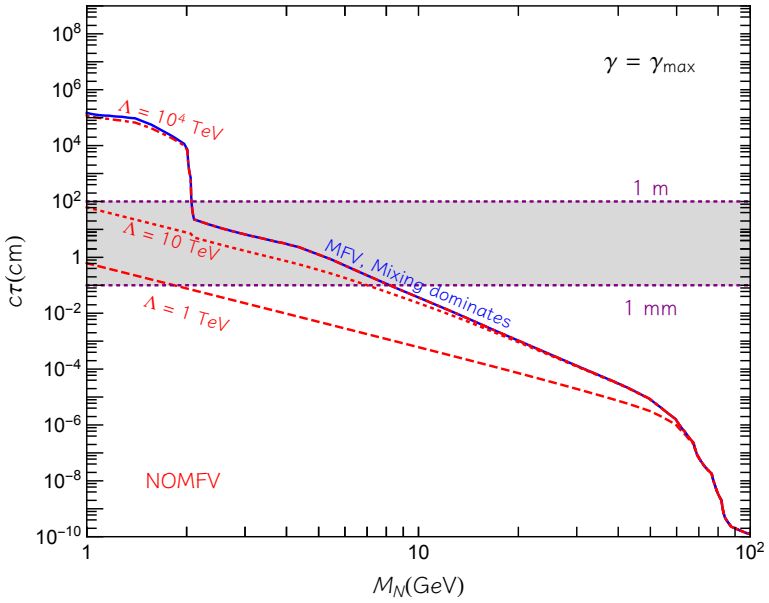

Figure 3.5: Longitud de desintegración $c\tau$ de los neutrinos estériles como función de su masa M_N para $\gamma = \gamma_{max}$ (valor máximo de este parámetro permitido experimentalmente) y $\theta = 0$. Las lineas rojas muestran los resultados sin asumir MFV para tres valores diferentes de la escala de nueva física: $\Lambda = 1$ TeV (linea discontinua),$\Lambda = 10$ TeV (linea punteada) y $\Lambda = 10^4$ TeV (linea puteada y discontinua). Las líneas azules asumen MFV, donde la razón de desintegración depende de la mezcla.

[75, 76] implica una supresión natural de las corrientes neutras que cambian sabor (FNCN) y los procesos que violan número leptónico (LNV) en el contexto de modelos de nueva física, a partir de un principio de simetría. La hipótesis asume que todos los efectos de cambio de sabor se originan en los del Langrangiano renormalizable. En nuestro trabajo, Ref. [7] , investigamos por primera vez las implicaciones fenomenológicas de esta hipotesis en el contexto del νSMEFT. Estudiamos en detalle como afecta esta hipótesis a las propiedades de las desintegraciones de los neutrinos pesados, lo cual es esencial para definir la estrategia de búsqueda. Este resultado se muestra en la Fig. 3.5.

Nuestro estudio nos ha permitido establecer la relevancia relativa de los operadores de $d = 6$, demostrando que en este escenario, el canal de producción dominante para los neutrinos pesados es la desintegración del Higgs estudiada en la sección anterior y un operador de $d = 6$ con dos neutrinos pesados que preservan número leptónico, $\mathcal{O}_{NX} = (\bar{N}_R \gamma^\mu N_R)(\bar{X}\gamma_\mu X)$ con $X = e, u, d, q, L, N$.

3.2.2 Explorando la materia oscura

El trabajo de esta tesis relativo a la materia oscura se ha centrado en dos aspectos. Por una parte, se hizo un trabajo de construcción de un modelo capaz de explicar las masas de los neutrinos, la asimetría bariónica y la materia oscura. Por otra parte, se han explorado varias estrategias no estándar para detectar materia oscura en la forma de keV neutrinos y de axiones.

3.2.2.1 Materia oscura frente a masas de neutrinos y asimetriá bariónica

Nuestro artículo [4] tuvo como objetivo explorar extensiones del modelo de masas de neutrinos presentado anteriormente, que sabemos que puede explicar la asimetrí bariónica, para además explicar la materia oscura.

La asimetría bariónica se origina a temperaturas por encima de la transición de fase electrodébil, $T_{\rm EW}$, por el mecanismo propuesto por Akhmedov, Rubakov y Smirnov [84, 85]. La fases de violación de CP en M_N y Y_ν inducen una asimetría de carga leptóncia en las distintas familias de neutrinos, que globalmente se anulan, pero que no se transfieren con igual eficiencia a los bariones, por lo que hay un número bariónico neto durante un tiempo antes de que todos los neutrinos pesados alcancen el equilibrio térmico. Es natural para los valores de masas en el rango $1-100$ GeV que esto no ocurra antes de la transición de fase electrodébil, por lo que si el número bariónico neto sobrevive hasta ese instante, posteriormente se congela porque los esfalerones dejan de ser eficientes. Encontrar un candidato a materia oscura en estos modelos es un reto, porque es necesario que al menos una familia de neutrinos pesados no alcance el equilibrio antes de $T_{\rm EW}$ y ello requiere constantes de acoplamiento con la materia oscura muy pequeñas, por lo que el mecanismo de producción no puede ser térmico. Típicamente es necesario que la partícula de la materia oscura no alcance tampoco el equilibrio térmico. Varios modelos fueron analizados en [4] y el más interesante resultó ser una extensión con una campo gauge $U(1)_{B-L}$, donde el candidato a materia oscura es un tercer neutrino pesado, con masa en el rango del keV como en el νMSM [85], pero donde la producción de este neutrino no es por mixing sino en el decay del $B-L$ gauge boson. Este resultado se muestra en la Fig. 3.6.

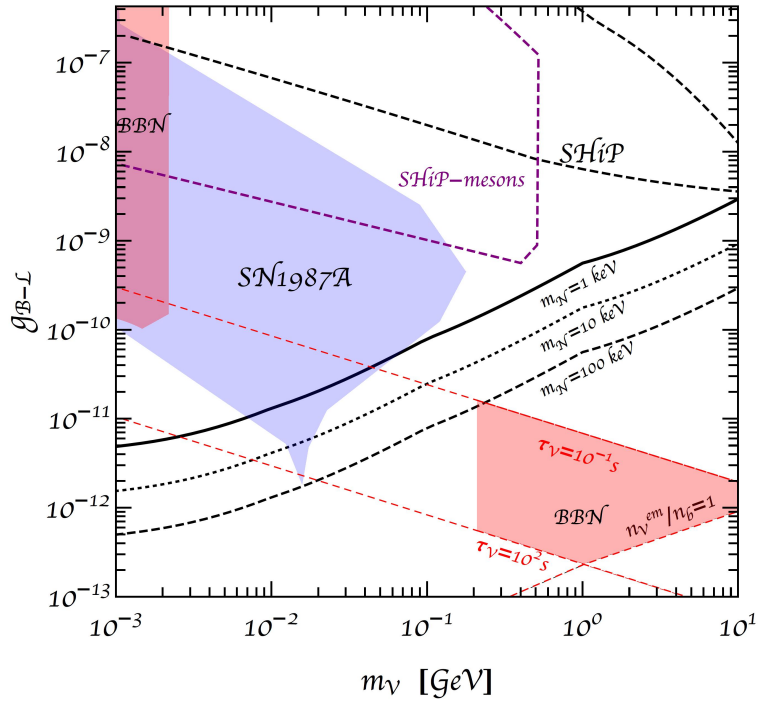

Figure 3.6: Las regiones sombreadas están actualmente excluidas por las observaciones de supernova [86], límites de BBN in [87]y beam dump experiments [88]. Las regiones no sombreadas representan el alcance de SHIP desde la descomposición del mesón y bremsstrahlung busca [89]. Las curvas indican los valores de (g_{B-L}, m_V) donde el neutrino estéril más ligero N_1 puede representar toda la materia oscura para tres valores de las masas de neutrinos, $m_N = 1, 10, 100$keV.

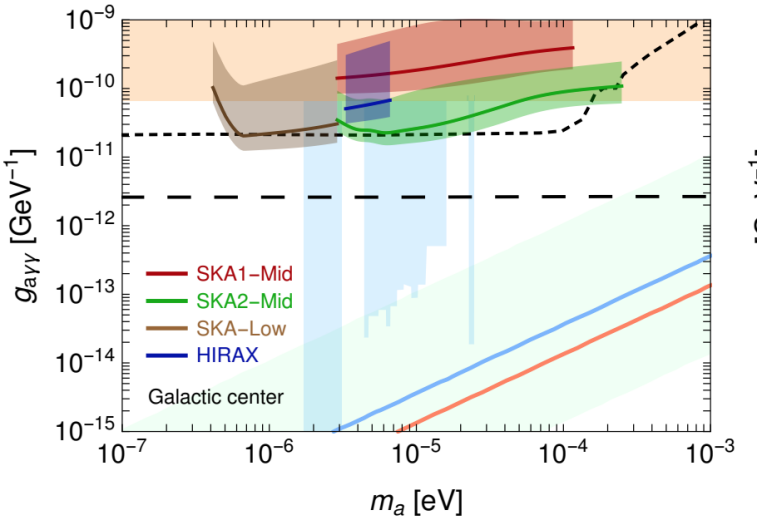

Figure 3.7: Sensibilidades proyectadas para el Centro Galáctico. Las bandas verde, roja y marrón corresponden a diferentes fases y configuraciones de [155]. La banda azul corresponde en cambio a un telescopio diferente, con un campo de visión más amplio, el interferómetro HIRAX [156]. Se muestran los resultados juntos a los límites actuales de los haloscopios [157, 158](light blue) y helioscopios [159](naranja), límites proyectados de ALPS-II [160] (negro, guión corto) y IAXO [161, 162] (negro, guión largo), y modelos de QCD axion [163, 125](banda verde claro, línea azul , línea naranja).

3.2.2.2 Detección de axiones con radiotelescopios

En los artículos Ref. [5, 3, 6] estudié posibles formas de detectar la materia oscura. Recientemente ha habido varios intentos de utilizar radiotelescopios para detectar axiones de materia oscura [151, 152, 153]; pero posteriormente se ha demostrado que, a menos que se explote una conversión resonante de axíon-fotón, la tasa de desintegración del axión en dos fotones domina a la conversión de axión-fotón en entornos astrofísicos. Una de las dificultades con las búsquedas resonantes es que dependen de las propiedades de los entornos astrofísicos muy inciertas [154]. En [3, 5] desarrollamos un enfoque alternativo, estudiando la sensitividad a su desintegración en fotones, en frecuencias de radio. Exploramos una variedad de entornos astrofísicos, como las galaxias esferoidales enanas, el centro galáctico y el halo, así como los cúmulos de galaxias. Hemos demostrado que las observaciones de radio que se esperan del experimento SKA, será posible aumentar la sensitividad al acoplamiento axión-fotón en un orden de magnitud con respecto a los límites actuales. Es interesante que el rango de parámetros del modelo que estas medidas permiten explorar coincide con el rango en que es posible explicar el mecanismo de enfriamiento no estándar observado en varios sistemas estelares. Los resultados se muestran en la Fig. 3.7.

Finalmente, en el contexto de la materia oscura de keV neutrinos, como los explorados en la sección anterior, en la publicación [6], exploramos una posible técnica experimental para detectar la radiación de rayos X proveniente de la desintegración radiativa de $N_R \to \gamma\nu$ que daría una señal monocromática en los rayos X. La emisión cosmológica de rayos X asociada a la posible desintegración radiactiva de los neutrinos estériles se compone de una colección de líneas a diferentes energías. Para una masa dada, cada línea corresponde a un desplazamiento al rojo dado. La no observación de estas líneas en distintos contextos: las galaxias esferoidales enanas, los cúmulos de galaxias, la Vía Láctea y el fondo de rayos X (ver nuevamente, por ejemplo, Refs. [170, 164, 110]), nos ha permitido derivar nuevos límites en el ángulo de mezcla del neutrino de materia oscura. Curiosamente, la detección de una línea no identificada a la energía $E \simeq 3.5$ keV ha sido objeto de un gran interés aunque aún no ha sido confirmada con suficiente nivel de confianza. En [6] correlacionamos la emisión de líneas con loscatálogos de galaxias que rastrean la distribución de la materia oscura en diferentes desplazamientos al rojo. Este resultado se muestra en la Fig. 3.8.

En resumen, en esta tesis hemos investigado las implicaciones fenomenológicas de los neutrinos pesados, la posibilidad de ampliar el modelo ARS y nuevas maneras para descubrir la materia oscura, usando distintos datos astrofísicos. Mi opinión es que en el futuro será cada vez más relevante para los físicos de partículas extraer información de los datos astrofísicos y cosmológicos.

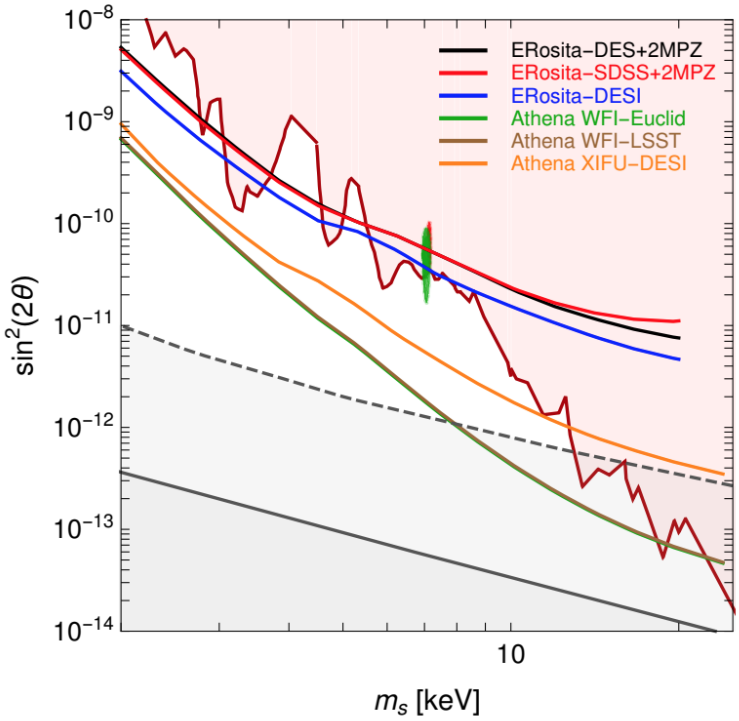

Figure 3.8: Límites proyectado 95% C.L. para los diferentes análisis de correlación cruzada de diferentes catálogos. El gráfico presenta los resultados en el plano de mezcla estéril frente a masa. La región roja clara está excluida por las observaciones actuales de rayos X [164]. Los contornos rojo y verde son las regiones $2-\sigma$ para el exceso de línea de 3.55 keV respectivamente de los grupos the MOS stacked clusters [165] y M31 [166]. Para el caso de la producción resonante, el sólido (discontinua) la línea gris muestra dónde el neutrino estéril representa todo el DM para una asimetría de leptones $L = 7 \cdot 10^{-5}$ ($L = 2.5 \cdot 10^{-3}$, el valor máximo permitido por BBN [167]). Debajo de estas líneas, el neutrino estéril es un componente de DM subdominante (para estas opciones de L y considerando solo la producción resonante).

Bibliography

[1] A. Caputo, P. Hernandez, M. Kekic, J. LÃşpez-PavÃşn and J. Salvado, *The seesaw path to leptonic CP violation*, *Eur. Phys. J.* **C77** (2017) 258, [1611.05000]. Cited on page i, 29, 30, 31, 59, 60, and 61.

[2] A. Caputo, P. Hernandez, J. Lopez-Pavon and J. Salvado, *The seesaw portal in testable models of neutrino masses*, *JHEP* **06** (2017) 112, [1704.08721]. Cited on page i, 31, 59, and 62.

[3] A. Caputo, C. P. Garay and S. J. Witte, *Looking for axion dark matter in dwarf spheroidal galaxies*, *Phys. Rev.* **D98** (2018) 083024, [1805.08780]. Cited on page i, 47, and 67.

[4] A. Caputo, P. Hernandez and N. Rius, *Leptogenesis from oscillations and dark matter*, *Eur. Phys. J.* **C79** (2019) 574, [1807.03309]. Cited on page i, 37, 40, 41, 59, and 65.

[5] A. Caputo, M. Regis, M. Taoso and S. J. Witte, *Detecting the Stimulated Decay of Axions at RadioFrequencies*, *JCAP* **1903** (2019) 027, [1811.08436]. Cited on page i, 47, and 67.

[6] A. Caputo, M. Regis and M. Taoso, *Searching for Sterile Neutrino with X-ray Intensity Mapping*, 1911.09120. Cited on page i, 41, 48, 50, 67, and 68.

[7] D. Barducci, E. Bertuzzo, A. Caputo and P. Hernandez, *Minimal flavor violation in the see-saw portal*, 2003.08391. Cited on page i, 33, 59, 63, and 64.

[8] A. Caputo, L. Sberna, M. Frias, D. Blas, P. Pani, L. Shao et al., *Constraints on millicharged dark matter and axionlike particles from timing of radio waves*, *Phys. Rev.* **D100** (2019) 063515, [1902.02695]. Cited on page ii.

[9] A. Caputo, A. Esposito and A. D. Polosa, *Sub-MeV Dark Matter and the Goldstone Modes of Superfluid Helium*, *Phys. Rev.* **D100** (2019) 116007, [1907.10635]. Cited on page ii, and 46.

[10] A. Caputo, A. Esposito, E. Geoffray, A. D. Polosa and S. Sun, *Dark Matter, Dark Photon and Superfluid He-4 from Effective Field Theory*, 1911.04511. Cited on page ii, and 46.

[11] A. Caputo, J. Zavala and D. Blas, *Binary pulsars as probes of a Galactic dark matter disk*, *Phys. Dark Univ.* **19** (2018) 1–11, [1709.03991]. Cited on page ii.

[12] A. Caputo and M. Reig, *Cosmic implications of a low-scale solution to the axion domain wall problem*, *Phys. Rev.* **D100** (2019) 063530, [1905.13116]. Cited on page ii.

[13] A. Caputo, *Radiative Axion Inflation*, *Phys. Lett.* **B797** (2019) 134824, [1902.02666]. Cited on page ii.

[14] D. Blas, A. Caputo, M. M. Ivanov and L. Sberna, *No chiral light bending by clumps of axion-like particles*, *Phys. Dark Univ.* **27** (2020) 100428, [1910.06128]. Cited on page ii.

[15] A. Caputo, L. Sberna, A. Toubiana, S. Babak, E. Barausse, S. Marsat et al., *Gravitational-wave detection and parameter estimation for accreting black-hole binaries and their electromagnetic counterpart*, 2001.03620. Cited on page ii.

[16] A. Caputo, H. Liu, S. Mishra-Sharma and J. T. Ruderman, *Dark Photon Oscillations in Our Inhomogeneous Universe*, 2002.05165. Cited on page iii.

[17] A. Caputo, H. Liu, S. Mishra-Sharma and J. T. Ruderman, *Modeling Dark Photon Oscillations in Our Inhomogeneous Universe*, 2004.06733. Cited on page iii.

[18] A. Caputo, A. J. Millar and E. Vitagliano, *Revisiting longitudinal plasmon-axion conversion in external magnetic fields*, 2005.00078. Cited on page iii.

[19] C. A. O'Hare, A. Caputo, A. J. Millar and E. Vitagliano, *Axion helioscopes as solar magnetometers*, 2006.10415. Cited on page iii.

[20] I. M. Bloch, A. Caputo, R. Essig, D. Redigolo, M. Sholapurkar and T. Volansky, *Exploring New Physics with O(keV) Electron Recoils in Direct Detection Experiments*, 2006.14521. Cited on page iii.

[21] P. W. Higgs, *Broken symmetries, massless particles and gauge fields*, *Phys. Lett.* **12** (1964) 132–133. Cited on page 1, 3, and 51.

[22] P. W. Higgs, *Broken Symmetries and the Masses of Gauge Bosons*, *Phys. Rev. Lett.* **13** (1964) 508–509. Cited on page 1, 3, and 51.

[23] S. Glashow, *Partial Symmetries of Weak Interactions*, *Nucl. Phys.* **22** (1961) 579–588. Cited on page 1, and 51.

[24] S. Weinberg, *A Model of Leptons*, *Phys. Rev. Lett.* **19** (1967) 1264–1266. Cited on page 1, and 51.

[25] A. Salam, *Weak and Electromagnetic Interactions*, *Conf. Proc. C* **680519** (1968) 367–377. Cited on page 1, and 51.

[26] F. Englert and R. Brout, *Broken Symmetry and the Mass of Gauge Vector Mesons*, *Phys. Rev. Lett.* **13** (1964) 321–323. Cited on page 1, 3, and 51.

[27] H. Watanabe, T. s. Brauner and H. Murayama, *Massive Nambu-Goldstone Bosons*, *Phys. Rev. Lett.* **111** (2013) 021601, [1303.1527]. Cited on page 2.

[28] A. Nicolis, R. Penco and R. A. Rosen, *Relativistic Fluids, Superfluids, Solids and Supersolids from a Coset Construction*, *Phys. Rev. D* **89** (2014) 045002, [1307.0517]. Cited on page 2.

[29] A. Nicolis, R. Penco, F. Piazza and R. Rattazzi, *Zoology of condensed matter: Framids, ordinary stuff, extra-ordinary stuff*, *JHEP* **06** (2015) 155, [1501.03845]. Cited on page 2.

[30] I. Low and A. V. Manohar, *Spontaneously broken space-time symmetries and Goldstone's theorem*, *Phys. Rev. Lett.* **88** (2002) 101602, [hep-th/0110285]. Cited on page 2.

[31] G. 't Hooft, *Renormalization of Massless Yang-Mills Fields*, *Nucl. Phys. B* **33** (1971) 173–199. Cited on page 3.

[32] G. 't Hooft, *Renormalizable Lagrangians for Massive Yang-Mills Fields*, *Nucl. Phys. B* **35** (1971) 167–188. Cited on page 3.

[33] R. N. Cahn, *The Eighteen arbitrary parameters of the standard model in your everyday life*, *Rev. Mod. Phys.* **68** (1996) 951–960. Cited on page 9.

[34] L. Wolfenstein, *Parametrization of the Kobayashi-Maskawa Matrix*, *Phys. Rev. Lett.* **51** (1983) 1945. Cited on page 10.

[35] M. E. Peskin and D. V. Schroeder, *An Introduction to quantum field theory*. Addison-Wesley, Reading, USA, 1995. Cited on page 11.

[36] G. C. Branco, L. Lavoura and J. P. Silva, *CP Violation*, vol. 103. 1999. Cited on page 11, and 12.

[37] C. Jarlskog, *Commutator of the Quark Mass Matrices in the Standard Electroweak Model and a Measure of Maximal CP Violation*, *Phys. Rev. Lett.* **55** (1985) 1039. Cited on page 12.

[38] J. M. Pendlebury et al., *Revised experimental upper limit on the electric dipole moment of the neutron*, *Phys. Rev. D* **92** (2015) 092003, [1509.04411]. Cited on page 12.

[39] B. Guberina and R. Peccei, *Quantum Chromodynamic Effects and CP Violation in the Kobayashi-Maskawa Model*, *Nucl. Phys. B* **163** (1980) 289–311. Cited on page 12.

[40] R. Crewther, P. Di Vecchia, G. Veneziano and E. Witten, *Chiral Estimate of the Electric Dipole Moment of the Neutron in Quantum Chromodynamics*, *Phys. Lett. B* **88** (1979) 123. Cited on page 12.

[41] J. R. Ellis and M. K. Gaillard, *Strong and Weak CP Violation*, *Nucl. Phys. B* **150** (1979) 141–162. Cited on page 12.

[42] M. Gavela, P. Hernandez, J. Orloff and O. Pene, *Standard model CP violation and baryon asymmetry*, *Mod. Phys. Lett. A* **9** (1994) 795–810, [hep-ph/9312215]. Cited on page 13, 24, 36, and 56.

[43] M. Gavela, P. Hernandez, J. Orloff, O. Pene and C. Quimbay, *Standard model CP violation and baryon asymmetry. Part 2: Finite temperature*, *Nucl. Phys. B* **430** (1994) 382–426, [hep-ph/9406289]. Cited on page 13, 24, 36, and 56.

[44] I. Esteban, M. Gonzalez-Garcia, M. Maltoni, I. Martinez-Soler and T. Schwetz, *Updated fit to three neutrino mixing: exploring the accelerator-reactor complementarity*, *JHEP* **01** (2017) 087, [1611.01514]. Cited on page 17, and 53.

[45] I. Esteban, M. Gonzalez-Garcia, A. Hernandez-Cabezudo, M. Maltoni and T. Schwetz, *Global analysis of three-flavour neutrino oscillations: synergies and tensions in the determination of θ_{23}, δ_{CP}, and the mass ordering*, *JHEP* **01** (2019) 106, [1811.05487]. Cited on page 17, 53, and 54.

[46] P. de Salas, D. Forero, C. Ternes, M. Tortola and J. Valle, *Status of neutrino oscillations 2018: 3σ hint for normal mass ordering and improved CP sensitivity*, *Phys. Lett. B* **782** (2018) 633–640, [1708.01186]. Cited on page 17, and 53.

[47] Troitsk collaboration, V. Aseev et al., *An upper limit on electron antineutrino mass from Troitsk experiment*, *Phys. Rev. D* **84** (2011) 112003, [1108.5034]. Cited on page 17.

[48] C. Kraus et al., *Final results from phase II of the Mainz neutrino mass search in tritium beta decay*, *Eur. Phys. J. C* **40** (2005) 447–468, [hep-ex/0412056]. Cited on page 17.

[49] KATRIN collaboration, A. Osipowicz et al., *KATRIN: A Next generation tritium beta decay experiment with sub-eV sensitivity for the electron neutrino mass. Letter of intent*, hep-ex/0109033. Cited on page 17, and 54.

[50] Planck collaboration, N. Aghanim et al., *Planck 2018 results. VI. Cosmological parameters*, 1807.06209. Cited on page 17, 40, and 54.

[51] G. Degrassi, S. Di Vita, J. Elias-Miro, J. R. Espinosa, G. F. Giudice, G. Isidori et al., *Higgs mass and vacuum stability in the Standard Model at NNLO*, *JHEP* **08** (2012) 098, [1205.6497]. Cited on page 18, and 19.

[52] D. Buttazzo, G. Degrassi, P. P. Giardino, G. F. Giudice, F. Sala, A. Salvio et al., *Investigating the near-criticality of the Higgs boson*, *JHEP* **12** (2013) 089, [1307.3536]. Cited on page 18.

[53] M. Sher, *Electroweak Higgs Potentials and Vacuum Stability*, *Phys. Rept.* **179** (1989) 273–418. Cited on page 18.

[54] S. R. Coleman and E. J. Weinberg, *Radiative Corrections as the Origin of Spontaneous Symmetry Breaking*, *Phys. Rev. D* **7** (1973) 1888–1910. Cited on page 18.

[55] G. Isidori, G. Ridolfi and A. Strumia, *On the metastability of the standard model vacuum*, *Nucl. Phys. B* **609** (2001) 387–409, [hep-ph/0104016]. Cited on page 18.

[56] H. Georgi, *Effective field theory*, *Ann. Rev. Nucl. Part. Sci.* **43** (1993) 209–252. Cited on page 22.

[57] J. Polchinski, *Renormalization and Effective Lagrangians*, *Nucl. Phys. B* **231** (1984) 269–295. Cited on page 22.

[58] K. Kajantie, M. Laine, K. Rummukainen and M. E. Shaposhnikov, *Is there a hot electroweak phase transition at m(H) larger or equal to m(W)?*, *Phys. Rev. Lett.* **77** (1996) 2887–2890, [hep-ph/9605288]. Cited on page 24, 36, and 56.

[59] K. Rummukainen, M. Tsypin, K. Kajantie, M. Laine and M. E. Shaposhnikov, *The Universality class of the electroweak theory*, *Nucl. Phys. B* **532** (1998) 283–314, [hep-lat/9805013]. Cited on page 24, 36, and 56.

[60] S. Weinberg, *Baryon and Lepton Nonconserving Processes*, *Phys. Rev. Lett.* **43** (1979) 1566–1570. Cited on page 25.

[61] P. Minkowski, $\mu \to e\gamma$ *at a Rate of One Out of* 10^9 *Muon Decays?*, *Phys. Lett. B* **67** (1977) 421–428. Cited on page 25.

[62] R. N. Mohapatra and G. Senjanovic, *Neutrino Mass and Spontaneous Parity Nonconservation*, *Phys. Rev. Lett.* **44** (1980) 912. Cited on page 25, and 41.

[63] S. M. Bilenky, J. Hosek and S. Petcov, *On Oscillations of Neutrinos with Dirac and Majorana Masses*, *Phys. Lett. B* **94** (1980) 495–498. Cited on page 26.

[64] J. Schechter and J. Valle, *Neutrino Masses in SU(2) x U(1) Theories*, *Phys. Rev. D* **22** (1980) 2227. Cited on page 26.

[65] KamLAND-Zen collaboration, A. Gando et al., *Search for Majorana Neutrinos near the Inverted Mass Hierarchy Region with KamLAND-Zen*, *Phys. Rev. Lett.* **117** (2016) 082503, [1605.02889]. Cited on page 26, and 27.

[66] SHiP collaboration, M. Anelli et al., *A facility to Search for Hidden Particles (SHiP) at the CERN SPS*, 1504.04956. Cited on page 30, and 61.

[67] SHiP Collaboration collaboration, E. Graverini, *SHiP sensitivity to Heavy Neutral Leptons*, . Cited on page 30, and 61.

[68] FCC-ee study Team collaboration, A. Blondel, E. Graverini, N. Serra and M. Shaposhnikov, *Search for Heavy Right Handed Neutrinos at the FCC-ee*, *Nucl. Part. Phys. Proc.* **273-275** (2016) 1883–1890, [1411.5230]. Cited on page 30, and 61.

[69] A. Atre, T. Han, S. Pascoli and B. Zhang, *The Search for Heavy Majorana Neutrinos*, *JHEP* **05** (2009) 030, [0901.3589]. Cited on page 30.

[70] M. L. Graesser, *Broadening the Higgs boson with right-handed neutrinos and a higher dimension operator at the electroweak scale*, *Phys. Rev.* **D76** (2007) 075006, [0704.0438]. Cited on page 32, and 62.

[71] M. L. Graesser, *Experimental Constraints on Higgs Boson Decays to TeV-scale Right-Handed Neutrinos*, 0705.2190. Cited on page 32, and 62.

[72] F. del Aguila, S. Bar-Shalom, A. Soni and J. Wudka, *Heavy Majorana Neutrinos in the Effective Lagrangian Description: Application to Hadron Colliders*, *Phys. Lett.* **B670** (2009) 399–402, [0806.0876]. Cited on page 32, and 62.

[73] A. Aparici, K. Kim, A. Santamaria and J. Wudka, *Right-handed neutrino magnetic moments*, *Phys. Rev.* **D80** (2009) 013010, [0904.3244]. Cited on page 32, and 62.

[74] P. Hernandez, M. Kekic, J. Lopez-Pavon, J. Racker and J. Salvado, *Testable Baryogenesis in Seesaw Models*, *JHEP* **08** (2016) 157, [1606.06719]. Cited on page 32, and 63.

[75] R. S. Chivukula and H. Georgi, *Composite Technicolor Standard Model*, *Phys. Lett.* **B188** (1987) 99–104. Cited on page 33, and 64.

[76] G. D'Ambrosio, G. F. Giudice, G. Isidori and A. Strumia, *Minimal flavor violation: An Effective field theory approach*, *Nucl. Phys.* **B645** (2002) 155–187, [hep-ph/0207036]. Cited on page 33, and 64.

[77] B. D. Fields, P. Molaro and S. Sarkar, *Big-Bang Nucleosynthesis*, *Chin. Phys. C* **38** (2014) 339–344, [1412.1408]. Cited on page 35.

[78] E. W. Kolb and M. S. Turner, *The Early Universe*, *Front. Phys.* **69** (1990) 1–547. Cited on page 35, 39, 40, and 55.

[79] A. Sakharov, *Violation of CP Invariance, C asymmetry, and baryon asymmetry of the universe*, *Sov. Phys. Usp.* **34** (1991) 392–393. Cited on page 35, and 55.

[80] G. 't Hooft, *Symmetry Breaking Through Bell-Jackiw Anomalies*, *Phys. Rev. Lett.* **37** (1976) 8–11. Cited on page 35.

[81] V. Kuzmin, V. Rubakov and M. Shaposhnikov, *On the Anomalous Electroweak Baryon Number Nonconservation in the Early Universe*, *Phys. Lett. B* **155** (1985) 36. Cited on page 35, and 56.

[82] A. G. Cohen, D. B. Kaplan and A. E. Nelson, *Baryogenesis at the weak phase transition*, *Nucl. Phys. B* **349** (1991) 727–742. Cited on page 36, and 56.

[83] M. Fukugita and T. Yanagida, *Baryogenesis Without Grand Unification*, *Phys. Lett.* **B174** (1986) 45–47. Cited on page 36.

[84] E. K. Akhmedov, V. Rubakov and A. Smirnov, *Baryogenesis via neutrino oscillations*, *Phys. Rev. Lett.* **81** (1998) 1359–1362, [hep-ph/9803255]. Cited on page 36, and 65.

[85] T. Asaka, S. Blanchet and M. Shaposhnikov, *The nuMSM, dark matter and neutrino masses*, *Phys. Lett.* **B631** (2005) 151–156, [hep-ph/0503065]. Cited on page 36, 41, and 65.

[86] J. H. Chang, R. Essig and S. D. McDermott, *Revisiting Supernova 1987A Constraints on Dark Photons*, *JHEP* **01** (2017) 107, [1611.03864]. Cited on page 38, and 66.

[87] A. Fradette, M. Pospelov, J. Pradler and A. Ritz, *Cosmological Constraints on Very Dark Photons*, *Phys. Rev. D* **90** (2014) 035022, [1407.0993]. Cited on page 38, and 66.

[88] M. Williams, C. Burgess, A. Maharana and F. Quevedo, *New Constraints (and Motivations) for Abelian Gauge Bosons in the MeV-TeV Mass Range*, *JHEP* **08** (2011) 106, [1103.4556]. Cited on page 38, and 66.

[89] D. Gorbunov, A. Makarov and I. Timiryasov, *Decaying light particles in the SHiP experiment: Signal rate estimates for hidden photons*, *Phys. Rev. D* **91** (2015) 035027, [1411.4007]. Cited on page 38, and 66.

[90] Y. Sofue and V. Rubin, *Rotation curves of spiral galaxies*, *Ann. Rev. Astron. Astrophys.* **39** (2001) 137–174, [astro-ph/0010594]. Cited on page 38, and 57.

[91] M. Bartelmann and P. Schneider, *Weak gravitational lensing*, *Phys. Rept.* **340** (2001) 291–472, [astro-ph/9912508]. Cited on page 38, and 57.

[92] M. Mateo, *Dwarf galaxies of the Local Group*, *Ann. Rev. Astron. Astrophys.* **36** (1998) 435–506, [astro-ph/9810070]. Cited on page 39, and 57.

[93] T. Lin, *TASI lectures on dark matter models and direct detection*, 1904.07915. Cited on page 39, 46, and 57.

[94] M. Lisanti, *Lectures on Dark Matter Physics*, in *Proceedings, Theoretical Advanced Study Institute in Elementary Particle Physics: New Frontiers in Fields and Strings (TASI 2015): Boulder, CO, USA, June 1-26, 2015*, pp. 399–446, 2017. 1603.03797. DOI. Cited on page 39, and 57.

[95] T. R. Slatyer, *Indirect Detection of Dark Matter*, in *Proceedings, Theoretical Advanced Study Institute in Elementary Particle Physics : Anticipating the Next Discoveries in Particle Physics (TASI 2016): Boulder, CO, USA, June 6-July 1, 2016*, pp. 297–353, 2018. 1710.05137. DOI. Cited on page 39, and 57.

[96] G. Bertone, D. Hooper and J. Silk, *Particle dark matter: Evidence, candidates and constraints*, *Phys. Rept.* **405** (2005) 279–390, [hep-ph/0404175]. Cited on page 39, 40, and 57.

[97] D. Racco, *Theoretical models for Dark Matter: from WIMPs to Primordial Black Holes*. PhD thesis, Geneva U., 9, 2018. 10.13097/archive-ouverte/unige:108633. Cited on page 39.

[98] P. Gondolo and G. Gelmini, *Cosmic abundances of stable particles: Improved analysis*, *Nucl. Phys. B* **360** (1991) 145–179. Cited on page 39.

[99] K. Griest and D. Seckel, *Three exceptions in the calculation of relic abundances*, *Phys. Rev. D* **43** (1991) 3191–3203. Cited on page 39.

[100] M. Bauer and T. Plehn, *Yet Another Introduction to Dark Matter: The Particle Physics Approach*, vol. 959 of *Lecture Notes in Physics*. Springer, 2019, 10.1007/978-3-030-16234-4. Cited on page 40.

[101] L. J. Hall, K. Jedamzik, J. March-Russell and S. M. West, *Freeze-In Production of FIMP Dark Matter*, *JHEP* **03** (2010) 080, [0911.1120]. Cited on page 40.

[102] J. McDonald, *Thermally generated gauge singlet scalars as selfinteracting dark matter*, *Phys. Rev. Lett.* **88** (2002) 091304, [hep-ph/0106249]. Cited on page 40.

[103] Y. Ali-HaÃŕmoud and M. Kamionkowski, *Cosmic microwave background limits on accreting primordial black holes*, *Phys. Rev. D* **95** (2017) 043534, [1612.05644]. Cited on page 41.

[104] A. Katz, J. Kopp, S. Sibiryakov and W. Xue, *Femtolensing by Dark Matter Revisited*, *JCAP* **12** (2018) 005, [1807.11495]. Cited on page 41.

[105] A. Katz, J. Kopp, S. Sibiryakov and W. Xue, *Looking for MACHOs in the Spectra of Fast Radio Bursts*, 1912.07620. Cited on page 41.

[106] H. Niikura et al., *Microlensing constraints on primordial black holes with Subaru/HSC Andromeda observations*, *Nat. Astron.* **3** (2019) 524–534, [1701.02151]. Cited on page 41.

[107] EROS-2 collaboration, P. Tisserand et al., *Limits on the Macho Content of the Galactic Halo from the EROS-2 Survey of the Magellanic Clouds*, *Astron. Astrophys.* **469** (2007) 387–404, [astro-ph/0607207]. Cited on page 41.

[108] J. Garcia-Bellido, S. Clesse and P. Fleury, *Primordial black holes survive SN lensing constraints*, *Phys. Dark Univ.* **20** (2018) 95–100, [1712.06574]. Cited on page 41.

[109] M. Sasaki, T. Suyama, T. Tanaka and S. Yokoyama, *Primordial black holes—perspectives in gravitational wave astronomy*, *Class. Quant. Grav.* **35** (2018) 063001, [1801.05235]. Cited on page 41.

[110] A. Boyarsky, M. Drewes, T. Lasserre, S. Mertens and O. Ruchayskiy, *Sterile Neutrino Dark Matter*, *Prog. Part. Nucl. Phys.* **104** (2019) 1–45, [1807.07938]. Cited on page 41, 48, and 68.

[111] S. Dodelson and L. M. Widrow, *Sterile-neutrinos as dark matter*, *Phys. Rev. Lett.* **72** (1994) 17–20, [hep-ph/9303287]. Cited on page 41.

[112] R. Barbieri and A. Dolgov, *Neutrino oscillations in the early universe*, *Nucl. Phys. B* **349** (1991) 743–753. Cited on page 41.

[113] K. Kainulainen, *Light Singlet Neutrinos and the Primordial Nucleosynthesis*, *Phys. Lett. B* **244** (1990) 191–195. Cited on page 41.

[114] R. Barbieri and A. Dolgov, *Bounds on Sterile-neutrinos from Nucleosynthesis*, *Phys. Lett. B* **237** (1990) 440–445. Cited on page 41.

[115] X.-D. Shi and G. M. Fuller, *A New dark matter candidate: Nonthermal sterile neutrinos*, *Phys. Rev. Lett.* **82** (1999) 2832–2835, [astro-ph/9810076]. Cited on page 41.

[116] A. Merle, V. Niro and D. Schmidt, *New Production Mechanism for keV Sterile Neutrino Dark Matter by Decays of Frozen-In Scalars*, *JCAP* **1403** (2014) 028, [1306.3996]. Cited on page 41.

[117] A. Merle and M. Totzauer, *keV Sterile Neutrino Dark Matter from Singlet Scalar Decays: Basic Concepts and Subtle Features*, *JCAP* **1506** (2015) 011, [1502.01011]. Cited on page 41.

[118] B. Shuve and I. Yavin, *Dark matter progenitor: Light vector boson decay into sterile neutrinos*, *Phys. Rev.* **D89** (2014) 113004, [1403.2727]. Cited on page 41.

[119] J. KÃűnig, A. Merle and M. Totzauer, *keV Sterile Neutrino Dark Matter from Singlet Scalar Decays: The Most General Case*, *JCAP* **1611** (2016) 038, [1609.01289]. Cited on page 41.

[120] R. D. Peccei and H. R. Quinn, *CP Conservation in the Presence of Instantons*, *Phys. Rev. Lett.* **38** (1977) 1440–1443. Cited on page 42.

[121] R. D. Peccei and H. R. Quinn, *Constraints Imposed by CP Conservation in the Presence of Instantons*, *Phys. Rev.* **D16** (1977) 1791–1797. Cited on page 42.

[122] J. Preskill, M. B. Wise and F. Wilczek, *Cosmology of the Invisible Axion*, *Phys. Lett.* **B120** (1983) 127–132. Cited on page 43, and 58.

[123] M. S. Turner, *Coherent Scalar Field Oscillations in an Expanding Universe*, *Phys. Rev. D* **28** (1983) 1243. Cited on page 43, and 58.

[124] L. Abbott and P. Sikivie, *A Cosmological Bound on the Invisible Axion*, *Phys. Lett. B* **120** (1983) 133–136. Cited on page 43, and 58.

[125] L. Di Luzio, M. Giannotti, E. Nardi and L. Visinelli, *The landscape of QCD axion models*, 2003.01100. Cited on page 45, 48, and 67.

[126] D. J. E. Marsh, *Axion Cosmology*, *Phys. Rept.* **643** (2016) 1–79, [1510.07633]. Cited on page 45.

[127] M. W. Goodman and E. Witten, *Detectability of Certain Dark Matter Candidates*, *Phys. Rev. D* **31** (1985) 3059. Cited on page 45.

[128] R. Essig, J. Mardon and T. Volansky, *Direct Detection of Sub-GeV Dark Matter*, *Phys. Rev.* **D85** (2012) 076007, [1108.5383]. Cited on page 46.

[129] P. W. Graham, D. E. Kaplan, S. Rajendran and M. T. Walters, *Semiconductor Probes of Light Dark Matter*, *Phys. Dark Univ.* **1** (2012) 32–49, [1203.2531]. Cited on page 46.

[130] L. M. Capparelli, G. Cavoto, D. Mazzilli and A. D. Polosa, *Directional Dark Matter Searches with Carbon Nanotubes*, *Phys. Dark Univ.* **9-10** (2015) 24–30, [1412.8213]. Cited on page 46.

[131] R. Essig, M. Fernandez-Serra, J. Mardon, A. Soto, T. Volansky and T.-T. Yu, *Direct Detection of sub-GeV Dark Matter with Semiconductor Targets*, *JHEP* **05** (2016) 046, [1509.01598]. Cited on page 46.

[132] Y. Hochberg, Y. Zhao and K. M. Zurek, *Superconducting Detectors for Superlight Dark Matter*, *Phys. Rev. Lett.* **116** (2016) 011301, [1504.07237]. Cited on page 46.

[133] Y. Hochberg, M. Pyle, Y. Zhao and K. M. Zurek, *Detecting Superlight Dark Matter with Fermi-Degenerate Materials*, *JHEP* **08** (2016) 057, [1512.04533]. Cited on page 46.

[134] G. Cavoto, E. N. M. Cirillo, F. Cocina, J. Ferretti and A. D. Polosa, *WIMP detection and slow ion dynamics in carbon nanotube arrays*, *Eur. Phys. J.* **C76** (2016) 349, [1602.03216]. Cited on page 46.

[135] Y. Hochberg, Y. Kahn, M. Lisanti, C. G. Tully and K. M. Zurek, *Directional detection of dark matter with two-dimensional targets*, *Phys. Lett.* **B772** (2017) 239–246, [1606.08849]. Cited on page 46.

[136] G. Cavoto, F. Luchetta and A. D. Polosa, *Sub-GeV Dark Matter Detection with Electron Recoils in Carbon Nanotubes*, *Phys. Lett.* **B776** (2018) 338–344, [1706.02487]. Cited on page 46.

[137] Y. Hochberg, Y. Kahn, M. Lisanti, K. M. Zurek, A. G. Grushin, R. Ilan et al., *Detection of sub-MeV Dark Matter with Three-Dimensional Dirac Materials*, *Phys. Rev.* **D97** (2018) 015004, [1708.08929]. Cited on page 46.

[138] S. Fichet, *Quantum Forces from Dark Matter and Where to Find Them*, *Phys. Rev. Lett.* **120** (2018) 131801, [1705.10331]. Cited on page 46.

[139] R. Alonso, D. Blas and P. Wolf, *Exploring the ultra-light to sub-MeV dark matter window with atomic clocks and co-magnetometers*, *JHEP* **07** (2019) 069, [1810.00889]. Cited on page 46.

[140] T. Trickle, Z. Zhang and K. M. Zurek, *Direct Detection of Light Dark Matter with Magnons*, 1905.13744. Cited on page 46.

[141] T. Cheng, R. Primulando and M. Spinrath, *Dark Matter Induced Brownian Motion*, 1906.07356. Cited on page 46.

[142] J. A. Dror, G. Elor and R. Mcgehee, *Direct Detection Signals from Absorption of Fermionic Dark Matter*, 1905.12635. Cited on page 46.

[143] J. Alexander et al., *Dark Sectors 2016 Workshop: Community Report*, 2016. 1608.08632. Cited on page 46.

[144] M. Battaglieri et al., *US Cosmic Visions: New Ideas in Dark Matter 2017: Community Report*, in *U.S. Cosmic Visions: New Ideas in Dark Matter College Park, MD, USA, March 23-25, 2017*, 2017. 1707.04591. Cited on page 46.

[145] K. Schutz and K. M. Zurek, *Detectability of Light Dark Matter with Superfluid Helium*, *Phys. Rev. Lett.* **117** (2016) 121302, [1604.08206]. Cited on page 46.

[146] S. Knapen, T. Lin and K. M. Zurek, *Light Dark Matter in Superfluid Helium: Detection with Multi-excitation Production*, *Phys. Rev. D* **95** (2017) 056019, [1611.06228]. Cited on page 46.

[147] W. Guo and D. N. McKinsey, *Concept for a dark matter detector using liquid helium-4*, *Phys. Rev. D* **87** (2013) 115001, [1302.0534]. Cited on page 46.

[148] F. Acanfora, A. Esposito and A. D. Polosa, *Sub-GeV Dark Matter in Superfluid He-4: an Effective Theory Approach*, *Eur. Phys. J.* **C79** (2019) 549, [1902.02361]. Cited on page 46.

[149] D. Son, *Low-energy quantum effective action for relativistic superfluids*, hep-ph/0204199. Cited on page 46.

[150] A. Nicolis, *Low-energy effective field theory for finite-temperature relativistic superfluids*, 1108.2513. Cited on page 46.

[151] A. Hook, Y. Kahn, B. R. Safdi and Z. Sun, *Radio Signals from Axion Dark Matter Conversion in Neutron Star Magnetospheres*, 1804.03145. Cited on page 47, and 67.

[152] F. P. Huang, K. Kadota, T. Sekiguchi and H. Tashiro, *The radio telescope search for the resonant conversion of cold dark matter axions from the magnetized astrophysical sources*, 1803.08230. Cited on page 47, and 67.

[153] B. R. Safdi, Z. Sun and A. Y. Chen, *Detecting Axion Dark Matter with Radio Lines from Neutron Star Populations*, 1811.01020. Cited on page 47, and 67.

[154] G. Sigl, *Astrophysical Haloscopes*, *Phys. Rev.* **D96** (2017) 103014, [1708.08908]. Cited on page 47, and 67.

[155] F. Combes, *The Square Kilometer Array: cosmology, pulsars and other physics with the SKA*, *JINST* **10** (2015) C09001, [1504.00493]. Cited on page 47, 48, and 67.

[156] L. B. Newburgh et al., *Calibrating CHIME, A New Radio Interferometer to Probe Dark Energy*, *Proc. SPIE Int. Soc. Opt. Eng.* **9145** (2014) 4V, [1406.2267]. Cited on page 48, and 67.

[157] C. Hagmann, P. Sikivie, N. S. Sullivan and D. B. Tanner, *Results from a search for cosmic axions*, *Phys. Rev.* **D42** (1990) 1297–1300. Cited on page 48, and 67.

[158] ADMX collaboration, C. Hagmann et al., *Results from a high sensitivity search for cosmic axions*, *Phys. Rev. Lett.* **80** (1998) 2043–2046, [astro-ph/9801286]. Cited on page 48, and 67.

[159] CAST collaboration, V. Anastassopoulos et al., *New CAST Limit on the Axion-Photon Interaction*, *Nature Phys.* **13** (2017) 584–590, [1705.02290]. Cited on page 48, and 67.

[160] R. BÃďhre et al., *Any light particle search II âĂŤTechnical Design Report*, *JINST* **8** (2013) T09001, [1302.5647]. Cited on page 48, and 67.

[161] IAXO collaboration, I. Irastorza et al., *The International Axion Observatory IAXO. Letter of Intent to the CERN SPS committee*, . Cited on page 48, and 67.

[162] E. Armengaud et al., *Conceptual Design of the International Axion Observatory (IAXO)*, *JINST* **9** (2014) T05002, [1401.3233]. Cited on page 48, and 67.

[163] L. Di Luzio, F. Mescia and E. Nardi, *Redefining the Axion Window*, *Phys. Rev. Lett.* **118** (2017) 031801, [1610.07593]. Cited on page 48, and 67.

[164] K. N. Abazajian, *Sterile neutrinos in cosmology*, *Phys. Rept.* **711-712** (2017) 1–28, [1705.01837]. Cited on page 48, 49, 68, and 69.

[165] E. Bulbul, M. Markevitch, A. Foster, R. K. Smith, M. Loewenstein and S. W. Randall, *Detection of An Unidentified Emission Line in the Stacked X-ray spectrum of Galaxy Clusters*, *Astrophys. J.* **789** (2014) 13, [1402.2301]. Cited on page 49, and 69.

[166] A. Boyarsky, O. Ruchayskiy, D. Iakubovskyi and J. Franse, *Unidentified Line in X-Ray Spectra of the Andromeda Galaxy and Perseus Galaxy Cluster*, *Phys. Rev. Lett.* **113** (2014) 251301, [1402.4119]. Cited on page 49, and 69.

[167] A. Boyarsky, O. Ruchayskiy and M. Shaposhnikov, *The Role of sterile neutrinos in cosmology and astrophysics*, *Ann. Rev. Nucl. Part. Sci.* **59** (2009) 191–214, [0901.0011]. Cited on page 49, and 69.

[168] B. W. Lee and R. E. Shrock, *Natural Suppression of Symmetry Violation in Gauge Theories: Muon - Lepton and Electron Lepton Number Nonconservation*, *Phys. Rev.* **D16** (1977) 1444. Cited on page 48.

[169] P. B. Pal and L. Wolfenstein, *Radiative Decays of Massive Neutrinos*, *Phys. Rev.* **D25** (1982) 766. Cited on page 48.

[170] M. Drewes et al., *A White Paper on keV Sterile Neutrino Dark Matter*, *JCAP* **1701** (2017) 025, [1602.04816]. Cited on page 48, and 68.

[171] F. Zandanel, C. Weniger and S. Ando, *The role of the eROSITA all-sky survey in searches for sterile neutrino dark matter*, *JCAP* **1509** (2015) 060, [1505.07829]. Cited on page 50.

[172] A. Merloni, P. Predehl, W. Becker, H. Böhringer, T. Boller, H. Brunner et al., *eROSITA Science Book: Mapping the Structure of the Energetic Universe*, *arXiv e-prints* (Sept., 2012) arXiv:1209.3114, [1209.3114]. Cited on page 50.

[173] K. Nandra et al., *The Hot and Energetic Universe: A White Paper presenting the science theme motivating the Athena+ mission*, 1306.2307. Cited on page 50.

[174] DESI collaboration, A. Aghamousa et al., *The DESI Experiment Part I: Science,Targeting, and Survey Design*, 1611.00036. Cited on page 50.

[175] M. Bilicki, T. H. Jarrett, J. A. Peacock, M. E. Cluver and L. Steward, *Two Micron All Sky Survey Photometric Redshift Catalog: A Comprehensive Three-dimensional Census of the Whole Sky*, *ApJ Suppl.* **210** (Jan., 2014) 9, [1311.5246]. Cited on page 50.

[176] J. Casas and A. Ibarra, *Oscillating neutrinos and $\mu \to e, \gamma$*, *Nucl. Phys. B* **618** (2001) 171–204, [hep-ph/0103065]. No cited.

Part II

Scientific Research

Eur. Phys. J. C (2017) 77:258
DOI 10.1140/epjc/s10052-017-4823-8

THE EUROPEAN PHYSICAL JOURNAL C

Letter

The seesaw path to leptonic CP violation

A. Caputo[1,2,a], **P. Hernandez**[1,2,b], **M. Kekic**[1,c], **J. López-Pavón**[2,d], **J. Salvado**[1,e]

[1] Instituto de Física Corpuscular, Universidad de Valencia and CSIC, Edificio Institutos Investigación, Catedrático José Beltrán 2, 46980 Paterna, Spain
[2] CERN, Theoretical Physics Department, Geneva, Switzerland

Received: 4 January 2017 / Accepted: 7 April 2017 / Published online: 24 April 2017

Abstract Future experiments such as SHiP and high-intensity e^+e^- colliders will have a superb sensitivity to heavy Majorana neutrinos with masses below M_Z. We show that the measurement of the mixing to electrons and muons of one such state could establish the existence of CP violating phases in the neutrino mixing matrix, in the context of low-scale seesaw models. We quantify in the minimal model the CP reach of these future experiments, and demonstrate that CP violating phases in the mixing matrix could be established at 5σ CL in a very significant fraction of parameter space.

1 Introduction

The simplest extension of the standard model that can accommodate naturally light neutrino masses is the well-known seesaw model [1–4], where at least two singlet Majorana fermions, N_R^i, are added and can couple to the lepton doublets via a Higgs–Yukawa coupling.

The Lagrangian of the model is given by

$$\mathscr{L} = \mathscr{L}_{\rm SM} - \sum_{\alpha,i} \bar{L}^\alpha Y^{\alpha i} \tilde{\Phi} N_R^i - \sum_{i,j=1}^{2} \frac{1}{2} \bar{N}_R^{ic} M^{ij} N_R^j + h.c.,$$

where Y is a 3×2 complex matrix and M is a two-dimensional complex symmetric matrix.

While the Majorana mass scale, M, has been traditionally assumed to be very large so that the light neutrino masses can be explained with Yukawa couplings of $\mathcal{O}(1)$, the absence of any indication of new physics that solves the hierarchy problem suggests that a more natural option might be to assume a Majorana scale of the order of the electroweak scale. The lepton flavour puzzle would not be qualitatively very different from the quark one, in particular there would not be a large gap between neutrino Yukawas and those of the charged leptons, since the neutrino Yukawas would need to be only slightly smaller than the electron one:

$$\frac{y_\nu}{y_e} \simeq 0.2 \sqrt{\frac{m_\nu}{0.05\text{eV}} \frac{M}{v}}. \tag{1}$$

From a phenomenological point of view this is of course a very interesting possibility since the heavy Majorana neutrino states might be searched for in fixed-target experiments and at colliders.

In this letter we explore the opportunities that this opens for the discovery of leptonic CP violation. In particular we concentrate on the observables that could be provided by direct searches of these heavy neutrino states, more concretely their mixings to electrons and muons. It is well known that in seesaw models there is a strong correlation between the mixings of the heavy states and the light and heavy neutrino spectrum. In particular for just one neutrino species/flavour, the mixing of the heavy state is fixed to be

$$|U_{\alpha h}|^2 = \frac{m_{\rm l}}{M_{\rm h}}, \tag{2}$$

where $m_{\rm l}$ is the light neutrino mass and $M_{\rm h}$ is the heavy one. This is the naive seesaw scaling which implies that the mixing of heavy states is highly suppressed when $M_{\rm h} \gg m_{\rm l}$.

In the case of more families the correlation still exists but it is not so strong. In particular, for the minimal model with two heavy neutrinos, using the Casas–Ibarra parametrization of the model [5], the mixing of the heavy neutrinos is given in all generality by

$$U_{\alpha h} = i U_{\rm PMNS} \sqrt{m_{\rm l}}\, P_{\rm NO}\, R^\dagger(z) M^{-1/2}, \tag{3}$$

where $m_{\rm l}$ is the diagonal matrix of the light neutrino masses (note that the lightest neutrino is massless) and $U_{\rm PMNS}$ is the PMNS matrix in the standard parametrization, which

[a] e-mail: andrea.caputo@cern.ch
[b] e-mail: m.pilar.hernandez@uv.es
[c] e-mail: marija.kekic@ific.uv.es
[d] e-mail: jacobo.lopez.pavon@cern.ch
[e] e-mail: jordi.salvado@ific.uv.es

depends only on two CP violating phases [6–8]. $P_{\rm NO}$ is a 3×2 matrix that depends on the neutrino ordering (NH, IH)

$$P_{\rm NH} = \begin{pmatrix} \mathbf{0} \\ \mathbf{I} \end{pmatrix}, \quad P_{\rm IH} = \begin{pmatrix} \mathbf{I} \\ \mathbf{0} \end{pmatrix}, \tag{4}$$

where $\mathbf{I}$ is the 2×2 identity matrix and $\mathbf{0} = (0, 0)$ [9]. The unknown parameters are $M = \text{Diag}(M_1, M_2)$, the diagonal matrix of the heavy neutrino masses, and R, a two-dimensional complex orthogonal matrix, that depends generically on one complex angle, $z = \theta + i\gamma$. The entries in this matrix can be very large and therefore the naive seesaw scaling of Eq. (2) is not generically satisfied in the case of more than one family. In this work we will fix the known oscillation parameters to their best fit values as taken from [10].

In [11], we pointed out that in the region of large mixings the ratio of mixings to electron and muons of the heavy states are essentially fixed by the PMNS matrix, and is therefore very sensitive to its unknown CP phases. In this paper, our aim is to quantify the CP discovery potential of such measurement. Interestingly this measurement provides an example of a CP conserving observable that is sensitive to leptonic CP violation.

It should be noted that the results below will also apply to the model with three neutrinos, where one of them is sufficiently decoupled, as in the νMSM [12], and more generally to more complex seesaw models where the dominant contribution to neutrino masses comes from the two singlet states considered.

2 Heavy neutrino mixings versus leptonic CP phases

Given the upper bound on the light neutrino masses of $\mathcal{O}(1)$eV, the naive seesaw scaling formula of Eq. (2) implies that the mixings of the heavy states are of $|U_{\alpha h}|^2 \simeq \mathcal{O}\left(\frac{10^{-9}\text{GeV}}{M}\right)$, a value at the limit of sensitivity of SHiP [13] in the GeV range or FCC-e in the $\mathcal{O}(10)$ GeV range [14]. This implies that in most of the sensitivity range of SHiP and other collider experiments the entries of R need to be largish (i.e. $\gamma \gtrsim 1$), and in this case the dependence of the mixings on the unknown parameters simplifies greatly. Indeed, a perturbative expansion to $\mathcal{O}(\epsilon)$ in the small parameters

$$\epsilon \sim r \equiv \sqrt{\frac{\Delta m^2_{\rm sol}}{\Delta m^2_{\rm atm}}} \sim \theta_{13} \sim e^{-\frac{\gamma}{2}}, \tag{5}$$

shows that the ratio of electron/muon mixings does not depend on the complex angle γ, θ, nor on the masses of the heavy states, and only depends on the the mixing angles and CP phases of the PMNS matrix [11]. Defining $A \equiv \frac{e^{2\gamma}\sqrt{\Delta m^2_{\rm atm}}}{4}$, the result for the inverted ordering (IH) is

$$\begin{aligned} |U_{ei}|^2 M_i &\simeq A\Big[(1 + \sin\phi_1 \sin 2\theta_{12})(1 - \theta_{13}^2) \\ &\quad + \frac{1}{2} r^2 s_{12}(c_{12}\sin\phi_1 + s_{12}) + \mathcal{O}(\epsilon^3)\Big], \\ |U_{\mu i}|^2 M_i &\simeq A\Big[\left(1 - \sin\phi_1 \sin 2\theta_{12}\left(1 + \frac{1}{4}r^2\right) + \frac{1}{2}r^2 c_{12}^2\right) c_{23}^2 \\ &\quad + \theta_{13}(\cos\phi_1 \sin\delta - \sin\phi_1 \cos 2\theta_{12}\cos\delta)\sin 2\theta_{23} \\ &\quad + \theta_{13}^2(1 + \sin\phi_1 \sin 2\theta_{12}) s_{23}^2 + \mathcal{O}(\epsilon^3)\Big], \end{aligned} \tag{6}$$

while for the normal one (NH) we have

$$\begin{aligned} |U_{ei}|^2 M_i &\simeq A\Big[r s_{12}^2 - 2\sqrt{r}\theta_{13}\sin(\delta + \phi_1) s_{12} + \theta_{13}^2 + \mathcal{O}(\epsilon^{5/2})\Big], \\ |U_{\mu i}|^2 M_i &\simeq A\Big[s_{23}^2 - \sqrt{r}\, c_{12}\sin\phi_1 \sin 2\theta_{23} + r c_{12}^2 c_{23}^2 \\ &\quad + 2\sqrt{r}\,\theta_{13}\sin(\phi_1 + \delta) s_{12} s_{23}^2 - \theta_{13}^2 s_{23}^2 + \mathcal{O}(\epsilon^{5/2})\Big]. \end{aligned} \tag{7}$$

On the other hand, the parameter γ and the Majorana masses determine the global size of the mixings, and therefore the statistical uncertainty in the measurement of the ratio of mixings.

However, values of the heavy mixings much larger that the naive seesaw scaling in Eq. (2) imply generically large one loop corrections to neutrino masses [15] except in the region where an approximate lepton number symmetry holds [16–19], which implies highly degenerate neutrinos, besides large γ.

We want to quantify the range of the PMNS CP phase parameter space, that is, the rectangle $\delta, \phi_1 \in [0, 2\pi]$, in which leptonic CP violation can be discovered via the measurement of the electron and muon mixings of one of the heavy neutrinos. In other words, we wonder for which values of the true parameters (δ, ϕ_1) can these mixings be distinguished from those at the CP conserving points $(0, 0)$, $(0, \pi)$, $(\pi, 0)$, (π, π).

3 Discovery of Majorana neutrinos

We consider two future experiments that have the potential to discover sterile neutrinos in complementary regions of masses: SHiP [13] and FCC-ee [14].

3.1 The SHiP experiment

The SHiP experiment [13] will search for the heavy neutrinos of the seesaw model in charmed and b meson decays. Neutrinos with masses below charmed and b meson masses could

be discovered, and the best sensitivity is expected for masses around 1 GeV. In order to carry out our study we would ideally need an estimate of the uncertainty in the determination of the mixing angles of the sterile neutrinos to electrons and muons as a function of those mixings and the heavy neutrino masses. Such information has not been published yet by the collaboration. The only publicly available result is the sensitivity reach (corresponding to 2 expected events in a 5 year run with 0.1 estimated background events) on the plane $U^2 \equiv \sum_\alpha |U_{\alpha i}|^2$ vs. M_i for five scenarios, where the contribution of electron and muon channels is combined, and only the channels with two charged particles in the final state are considered. These scenarios also correspond to two highly degenerate neutrinos with equal mixings that contribute equally to the signal. Since we are interested in a more general case, where neutrinos might not be degenerate, we consider the contribution of just one of the states, so we will assume that at the sensitivity limit the number of events is one instead of two.

The number of events in the charged-current two-body decays $N \to l_\alpha^\pm H^\mp$, for different hadrons $H = \pi, \rho, \ldots$, is expected to scale as

$$N_\alpha(M_i) \propto |U_{\alpha i}|^2 U^2, \tag{8}$$

because U^2 controls the number of charm decays into sterile neutrinos, while $|U_{\alpha i}|^2$ controls the fraction of those that decay to the lepton flavour α via a charged current within the detector length (which is assumed to be much smaller than the decay length). Note that in the charged-current three-body decays $N \to l_\alpha^- l_\beta^+ \nu_\beta$ with $\alpha \neq \beta$, the contributions from the charged-current muon and electron mixings cannot be distinguished, because the N are Majorana. Also those decays with $\alpha = \beta$ cannot be distinguished from the corresponding neutral-current process. These three-body decays are, however, subleading in the sensitivity regime of SHiP so we will consider only the information from the two-body decays.

Among the five scenarios studied in [13,20], there are, however, two of them where either the mixing to electrons or the mixing to muons dominates by a large factor. In Fig. 1 we reproduce the SHiP sensitivity curves for these electron-dominated (IV) and muon-dominated (II) scenarios. As an illustration, we also indicate in Fig. 1 the mixings corresponding to different values of the Casas–Ibarra parameter γ. Stringent bounds exist from direct searches. We do not include them in the plot because they are flavour dependent and cannot easily be interpreted in terms of U^2. They restrict severely the region of masses below 0.5 GeV and cut slightly the range of largest mixings. We will therefore not consider this region of parameter space. In the figure we also indicate the line that corresponds to one-loop corrections to neutrino mass differences being of the same order as the atmospheric mass splitting, for a level of degeneracy $\Delta M/M_1 = 1$. No degeneracy is therefore required in this range of masses to reach mixings up to $U^2 \sim 10^{-6}$ without fine-tunning.

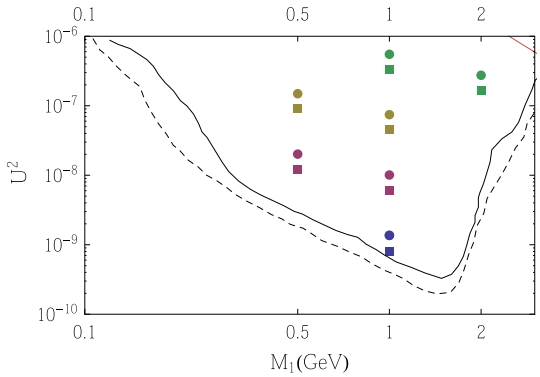

Fig. 1 *Lines* corresponding to two expected events for scenarios II (*solid*) and IV (*dashed*) in [13]. The indicated points correspond to the CP conserving case and $\gamma = 2, 3, 4, 5$ in ascending order for IH (*circles*) and NH (*squares*). The *red line in the top right corner* corresponds to one-loop corrections to neutrino masses being of the same order as the atmospheric splitting for $\Delta M/M_1 = 1$

In order to estimate the number of electron and muon events as a function of the Casas–Ibarra parameters, we assume that the total number of events (with two charged particles in the final state) is one at the sensitivity limit curve in the two scenarios, and we compute the contribution to this total of the electron and muon two-body decay channels. Note that for $M \sim 1$ GeV the three-body decays are subleading. At each mass, the number of electron and muon events at different value of the mixings is obtained by scaling this number according to Eq. (8).

Besides the number of electron and muon events we assume that the mass of the heavy neutrino is measured, which should be easy in these two-body channels. Again the uncertainty in the determination of the mass as a function of the mass and mixing has not yet been presented by the SHiP collaboration. A realistic error is much harder to estimate in this case, since it involves reconstructing a peak in the invariant mass. We will therefore assume a fixed relative error of 1%. We note that this uncertainty is not expected to be very relevant, since most information on the phases comes from the ratio of mixings where the mass dependence drops.

3.2 FCC-ee collider

For masses above 2 GeV, the heavy neutrinos can be searched for in high luminosity colliders such as the future e^+e^- circular collider (FCC-ee) [14,21–23] that can provide $10^{12}-10^{13}$ Z boson decays at rest per year. Sterile neutrinos with masses $m_N \leq M_Z$ can be produced in the decay $Z \to N\nu$, and they leave a very characteristic signal of a displaced vertex produced by the decay of the long-lived heavy neutrino. A simplified estimate of the number of events to visible leptonic channels within the detector can be obtained as follows:

$$N_{\text{total}} = N_Z \text{BR}(Z \to N\nu)\text{BR}(N \to \text{leptonic}) \times \left(e^{-l_{\min}/\gamma_L c\tau_N} - e^{-l_{\max}/\gamma_L c\tau_N}\right), \quad (9)$$

where N_Z is the number of Z decays, $\gamma_L = \frac{1}{2}\left(\frac{M_Z}{M_1} + \frac{M_1}{M_Z}\right)$ is the heavy neutrino Lorentz boost gamma factor and τ_N is its lifetime. $l_{\min}$ and $l_{\max}$ are the minimum and maximum displacement of the secondary vertex that can be measured. The $Z \to N\nu$ branching ratio has been computed in [24] to be

$$\text{BR}(Z \to N_i\nu) = 2U^2\text{BR}(Z \to \nu\bar{\nu})\left(1 - \frac{M_i^2}{M_Z^2}\right)^2 \times \left(1 + \frac{1}{2}\frac{M_i^2}{M_Z^2}\right), \quad (10)$$

where $\text{BR}(Z \to \nu\bar{\nu})$ corresponds to one family.

The partial width to the leptonic channels can be found in many references, see for example [25,26], while the total width requires an estimate of the hadronic width. While in the SHiP case, exclusive hadronic channels where considered, for the heavier masses relevant at FCC-ee, the inclusive hadronic decay width is approximated by the parton model [27]. This is sufficient for our purposes. Note, however, that a precise determination of this width would be possible, applying similar methods to those used in τ decays [28].

In the recent analysis of [20], a FCC-ee configuration with 10^{13} Z decays per year and an inner tracker that can resolve a displaced vertex at a distance between $l_{\min} = 0.1$ mm and $l_{\max} = 5$ m has been assumed in the context of the same two scenarios above. The sensitivity reach using only leptonic channels and assuming 100% efficiency and zero background is reproduced in Fig. 2, which agrees reasonably well with the results of [20]. The regions of mixings above the red lines would imply fine-tunning between the tree level and one-loop contributions to the light neutrino masses for a level of degeneracy of $\Delta M/M_1 = 1$ (solid) and $\Delta M/M_1 = 0.01$ (dashed).

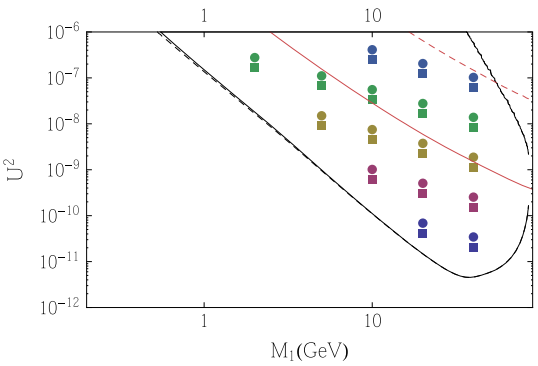

Fig. 2 *Lines* corresponding to two expected events for scenarios II (*solid*) and IV (*dashed*) in [20]. The indicated points correspond to the CP conserving case and $\gamma = 2, 3, 4, 5, 6$ in ascending order for IH (*circles*) and NH (*squares*). The *red lines in the top right corner* correspond to one-loop corrections to neutrino masses being of the same order as the atmospheric splitting for $\Delta M/M_1 = 1$ (*solid*) and $\Delta M/M_1 = 0.01$ (*dashed*)

Since we are interested in measuring separately the mixings to electrons and muons, we will separate the distinguishable leptonic channels $l_\alpha l_\beta = ee, e\mu, \mu\mu$. Note that each of these channels depends on several mixings, either because they get a contribution from neutral currents in the case of $\beta = \alpha$ or because the channels where the leading lepton (i.e. that coupled to the N_i) is α or $\beta \neq \alpha$ are indistinguishable. We also consider the inclusive hadronic ones, $N \to l_\alpha + q + \bar{q}'$, that depend only on the mixing $|U_{\alpha i}|$. Finally we assume an angular acceptance of ~80% (i.e. we require the N direction is at least 15° off the beam axis) and include just statistical uncertainties.

4 CP reach

In order to quantify the discovery CP potential we consider that SHiP or FCC-ee will measure the number of electron and muon events in the decay of one of the heavy neutrino states (without loss of generality we assume to be that with mass M_1), estimated as explained in the previous section. We will only consider statistical errors.

The test statistics (TS) for leptonic CP violation is then defined as follows:

$$\Delta\chi^2 \equiv -2 \sum_{\alpha=\text{channel}} N_\alpha^{\text{true}} - N_\alpha^{\text{CP}} + N_\alpha^{\text{true}} \log\left(\frac{N_\alpha^{\text{CP}}}{N_\alpha^{\text{true}}}\right) + \left(\frac{M_1 - M_1^{\min}}{\Delta M_1}\right)^2, \quad (11)$$

where $N_\alpha^{\text{true}} = N_\alpha(\delta, \phi_1, M_1, \gamma, \theta)$ is the number of events for the true model parameters, and $N_\alpha^{\text{CP}} = N_\alpha(\text{CP}, \gamma^{\min}, \theta^{\min}, M_1^{\min})$ is the number of events for the CP conserving test hypothesis that minimizes $\Delta\chi^2$ among the four CP conserving phase choices $\text{CP} = (0/\pi, 0/\pi)$ and over the unknown test parameters. ΔM_1 is the uncertainty in the mass, which is assumed to be 1%.

Surface plots for $\Delta\chi^2$ are shown in Fig. 3 for SHiP and the true parameters $\{\gamma, \theta, M_1\} = \{3.5, 0, 1\,\text{GeV}\}$. The basic features of these contours can be understood analytically, as shown by the superimposed lines corresponding to a constant electron–muon mixing ratio, as obtained from the analytical formulae in Eqs. (6) and (7).

We have evaluated via Monte Carlo the statistical distribution of this test statistics in order to define confidence intervals for the exclusion of the CP conserving hypothesis, following the approach of [29]. In Fig. 4 we show the result of $\mathcal{O}(10^7)$ experiments where the true value for the phases

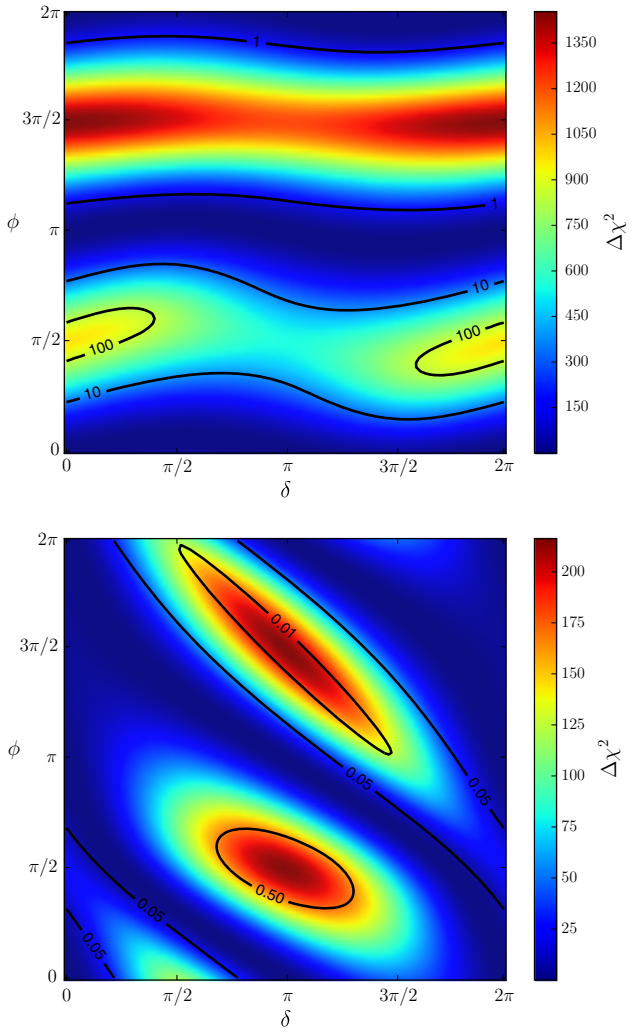

Fig. 3 Surface plots of $\Delta\chi^2$ for $(\gamma, \theta, M_1) = (3.5, 0, 1\ \text{GeV})$ as a function of the true (δ, ϕ_1) of IH (*up*) and NH (*down*) for SHiP. The *lines* correspond to the constant value indicated of the ratio of electron–muon mixing as obtained from the analytical formulae of Eqs. (6) and (7)

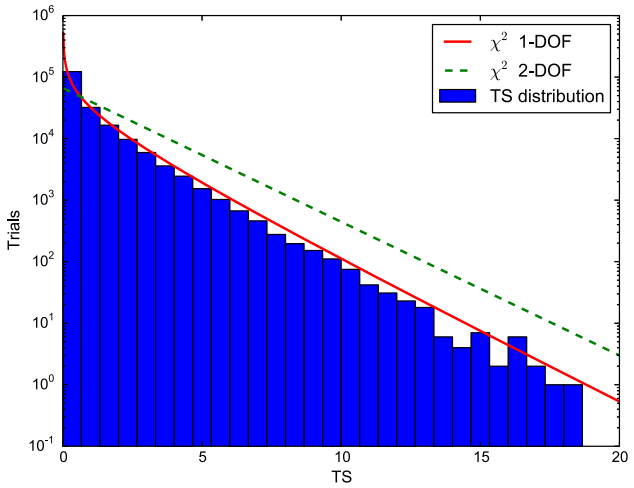

Fig. 4 Distribution of the test statistics for $\mathcal{O}(10^7)$ number of experimental measurements of the number of events for true values of the phases $(\delta, \phi_1) = (0, 0)$ for IH and $(\gamma, \theta, M_1) = (3.5, 0, 1)$ GeV, compared to the χ^2 distribution for 1 or 2 degrees of freedom

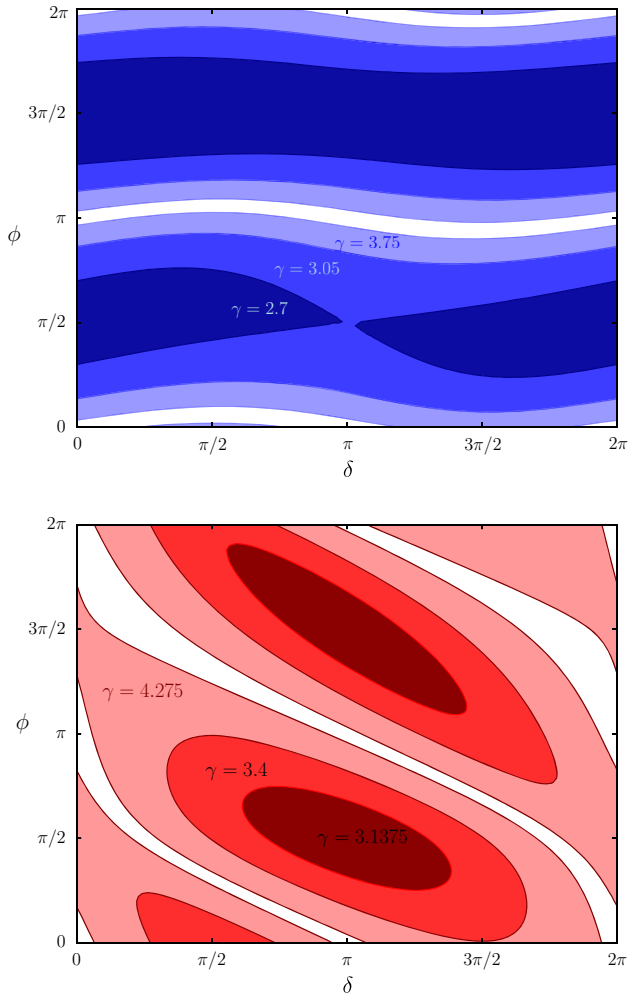

Fig. 5 5σ CP violation SHiP discovery regions on the plane (δ, ϕ_1) for various true values of γ for IH (*up*) and NH (*down*) and for the true parameters $M_1 = 1$ GeV and $\theta = 0$

is any of the CP conserving hypotheses and the number of events is distributed according to Poisson statistics. The distribution is compared with a χ^2 distribution of one or two degrees of freedom. The true distribution is very similar for NH/IH and is very well approximated by the $\chi^2(1\text{dof})$. This is probably due to the strong correlation between the two CP phases. We conclude from this exercise that is a good approximation to define the 5σ regions in the following as those corresponding to $\Delta\chi^2 = 25$.

As indicated by the analytical results, we expect almost no dependence on the parameter θ, while the sensitivity to CP violation is expected to depend significantly on γ and M_1, which control the size of the mixing. In Fig. 5 we show the 5σ contours with $M_1 = 1$ GeV and for different values of true γ on the plane (δ, ϕ_1). The coloured regions limited by

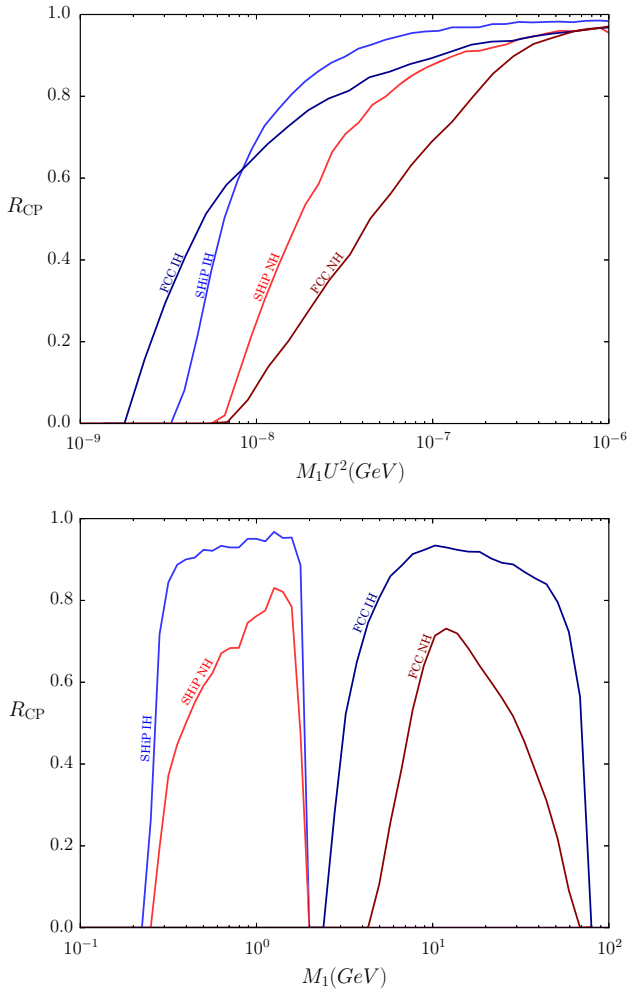

Fig. 6 CP fractions for a 5σ discovery of leptonic CP violation for the two neutrino orderings and the two experiments SHiP and FCC-ee, as a function of γ (shown in units of the more physical quantity M_1U^2) for $M_1 = 1$ GeV in SHiP and $M_1 = 30$ GeV in FCC-ee (*up*), and as a function of M_1 for $\gamma = 4$ (*down*)

the contours indicate the range of true CP phases for which leptonic CP conservation can be excluded at 5σ CL.

A nice way of quantifying the potential of SHiP and FCC-ee is provided by the CP fraction, R_{CP}, defined as the fraction of the area of the CP phase square $\delta, \phi_1 \in [0, 2\pi]$ where leptonic CP violation can be discovered (i.e. the CP conserving hypothesis excluded) at 5σ CL, in complete analogy to the CP fraction for the δ phase, often used in evaluating the sensitivity to CP violation of future long-baseline neutrino oscillation experiments. In Fig. 6 we show the R_{CP} as a function of γ and M_1.

Some observations are in order. CP fractions are significantly larger for IH than for NH, for the same γ. This can be understood because the dependence of the mixings on the phases is more suppressed in the latter. There is a very significant sensitivity to leptonic CP violation in these observables (mass and mixing to electron and muon). In SHiP with $M_1 = 1$ GeV, we obtain fractions above 70% for $\gamma \geq 3$ for IH (mixings of $\geq \mathcal{O}(10^{-8})$) and for $\gamma \geq 3.8$ for NH (mixings of $\geq \mathcal{O}(3 \times 10^{-8})$). For FCC-ee, with a mass 30 GeV, we get fractions above 70% for $\gamma \geq 3.1$ (mixings above $\mathcal{O}(4 \times 10^{-10})$) for IH and for $\gamma \geq 4.5$ (mixings above $\mathcal{O}(4 \times 10^{-9})$) for NH. The complementarity of SHiP and FCC-ee is clear, since they have sensitivity in different mass ranges. For mixings in the middle of their sensitivity region, they can reach fractions above 50% (90%) for NH(IH) in the mass range 0.4–2 GeV in SHiP, and above 50% (80%) for NH (IH) in the range 7–30 GeV in FCC-ee.

For simplicity, we have not included errors on the known oscillation parameters. In order to get a rough idea of the effect, we have considered an error on the atmospheric angle of 0.02 radians. The effect is only visible in the high sensitivity region, where the CP fraction saturates at ∼90%. We have also studied the impact of increasing the error on the determination of M_1 to 5%, and we observe a small effect in the high sensitivity region, for IH the CP fraction decreases from 98 → 96%, while for the NH the effect is a bit bigger changing from 96 → 88%. These effects are not expected to change significantly the results, but an analysis including all errors in the oscillation parameters should be done in future work.

Our analysis relies on rather simple assumptions, and should be further improved by including a realistic detector response and systematic errors. However, the potential of this measurement is excellent and we do not expect a big difference in the results when a more realistic simulation is implemented. It will also be interesting to include the extra information, provided by the measurement of the mixing to τ leptons, that should break the δ, ϕ_1 correlation to a discrete degeneracy [11]. Note also that we have only considered the contribution of one sterile state, but if there is another state in the same mass range, the statistics would improve by a factor of 2.

5 Conclusions

In seesaw models, the size of the mixing of the heavy Majorana neutrinos is strongly correlated with their masses, while their flavour structure is strongly dependent on the structure of the PMNS matrix. In the minimal seesaw model with just two right-handed neutrinos giving the largest contribution to neutrino masses, this correlation is strong enough for the ratio of the mixings to electron and muon flavours to be essentially fixed by the PMNS CP phases. In this letter we have quantified for the first time the sensitivity of these observables to leptonic CP violation in the mixing matrix. We have considered two proposed experiments SHiP and FCC-ee that have a superb sensitivity to heavy neutrinos in the mass range

between $\mathcal{O}(1–100)$ GeV. Within their range of sensitivity, we have demonstrated that the discovery of one of these massive neutrinos and the measurement of its mass and its mixings to electrons and muons can establish the existence of CP violating phases in the mixing matrix at 5σ CL, in a very significant fraction of the CP phase parameter space (>70% for mixings above $\mathcal{O}(1/3 \times 10^{-8})$ for IH/NH in SHiP and above $\mathcal{O}(4 \times 10^{-10}/4 \times 10^{-9})$ in FCC-ee).

Acknowledgements We thank A. Blondel and N. Serra useful discussions. This work was partially supported by Grants FPA2014-57816-P, PROMETEOII/2014/050 and SEV-2014-0398, as well as by the EU projects 690575—InvisiblesPlus—H2020-MSCA-RISE-2015 and 2020-MSCA-ITN-2015//674896-ELUSIVES.

References

1. P. Minkowski, Phys. Lett. B **67**, 421 (1977)
2. M. Gell-Mann, P. Ramond, R. Slansky, in *Supergravity*, ed. by P. van Nieuwenhuizen, D. Freedman (North-Holland, 1979), p. 315
3. T. Yanagida in *Proceedings of the Workshop on the Unified Theory and the Baryon Number in the Universe*, ed. by O. Sawada, A. Sugamoto (KEK Report No. 79-18, Tsukuba, 1979), p. 95
4. R.N. Mohapatra, G. Senjanovic, Phys. Rev. Lett. **44**, 912 (1980)
5. J.A. Casas, A. Ibarra, Nucl. Phys. B **618**, 171 (2001). arXiv:hep-ph/0103065
6. N. Cabibbo, Phys. Lett. **72B**, 333 (1978)
7. S.M. Bilenky, J. Hosek, S.T. Petcov, Phys. Lett. **94B**, 495 (1980). doi:10.1016/0370-2693(80)90927-2
8. J. Schechter, J.W.F. Valle, Phys. Rev. D **22**, 2227 (1980)
9. A. Donini, P. Hernandez, J. Lopez-Pavon, M. Maltoni, T. Schwetz, JHEP **1207**, 161 (2012). arXiv:1205.5230 [hep-ph]
10. I. Esteban, M.C. Gonzalez-Garcia, M. Maltoni, I. Martinez-Soler, T. Schwetz, arXiv:1611.01514 [hep-ph]
11. P. Hernandez, M. Kekic, J. Lopez-Pavon, J. Racker, J. Salvado, JHEP **1608**, 157 (2016). arXiv:1606.06719 [hep-ph]
12. T. Asaka, M. Shaposhnikov, Phys. Lett. B **620**, 17 (2005). arXiv:hep-ph/0505013
13. M. Anelli et al. [SHiP Collaboration], arXiv:1504.04956 [physics.ins-det]
14. A. Blondel et al. [FCC-ee study Team Collaboration], arXiv:1411.5230 [hep-ex]
15. J. Lopez-Pavon, S. Pascoli, C.F. Wong, Phys. Rev. D **87**(9), 093007 (2013). arXiv:1209.5342 [hep-ph]
16. D. Wyler, L. Wolfenstein, Nucl. Phys. B **218**, 205 (1983)
17. R.N. Mohapatra, J.W.F. Valle, Phys. Rev. D **34**, 1642 (1986)
18. J. Kersten, A.Y. Smirnov, Phys. Rev. D **76**, 073005 (2007). arXiv:0705.3221 [hep-ph]
19. M.B. Gavela, T. Hambye, D. Hernandez, P. Hernandez, JHEP **0909**, 038 (2009). arXiv:0906.1461 [hep-ph]
20. E. Graverini, *SHiP sensitivity to Heavy Neutral Leptons*, CERN-SHiP-NOTE-2016-003
21. A. Abada, V. De Romeri, S. Monteil, J. Orloff, A.M. Teixeira, JHEP **1504**, 051 (2015). arXiv:1412.6322 [hep-ph]
22. S. Antusch, O. Fischer, JHEP **1505**, 053 (2015). arXiv:1502.05915 [hep-ph]
23. S. Antusch, E. Cazzato, O. Fischer, arXiv:1612.02728 [hep-ph]
24. M. Dittmar, A. Santamaria, M.C. Gonzalez-Garcia, J.W.F. Valle, Nucl. Phys. B **332**, 1 (1990)
25. D. Gorbunov, M. Shaposhnikov, JHEP **0710**, 015 (2007). Erratum: [JHEP **1311**, 101 (2013)]. arXiv:0705.1729 [hep-ph]
26. A. Atre, T. Han, S. Pascoli, B. Zhang, JHEP **0905**, 030 (2009). arXiv:0901.3589 [hep-ph]
27. M. Gronau, C.N. Leung, J.L. Rosner, Phys. Rev. D **29**, 2539 (1984)
28. E. Braaten, Phys. Rev. Lett. **60**, 1606 (1988)
29. M. Blennow, P. Coloma, E. Fernandez-Martinez, JHEP **1503**, 005 (2015). arXiv:1407.3274 [hep-ph]

JHEP

Published for SISSA by Springer

Received: May 8, 2017
Accepted: June 6, 2017
Published: June 21, 2017

The seesaw portal in testable models of neutrino masses

A. Caputo,[a,b] **P. Hernández,**[a,b] **J. López-Pavón**[b] **and J. Salvado**[a]

[a] *Instituto de Física Corpuscular, Universidad de Valencia and CSIC, Edificio Institutos Investigación, Catedrático José Beltrán 2, 46980 Spain*

[b] *Theory Division, CERN, 1211 Geneve 23, Switzerland*

E-mail: andrea.caputo@cern.ch, pilar.hernandez@ific.uv.es, jacobo.lopez.pavon@cern.ch, jsalvado@ific.uv.es

Abstract: A Standard Model extension with two Majorana neutrinos can explain the measured neutrino masses and mixings, and also account for the matter-antimatter asymmetry in a region of parameter space that could be testable in future experiments. The testability of the model relies to some extent on its minimality. In this paper we address the possibility that the model might be extended by extra generic new physics which we parametrize in terms of a low-energy effective theory. We consider the effects of the operators of the lowest dimensionality, $d = 5$, and evaluate the upper bounds on the coefficients so that the predictions of the minimal model are robust. One of the operators gives a new production mechanism for the heavy neutrinos at LHC via higgs decays. The higgs can decay to a pair of such neutrinos that, being long-lived, leave a powerful signal of two displaced vertices. We estimate the LHC reach to this process.

Keywords: Beyond Standard Model, Neutrino Physics

ArXiv ePrint: 1704.08721

https://doi.org/10.1007/JHEP06(2017)112

JHEP06(2017)112

Contents

JHEP06(2017)112

1 Introduction

The measured neutrino masses and mixings provide a strong hint of physics beyond the Standard Model, and this new physics might involve new weakly coupled fields at the electroweak scale. The simplest of these possibilities is an extension of the Standard Model with just two singlet Majorana fermions. This model has been shown to provide a natural explanation of the matter-antimatter asymmetry of the Universe [1–15] via neutrino oscillations [16] if the two heavy singlets have masses in the range $[1, 10^2]$ GeV, a range that implies that these states could be produced and searched for in beam dump experiments (for a recent review see [17]) and colliders (for a sample set of references see [18–33]). This opens the possibility of making this baryogenesis scenario testable: the combination of measurements of the mixings and masses of the heavy neutrino states, together with the determination of the CP phase δ in future oscillation experiments and the amplitude of neutrinoless double beta decay might lead to a quantitative prediction of the baryon asymmetry in the universe [13].

The constraint of the measured neutrino masses and mixings fixes to a large extent the flavour mixings of the heavy neutrino states [13]. In particular, it has been shown that the ratios of mixings to different lepton flavours are strongly correlated with the CP violating phases of the PMNS matrix [34]. One of the most drastic implications of this minimal model is the vanishing of the lightest neutrino mass. If evidence of a non-vanishing lightest neutrino mass would come from future beta-decay experiments or from cosmological measurements, the minimal model with two neutrinos would not be able to explain it and an extension would be required.

The question we would like to address in this paper is the following. If there is some extra new physics at a higher scale (for example more singlet states), how does this new

physics would modify the predictions of the low-energy theory represented by the minimal model with the two singlet states. In particular, we would like to understand if the strong correlations between the light and heavy neutrino masses and mixings [34] that underlie the predictivity and testability of this model could be preserved or under what conditions they might be.

A model independent way of answering this question is by building the effective theory and analysing what modifications on the correlations higher dimensional operators can induce. The list of higher dimensional operators in the SM up to dimension $d = 6$ is well-known [35–37] and has been studied extensively. Interestingly however in the extended theory with fermion singlets [38–40], there are more $d = 5$ operators than in the SM. The relatively light singlet states provide a new portal into BSM physics. In this paper we will restrict ourselves to the lowest dimensional operators of $d = 5$, which are expected to be dominant.

The paper is organized as follows. In the section 2 we describe the minimal model and the extension by $d = 5$ operators. In section 3 we consider the different constraints on the $d = 5$ operators from neutrino masses and LHC and in section 4 we conclude.

2 The seesaw effective theory

At energies much smaller than the new physics scale, Λ, the theory is just a type I seesaw model [41–44] with two Majorana neutrinos in the GeV range, with the Lagrangian

$$\mathcal{L}_{SS} = \mathcal{L}_{SM} - \sum_{\alpha,i} \bar{L}_\alpha Y^{\alpha i} \tilde{\Phi} N_i - \sum_{i,j=1}^{2} \frac{1}{2} \overline{N_i^c} M_N^{ij} N_j + h.c.$$

The leading effects of the new physics should be well described by higher dimensional operators of $d = 5$ that can be constructed in a gauge invariant way with the Standard Model fields and the heavy Majorana neutrinos. These have been classified in refs. [38–40]. There are three independent operators:

$$\mathcal{O}_W = \sum_{\alpha,\beta} \frac{(\alpha_W)_{\alpha\beta}}{\Lambda} \overline{L}_\alpha \tilde{\Phi} \Phi^\dagger L_\beta^c + h.c., \tag{2.1}$$

$$\mathcal{O}_{N\Phi} = \sum_{i,j} \frac{(\alpha_{N\Phi})_{ij}}{\Lambda} \overline{N}_i N_j^c \Phi^\dagger \Phi + h.c., \tag{2.2}$$

$$\mathcal{O}_{NB} = \sum_{i \neq j} \frac{(\alpha_{NB})_{ij}}{\Lambda} \overline{N}_i \sigma_{\mu\nu} N_j^c B_{\mu\nu} + h.c. \tag{2.3}$$

The first is the well known Weinberg operator $\mathcal{O}_W$ [35] that induces a new contribution to the light neutrino masses, independent of the contribution of the N fields. The new operator $\mathcal{O}_{N\Phi}$ contributes to the N Majorana masses, and interestingly gives additional couplings of these heavy neutrinos to the Higgs [19, 38], which are not necessarily suppressed with the Yukawa couplings. Constrains on this operator have been extensively studied in the context of Higgs portal dark matter [45]. In that case however, it is assumed that the

JHEP06(2017)112

Majorana fermion constitutes the dark matter and therefore does not decay, for which it is necessary to forbid the yukawa coupling to the lepton doublet. In our case the states can decay visibly in the detector. The last operator induces magnetic moments of the heavy neutrinos and the constraints have been studied in [40].

We will see in the following that the direct constraints on the coefficients of these operators are very different. It is therefore an important question whether large hierarchies could exist between the coefficients. On naturality grounds we would expect they should of the same order

$$\frac{\alpha_W}{\Lambda} \sim \frac{\alpha_{N\Phi}}{\Lambda} \sim \frac{\alpha_{NB}}{\Lambda}. \tag{2.4}$$

However this might not be the case if there exists an approximate global $\mathrm{U}(1)_L$ symmetry [46, 47]. If the two Majorana neutrinos carry opposite lepton number charges, the Majorana mass term can be chosen to be of the form

$$M_N = \begin{pmatrix} 0 & M \\ M & 0 \end{pmatrix}, \tag{2.5}$$

to ensure an exact symmetry, implying degenerate heavy neutrinos and massless light neutrinos. We note that this approximate $\mathrm{U}(1)_L$ symmetry is also usually invoked in the minimal model to justify yukawa couplings larger than the naive seesaw relation $Y \sim \sqrt{\frac{Mm_\nu}{v^2}}$, that are required to be within the sensitivity reach of future experiments.

The operator $\mathcal{O}_{NB}$ is invariant, while the operator $\mathcal{O}_{N\Phi}$ is invariant provided the flavour structure of the coefficient is of the same form as the Majorana mass,

$$\alpha_{N\Phi} = \begin{pmatrix} 0 & \alpha \\ \alpha & 0 \end{pmatrix}. \tag{2.6}$$

Only the Weinberg operator violates lepton number in this case. If we assume the symmetry is approximately conserved, since we need to accommodate neutrino masses, it is technically natural in this context to assume the following hierarchy

$$\frac{\alpha_W}{\Lambda} \ll \frac{\alpha_{N\Phi}}{\Lambda} \sim \frac{\alpha_{NB}}{\Lambda}. \tag{2.7}$$

A hierarchy also arises in the context of minimal flavour violation [48–50]. As discussed in [38], in this case the coefficients $\alpha_W \sim \alpha_{NB} \sim \mathcal{O}(Y^2)$, while there is no suppression of $\alpha_{N\Phi}$.

On the other hand, if we drop completely the naturalness argument, we have to confront a hierarchy problem. All the $d = 5$ operators generically mix under renormalization. For example the diagram of figure 1 induces a contribution to the Weinberg operator at one loop of the form

$$\delta\left(\frac{\alpha_W}{\Lambda}\right) \propto \frac{1}{(4\pi)^2} \frac{Y \alpha_{N\Phi} Y^T}{4\Lambda} \log \frac{\mu^2}{M^2}. \tag{2.8}$$

JHEP06(2017)112

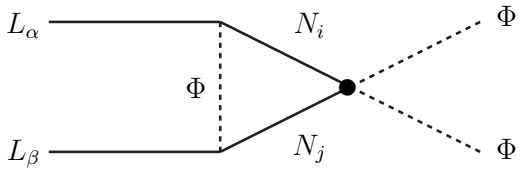

Figure 1. One loop contribution of $\mathcal{O}_{N\Phi}$ to the neutrino masses.

Requiring this contribution to be of the same order or smaller than the tree level contribution implies the following bound

$$\frac{\alpha_{N\phi}}{\Lambda} \lesssim \frac{2 \cdot 10^{13}}{\log \frac{\mu^2}{M^2}} \left(\frac{10^{-6}}{\theta^2}\right) \left(\frac{\text{GeV}}{M}\right)^2 \frac{\alpha_W}{\Lambda}, \tag{2.9}$$

where θ is the mixing of the heavy states with the leptons. This constraint is rather mild and leaves significant freedom to have a large hierarchy, even if no symmetry principle is assumed.

3 Constraints on the $d = 5$ operators

3.1 Neutrino masses

The operator $\mathcal{O}_{N\Phi}$ gives a correction to the Majorana neutrino mass matrix:

$$M' = M + v^2 \frac{\alpha_{N\Phi}}{\Lambda}. \tag{3.1}$$

The light neutrino masses get a contribution from the two light states, and from new physics at the scale Λ. We call this latter contribution δm_ν^W:

$$m_\nu = \left(-Y \frac{1}{M'} Y^T + 2\frac{\alpha_W}{\Lambda}\right) \frac{v^2}{2} \equiv -Y \frac{1}{M'} Y^T \frac{v^2}{2} + \delta m_\nu^W. \tag{3.2}$$

The diagonalization of the complete light neutrino mass matrix gives:

$$m_\nu = -\frac{v^2}{2} Y \frac{1}{M'} Y^T + \delta m_\nu^W = U m_l U^T. \tag{3.3}$$

where U is the standard PMNS matrix, $m_l = \text{diag}\,(m_1, m_2, m_3)$ are the light neutrino masses. We know that in the limit $\delta m_\nu^W \to 0$, $m_1(m_3) \to 0$ for the normal (inverted) hierarchy (NH/IH) or equivalently the condition

$$\det\left[U m_l U^T - \delta m_\nu^W\right] = 0 \tag{3.4}$$

must hold. Perturbing in $(\delta m_\nu^W)_{ij} = \delta_{ij}$ and the small light neutrino parameters $\theta_{13} \sim \theta_{23} - \pi/4 \sim r \equiv \Delta m^2_{\text{sol}}/\Delta m^2_{\text{atm}}$, all of which are taken of the same order, $\mathcal{O}(\epsilon) \sim \mathcal{O}(\delta)$, we

obtain at leading order:

NH: (3.5)

$$m_1 = -\left[U^\dagger m_l U^*\right]_{11} = \frac{-e^{2i\phi_1}}{2}\left[2\delta_{11}c_{12}^2 + (\delta_{22} - 2\delta_{23} + \delta_{33})s_{12}^2 + \sqrt{2}(\delta_{13} - \delta_{12})\sin 2\theta_{12}\right] + \mathcal{O}(\epsilon\,\delta)\,,$$

IH: (3.6)

$$m_3 = -\left[U^\dagger m_l U^*\right]_{33} = \frac{-e^{2i\phi_1}}{2}(\delta_{22} + 2\delta_{23} + \delta_{33}) + \mathcal{O}(\epsilon\,\delta)\,. \tag{3.7}$$

Barring fine-tuned cancellations among the δ_{ij} coefficients, we have therefore

$$\delta_{ij} = \frac{(\alpha_W)_{ij}v^2}{\Lambda} \sim \mathcal{O}(1)\, m_{1,3}. \tag{3.8}$$

The lightest neutrino mass is thus the measure of the non-standard contributions from $\mathcal{O}_W$.

3.2 Heavy neutrino mixing

The heavy states mix with the charged leptons inducing charged and neutral currents as well as higgs interactions. All these get modified by the $d = 5$ operators. In the mass basis the heavy neutrinos interact with the Z and W via the interactions:

$$-\frac{g}{\sqrt{8}}U_{\alpha 3+i}\bar{l}_\alpha\gamma_\mu(1-\gamma_5)N_i W_\mu^- - \frac{g}{4\cos\theta_W}U_{\alpha 3+i}\bar{\nu}^\alpha\gamma_\mu(1-\gamma_5)N_i Z_\mu + h.c. \tag{3.9}$$

where N_i are now the mass eigenstates, $i = 1, 2$ and $U_{\alpha 3+i}$ are their mixings to the flavours $\alpha = e, \mu, \tau$. These mixings are related to the Yukawa couplings as

$$U_{\alpha 3+i} \simeq \frac{v}{\sqrt{2}}(Y M'^{-1})_{\alpha i}. \tag{3.10}$$

We can use the Casas-Ibarra trick [51] to parametrize Y in terms of $\widetilde{m}$ and $\widetilde{U}$ where

$$m_\nu - \delta m_\nu^W = -\frac{v^2}{2}Y M^{-1} Y^T \equiv \widetilde{U}\widetilde{m}\widetilde{U}^T, \tag{3.11}$$

and a generic 2×2 complex orthogonal matrix R. In this parametrization the mixings are

$$U_{\alpha 3+i} = i(\widetilde{U}\widetilde{m}^{1/2}R^\dagger M'^{-1/2})_{\alpha i}. \tag{3.12}$$

In the limit $\delta m_\nu^W \to 0$, $\widetilde{m}$ and $\widetilde{U}$ coincide with the light neutrino masses and mixing matrix. It has been shown that in this case the flavour structure of the mixings is approximately fixed those neutrino oscillation observables [13, 50, 52]. Simple analytical approximations were worked out in [13] that should be accurate in the sensitivity region of future experiments. These are shown in figure 2, where we show the allowed range for normalized flavour mixings: $|U_{\alpha 3+i}|^2/\bar{U}^2$, with $\bar{U}^2 \equiv \sum_\alpha |U_{\alpha 3+i}|^2$, fixing the known oscillation parameters to their best fit values [53], and varying the CP violating phases δ and ϕ_1 in the whole physical range (the second Majorana phase is unphysical for two heavy neutrinos). It has

JHEP06(2017)112

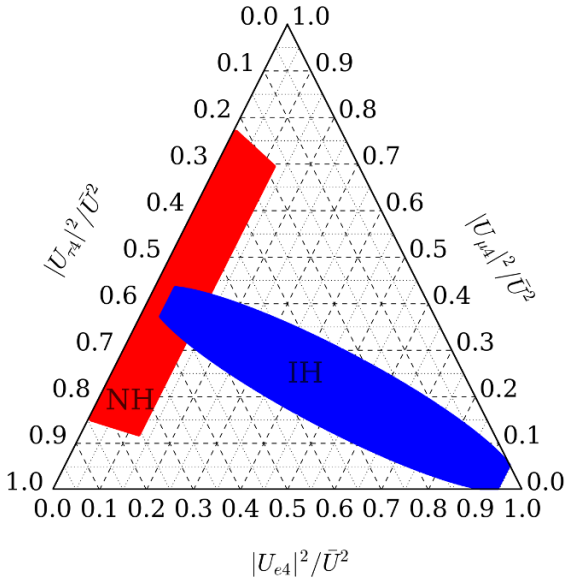

Figure 2. Ternary diagram for the normalized flavour mixings $|U_{\alpha i}|^2/\bar{U}^2$ (in the large mixing regime) fixing the known oscillation parameters to their best fit values and varying the CP phases from $[0, 2\pi]$ for NH (red) and IH (blue).

been shown that the determination of these ratios in future experiments would give very valuable information on the CP phases [34].

In general however the parameters $\tilde{U}$ and $\tilde{m}$ are sensitive to new physics. We can relate them to the physical mixings and masses using perturbation theory in $\delta m_\nu^W = \mathcal{O}(\delta)$. For NH we have

$$\widetilde{U}\widetilde{m}^2\widetilde{U}^\dagger = U\mathrm{diag}\left(0, m_2^2, m_3^2\right)U^T + \left\{U\mathrm{diag}\left(0, m_2, m_3\right)U^T, \delta m_\nu^{W\dagger}\right\} + \mathcal{O}\left(\delta^2\right), \quad (3.13)$$

where $\{,\}$ is the anticommutator. For IH the result is the same with $m_3 \to m_1$ and moved to the first position. Here we have used that $m_1/m_3 = \mathcal{O}(\delta)$. The first order corrections $\mathcal{O}(\delta)$ to $\tilde{m}$ and $\tilde{U}$ are presented in appendix A.

Including these in eq. (3.12) we find that the approximate expressions for the mixings in the absence of extra dynamics derived in ref. [13] get modified by corrections $\delta|U_{\alpha i}|^2$. For NH we get

$$\delta|U_{e4}|^2 M_1 = A\, c_e \frac{m_1}{\sqrt{\Delta m^2_{\mathrm{atm}}}}, \quad \delta|U_{\mu 4}|^2 M_1 = A\, c_\mu \frac{m_1}{\sqrt{r\Delta m^2_{\mathrm{atm}}}}, \quad (3.14)$$

where $A = e^{2\gamma}\sqrt{\Delta m^2_{\mathrm{atm}}}/4$. Similarly for IH:

$$\delta|U_{e4}|^2 M_1 = A\, c'_e \frac{m_3}{\sqrt{\Delta m^2_{\mathrm{atm}}}}, \quad \delta|U_{\mu 4}|^2 M_1 = A\, c'_\mu \frac{m_3}{\sqrt{\Delta m^2_{\mathrm{atm}}}}, \quad (3.15)$$

and $\delta|U_{\alpha 4}|^2 M_1 = \delta|U_{\alpha 5}|^2 M_2$ at this order for both hierarchies. Barring fine tuning among the different entries in δm_ν^W and taking into account eq. (3.8), the coefficients c_α and c'_α are expected to be $\mathcal{O}(1)$. In figure 3 we show the impact of these corrections to the ratio

JHEP06(2017)112

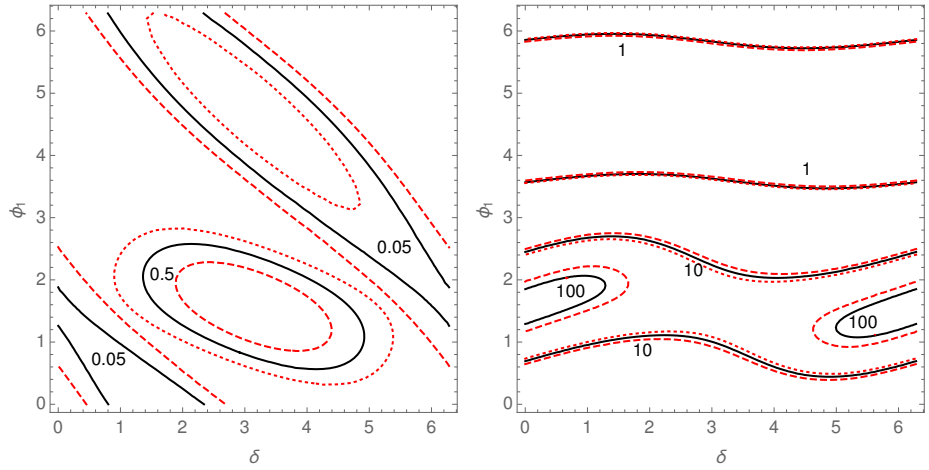

Figure 3. Contours of constant ratio $|U_{ei}|^2/|U_{\mu i}|^2$ as a function of the two CP phases δ, ϕ_1 for NH(left) and IH(right). The three curves correspond to no Λ^{-1} corrections (solid black) and minimal or maximal (red dashed) deviations within the range $c_\alpha, c'_\alpha \in [-1, 1]$.

$|U_{e4}|^2/|U_{\mu 4}|^2$ dependence on the CP phases for $m_{1,3} = 0.1\sqrt{\Delta m^2_{\rm sol}}$ and varying c_α and c'_α between -1 and 1 to maximize the difference. The corrections to the flavour ratios are therefore of $O(m_{\rm lightest}/\sqrt{\Delta m^2_{\rm atm}})$ for IH and of $O(m_{\rm lightest}/\sqrt{\Delta m^2_{\rm solar}})$ for NH. It will be hard experimentally to ensure that these corrections are sufficiently small, in other words to prove that $m_{\rm lightest}$ is significantly smaller than $\sqrt{\Delta m^2_{\rm atm}}$ for IH and $\sqrt{\Delta m^2_{\rm solar}}$ for NH. On the other hand, measuring a lightest neutrino mass above this value will surely imply that corrections to the predictions of the minimal model are likely to be significant. Alternatively finding the flavour ratios in the regions given by figure 2 would be a strong indication that only two Majorana states give the dominant contribution to the light neutrino masses and therefore the lightest neutrino mass is significantly smaller than the mass splittings.

3.3 Higgs-neutrino interactions

Interestingly the operator $\mathcal{O}_{N\Phi}$ induces new higgs interactions with the right handed neutrinos. In particular for $M_i \leq \frac{M_H}{2}$, the Higgs can decay to two heavy neutrinos via this coupling

$$\mathcal{L} \supset -\frac{v}{\sqrt{2}\Lambda} H \overline{N}^c \alpha_{N\Phi} N + h.c. \tag{3.16}$$

This decay leads to a spectacular signal at LHC, which is that of a pair of displaced vertices (DVs) since the N decay only via mixing and they have a long decay length. The process is depicted in figure 4 Note that compared to the minimal model, where the sterile neutrinos are singly produced via mixing, in this case the production is controlled by the coefficient $\alpha_{N\Phi}$ and therefore one should have access to much smaller mixings, as long as they lead to lifetimes are within reach of DV searches within the detectors.

Our aim in this section is to do a simple estimate of the bounds on the coupling $\alpha_{N\Phi}/\Lambda$ from searches of higgs decays to two displaced vertices at LHC. A closely related calculation

JHEP06(2017)112

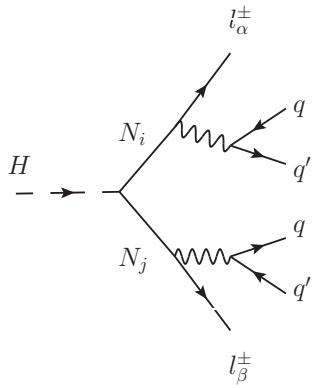

Figure 4. Higgs decay to two heavy neutrinos leading to displaced vertices.

has been done in the context of U(1)′ models in [54], where the signal selection has been performed following recent searches by the CMS collaboration [55, 56]. We have considered two different analyses: 1) a search of displaced tracks in the inner tracker where at least one displaced lepton, e or μ, is reconstructed from each vertex; 2) a search for displaced tracks in the muon chambers and outside the inner tracker where at least one μ is reconstructed from each vertex. The charges are not restricted and therefore events with same-sign or opposite sign leptons are possible.

For simplicity we will consider only semileptonic decays of the N_i which give rise to two lepton final states through the decay

$$N_i \to l^{\pm} W^{\mp} \to l^{\pm} q \bar{q}'. \tag{3.17}$$

We consider a parton-level Monte Carlo analysis using Madgraph5 [57] at LHC with a center-of-mass energy of 13TeV and $300\,\mathrm{fb}^{-1}$ luminosity. We include only the dominant gluon fusion higgs production and we consider the production of just one neutrino species, N_1. The production cross section $pp \to h \to N_1 N_1$ is shown in figure 5 as a function of the heavy neutrino mass for various values of the coupling $g_{N\Phi} \equiv \frac{v(\alpha_{N\Phi})_{11}}{\sqrt{2}\Lambda}$. In figure 6 we show the $\mathrm{Br}(H \to N_1 N_1)$ as a function of $g_{N\Phi}$ for various values of the mass (here we assume the higgs decays just to one neutrino).

The p_T of the two leading leptons is shown in figure 7. Following [54], the signal selection is done by requiring two lepton tracks, e or μ that satisfy the following kinematical cuts on transverse momentum, pseudorapidity and isolation of the two tracks:

$$p_T(l) > 26\ \mathrm{GeV}, \quad |\eta| < 2, \quad \Delta R > 0.2, \quad \cos\theta_{\mu\mu} > -0.75. \tag{3.18}$$

In the case of muons a constraint in the opening angle $\theta_{\mu\mu}$ is imposed in order to reduce the cosmic muon background. The efficiencies resulting from these consecutive cuts for various neutrino masses are shown in tables 1 and 2. Note that they do not depend on the mixings $|U_{\alpha i}|^2$.

For each event the decay length of each neutrino in the laboratory frame is obtained from their simulated momenta and the distance travelled, L, is randomly sampled according

JHEP06(2017)112

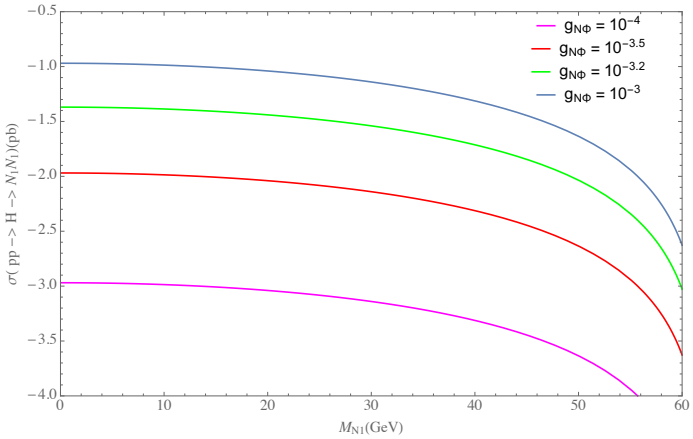

Figure 5. Cross section $pp \to H \to N_1 N_1$ in pb as a function of the heavy neutrino mass, M_1 for a few values of $g_{N\Phi} \equiv \frac{v(\alpha_{N\Phi})_{11}}{\sqrt{2}\Lambda}$.

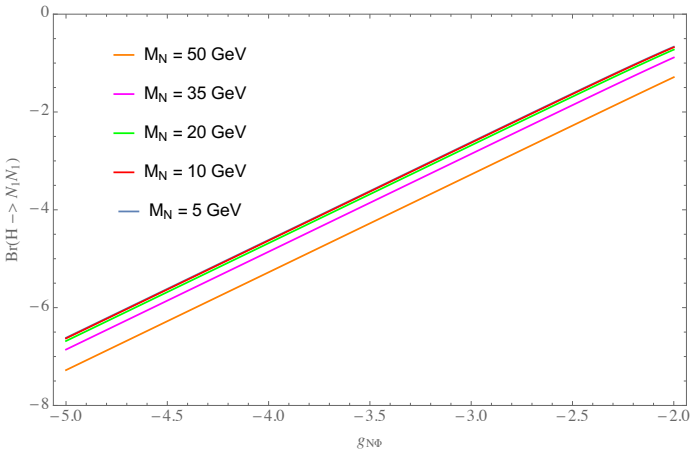

Figure 6. $\mathrm{Br}(H \to N_1 N_1)$ as a function of the $g_{N\Phi}$ for various masses M_1.

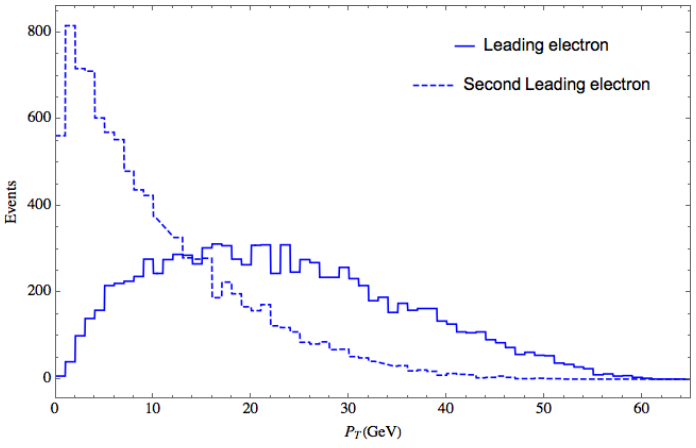

Figure 7. p_T distribution of the two leading electrons for $M = 15\mathrm{GeV}$.

JHEP06(2017)112

ee	$M_1 = 10\,\text{GeV}$	$M_1 = 20\,\text{GeV}$	$M_1 = 30\text{GeV}$	$M_1 = 40\,\text{GeV}$
p_T	6.4%	7.0%	5.6%	4.5%
η	4.2%	4.8%	4%	2.9%
ΔR	4.2%	4.8%	4%	2.9%

Table 1. Signal efficiciencies after consecutive cuts on p_T, η and ΔR for the ee channel in the inner tracker, for various heavy neutrino masses.

$\mu\mu$	$M_1 = 10\text{G}\,\text{eV}$	$M_1 = 20\,\text{GeV}$	$M_1 = 30\,\text{GeV}$	$M_1 = 40\,\text{GeV}$
p_T	7.0%	6.8%	6.0%	4.7 %
η	4.7%	4.9%	4%	3.2%
ΔR	4.7%	4.9%	4%	3.2%
$\cos\theta_{\mu\mu}$	3.2%	3.6%	3.0%	2.7%

Table 2. Signal efficiciencies after consecutive cuts on p_T, η and ΔR for the $\mu\mu$ channel in the muon chamber for various heavy neutrino masses.

to the expected exponential distribution. The impact parameter of the lepton in the transverse direction d_0 is defined as

$$d_0 = |L_x p_y - L_y p_x|/p_T, \tag{3.19}$$

where $L_{x,y,z}$ are the X, Y, Z projections of the vector $L\vec{u}$, where $\vec{u}$ is the velocity of the heavy neutrino, and (p_x, p_y) is the momentum of the lepton in the transverse direction.

The cuts associated to the displaced tracks are different for the two analyses [54]:

- Inner tracker (IT):

$$10\,\text{cm} < |L_{xy}| < 50\,\text{cm}, \quad |L_z| \leq 1.4\,\text{m}, \quad d_0/\sigma_d^t > 12, \tag{3.20}$$

  where $\sigma_d^t \simeq 20\,\mu\text{m}$ is the resolution in the tracker.

- Muon chambers (MC):

$$|L_{xy}| \leq 5\,\text{m}, \quad |L_z| \leq 8\,\text{m}, \quad d_0/\sigma_d^\mu > 4, \tag{3.21}$$

  where the impact parameter resolution in the chambers is $\sigma_d^\mu \sim 2\,\text{cm}$.

Since $\langle L^{-1}\rangle \propto U^2 M^6$, we expect that these cuts depend mostly on this combination of mass and mixing with some dispersion. In figure 8 we show the acceptance given by cuts of eqs. (3.20) and (3.21) as a function of $U^2 M^6$. As expected the two analyses are sensitive to different decay lengths. We have checked that the global efficiencies resulting for each of these cuts agree reasonably well with the results quoted in [54].

Concerning the flavour structures, we have considered two scenarios:

- Scenario A: only the decay of the higgs to one neutrino species, N_1, is considered. Obviously if the other state has a mass below $M_H/2$, it will also contribute via the

JHEP06(2017)112

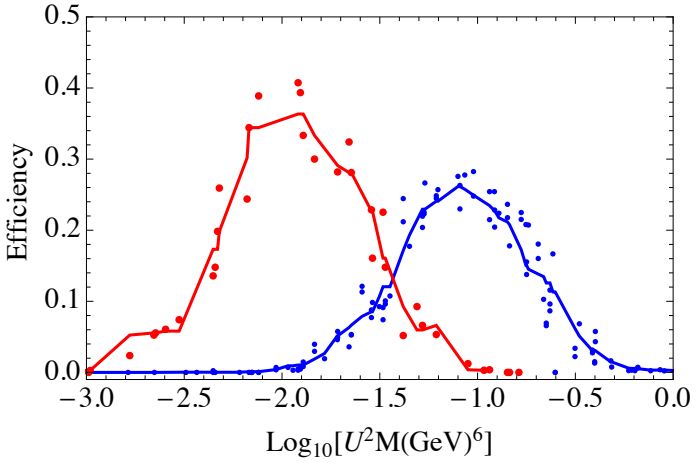

Figure 8. Acceptance of the cuts in eqs. (3.20) in blue and (3.21) in red as a function of the combination U^2M^6.

decays $H \to N_2N_2$ and $H \to N_1N_2$. These will be sensitive however to different entries of the matrix $\alpha_{N\Phi}$.

In figure 9 we show the $BR(H \to N_1N_1)$ corresponding to 4 signal events as a function of $\frac{M_H}{2M} \times c\tau$ which is approximately the decay length in the laboratory frame. We present the results that include the events producing two displaced electrons in the inner tracker, and either two displaced μ in the inner tracker (IT analysis) or two displaced muons in the muon chamber (MC analysis). We compare these limits with the those of the Mathusla project of the HL-LHC with $3000\, fb^{-1}$ as obtained in ref. [58], where all the decays of the N_1 are assumed observed. The limit this implies on the coefficient of the operator, $g_{N\Phi}$ can then be read from figure 6.

As we have seen the flavour structure of the mixings depends strongly on the hierarchy and the CP phases (see figure 2). We fix the CP phases to $\delta = 0, \phi_1 = \pi/2$. For this choice and NH, the muon channels dominates, while for IH it is the electron that dominates. In the former case therefore the reach of the two analysis IT and MC are quite different, showing the reach in complementary regions of $c\tau$, while for the latter most of the sensitivity comes from the electron search which contributes the same to both analyses as it can only be done with the tracker. The dependence on the phases is illustrated in figure 10 where the phase ϕ_1 is chosen approximately to maximize/minimize the sensitivity.

- Scenario B: the flavour structure of the matrix $\alpha_{N\Phi}$ is such that the operator is symmetric under a global $U(1)_L$ symmetry. The symmetry is very transparent in the basis where the Majorana neutrino mass matrix and $\alpha_{N\Phi}$ are of the form

$$M = \begin{pmatrix} 0 & M \\ M & 0 \end{pmatrix}, \alpha_{N\Phi} = \begin{pmatrix} 0 & \alpha \\ \alpha & 0 \end{pmatrix}. \tag{3.22}$$

This pattern ensures that a lepton number is preserved under which N_1 and N_2 have opposite charges. In the same basis only N_1 has Yukawa couplings. As a result of the

JHEP06(2017)112

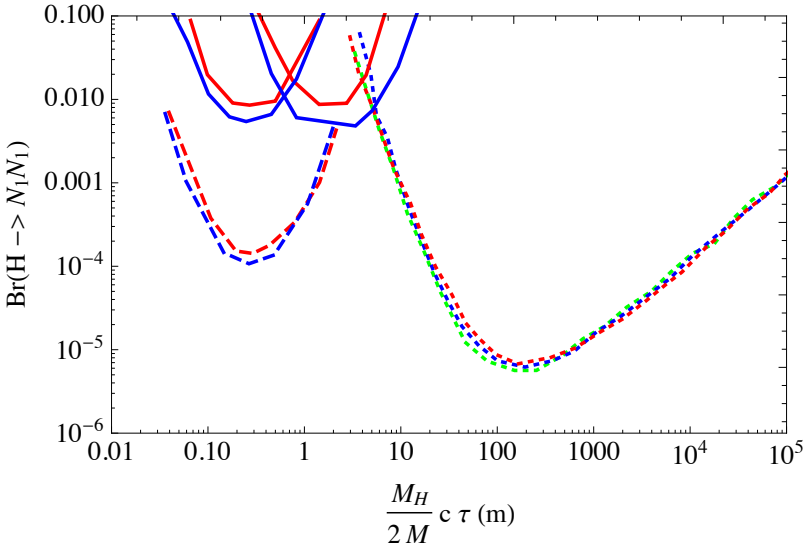

Figure 9. Expected limits at LHC (13 TeV, 300 fb^{-1}) on the $BR(H \to N_1N_1)$ for scenario A as a function of $\frac{M_H}{2M}c\tau$ in meters. The solid lines correspond to the IT and MC analyses with $M_1 = 20$GeV (blue) and $M_1 = 35$GeV (red) for NH and CP phases $\delta = 0, \phi_1 = \pi/2$. The dashed lines are for IH and the same CP phases for IT/MC . The dotted lines correspond to the estimated reach of Mathusla in the HL-LHC (14TeV, 3000 fb^{-1}) [58] for masses $5, 20, 40$GeV, assuming that all the decays of N_1 are observable.

approximate symmetry same sign lepton decays vanish, the massive state is a Dirac fermion. The branching ratios are however unchanged. The bounds on this scenario also can be read from figure 9, if we interpret the y-axis as the total branching ratio of the higgs to the heavy Dirac state. On other hand the dependence of this branching ratio on the coupling $g_{N\Phi}$ is twice larger as that shown in figure 6.

4 Discussion

In order to explain the observed neutrino masses in the context of Type I seesaw models, only two heavy Majorana singlets are required. This is the minimal extension of the Standard Model that can accommodate neutrino masses. The flavour structure of the mixings of the heavy neutrino mass eigenstates is strongly correlated with the light neutrino masses and the PMNS matrix. If the mass of these heavy states is in the electroweak range, they can be searched for in future experiments within the high intensity frontier. A putative measurement of their masses and mixings might demonstrate the origin of neutrino masses. The predictivity of this minimal model relies on the assumption that only these two states give the dominant contribution to neutrino masses. Any extension of this minimal scenario can modify these predictions. We have considered the possible modifications on the minimal scenario induced by generic new physics at some higher scale Λ. Three operators can parametrize these modifications at leading order in Λ^{-1}.

JHEP06(2017)112

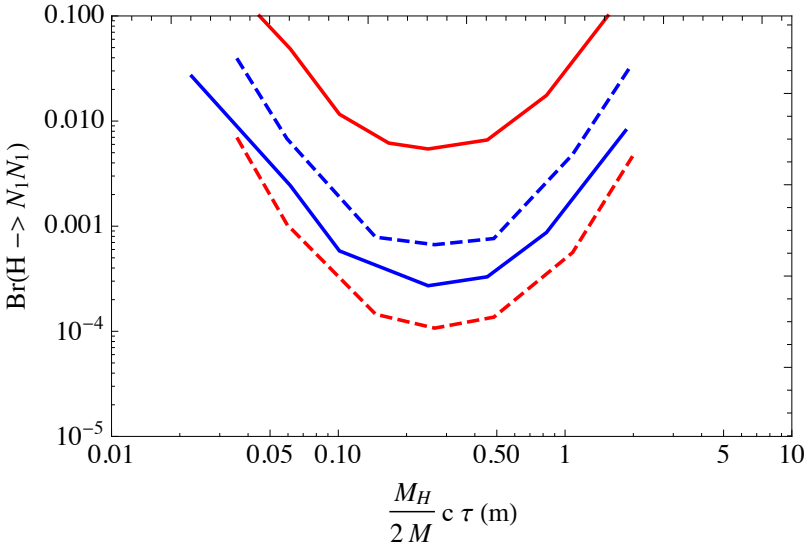

Figure 10. Expected limits at LHC (13 TeV, 300 fb^{-1}) on the $BR(H \to N_1 N_1)$ for scenario A as a function of $\frac{M_H}{2M} c\tau$ in meters. The mass is 20 GeV and the CP phase $\phi_1 = -\pi/2$ (blue) or $\phi_1 = \pi/2$ (red) for NH (solid) and IH (dashed).

Assuming the coefficients of these operators are all of the same order, the strongest bound comes from the bound on the lightest neutrino mass:

$$\left|\frac{\alpha_W v^2}{\Lambda}\right| \leq \mathcal{O}(1) m_{\text{lightest}} \to \frac{\alpha_W}{\Lambda} \leq 3 \times 10^{-12} \text{TeV}^{-1} \left(\frac{m_{\text{lightest}}}{0.2\text{eV}}\right) \tag{4.1}$$

A more stringent bound needs to be imposed generically to preserve the flavour predictions of the minimal model in the presence of new physics. Corrections to these predictions from the Weinberg operator are of $\mathcal{O}\left(\frac{m_{\text{light}}}{\sqrt{\Delta m^2_{\text{atm}}}}\right)$ for IH or $\mathcal{O}\left(\frac{m_{\text{light}}}{\sqrt{\Delta m^2_{\text{sol}}}}\right)$ for NH, and this is only warrantied in the hierarchical scenario where m_{light} is smaller than 0.05 eV.

A possible extension of the minimal scenario that gives rise to the Weinberg operator is obviously the addition of extra Majorana singlets. In particular, in the case where one more neutrino is added, it is necessary that the mass is larger and/or the mixings smaller. This is for example the case in the νMSM [1], where the extra keV state is very weakly coupled, so that the contribution to the lightest neutrino mass is below 10^{-5}eV, well below the above requirement.

On the other hand, large hierarchies $\alpha_W \ll \alpha_{N\Phi} \sim \alpha_B$ could be present undisrupted by radiative corrections. In this case, direct bounds on the other two $d = 5$ operators might be competitive and offer a new window into neutrino physics at the LHC. We have considered the bounds on $\alpha_{N\Phi}$ from searches of displaced leptons at LHC and we have found that LHC with 300 fb^{-1} at 13TeV could set bounds

$$\left|\frac{\alpha_{N\Phi} v}{\sqrt{2}\Lambda}\right| \leq 10^{-3} - 10^{-2} \to \frac{\alpha_{N\Phi}}{\Lambda} \leq 6 \times (10^{-3} - 10^{-2}) \text{TeV}^{-1}. \tag{4.2}$$

It is important to note that if the coefficient of this operator is above this sensitivity limit, LHC could detect the sterile neutrinos for significantly smaller mixings than it is possible

JHEP06(2017)112

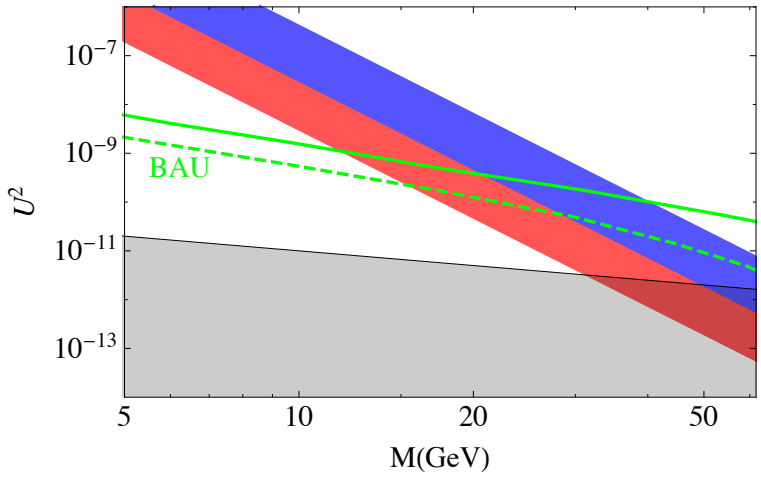

Figure 11. Regions on the plane (M, U^2) where LHC displaced track selection efficiency (eq. (3.20) and (3.21)) is above 10% in the IT (blue band) and MC (red band). The grey shaded region cannot explain the light neutrino masses and the green lines correspond to the upper limits of the 90%CL bayesian region for successful baryogenesis in the minimal model for NH (solid) and IH (dashed), taken from [13].

in the minimal model, in particular LHC could even reach the seesaw limit as shown in figure 11. This is because the production rate of these neutrinos depends on $\alpha_{N\Phi}$ and not on the mixing, while the possibility of detection depends on the lifetime in the laboratory frame and therefore scales with M^6U^2.

The bounds on α_{NB} were considered in ref. [40] and found to be

$$\frac{\alpha_{NB}}{\Lambda} \leq 10^{-2} - 10^{-1}\text{TeV}^{-1}. \tag{4.3}$$

These operators could appear at tree level in extensions with scalar singlets, such as the Majoron model, where the singlet can couple to the singlet Majorana contraction $\bar{N}N^c$ and the Higgs portal $\Phi^\dagger\Phi$. The exchange of the singlet scalar leads at tree level to the operator $\mathcal{O}_{N\Phi}$. On the other hand the operator $\mathcal{O}_{NB}$ needs to be generated at one loop.

It is important to note that, while the operators $\mathcal{O}_{N\Phi}$ and $\mathcal{O}_{NB}$ do not contribute to neutrino masses directly and therefore do not modify the predictions of the minimal model, they in general mix with the operator $\mathcal{O}_W$ that does. We have estimated this correction in eq. (2.8). If we saturate the bounds that can be obtained from LHC, eq. (4.2), the correction to α_W/Λ is

$$\delta\left(\frac{\alpha_W}{\Lambda}\right) \sim 6 \times (10^{-16} - 10^{-15})\text{TeV}^{-1}\left(\frac{\theta^2}{10^{-6}}\right)\left(\frac{M}{\text{GeV}}\right)^2 \log\left(\frac{\mu}{M}\right), \tag{4.4}$$

leading to contribution to the light neutrino masses of order

$$\delta m_{\text{light}} \sim 4 \times (10^{-3} - 10^{-2})\sqrt{\Delta m^2_{\text{sol}}}\left(\frac{\theta^2}{10^{-6}}\right)\left(\frac{M}{\text{GeV}}\right)^2 \log\left(\frac{\mu}{M}\right), \tag{4.5}$$

below the limit that would significantly modify the predictions of the minimal model on the heavy flavour mixing ratios.

JHEP06(2017)112

Flavour symmetries could explain a large hierarchy between α_W and $\alpha_{N\Phi}$ or α_{NB}. An approximate $\mathrm{U}(1)_L$ could explain the hierarchy $\alpha_W \ll \alpha_{N\Phi}, \alpha_{NB}$. Such symmetry is also the most natural scenario within the minimal model to have mixings significantly larger than the naive seesaw limit as required for their observability. Similarly, hierarchies of this type or $\alpha_W, \alpha_{NB} \ll \alpha_{N\Phi}$ are expected in the context of minimal flavour violation [38].

As we have seen, the presence of large contributions from these operators do not modify the predictions concerning the flavour structure of the mixings of the heavy neutrinos, but they could provide a new portal at colliders to reveal the mechanism behind neutrino masses. On the other hand the same interactions will surely affect the baryogenesis scenario with respect to the minimal model, since the sterile neutrinos can reach thermal equilibrium if the interactions induced by the higher dimensional operators are within LHC reach. The impact of $\mathcal{O}_{N\Phi}$ in the context of baryogenesis has been recenlty considered in [59].

A Perturbative corrections from $\mathcal{O}_W$

We list the relation between $\widetilde{m}$ and $\widetilde{U}$ and the physical neutrino masses, m_i, and mixings, at leading order in a perturbative expansion in δm_ν^W:

$$
\begin{aligned}
&\text{NH}\\
&\widetilde{m_1} = 0,\\
&\widetilde{m_2} = m_2 + \mathrm{Re}\left(\frac{-e^{2i\phi_1}}{2}\left[2\delta_{11}s_{12}^2 + (\delta_{22} - 2\delta_{23} + \delta_{33})c_{12}^2 + \sqrt{2}(\delta_{12} - \delta_{13})\sin 2\theta_{12}\right]\right) + \mathcal{O}(\delta\epsilon),\\
&\widetilde{m_3} = m_3 + \mathrm{Re}\left(\frac{-e^{2i\phi_1}}{2}\left[\delta_{22} + 2\delta_{23} + \delta_{33}\right]\right) + \mathcal{O}(\delta\epsilon),\\
&\text{IH}\\
&\widetilde{m_1} = m_1 + \mathrm{Re}\left(\frac{1}{2}\left[2\delta_{11}c_{12}^2 + (\delta_{22} - 2\delta_{23} + \delta_{33})s_{12}^2 + \sqrt{2}(\delta_{12} - \delta_{13})\sin 2\theta_{12}\right]\right) + \mathcal{O}(\delta\epsilon),\\
&\widetilde{m_2} = m_2 + \mathrm{Re}\left(\frac{-e^{2i\phi_1}}{2}\left[2\delta_{11}s_{12}^2 + (\delta_{22} - 2\delta_{23} + \delta_{33})c_{12}^2 + \sqrt{2}(\delta_{12} - \delta_{13})\sin 2\theta_{12}\right]\right) + \mathcal{O}(\delta\epsilon),\\
&\widetilde{m_3} = 0.
\end{aligned}
\tag{A.1}
$$

the next to leading order contributions are $\mathcal{O}(\epsilon\,\delta m)$.

Defining

$$
\widetilde{U} = U(1 + \delta\tilde{U}),
\tag{A.2}
$$

at leading order we find

$$
\delta\tilde{U} = \begin{pmatrix} 0 & \delta\tilde{U}_{12} & \delta\tilde{U}_{13} \\ -\delta\tilde{U}_{12}^* & 0 & \delta\tilde{U}_{23} \\ -\delta\tilde{U}_{13}^* & -\delta\tilde{U}_{23}^* & 0 \end{pmatrix} + \mathcal{O}(\delta^2),
\tag{A.3}
$$

JHEP06(2017)112

with

NH

$$\delta\tilde{U}_{12} = \frac{e^{-i(\phi_1+\phi_2)}}{2r\sqrt{\Delta m^2_{\rm atm}}}\left[2\sqrt{2}(\delta_{12}-\delta_{13})\cos 2\theta_{12} + (2\delta_{11}+2\delta_{23}-\delta_{22}-\delta_{33})\sin 2\theta_{12}\right], \\ +\mathcal{O}(\delta)$$

$$\delta\tilde{U}_{13} = \frac{e^{-i\phi_2}}{2\sqrt{\Delta m^2_{\rm atm}}}\left[\sqrt{2}(\delta_{12}+\delta_{13})c_{12} + (\delta_{33}-\delta_{22})s_{12}\right] + \mathcal{O}(\epsilon\,\delta),$$

$$\delta\tilde{U}_{23} = \frac{e^{-i\phi_1}}{2\sqrt{\Delta m^2_{\rm atm}}}\left[-\sqrt{2}(\delta_{12}+\delta_{13})s_{12} + (\delta_{33}-\delta_{22})c_{12}\right] + \mathcal{O}(\epsilon\,\delta),$$

IH

$$\delta\tilde{U}_{12} = {\rm Re}\left(\frac{e^{-i\phi_1}}{2r^2\sqrt{\Delta m^2_{\rm atm}}}\left[2\sqrt{2}(\delta_{12}-\delta_{13})\cos 2\theta_{12} - (2\delta_{11}+2\delta_{23}-\delta_{22}-\delta_{33})\sin 2\theta_{12}\right]\right), \\ +\mathcal{O}(\delta)$$

$$\delta\tilde{U}_{13} = \frac{e^{i\phi_2}}{2\sqrt{\Delta m^2_{\rm atm}}}\left\{(\delta^*_{22}-\delta^*_{33})s_{12} - \sqrt{2}(\delta^*_{12}+\delta^*_{13})c_{12}\right\} + \mathcal{O}(\epsilon\,\delta),$$

$$\delta\tilde{U}_{23} = \frac{e^{i(\phi_1+\phi_2)}}{2\sqrt{\Delta m^2_{\rm atm}}}\left\{(\delta^*_{33}-\delta^*_{22})c_{12} - \sqrt{2}(\delta^*_{12}+\delta^*_{13})s_{12}\right\} + \mathcal{O}(\epsilon\,\delta). \tag{A.4}$$

Acknowledgments

We thank P. Coloma, L. Delle Rose, E. Fernández-Martínez, O. Mattelaer, R. Ruiz and T. Schwetz for useful discussions and/or clarifications. This work was partially supported by grants FPA2014-57816-P, PROMETEOII/2014/050, MINECO's Centro de Excelencia Severo Ocho Programme under grants SEV-2014-0398, and the European projects H2020-MSCA-ITN-2015//674896-ELUSIVES and 690575-InvisiblesPlus-H2020-MSCA-RISE-2015.

References

[1] T. Asaka and M. Shaposhnikov, *The nuMSM, dark matter and baryon asymmetry of the universe*, *Phys. Lett.* **B 620** (2005) 17 [hep-ph/0505013] [INSPIRE].

[2] M. Shaposhnikov, *The nuMSM, leptonic asymmetries and properties of singlet fermions*, *JHEP* **08** (2008) 008 [arXiv:0804.4542] [INSPIRE].

[3] T. Asaka, S. Eijima and H. Ishida, *Kinetic Equations for Baryogenesis via Sterile Neutrino Oscillation*, *JCAP* **02** (2012) 021 [arXiv:1112.5565] [INSPIRE].

[4] L. Canetti and M. Shaposhnikov, *Baryon Asymmetry of the Universe in the NuMSM*, *JCAP* **09** (2010) 001 [arXiv:1006.0133] [INSPIRE].

JHEP06(2017)112

[5] D. Besak and D. Bödeker, *Thermal production of ultrarelativistic right-handed neutrinos: Complete leading-order results*, *JCAP* **03** (2012) 029 [arXiv:1202.1288] [INSPIRE].

[6] L. Canetti, M. Drewes, T. Frossard and M. Shaposhnikov, *Dark Matter, Baryogenesis and Neutrino Oscillations from Right Handed Neutrinos*, *Phys. Rev.* **D 87** (2013) 093006 [arXiv:1208.4607] [INSPIRE].

[7] M. Drewes and B. Garbrecht, *Leptogenesis from a GeV Seesaw without Mass Degeneracy*, *JHEP* **03** (2013) 096 [arXiv:1206.5537] [INSPIRE].

[8] I. Ghisoiu and M. Laine, *Right-handed neutrino production rate at $T > 160$ GeV*, *JCAP* **12** (2014) 032 [arXiv:1411.1765] [INSPIRE].

[9] B. Garbrecht, *More Viable Parameter Space for Leptogenesis*, *Phys. Rev.* **D 90** (2014) 063522 [arXiv:1401.3278] [INSPIRE].

[10] B. Shuve and I. Yavin, *Baryogenesis through Neutrino Oscillations: A Unified Perspective*, *Phys. Rev.* **D 89** (2014) 075014 [arXiv:1401.2459] [INSPIRE].

[11] A. Abada, G. Arcadi, V. Domcke and M. Lucente, *Lepton number violation as a key to low-scale leptogenesis*, *JCAP* **11** (2015) 041 [arXiv:1507.06215] [INSPIRE].

[12] P. Hernández, M. Kekic, J. López-Pavón, J. Racker and N. Rius, *Leptogenesis in GeV scale seesaw models*, *JHEP* **10** (2015) 067 [arXiv:1508.03676] [INSPIRE].

[13] P. Hernández, M. Kekic, J. López-Pavón, J. Racker and J. Salvado, *Testable Baryogenesis in Seesaw Models*, *JHEP* **08** (2016) 157 [arXiv:1606.06719] [INSPIRE].

[14] M. Drewes, B. Garbrecht, D. Gueter and J. Klaric, *Testing the low scale seesaw and leptogenesis*, arXiv:1609.09069 [INSPIRE].

[15] J. Ghiglieri and M. Laine, *GeV-scale hot sterile neutrino oscillations: a derivation of evolution equations*, *JHEP* **05** (2017) 132 [arXiv:1703.06087] [INSPIRE].

[16] E.K. Akhmedov, V.A. Rubakov and A. Yu. Smirnov, *Baryogenesis via neutrino oscillations*, *Phys. Rev. Lett.* **81** (1998) 1359 [hep-ph/9803255] [INSPIRE].

[17] S. Alekhin et al., *A facility to Search for Hidden Particles at the CERN SPS: the SHiP physics case*, *Rept. Prog. Phys.* **79** (2016) 124201 [arXiv:1504.04855] [INSPIRE].

[18] A. Ferrari et al., *Sensitivity study for new gauge bosons and right-handed Majorana neutrinos in pp collisions at $s = 14$-TeV*, *Phys. Rev.* **D 62** (2000) 013001 [INSPIRE].

[19] M.L. Graesser, *Experimental Constraints on Higgs Boson Decays to TeV-scale Right-Handed Neutrinos*, arXiv:0705.2190 [INSPIRE].

[20] F. del Aguila and J.A. Aguilar-Saavedra, *Distinguishing seesaw models at LHC with multi-lepton signals*, *Nucl. Phys.* **B 813** (2009) 22 [arXiv:0808.2468] [INSPIRE].

[21] F. del Aguila and J.A. Aguilar-Saavedra, *Electroweak scale seesaw and heavy Dirac neutrino signals at LHC*, *Phys. Lett.* **B 672** (2009) 158 [arXiv:0809.2096] [INSPIRE].

[22] P.S. Bhupal Dev, R. Franceschini and R.N. Mohapatra, *Bounds on TeV Seesaw Models from LHC Higgs Data*, *Phys. Rev.* **D 86** (2012) 093010 [arXiv:1207.2756] [INSPIRE].

[23] A. Das, P.S. Bhupal Dev and N. Okada, *Direct bounds on electroweak scale pseudo-Dirac neutrinos from $\sqrt{s} = 8$ TeV LHC data*, *Phys. Lett.* **B 735** (2014) 364 [arXiv:1405.0177] [INSPIRE].

JHEP06(2017)112

[24] FCC-ee study Team collaboration, A. Blondel, E. Graverini, N. Serra and M. Shaposhnikov, *Search for Heavy Right Handed Neutrinos at the FCC-ee*, *Nucl. Part. Phys. Proc.* **273-275** (2016) 1883 [arXiv:1411.5230] [INSPIRE].

[25] A. Abada, V. De Romeri, S. Monteil, J. Orloff and A.M. Teixeira, *Indirect searches for sterile neutrinos at a high-luminosity Z-factory*, *JHEP* **04** (2015) 051 [arXiv:1412.6322] [INSPIRE].

[26] J.C. Helo, M. Hirsch and S. Kovalenko, *Heavy neutrino searches at the LHC with displaced vertices*, *Phys. Rev.* **D 89** (2014) 073005 [arXiv:1312.2900] [INSPIRE].

[27] S. Antusch and O. Fischer, *Testing sterile neutrino extensions of the Standard Model at future lepton colliders*, *JHEP* **05** (2015) 053 [arXiv:1502.05915] [INSPIRE].

[28] F.F. Deppisch, P.S. Bhupal Dev and A. Pilaftsis, *Neutrinos and Collider Physics*, *New J. Phys.* **17** (2015) 075019 [arXiv:1502.06541] [INSPIRE].

[29] A. Maiezza, M. Nemevšek and F. Nesti, *Lepton Number Violation in Higgs Decay at LHC*, *Phys. Rev. Lett.* **115** (2015) 081802 [arXiv:1503.06834] [INSPIRE].

[30] E. Izaguirre and B. Shuve, *Multilepton and Lepton Jet Probes of Sub-Weak-Scale Right-Handed Neutrinos*, *Phys. Rev.* **D 91** (2015) 093010 [arXiv:1504.02470] [INSPIRE].

[31] A.M. Gago, P. Hernández, J. Jones-Pérez, M. Losada and A. Moreno Briceño, *Probing the Type I Seesaw Mechanism with Displaced Vertices at the LHC*, *Eur. Phys. J.* **C 75** (2015) 470 [arXiv:1505.05880] [INSPIRE].

[32] M. Nemevšek, F. Nesti and J.C. Vasquez, *Majorana Higgses at colliders*, *JHEP* **04** (2017) 114 [arXiv:1612.06840] [INSPIRE].

[33] A. Das, P.S.B. Dev and C.S. Kim, *Constraining Sterile Neutrinos from Precision Higgs Data*, arXiv:1704.00880 [INSPIRE].

[34] A. Caputo, P. Hernández, M. Kekic, J. López-Pavón and J. Salvado, *The seesaw path to leptonic CP-violation*, *Eur. Phys. J.* **C 77** (2017) 258 [arXiv:1611.05000] [INSPIRE].

[35] S. Weinberg, *Baryon and Lepton Nonconserving Processes*, *Phys. Rev. Lett.* **43** (1979) 1566 [INSPIRE].

[36] W. Buchmüller and D. Wyler, *Effective Lagrangian Analysis of New Interactions and Flavor Conservation*, *Nucl. Phys.* **B 268** (1986) 621 [INSPIRE].

[37] B. Grzadkowski, M. Iskrzynski, M. Misiak and J. Rosiek, *Dimension-Six Terms in the Standard Model Lagrangian*, *JHEP* **10** (2010) 085 [arXiv:1008.4884] [INSPIRE].

[38] M.L. Graesser, *Broadening the Higgs boson with right-handed neutrinos and a higher dimension operator at the electroweak scale*, *Phys. Rev.* **D 76** (2007) 075006 [arXiv:0704.0438] [INSPIRE].

[39] F. del Aguila, S. Bar-Shalom, A. Soni and J. Wudka, *Heavy Majorana Neutrinos in the Effective Lagrangian Description: Application to Hadron Colliders*, *Phys. Lett.* **B 670** (2009) 399 [arXiv:0806.0876] [INSPIRE].

[40] A. Aparici, K. Kim, A. Santamaria and J. Wudka, *Right-handed neutrino magnetic moments*, *Phys. Rev.* **D 80** (2009) 013010 [arXiv:0904.3244] [INSPIRE].

[41] P. Minkowski, $\mu \to e\gamma$ *at a Rate of One Out of* 10^9 *Muon Decays?*, *Phys. Lett.* **B 67** (1977) 421 [INSPIRE].

[42] M. Gell-Mann, P. Ramond and R. Slansky, *Complex Spinors and Unified Theories*, *Conf. Proc.* **C 790927** (1979) 315 [arXiv:1306.4669] [INSPIRE].

JHEP06(2017)112

[43] T. Yanagida, *Horizontal symmetry and masses of neutrinos*, *Conf. Proc.* **C 7902131** (1979) 95.

[44] R.N. Mohapatra and G. Senjanović, *Neutrino Mass and Spontaneous Parity Violation*, *Phys. Rev. Lett.* **44** (1980) 912 [INSPIRE].

[45] B. Patt and F. Wilczek, *Higgs-field portal into hidden sectors*, hep-ph/0605188 [INSPIRE].

[46] D. Wyler and L. Wolfenstein, *Massless Neutrinos in Left-Right Symmetric Models*, *Nucl. Phys.* **B 218** (1983) 205 [INSPIRE].

[47] R.N. Mohapatra and J.W.F. Valle, *Neutrino Mass and Baryon Number Nonconservation in Superstring Models*, *Phys. Rev.* **D 34** (1986) 1642 [INSPIRE].

[48] V. Cirigliano, B. Grinstein, G. Isidori and M.B. Wise, *Minimal flavor violation in the lepton sector*, *Nucl. Phys.* **B 728** (2005) 121 [hep-ph/0507001] [INSPIRE].

[49] S. Davidson and F. Palorini, *Various definitions of Minimal Flavour Violation for Leptons*, *Phys. Lett.* **B 642** (2006) 72 [hep-ph/0607329] [INSPIRE].

[50] M.B. Gavela, T. Hambye, D. Hernandez and P. Hernández, *Minimal Flavour Seesaw Models*, *JHEP* **09** (2009) 038 [arXiv:0906.1461] [INSPIRE].

[51] J.A. Casas and A. Ibarra, *Oscillating neutrinos and* $\mu \to e\gamma$, *Nucl. Phys.* **B 618** (2001) 171 [hep-ph/0103065] [INSPIRE].

[52] A. Ibarra, E. Molinaro and S.T. Petcov, *TeV Scale See-Saw Mechanisms of Neutrino Mass Generation, the Majorana Nature of the Heavy Singlet Neutrinos and* $(\beta\beta)_{0\nu}$*-Decay*, *JHEP* **09** (2010) 108 [arXiv:1007.2378] [INSPIRE].

[53] I. Esteban, M.C. Gonzalez-Garcia, M. Maltoni, I. Martinez-Soler and T. Schwetz, *Updated fit to three neutrino mixing: exploring the accelerator-reactor complementarity*, *JHEP* **01** (2017) 087 [arXiv:1611.01514] [INSPIRE].

[54] E. Accomando, L. Delle Rose, S. Moretti, E. Olaiya and C.H. Shepherd-Themistocleous, *Novel SM-like Higgs decay into displaced heavy neutrino pairs in* U(1)′ *models*, *JHEP* **04** (2017) 081 [arXiv:1612.05977] [INSPIRE].

[55] CMS collaboration, *Search for long-lived particles that decay into final states containing two electrons or two muons in proton-proton collisions at* $\sqrt{s} = 8$ *TeV*, *Phys. Rev.* **D 91** (2015) 052012 [arXiv:1411.6977] [INSPIRE].

[56] CMS collaboration, *Search for long-lived particles that decay into final states containing two muons, reconstructed using only the CMS muon chambers*, CMS-PAS-EXO-14-012 (2014).

[57] J. Alwall et al., *The automated computation of tree-level and next-to-leading order differential cross sections and their matching to parton shower simulations*, *JHEP* **07** (2014) 079 [arXiv:1405.0301] [INSPIRE].

[58] J.P. Chou, D. Curtin and H.J. Lubatti, *New Detectors to Explore the Lifetime Frontier*, *Phys. Lett.* **B 767** (2017) 29 [arXiv:1606.06298] [INSPIRE].

[59] T. Asaka, S. Eijima, H. Ishida, K. Minogawa and T. Yoshii, *Initial condition for baryogenesis via neutrino oscillation*, arXiv:1704.02692 [INSPIRE].

JHEP06(2017)112

Looking for axion dark matter in dwarf spheroidal galaxies

Andrea Caputo,[1] Carlos Peña Garay,[2,3] and Samuel J. Witte[1]
[1]Instituto de Física Corpuscular (IFIC), CSIC-Universitat de València, Apartado de Correos 22085, E-46071, Spain
[2]I2SysBio, CSIC-UVEG, P.O. 22085, Valencia 46071, Spain
[3]Laboratorio Subterráneo de Canfranc, Estación de Canfranc 22880, Spain

(Received 30 May 2018; published 26 October 2018)

We study the extent to which the decay of cold dark matter axions can be probed with forthcoming radio telescopes such as the Square Kilometer Array (SKA). In particular, we focus on signals arising from dwarf spheroidal galaxies, where astrophysical uncertainties are reduced and the expected magnetic field strengths are such that signals arising from axion decay may dominate over axion-photon conversion in a magnetic field. We show that with ∼100 hr of observing time, SKA could improve current sensitivity by 2–3 orders of magnitude—potentially obtaining sufficient sensitivity to begin probing the decay of cold dark matter axions.

DOI: 10.1103/PhysRevD.98.083024

I. INTRODUCTION

Perhaps the most promising solution to the strong CP problem involves the introduction of a new global $U(1)$ symmetry, which when spontaneously broken at high energies produces a pseudo-Nambu-Goldstone boson known as the "axion" [1–4] (see, e.g., [5] for a recent review). Despite the small mass of the axion, nonthermal production mechanisms in the early Universe allow for the possibility that this particle accounts for the observed abundance of cold dark matter [6–10].[1]

The potential of simultaneously solving two of the largest outstanding problems in particle physics has led to a large and diverse experimental program aimed at probing the parameter space associated with axion dark matter (see, e.g., [11] for a review of experimental search techniques). Many of these experiments have been focused on exploiting the conversion of axions to and from photons, a process which occurs in the presence of a strong magnetic field; this is the so-called Primakoff effect. In this work, we instead focus on the often neglected process of the spontaneous decay of the axion into two photons and show that near-future radio telescopes can significantly improve the existing sensitivity to axions with masses $m_a \sim 10^{-6}$–10^{-4} eV.

Here, we focus on the signal arising from on one particular class of astrophysical objects, dwarf spheroidal galaxies (dSphs)—these are dark-matter-dominated objects with a low radio background and are thus capable of yielding significant unabated signatures of axion dark matter. Conventional astrophysical searches for axion conversion (e.g., targeting the Galactic center [12] or highly magnetized pulsars [13,14]), on the other hand, typically require targeting highly uncertain environments with many assumptions on, e.g., the magnetic field strength, the magnetic field distribution, radio backgrounds arising from synchrotron emission and free-free absorption, and the dark matter distribution.

The possibility of detecting axion decay in dSphs with a radio telescope was first explored in Ref. [15] and, to our knowledge, not discussed since. The subsequent ∼20 yr have provided significant improvement in the sensitivity of radio telescopes and the discovery of many new dSphs. In this work, we evaluate the sensitivity of current and future radio telescopes to axion decay in a variety of known dSphs. In particular, we show that with ∼100 hr of observation, the Square Kilometer Array (SKA) [16] can potentially improve the constraints from helioscopes by ∼2–3 orders of magnitude depending on the axion mass. For completeness, we also present a comparison of the signal arising from axion decay with that produced by the process of magnetic field conversion.

II. THE SIGNAL

A. Axion decay

The spontaneous decay of an axion with mass m_a proceeds through the chiral anomaly to two photons, each with a frequency $\nu = m_a/4\pi$, and with a lifetime given by

$$\tau_a = \frac{64\pi}{m_a^3 g^2}, \tag{1}$$

where g is the axion-to-two-photon coupling constant. It is perhaps straightforward to understand why axion decay has

[1]It is worth noting that there has been a recent interest in the community in searching for axionlike particles (ALPs); in such models, one sacrifices the ability to solve the strong CP problem for the freedom to independently choose the mass and coupling of the pseudoscalar [11].

been largely neglected in the literature—if one evaluates Eq. (1) for $m_a \sim 10^{-4}$ eV and $g \sim 7 \times 10^{-11}$ (i.e., the upper limit imposed by helioscopes), it is found that the axion has a lifetime of $\sim 10^{30}$ yr.

The observed power per unit area per unit frequency from the spontaneous decay of an axion by a radio telescope is then given by

$$S_{\rm sd} = \frac{m_a}{4\pi\Delta\nu} \int d\Omega d\ell \frac{n(\ell,\Omega)}{\tau_a}, \tag{2}$$

where $\Delta\nu$ is the width of the axion line, given by $\Delta\nu = \nu_{\rm center}\sigma_{\rm disp}$ where $\sigma_{\rm disp}$ is the dispersion of the line resulting from the velocity dispersion of dark matter within the dwarf,[2] and $n(\ell,\Omega)$ is the axion number density at a distance along the line of sight ℓ in the solid angle Ω. For convenience, we define the astrophysical quantity

$$D(\alpha_{\rm int}) = \int d\Omega d\ell \rho(\ell,\Omega), \tag{3}$$

which allows us to write Eq. (2) as

$$S_{\rm sd} = \frac{m_a^2 g^2}{64\pi} \frac{D(\alpha_{\rm int})}{\sigma_{\rm disp}}, \tag{4}$$

where $\alpha_{\rm int}$ is the angle of integration defined between the center of a given dwarf galaxy and the largest observable radius. From Eq. (4), it should be clear that, given a radio telescope, the dwarf galaxies providing the best sensitivity to axion decay are those with the largest $D(\alpha_{\rm int})/\sigma_{\rm disp}$. The angle $\alpha_{\rm int}$ depends on both the size of the dishes used for observation and the frequency (and thus the axion mass). The observed field of view of a particular telescope is given by

$$\Omega_{\rm FoV} \sim \frac{\pi}{4}\left(\frac{66\lambda}{D_{\rm dish}}\right)^2, \tag{5}$$

where λ is the wavelength of the observed photons and $D_{\rm dish}$ is the diameter of the dish. Consequently, the maximum angle of the dwarf that can be probed is given by

$$\alpha_{\rm int} \sim 8.8 \times \left(\frac{\rm GHz}{\nu}\right)\left(\frac{1\ {\rm m}}{D_{\rm dish}}\right) \text{ degrees}. \tag{6}$$

Up until this point, we have focused solely on the spontaneous decay of axions into photons. However, these decays take place in the background of cosmic microwave background (CMB) photons with the same energy; this inherently enhances the photon production rate via stimulated emission. The power emitted by stimulated emission is given by

$$P_{\rm se} = m_a g(\nu) B_{21} \rho_{\rm cmb}(\nu) \Delta N, \tag{7}$$

where B_{21} is the Einstein coefficient, $\rho_{\rm cmb}(\nu)$ is the radiation density of CMB photons at a given frequency, ΔN is the difference between the number of axions and the number of photons with energy $m_a/2$ (which can be approximated as just N_a), and $g(\nu)$ is the spectral line shape function (which we take to be a delta function). Taking the Einstein coefficient to be

$$B_{21} = \left(\frac{\pi^2}{\omega^3}\right)\frac{1}{\tau} = \frac{g^2\pi}{8}, \tag{8}$$

one can express the observed power per unit area per unit frequency contributed from stimulated emission as

$$S_{\rm se} = 2\frac{m_a^2 g^2}{64\pi}\frac{D(\alpha_{\rm int})}{\sigma_{\rm disp}}\left(\frac{1}{e^{m_a/(2T_{\rm cmb})}-1}\right), \tag{9}$$

which is identical to the contribution of the spontaneous emission multiplied by two times the photon occupation number. We emphasize that the aforementioned effect of stimulated emission, described above using the language of atomic physics, is entirely equivalent to the quantum field theory computation performed assuming a background of photons rather than a vacuum. An identical result can be obtained using the Boltzmann equation and applying the limit in which the photon number density is much less than the axion number density. The total observed power $S_{\rm total}$ is then given by the sum of Eqs. (4) and (9).

B. Magnetic conversion

Signals arising from the conversion of axions to photons while traversing through a perpendicular magnetic field have been extensively studied in the context of both terrestrial and astrophysical environments (see, e.g., [12–14,17–22]). In this section, we will make a number of simplifying assumptions to estimate the potential signal arising from axion conversion in a magnetic field under rather optimistic assumptions. As shown below, the rate of magnetic field conversion in large astrophysical environments is almost certainly subdominant to the contribution from axion decay, largely due to the suppression arising from the fact that realistic magnetic fields are not homogenous.

In the case of a static magnetic field, the flux arising from axion conversion is proportional to $|\vec{B}(|k| = m_a)|^2$, where $\vec{B}(\vec{k})$ is the Fourier transform of the magnetic field. It is often convenient to characterize this contribution in terms of a characteristic magnetic field strength B_0 and a suppression factor $f(m_a)$, as $|\vec{B}(|k| = m_a)|^2 = B_0^2 f(m_a)$ [see, e.g., Eq. (20) of Ref. [23]]. Using this simplification, one can calculate the observed power per unit area per unit frequency from axion-photon conversion using [11,23,24]

[2]Note that we assume here that the velocity dispersion of dark matter follows that of the stellar component.

$$S_{\rm conv} = \frac{B_0^2 g^2}{m_a^2 \sigma_{\rm disp}} f(m_a) \int_{V_{B_0}} d\Omega d\ell \rho(\ell, \Omega), \quad (10)$$

where the integration runs over the volume containing the magnetic field, V_{B_0}. Naively, one may expect the astrophysical integral in Eq. (10) to be comparable to that of Eq. (3). Should this be the case, and should the suppression factor $f(m_a)$ be $\sim\mathcal{O}(1)$, one may approximate the ratio between the rate of axion decay and the rate of axion conversion as

$$\frac{R_{a\to\gamma\gamma}}{R_{a\to\gamma}} \sim \frac{m_a^4}{64\pi B_0^2}\left(1 + \frac{2}{e^{m_a/(2T_{\rm cmb})} - 1}\right). \quad (11)$$

In Fig. 1, we plot Eq. (11) as a function of the axion mass for various magnetic field strengths ranging from 100 to 10^{-4} μG. For comparison, we have also highlighted in Fig. 1 the approximate magnetic field strength expected in the Galactic center [25–29], dSphs [30], and the intergalactic medium [31,32]. This first-order comparison between the rate of decay and magnetic field conversion clearly illustrates an important point: The rate of axion decay can supersede that of magnetic field conversion for axion masses probed by radio telescopes.

At this point, we emphasize that the suppression factor for large-scale astrophysical environments is likely $f(m_a) \ll 1$. For example, it was shown in Ref. [23] that the rate of axion conversion in the Galactic center is generically reduced by a factor of $f(m_a) \sim 10^{-13}$, assuming the magnetic field distribution follows a power law and the coherence length in the Galactic center is of the order of $\sim$1 pc. While the coherence length of the magnetic field in dSphs is likely considerably smaller than that of the Galactic center, the length scales are still astrophysical and thus should reduce the overall rate of conversion by orders of magnitude. Thus, it should be clear that axion decay, and not magnetic field conversion, is the relevant mechanism for the detection of axions in large-scale astrophysical environments.

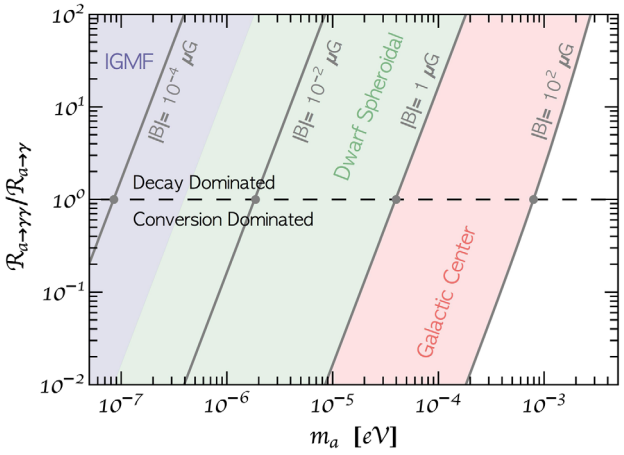

FIG. 1. Ratio of the rate of spontaneous decay $a \to \gamma\gamma$ to the conversion $a \to \gamma$ in a spatially uniform magnetic field of modulus $|B|$ as a function of the axion mass. While magnetic field conversion is far more efficient at small axion masses, the rate of spontaneous decay can be competitive for $m_a \sim 10^{-5}$ eV, depending on the value of the magnetic field. Approximate magnetic field strengths for the Galactic center (red), dSphs (green), and the intergalactic medium (gray) are also shown for comparison. Here, we have taken $f(m_a) = 1$.

C. Sensitivity

It is often conventional in radio astronomy to define the brightness temperature induced by a flux $S_{\rm total}$ as

$$T = \frac{A_{\rm eff} S_{\rm total}}{2}, \quad (12)$$

where $A_{\rm eff}$ is the effective collecting area of the telescope. Provided astrophysical backgrounds are low, the minimum observable temperature in a bandwidth ΔB given an observation time $t_{\rm obs}$ is given by

$$T_{\rm min} \sim \frac{T_{\rm sys}}{\sqrt{\Delta B \times t_{\rm obs}}}, \quad (13)$$

where $T_{\rm sys}$ consists of a sum over sky and instrumental noise, as well as residuals after background subtraction. For frequencies in the central part of the SKA band, it is typically valid to assume the sky temperature $T_{\rm sky}$ is subdominant to the contribution from instrumental noise. Actually, because we are interested in searching for narrow spectral lines, the only backgrounds expected to be truly detrimental are molecular lines.[3] However, it seems reasonable to neglect the possibility that photons arising in axion decay directly coincide with the location of a molecular line. For completeness, our estimation of the system temperature includes both the quoted 11 K instrumental noise and a frequency-dependent contribution from the sky temperature [16]. Throughout this analysis, we will assume an observation time of 100 hr and a bandwidth such that at least two bins with the Nyquist width of the autocorrelation spectrometer are inside the axion signal [15], a feat that should be easily achievable for SKA [note that SKA is expected to have $\mathcal{O}$(kHz) sensitivity [33], far below any requirements imposed here].

Combining Eq. (12) with Eq. (13), one can estimate the smallest detectable flux of a given radio telescope as

$$S_{\rm min} = 2\frac{T_{\rm sys}}{A_{\rm eff}\sqrt{\Delta B \times t_{\rm obs}}}. \quad (14)$$

[3]That is to say that spectrally smooth backgrounds are expected to be easily removed, implying that the dominant background temperature for a majority of the frequency range considered is set by the instrumental noise.

III. DWARF GALAXIES

In this analysis, we focus on signals arising in dSphs, as these targets offer large dark matter densities and low velocity dispersion. DSphs also make an intriguing target for radio telescopes, as the typical angular size of such objects is roughly the same order of magnitude as the field of view. Note that this is not inherently true of the Galactic center, implying that radio telescopes cannot take full advantage of the larger column density in this environment. It is also worth mentioning that targets like the Galactic center have (i) a larger velocity dispersion and (ii) a larger magnetic field, where the former implies a suppression of the flux and the latter an enhancement (large magnetic fields imply synchrotron emission, which can enhance the stimulated emission factor). These counteracting effects make it nontrivial to determine which environment is more promising. Here, we choose to focus on dSphs and leave a more careful analysis of other environments to future work.

As previously stated, we restrict our analysis to only the most promising dSphs, i.e., those producing the largest $D(\alpha_{\rm int})/\sigma_{\rm disp}$. The values of $D(\alpha_{\rm int})$ for a wide variety of dSphs have been inferred from kinematic distributions (see, e.g., [34–41]). In this work, we use the publicly available data provided in Refs. [35,36] to determine the value of $D(\alpha_{\rm int})/\sigma_{\rm disp}$ at each $\alpha_{\rm int}$. In Fig. 2, we show the maximum value of $D(\alpha_{\rm int})/\sigma_{\rm disp}$ for all dSphs considered in Refs. [35,36] as a function $\alpha_{\rm int}$, assuming the median best fit $D(\alpha_{\rm int})$ (black line) and ±95% CI $D(\alpha_{\rm int})$ (upper and lower green lines). The region bounded by the ±95% CIs has been shaded to illustrate the range of possible values. For each line and each value of $\alpha_{\rm int}$, the dSph giving rise to the largest value of $D(\alpha_{\rm int})$ is identified. Note that the surprisingly continuous nature of the lines in Fig. 2 arises from the fact that a number of dwarfs considered have very similar values of $D(\alpha_{\rm int})/\sigma_{\rm disp}$ (this is why we have chosen to mark the transitions with a vertical line segment). While the most promising dSph candidates are Reticulum II, Willman I,[4] Ursa Major II, and Draco, we emphasize that many of the dSphs considered here produce values of $D(\alpha_{\rm int})/\sigma_{\rm disp}$ comparable to those highlighted above; thus, the derived sensitivity is not specific to a particular choice of dSph.

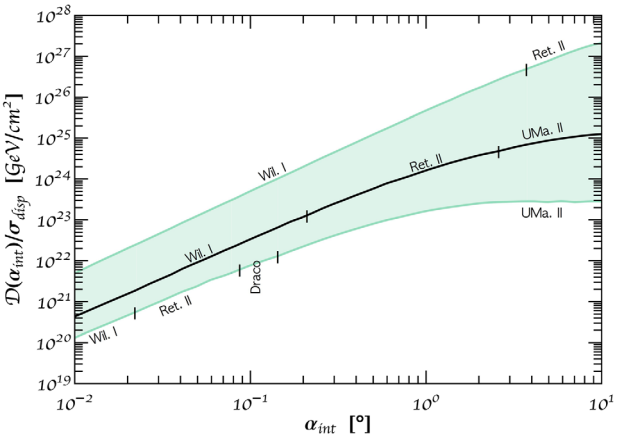

FIG. 2. Factor $D(\alpha_{\rm int})/\sigma_{\rm disp}$ as a function of the field of view of the telescope. For each value of $\alpha_{\rm int}$, we plot the median (black line) and ±95% CI (green band) of $D(\alpha_{\rm int})/\sigma_{\rm disp}$ for the dwarf galaxies providing the largest sensitivity. Depending on the field of view of a given radio telescope, the optimal dwarf galaxy is either Willman I, Reticulum II, Ursa Major II, or Draco.

IV. RESULTS

In this section, we present the projected sensitivity for the SKA-Mid, operated in the phase-2 upgrade which assumes an enhanced collection area of $(1\ {\rm km})^2$ and a system temperature of $T_{\rm sys} = 11\ {\rm K} + T_{\rm sky}(\nu)$, where $T_{\rm sky}(\nu)$ is taken from Ref. [16]. We have also considered the sensitivity for various current and future radio telescopes, namely, LOFAR, ASKAP, ParkesMB, WSRT, Arecibo, GBT, JVLA, FAST, and SKA-Low, which will be presented elsewhere.

Figure 3 shows the estimated sensitivity for SKA-Mid (phase 2) to axion decay in dSphs. At each axion mass, the sensitivity curves shown in Fig. 3 are produced using the dSph providing the largest $D(\alpha_{\rm int})/\sigma_{\rm disp}$, where the width of the sensitivity band reflects the ±95% C.L. of $D(\alpha_{\rm int})$.[5] This result is compared with current constraints from helioscopes [42] and haloscopes [43–48], projected sensitivity from future experiments IAXO [49] and ALPS-II [50], and with the QCD axion parameter space as identified in Ref. [51] (light green region). Note that, in the preinflationary scenario, the predicted axion mass that accounts for all the dark matter has been computed to be ∼26 μeV [52], which lies precisely in the range where the prospects of this paper are more relevant. Our results illustrate that SKA could potentially lead to the observation of the decay of the QCD axion and will allow for improvement upon existing helioscope constraints by roughly 2 orders of magnitude.

Before continuing, we comment briefly on the origin of the improvement in sensitivity relative to the original analysis performed in Ref. [15]. At low masses, the contribution from stimulated emission is significant; specifically, considering $m_a \sim 10^{-6}$ eV, stimulated emission enhances the signal by roughly a factor of 10^3 (which reduces to a factor of ∼10 for $m_a = 10^{-4}$ eV). With regard

[4]It is important to note that Willman I has irregular stellar kinematics indicative of a recent tidal disruption event, and thus the inferred distribution of dark matter may be untrustworthy.

[5]One may wonder whether the sensitivity could be significantly improved by performing a stacked dSph analysis, as is done, e.g., in gamma-ray searches for dark matter. Unfortunately, the narrow field of view of radio telescopes implies that they cannot simultaneously observe multiple dSphs, and thus stacked analyses performed using a fixed total observation time will not result in an increased sensitivity, although it will reduce systematic uncertainties.

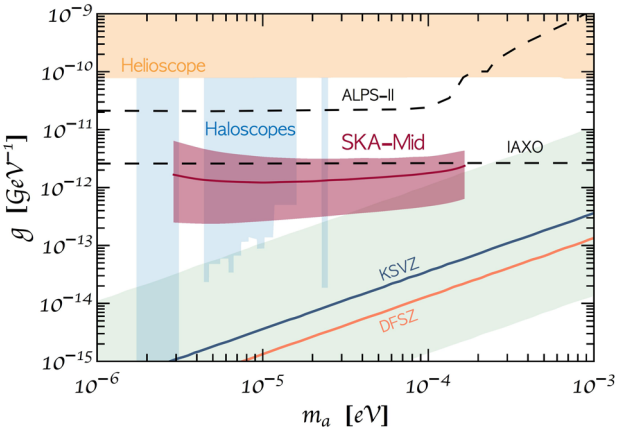

FIG. 3. Sensitivity of SKA to the axion dark matter parameter space. The solid red line (bands) denote the median (±95% CI) sensitivity to axion decay in the dSph providing the largest value of $D(\alpha_{\rm int})/\sigma_{\rm disp}$. Sensitivity estimates are compared with the QCD axion parameter space [51] (light green), existing bounds from helioscopes [42], existing bounds from haloscopes [43–47], and projected sensitivity for IAXO [49] and ALPS-II [50].

to telescope sensitivity, SKA-Mid offers more than one order of magnitude reduction in the system temperature and an enhancement in the effective area of ∼4 orders of magnitude. Lastly, the discovery of new dSphs in recent years has provided more promising astrophysical targets, subsequently allowing for a 1–2 order of magnitude improvement of the overall observed flux.

V. DISCUSSION

In this paper, we have demonstrated that axion decay can be competitive with axion-photon conversion for axion masses probed by radio telescopes, depending on the astrophysical environment. Therefore, it should be included in the sensitivity studies searching for cold dark matter axions with radio surveys. Among the many candidate astrophysical sources, we have identified the best nearby dwarf spheroidal galaxies as a function of the telescope field of view. We have shown that SKA can identify axion cold dark matter by observing the axion decay inside nearby dwarf spheroidal galaxies. Our proposal complements new projects searching for cold dark matter axions in the unexplored mass region near $m_a \sim 10^{-4}$ eV [11]. Furthermore, we emphasize that the sensitivity obtained here surpasses the projected coverage of future axion experiments such as ALPS-II and IAXO in the mass range of interest [49,50,53].

It should be understood that the projected sensitivity presented in this work represents what a particular *planned* experiment can accomplished with *known* astrophysical objects. In recent years, experiments such as the Dark Energy Survey have dramatically increased the rate of discovery of Milky Way dwarf galaxies, particularly those that offer promise for the indirect detection of dark matter [54–56]. With ongoing and future experiments such as Gaia [57] and the Large Synoptic Survey Telescope [58] providing unprecedented sensitivity to the gravitational effects of dark matter in the Galaxy, one may expect the rate of dwarf discovery to continue increasing. If more promising dwarf targets are observed in the near future, the projected sensitivity shown here may prove to be conservative. Furthermore, should future radio telescopes be developed with strong sensitivity at higher frequencies, one may expect searches for axion decay to significantly probe the QCD axion parameter space for masses as large as $m_a \sim 10^{-3}$ eV. Such instruments, however, would require good frequency resolution, with a Nyquist width of the autocorrelation spectrometer of ∼2 MHz at 100 GHz. Finally, we emphasize that, even in the absence of an axion detection, additional science can be obtained from observations of dSphs—e.g., molecular line searches in dSphs can enhance our current understanding of the limited star formation in these objects [59].

ACKNOWLEDGMENTS

C. P. G. thanks initial discussions on Ref. [15] with Matteo Viel and early work with Aaron Vincent and Francisco Villaescusa. The authors also thank the following individuals for their useful comments and discussions: Javier Redondo, Jordi Miralda, Jorge Peñarrubia, Leslie Rosenberg, Jose Carlos Guirado, Ivan Marti Vidal, Dan Hooper, Alfredo Urbano, Marco Taoso, Mauro Valli, Valentina De Romeri, Fernando Ballesteros, Marco Regis, Carlos Hernandez-Monteagudo, Jose Francisco Gomez, and the SOM group at IFIC in Valencia. We were supported by PROMETEO II/2014/050 of Generalitat Valenciana, FPA2014-57816-P and FPA2017-85985-P of MINECO, and the European Union's Horizon 2020 research and innovation program under H2020-MSCA-ITN-2015// 674896-ELUSIVES and H2020-MSCA-RISE-2015.

[1] R. D. Peccei and H. R. Quinn, Phys. Rev. Lett. **38**, 1440 (1977).
[2] R. D. Peccei and H. R. Quinn, Phys. Rev. D **16**, 1791 (1977).
[3] S. Weinberg, Phys. Rev. Lett. **40**, 223 (1978).
[4] F. Wilczek, Phys. Rev. Lett. **40**, 279 (1978).
[5] R. D. Peccei, Lect. Notes Phys. **741**, 3 (2008).

[6] J. Preskill, M. B. Wise, and F. Wilczek, Phys. Lett. **120B**, 127 (1983).
[7] M. Dine and W. Fischler, Phys. Lett. **120B**, 137 (1983).
[8] L. F. Abbott and P. Sikivie, Phys. Lett. **120B**, 133 (1983).
[9] R. L. Davis, Phys. Lett. B **180**, 225 (1986).
[10] D. H. Lyth, Phys. Lett. B **275**, 279 (1992).
[11] I. G. Irastorza and J. Redondo, Prog. Part. Nucl. Phys. **102**, 89 (2018).
[12] K. Kelley and P. J. Quinn, Astrophys. J. **845**, L4 (2017).
[13] F. P. Huang, K. Kadota, T. Sekiguchi, and H. Tashiro, Phys. Rev. D **97**, 123001 (2018).
[14] A. Hook, Y. Kahn, B. R. Safdi, and Z. Sun, arXiv: 1804.03145.
[15] B. D. Blout, E. J. Daw, M. P. Decowski, P. T. P. Ho, L. J. Rosenberg, and D. B. Yu, Astrophys. J. **546**, 825 (2001).
[16] SKA Whitepaper, https://www.skatelescope.org/wp-content/uploads/2014/03/SKA-TEL-SKO-0000308_SKA1_System_Baseline_v2_DescriptionRev01-part-1-signed.pdf.
[17] T. M. Shokair *et al.*, Int. J. Mod. Phys. A **29**, 1443004 (2014).
[18] D. Budker, P. W. Graham, M. Ledbetter, S. Rajendran, and A. Sushkov, Phys. Rev. X **4**, 021030 (2014).
[19] B. M. Brubaker *et al.*, Phys. Rev. Lett. **118**, 061302 (2017).
[20] S. Al Kenany *et al.*, Nucl. Instrum. Methods Phys. Res., Sect. A **854**, 11 (2017).
[21] B. Majorovits and J. Redondo (MADMAX Working Group), MADMAX: A new dark matter axion search using a dielectric haloscopein *Proceedings of the 12th Patras Workshop on Axions, WIMPs and WISPs (PATRAS 2016): Jeju Island, South Korea, 2016* (Verlag Deutsches Elektronen-Synchrotron, Hamburg, 2017), pp. 94–97.
[22] B. M. Brubaker, L. Zhong, S. K. Lamoreaux, K. W. Lehnert, and K. A. van Bibber, Phys. Rev. D **96**, 123008 (2017).
[23] G. Sigl, Phys. Rev. D **96**, 103014 (2017).
[24] P. Sikivie, Phys. Rev. Lett. **51**, 1415 (1983); **51**, 1415 (1983).
[25] T. N. LaRosa, S. N. Shore, T. Joseph, W. Lazio, and N. E. Kassim, J. Phys. Conf. Ser. **54**, 10 (2006).
[26] R. Beck, AIP Conf. Proc. **1085**, 83 (2009).
[27] K. Ferriere, Astron. Astrophys. **505**, 1183 (2009).
[28] J. L. Han, IAU Symp. **259**, 455 (2009).
[29] R. Beck and R. Wielebinski, arXiv:1302.5663.
[30] M. Regis, L. Richter, S. Colafrancesco, S. Profumo, W. J. G. de Blok, and M. Massardi, Mon. Not. R. Astron. Soc. **448**, 3747 (2015).
[31] T. C. Arlen, V. V. Vassiliev, T. Weisgarber, S. P. Wakely, and S. Y. Shafi, Astrophys. J. **796**, 18 (2014).
[32] J. D. Finke, L. C. Reyes, M. Georganopoulos, K. Reynolds, M. Ajello, S. J. Fegan, and K. McCann, Astrophys. J. **814**, 20 (2015).
[33] SKA Baseline Design, https://www.skatelescope.org/wp-content/uploads/2014/11/SKA-TEL-SKO-0000002-AG-BD-DD-Rev01-SKA1_System_Baseline_Design.pdf.
[34] A. Geringer-Sameth, S. M. Koushiappas, and M. Walker, Astrophys. J. **801**, 74 (2015).
[35] V. Bonnivard *et al.*, Mon. Not. R. Astron. Soc. **453**, 849 (2015).
[36] V. Bonnivard, C. Combet, D. Maurin, A. Geringer-Sameth, S. M. Koushiappas, M. G. Walker, M. Mateo, E. W. Olszewski, and J. I. Bailey III., Astrophys. J. **808**, L36 (2015).
[37] K. Hayashi, K. Ichikawa, S. Matsumoto, M. Ibe, M. N. Ishigaki, and H. Sugai, Mon. Not. R. Astron. Soc. **461**, 2914 (2016).
[38] J. L. Sanders, N. W. Evans, A. Geringer-Sameth, and W. Dehnen, Phys. Rev. D **94**, 063521 (2016).
[39] N. W. Evans, J. L. Sanders, and A. Geringer-Sameth, Phys. Rev. D **93**, 103512 (2016).
[40] K. Hayashi, M. Fabrizio, E. L. Łokas, G. Bono, M. Monelli, M. Dall'Ora, and P. B. Stetson, Mon. Not. R. Astron. Soc. **481**, 250 (2018).
[41] M. Petac, P. Ullio, and M. Valli, arXiv:1804.05052.
[42] V. Anastassopoulos *et al.* (CAST Collaboration), Nat. Phys. **13**, 584 (2017).
[43] C. Hagmann, P. Sikivie, N. S. Sullivan, and D. B. Tanner, Phys. Rev. D **42**, 1297 (1990).
[44] C. Hagmann *et al.* (ADMX Collaboration), Phys. Rev. Lett. **80**, 2043 (1998).
[45] S. J. Asztalos *et al.* (ADMX Collaboration), Phys. Rev. D **64**, 092003 (2001).
[46] N. Du *et al.* (ADMX Collaboration), Phys. Rev. Lett. **120**, 151301 (2018).
[47] L. Zhong *et al.* (HAYSTAC Collaboration), Phys. Rev. D **97**, 092001 (2018).
[48] A. Melcn *et al.*, J. Cosmol. Astropart. Phys. 05 (2018) 040.
[49] C. Hagmann, P. Sikivie, N. S. Sullivan, and D. B.Tanner, Phys. Rev. D **42**, 1297 (1990)
[50] R. Bhre *et al.*, J. Instrum. **8**, T09001 (2013).
[51] L. Di Luzio, F. Mescia, and E. Nardi, Phys. Rev. Lett. **118**, 031801 (2017).
[52] V. B. Klaer and G. D. Moore, J. Cosmol. Astropart. Phys. 11 (2017) 049.
[53] P. W. Graham, I. G. Irastorza, S. K. Lamoreaux, A. Lindner, and K. A. van Bibber, Annu. Rev. Nucl. Part. Sci. **65**, 485 (2015).
[54] S. E. Koposov, V. Belokurov, G. Torrealba, and N. W. Evans, Astrophys. J. **805**, 130 (2015).
[55] K. Bechtol *et al.* (DES Collaboration), Astrophys. J. **807**, 50 (2015).
[56] A. Drlica-Wagner *et al.* (DES Collaboration), Astrophys. J. **813**, 109 (2015).
[57] D. Massari and A. Helmi, arXiv:1805.01839.
[58] Z. Ivezic, J. A. Tyson, R. Allsman, J. Andrew, and R. Angel (LSST Collaboration), arXiv:0805.2366.
[59] S. M. Consiglio, J. L. Turner, S. Beck, D. S. Meier, S. Silich, and J.-H. Zhao, Astrophys. J. **850**, 54 (2017).

Eur. Phys. J. C (2019) 79:574
https://doi.org/10.1140/epjc/s10052-019-7083-y

THE EUROPEAN PHYSICAL JOURNAL C

Regular Article - Theoretical Physics

Leptogenesis from oscillations and dark matter

Andrea Caputo[a], **Pilar Hernandez**[b], **Nuria Rius**[c]

Instituto de Física Corpuscular, Universidad de Valencia and CSIC, Edificio Institutos Investigación, Catedrático Jose Beltrán 2, Paterna 46980, Spain

Received: 22 December 2018 / Accepted: 1 July 2019 / Published online: 9 July 2019

Abstract An extension of the Standard Model with Majorana singlet fermions in the 1–100 GeV range can explain the light neutrino masses and give rise to a baryon asymmetry at freeze-in of the heavy states, via their CP-violating oscillations. In this paper we consider extending this scenario to also explain dark matter. We find that a very weakly coupled $B-L$ gauge boson, an invisible QCD axion model, and the singlet majoron model can simultaneously account for dark matter and the baryon asymmetry.

1 Introduction

The standard model (SM) of particle physics needs to be extended to explain neutrino masses, the missing gravitating matter (DM) and the observed matter-antimatter asymmetry in the universe.

Some of the most minimal extensions of the SM include new fermions, namely two or three sterile Majorana neutrinos (singlets under the full gauge group), which can account for the tiny neutrino masses, through the seesaw mechanism [1–4], and explain the observed matter-antimatter asymmetry through leptogenesis [5]. The simplest version of leptogenesis establishes the source of the matter-antimatter asymmetry in the CP violating the out-of-equilibrium decay of the heavy neutrinos. This scenario requires however relatively large Majorana masses $> 10^8$ GeV [6] (or $\sim 10^6$ GeV with flavour effects [7] included), which makes these models difficult to test experimentally. For Majorana neutrinos in the 1–100 GeV range, it has been shown by Akhmedov, Rubakov and Smirnov (ARS) [8] and refined by Asaka and Shaposhnikov (AS) [9] that a different mechanism of leptogenesis is at work. In this case the asymmetries are produced at freeze-in of the sterile states via their CP-violating oscillations. The original ARS proposal did not include flavour effects and needs at least three Majorana species, while AS have shown that flavour effects can make it work with just two species. In the rest of the paper we will refer indistinctively to both scenarios as baryogenesis from oscillations (BO). In both cases, the lepton asymmetry is reprocessed into a baryonic one by electroweak sphalerons [10]. The extra heavy neutrinos in this case could be produced and searched for in beam dump experiments and colliders (see [11–23] for an incomplete list of works), possibly giving rise to spectacular signals such as displaced vertices [15,16,18,20,21]. Since only two sterile neutrinos are needed to generate the baryon asymmetry [9,24–39], the lightest sterile neutrino in the keV range can be very weakly coupled and play the role of DM [40]. This is the famous νMSM [9]. However the stringent X-ray bounds imply that this scenario can only work in the presence of a leptonic asymmetry [41] significantly larger than the baryonic one, which is quite difficult to achieve. A recent update of astrophysical bounds on this scenario can be found in [42,43].

In this paper our main goal is to consider scenarios compatible with Majorana masses in the 1–100 GeV range and study the conditions under which the models can explain DM without spoiling ARS leptogenesis.[1] In particular, we will focus on models that are minimal extensions of the type I seesaw model with three singlet neutrinos. We will first consider an extension involving a gauged $B-L$ model [45], which includes an extra gauge boson and can explain DM in the form of a non-thermal keV neutrino. We will then consider an extension which includes a CP axion [46] that can solve the strong CP problem and explain DM in the form of cold axions. Finally we consider the majoron singlet model [47,48] which can also explain DM under certain conditions both in the form of a heavy majorana neutrino or a majoron.

[a] e-mail: andrea.caputo@uv.es
[b] e-mail: pilar.hernandez@cern.ch
[c] e-mail: nuria.rius@ific.uv.es

[1] Some very recent work along these lines in the scotogenic model can be found in [44].

The plan of the paper is as follows. We start by briefly reviewing the ARS mechanism and the essential ingredients and conditions that need to be met when the sterile neutrinos have new interactions. In Sect. 3 we discuss the gauged $B-L$ model, in Sect. 4, we study the invisible axion model with sterile neutrinos and in Sect. 5 we reconsider the singlet majoron model. In Sect. 6 we conclude.

2 Leptogenesis from oscillations

For a recent extensive review of the ARS mechanism see [49]. The model is just the type I seesaw model with three neutrino singlets, N_i, $i=1-3$, which interact with the SM only through their Yukawa couplings. The Lagrangian in the Majorana mass basis is

$$\mathcal{L} = \mathcal{L}_{\rm SM} + i\overline{N}_i\gamma^\mu\partial_\mu N_i - \left(Y_{\alpha i}\overline{L}_\alpha N_i \Phi + \frac{m_{N_i}}{2}\overline{N}_i^c N_i + h.c.\right). \quad (1)$$

In the early Universe before the electroweak (EW) phase transition, the singlet neutrinos are produced through their Yukawa couplings in flavour states, which are linear combinations of the mass eigenstates. Singlet neutrinos then oscillate, and since CP is not conserved, lepton number L gets unevenly distributed between different flavours. At high enough temperatures $T \gg m_{N_i}$, total lepton number vanishes, in spite of which a surplus of baryons over antibaryons can be produced, because the flavoured lepton asymmetries are stored in the different species and transferred at different rates to the baryons. As long as full equilibration of the sterile states is not reached before the EW phase transition ($T_{\rm EW} \sim 140$GeV) , when sphaleron processes freeze-out, a net baryon asymmetry survives. It is *essential* that at least one of the sterile neutrinos does not equilibrate by $t_{\rm EW}$. The rate of interactions of these neutrinos at temperatures much higher than their mass can be estimated to be

$$\Gamma_\alpha \propto \kappa y_\alpha^2 T, \quad (2)$$

where y_α are the eigenvalues of the neutrino Yukawa matrix, T is the temperature and $\kappa =$ few 10^{-3} [50–52]. The Hubble expansion rate in the radiation dominated era is

$$H(T) = \sqrt{\frac{4\pi^3 G_N g_*}{45}}T^2 \equiv \frac{T^2}{M_P^*}. \quad (3)$$

where g_* is the number of relativistic degrees of freedom ($g_* \sim 100$ above the EW phase transition). The requirement that no equilibration is reached before $t_{\rm EW}$ is:

$$\Gamma_\alpha(T_{\rm EW}) \leq H(T_{\rm EW}), \quad (4)$$

which implies yukawa couplings of order

$$y_\alpha \lesssim 10^{-7}, \quad (5)$$

i.e. not much smaller than the electron yukawa. These yukawa couplings are compatible with the light neutrino masses for Majorana masses in the 1–100 GeV range.

Any model that extends the one described above with new fields/interactions should be such that the new interactions do not increase the equilibration rate of the sterile neutrinos for the out-of-equilibrium requirement in the ARS mechanism to be met. We will now consider the implications of this requirement on various extensions of the minimal seesaw model of Eq. (1) that are well motivated by trying to explain also the dark matter and in one case also the strong CP problem.

3 B-L gauge symmetry

The SM is invariant under an accidental global $U(1)_{B-L}$ symmetry, that couples to baryon minus lepton number. If one promotes this symmetry to a local one [45], the model needs to be extended with three additional right handed neutrinos to avoid anomalies, which interestingly makes the type I seesaw model the minimal particle content compatible with this gauge symmetry. In this case, we have interactions between SM lepton and quark fields with the new gauge boson, V_μ, as well as an additional term involving sterile neutrinos

$$\mathcal{L} \supset g_{B-L}\left(\sum_f Q^f_{B-L} V_\mu \overline{f}\gamma_\mu f - \sum_a V_\mu \overline{N}_a\gamma^\mu N_a\right), \quad (6)$$

where $Q^f_{B-L} = 1/3, -1$ for quarks and leptons respectively. We also assume the presence of a scalar field ϕ, with charge $B-L$ charge 2:

$$\mathcal{L} \supset (D_\mu\phi)^\dagger D_\mu\phi - V(\phi) - \frac{h_N}{2}\overline{N}^c N\phi + h.c., \quad (7)$$

that gets an expectation value $\langle\phi\rangle$, breaking $B-L$ spontaneously,[2] and giving a mass to both the gauge boson and the sterile neutrinos:

$$m_V = 2\sqrt{2}g_{B-L}\langle\phi\rangle, \quad m_{N_i} = h_{N_i}\langle\phi\rangle. \quad (8)$$

A massive higgs from the $B-L$ breaking, σ, remains in the spectrum with a mass that we can assume to be $M_\sigma \sim \langle\phi\rangle$.

Existing constraints on this model come from direct searches for V in elastic neutrino-electron scattering, V gauge boson production at colliders, Drell-Yan processes and new flavour changing meson decays [53–60]. The status of these searches is summarized in Fig. 1, adapted from [61] (see also [62–64]). For masses, 1 GeV $\leq m_V \leq$ 10 GeV, g_{B-L} is bounded to be smaller than $\sim 10^{-4}$, while the limit is weaker for larger masses. The improved prospects to search

[2] The Stuckelberg mechanism cannot be used here, because we need heavy neutrinos.

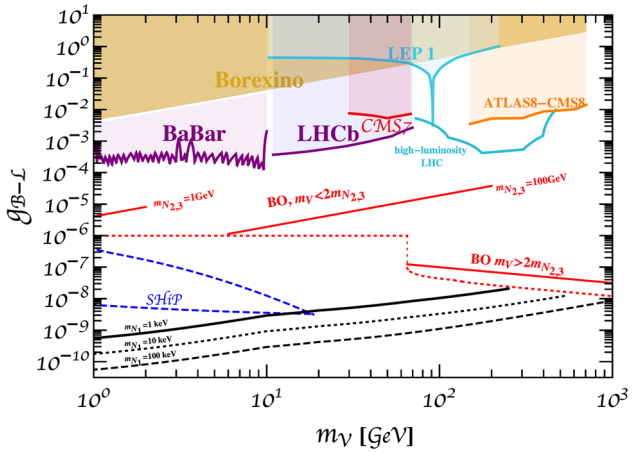

Fig. 1 Summary of present (shaded regions) and future (unshaded) constraints on g_{B-L} and m_V for the $B-L$ model, adapted from Ref. [61]. The dashed region labeled SHIP is the sensitivity of bremsstrahlung searches in SHIP [66,67]. The solid, dotted and dashed black lines correspond to the correct DM relic abundance in the form of sterile neutrinos of mass 1, 10 and 100 keV respectively. The dotted red line indicates the lower limit on the gauge coupling for which V is in thermal equilibrium. The solid red lines correspond to the upper bounds for successful BO leptogenesis for $m_{N_{2,3}} = 1$ and 100 GeV

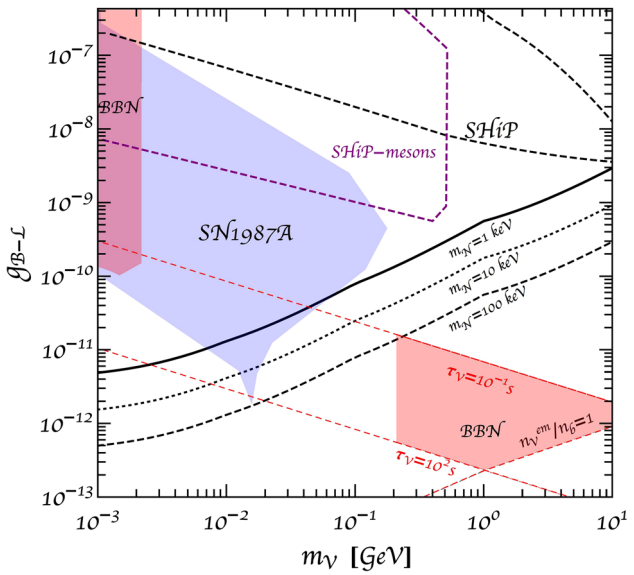

Fig. 2 Shaded regions are presently excluded by supernova observations [68], BBN bounds estimated in [69] and the combined beam dump experiments from [70]. Unshaded regions represent the reach of SHIP from meson decay and bremsstrahlung searches [66]. The curves indicate the values of (g_{B-L}, m_V) where the lightest sterile neutrino N_1 can account for the whole dark matter for three values of the neutrino masses, $m_N = 1$, 10, 100 keV in solid, dotted and dashed lines

for right-handed neutrinos exploiting the $U(1)_{B-L}$ interaction have been recently studied in [61], where the authors consider the displaced decay of the N at the LHC and the proposed SHIP beam dump experiment [65].

For $m_V \leq 1$GeV the strongest constraints come from supernova cooling [68,71–73], beam dump searches [70,74–78] and big bang nucleosynthesis (BBN) [69,70,79–81]. Recent updates on these bounds are compiled in Fig. 2. The lower mass region labeled BBN is excluded by the effect of $\Delta N_{\rm eff}$ on the expansion, while the higher mass BBN region is excluded because the injection of electromagnetic energy from the V decay to charged particles during nucleosynthesis distorts the abundance of light elements. These BBN constraints have been evaluated in detail in Refs. [79,80]. In the relevant region of parameter space, they are seen to depend on the lifetime of the decaying particle and its abundance per baryon prior to decay. The corresponding region in Fig. 2 is a sketch of the excluded region in the latter analysis, which is approximately bounded by the lines corresponding to the lifetimes $\tau_V \in [0.1-100]$s, the threshold for V hadronic decays, $m_V \geq 2m_\pi$, and the line corresponding to the fraction of the V decaying to charged particles per baryon, $n_V^{em}/n_b = 1$.

At least two of the neutrinos will be involved in the BO mechanism and their masses must be in the 1–100 GeV range. We need to ensure that the new $B-L$ interactions do not bring them to thermal equilibrium before t_{EW}, which will set an upper bound on g_{B-L}. It it important to know however if the $B-L$ gauge boson is in thermal equilibrium which also depends on g_{B-L}. For $m_V \lesssim 65$ GeV, the dominant process is the scattering $tt \leftrightarrow VH$ with a rate that can be estimated to be

$$\Gamma(tt \to VH) \simeq \frac{\zeta(3) g_{B-L}^2 y_t^2}{144\pi^3} T \log\left(\frac{T}{m_t(T)}\right), \tag{9}$$

where y_t is the Yukawa of the top quark and $m_t(T)$ is its thermal mass. This rate is larger than the Hubble expansion somewhere above the EW transition provided $g_{B-L} \gtrsim 10^{-6}$. For larger masses of the gauge boson ($m_V \gtrsim 65$GeV) the process $V \leftrightarrow f\bar{f}$ kinematically opens up at high temperature and one has to consider the decay and inverse decay with a rate

$$\Gamma(V \leftrightarrow f\bar{f}) = \sum_f \frac{g_{B-L}^2 N_C Q_f^2 m_V}{12\pi}\left(1+\frac{2m_f^2}{m_V^2}\right) \times \left(1-\frac{4m_f^2}{m_V^2}\right)^{1/2}, \tag{10}$$

where $N_C = 3(1)$ and $Q_f = 1/3(-1)$ for quarks(leptons). The sum is over all the standard model fermions whose thermal mass is such that $m_V(T) \geq 2m_f(T)$. The lower limit on g_{B-L} for the thermalization of the $B-L$ boson is shown as a dotted red line in Fig.1. Provided the $B-L$ boson is in thermal equilibrium we have to consider its interactions with the sterile neutrinos driving leptogenesis. Assuming that the V boson is lighter than $2m_N$, so that the decay $V \to NN$ is kinematically forbidden, the dominant contribution [82] comes from the scattering processes with the fermions and

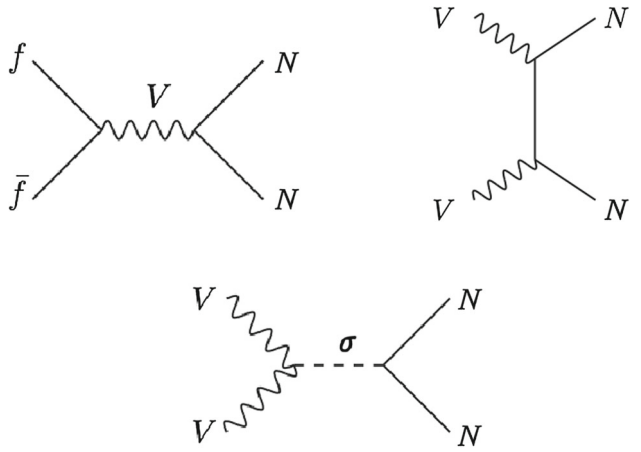

Fig. 3 Production of sterile neutrinos via the new gauge interaction

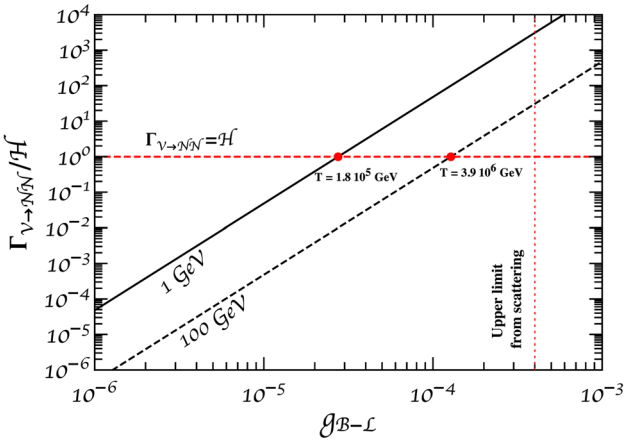

Fig. 4 $\Gamma(T)/H(T)$ including thermal effects for m_V and two values of the heavy neutrino masses $m_N = 1$, 100GeV for $T = 2\times$ the threshold temperature

gauge bosons in Fig. 3. To ensure these processes do not equilibrate the sterile neutrinos, we should have

$$\langle \Gamma(VV \to NN)\rangle_{T=\langle\phi\rangle} < H(T = \langle\phi\rangle) \tag{11}$$

Assuming $M_\sigma \sim \langle\phi\rangle \gg m_V, m_N$,

$$\langle \Gamma(VV \to NN)\rangle \sim \frac{g_{B-L}^4 m_N^2}{m_V^4}\frac{3\zeta(3)}{4\pi^3}T^3, \tag{12}$$

and using Eq. (8) we get

$$g_{B-L} < 5\cdot 10^{-6}\Big(\frac{m_V}{1\text{GeV}}\Big)\Big(\frac{1\text{GeV}}{m_N}\Big)^{2/3}. \tag{13}$$

This upper bound is shown by the red solid line in Fig. 1. In the next section we will include these new interactions in the equations for the generation of the baryon asymmetry, and our results confirm the naive estimate in Eq. (13).

Finally we consider the production of neutrinos through the decay of $\sigma \to NN$, which is relevant for $T \geq M_\sigma$, since $M_\sigma \gg m_N$. The requirement that this process does not thermalize the sterile neutrinos implies that the decay rate, Γ_σ, is slower than the Hubble rate at $T \geq M_\sigma$:

$$\Gamma_D(M_\sigma) = \frac{h_N^2 M_\sigma}{16\pi} \lesssim H(M_\sigma). \tag{14}$$

For $m_N = 1 - 100$ GeV, using Eq. (8), we get

$$M_\sigma \sim \langle\phi\rangle \geq 2\times 10^5 - 5\times 10^6\text{GeV}. \tag{15}$$

On the other hand, for $m_V \geq 2m_N$ the dominant production goes via the decay of the gauge boson into two sterile neutrinos $V \to NN$, which, if kinematically allowed, scales with g_{B-L}^2. In this case the decay rate is

$$\Gamma(V \to NN) = \frac{g_{B-L}^2 m_V}{24\pi}\left(1 - \frac{4m_N^2}{m_V^2}\right)^{3/2}. \tag{16}$$

Requiring that it is smaller than $H(T_{EW})$ implies for $m_N \ll m_V$

$$g_{B-L} \lesssim 10^{-7}\Big(\frac{100\text{GeV}}{m_V}\Big)^{\frac{1}{2}}. \tag{17}$$

One may worry if thermal mass corrections can allow the decay $V \to NN$ at large temperatures even if $m_V \leq 2m_N$. At high enough temperatures both sterile neutrinos and the gauge boson acquire thermal corrections to the masses of the form

$$m(T) \sim g_{B-L}T. \tag{18}$$

The thermal mass of the gauge boson is larger than that of the sterile neutrino, because all fermions charged under $B-L$ will contribute to the former and only the gauge boson loop contributes to the later [83]:

$$m_V^T = m_V + \sqrt{\frac{4}{3}}g_{B-L}T, \quad m_N^T = m_N + \frac{1}{\sqrt{8}}g_{B-L}T. \tag{19}$$

We substitute the temperature dependent mass in Eq. (16) and we show in Fig. 4 the ratio $\Gamma(V \to NN)/H$ close to the minimum threshold temperature (where $m_V^T \geq 2m_N^T$), for $m_N = 1$ and 100 GeV as a function of g_{B-L}. The upper limit for g_{B-L} are less stringent than those derived from $2 \to 2$ processes in Eq. (13).We now evaluate in detail the effect on BO induced by the new scatterings of Fig. 3. Leptogenesis in the presence of a new $B-L$ gauge interaction has been recently studied in [82], although not in the context of BO, which as far as we know has not been considered before.

3.1 Leptogenesis

The sterile neutrinos relevant for leptogenesis are the heavier ones, $m_{N_{2,3}}$, with masses in the 1–100 GeV, and we focus on the scenario where $m_V \leq 2m_{N_{2,3}}$. We now explain how to

include the terms involving the $B-L$ gauge interactions in the quantum kinetic equations for BO leptogenesis as derived in [31]. Following Raffelt-Sigl approach [84], we consider a density matrix, $\rho(k)$, describing the expectation value of number densities of N and a density matrix describing the corresponding anti-particles, $\bar{\rho}(k)$.[3] These equations are complemented with three equations involving the slow varying chemical potentials, $\mu_{B/3-L_\alpha}$. The modification of the kinetic equations induced by the $B-L$ interactions is the addition of new collision terms in the equations for ρ and $\bar{\rho}$, that have the same flavour structure as the neutral current contribution considered in [84]. As explained above the most relevant contributions come from the scattering processes: $\bar{f}f \leftrightarrow N\bar{N}$ and $VV \leftrightarrow N\bar{N}$. The latter is enhanced at high temperatures, but of course will only be relevant if the $V's$ are in thermal equilibrium, which we assume in the following.

The additional collision terms, from the first process, in the equation for the evolution $\rho(k)$ can be writen in the form:

$$\begin{aligned}(\dot{\rho}(k))^{ff\to NN}_{B-L} &= \frac{1}{2}\int\prod_i \frac{d^3p_i}{(2\pi)^3 2E_i}(2\pi)^4\delta(p_1+p_2-p_3-k)\\ &\times\sum_{spins}|\mathcal{M}(\bar{f}(p_1)f(p_2)\to\overline{N}(p_3)N(k))|^2\\ &\times f_1^{eq}f_2^{eq}\Big[2-\{r,\bar{r}\}-f_4^{eq}\{r,1-\bar{r}\}-f_3^{eq}\{\bar{r},1-r\}\Big],\end{aligned} \tag{20}$$

where $f_i^{eq}\equiv f_F(p_i)$ is the Fermi–Dirac equilibrium distribution function of the particle with momentum p_i with $p_4\equiv k$; $\{,\}$ is the anticommutator, and the normalized matrices are:

$$r(k)\equiv\frac{\rho(k)}{f_F(k)},\quad \bar{r}(p_3)\equiv\frac{\bar{\rho}(p_3)}{f_F(p_3)}. \tag{21}$$

The additional collision terms for $\bar{\rho}$ have the same form with the substitution $k\leftrightarrow p_3$.

For the second process we have similarly:

$$\begin{aligned}(\dot{\rho}(k))^{VV\to NN}_{B-L} &= \frac{1}{2}\int\prod_i \frac{d^3p_i}{(2\pi)^3 2E_i}(2\pi)^4\delta(p_1+p_2-p_3-k)\\ &\times\sum_{spins}|\mathcal{M}(V(p_1)V(p_2)\to\overline{N}(p_3)N(k))|^2\\ &\times f_1^{eq}f_2^{eq}\Big[2-\{r,\bar{r}\}-f_4^{eq}\{r,1-\bar{r}\}-f_3^{eq}\{\bar{r},1-r\}\Big],\end{aligned} \tag{22}$$

where f_i^{eq} is the equilibrium distribution function of the particle with momentum p_i, ie. Bose–Einstein, $f_i^{eq}\equiv f_B(p_i)$, for $i=1,2$ and Fermi–Dirac, $f_i^{eq}\equiv f_F(p_i)$, for $i=3,4$.

[3] We can neglect Majorana masses in the range of masses considered and therefore particles and antiparticles correspond to the two helicity states.

As usual we are interested in the evolution in an expanding universe, where the density matrices depend on momentum, $y\equiv p/T$ and the scale factor or inverse temperature $x\propto T^{-1}$. We consider the averaged momentum approximation, which assumes that all the momentum dependence factorizes in the Fermi–Dirac distribution and the density r is just a function of the scale factor, ie. $\rho(x,y)=f_F(y)r(x)$. In this approximation we can do the integration over momentum and the $B-L$ terms in the equation for r and $\bar{r}$ become:

$$\begin{aligned}\left(xH\frac{dr}{dx}\right)_{B-L} &= \left(xH\frac{d\bar{r}}{dx}\right)_{B-L} = \frac{\langle\gamma_V^{(0)}\rangle}{2}\Big(2-\{r,\bar{r}\}\Big)\\ &-\langle\gamma_V^{(1)}\rangle\Big(r+\bar{r}-\{r,\bar{r}\}\Big),\end{aligned} \tag{23}$$

where H is the Hubble expansion parameter.

The averaged rates including the two processes in Eqs. (20) and (22) (assuming in the latter the $Z's$ are in equilibrium) are computed in the appendix with the result:

$$\begin{aligned}\langle\gamma_V^{(0)}\rangle &= \left(3.2(3)\times10^{-3}+2.95\times10^{-4}\frac{m_N^2T^2}{m_V^4}\right)g_{B-L}^4T,\\ \langle\gamma_V^{(1)}\rangle &= \left(3.4(1)\times10^{-4}+3.55\times10^{-5}\frac{m_N^2T^2}{m_V^4}\right)g_{B-L}^4T,\end{aligned} \tag{24}$$

where the two terms inside the brackets correspond respectively to the $f\bar{f}$ and VV channels, and are valid for $T<T_{\max}\equiv M_\sigma\sim\langle\phi\rangle=\frac{m_V}{2\sqrt{2}g_{B-L}}$. Note the different temperature dependence of the two contributions. The growth of the $VV\leftrightarrow NN$ at high temperatures originates in the contribution of the longitudinal polarization of the V bosons when the temperature is below the scalar mass, M_σ. For higher temperature, $T\geq T_{\max}$, the contribution of the physical scalar σ has to be included, leading to a rate $\propto T$. The new interactions do not modify the chemical potential dependent terms, nor the evolution equation for $\mu_{B/3-L_\alpha}$. The equations are therefore those in [31] with the additional $B-L$ terms in Eq. (23).

To illustrate the effect of the $B-L$ gauge interaction, we have considered the test point of Ref. [31] with masses for the heavy steriles $m_{N_{2,3}}\sim0.8$ GeV. Within the parameter space of successful leptogenesis, this point was chosen because it leads to charmed meson decays to heavy sterile neutrinos that could be observable in SHIP, and furthermore this measurement, in combination with input from neutrinoless double beta decay and CP violation in neutrino oscillations, could provide a quantitative prediction of the baryon asymmetry. Adding the $B-L$ terms to the equations for r and $\bar{r}$ of [31], and solving them numerically (for details on the method see [31]) we obtain the curves in Fig. 5. The rates depend on m_V so we choose $m_V=1$GeV. The evolution of

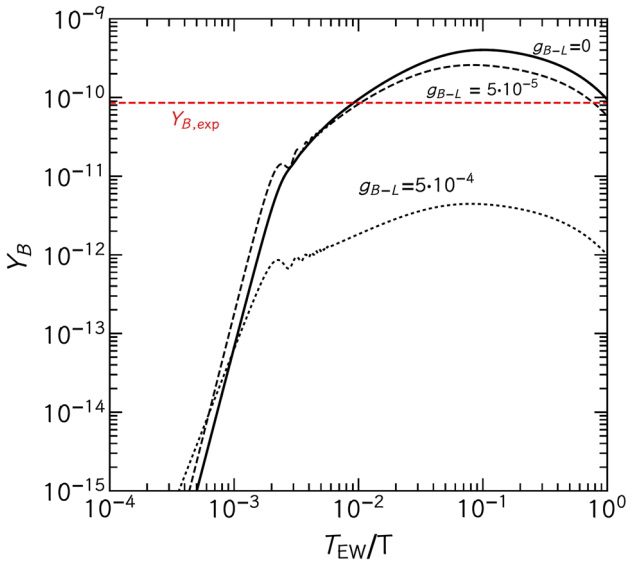

Fig. 5 Y_B as a function of $T_{\rm EW}/T$ for the Y and m_N parameters corresponding to the test point in [31] and $g_{B-L} = 0$ (solid), $g_{B-L} = 5 \times 10^{-5}$ (dashed), $g_{B-L} = 5 \times 10^{-4}$ (dotted). The horizontal line is the observed value

the baryon asymmetry as a function of $T_{\rm EW}/T$ is shown by the solid line of Fig. 5 in the absence of $B-L$ interactions or for a sufficiently small value of g_{B-L}. The suppression of the asymmetry is visible for larger values of $g_{B-L} \gtrsim \text{few} \times 10^{-5}$ as shown by the dashed and dashed-dotted lines. The naive expectations in Fig. 1 is therefore confirmed and we do not expect a significant modification of the baryon asymmetry of the minimal model, as long as g_{B-L} satisfies the bound in Eq. (13).

3.2 Dark matter

Now we want to discuss possible dark matter candidates in the $B-L$ scenario without spoiling the BO mechanism, which as we have seen imposes a stringent upper bound on the gauge coupling, g_{B-L}. We will be interested in the region where the V boson can decay to the lightest neutrino, ie $m_V \geq 2m_{N_1}$. The small value needed for g_{B-L} suggests to consider the possibility of a freeze-in scenario [85,86], where the gauge boson does not reach thermalization, and neither does the lightest sterile neutrino, N_1. The status of dark matter in a higher mass range through freeze-out has been recently updated in [64].

As it is well known, N_1 in the keV mass range is sufficiently long lived to provide a viable warm DM candidate [40,41]. The $B-L$ model is as we will see a simple extension of the νMSM [9], which avoids the need of huge lepton asymmetries to evade X-ray bounds. In our scenario the keV state is produced from the decay $V \to N_1 N_1$, while the lifetime of N_1, relevant in X-ray bounds, is controlled also by mixing, which can be sufficiently small, in a technically natural way, as in the νMSM scenario (provided the lightest neutrino mass is small enough). A similar scenario for DM has been studied in [67]. We now quantify the parameter space for successful DM and leptogenesis in this scenario.

We assume that the abundance of V and N_1 is zero at a temperature below the EW phase transition where all the remaining particles in the model are in thermal equilibrium. All fermions in the model couple to the V and therefore its production is dominated by the inverse decay process: $f\bar{f} \to V$. The kinetic equation describing the production of V is the following:

$$\begin{aligned}\dot{n}_V + 3Hn_V = \sum_f \int \frac{d^3p_f}{(2\pi)^3 2E_f} \frac{d^3p_{\bar{f}}}{(2\pi)^3 2E_{\bar{f}}} \frac{d^3p_V}{(2\pi)^3 2E_V} \\ \times (2\pi)^4 \delta^4(p_V - p_f - p_{\bar{f}}) [|M|^2_{f\bar{f}\to V} f_f f_{\bar{f}} (1+f_V) + \\ - |M|^2_{V\to f\bar{f}} f_V (1-f_f)(1-f_{\bar{f}})],\end{aligned} \tag{25}$$

where $f_i(p)$ are the distribution function of the particle, i, with momentum p, and

$$n_i = g_i \int \frac{d^3p}{(2\pi)^3} f_i(p), \tag{26}$$

is the number density, with g_i the number of spin degrees of freedom. $g_f = 4$ for a Dirac fermion, $g_N = 2$ for a Majorana fermion and $g_V = 3$ for a massive gauge boson. M is the amplitude for the decay $V \to f\bar{f}$ at tree level.

The sum over f is over all fermions, but we can safely neglect the contribution of the N_1 and also those that are non-relativistic. We can also neglect the Pauli-blocking and stimulated emission effects ($f_i \pm 1 \sim \pm 1$) and approximate the distribution function in equilibrium for fermions and bosons by the Maxwell-Boltzmann, $f_i(p_i) = f^{eq}(p_i) = e^{-E_i/T}$. Taking into account the relation

$$|M|^2_{V\to f\bar{f}} = |M|^2_{f\bar{f}\to V}, \tag{27}$$

and the principle of detailed balance

$$f^{eq}_f f^{eq}_{\bar{f}} = f^{eq}_V, \tag{28}$$

the equation can be simplified to

$$\begin{aligned}\dot{n}_V + 3Hn_V = -\sum_f \int \frac{d^3p_f}{(2\pi)^3 2E_f} \frac{d^3p_{\bar{f}}}{(2\pi)^3 2E_{\bar{f}}} \frac{d^3p_V}{(2\pi)^3 2E_V} \\ (2\pi)^4 \delta^4(p_V - p_f - p_{\bar{f}}) |M|^2_{V\to f\bar{f}} \left(f_V(p_V) - f^{eq}(p_V)\right).\end{aligned} \tag{29}$$

As long as $f_V \ll f^{eq}$, the first term on the right-hand side can be neglected and the equation simplifies further to:

$$\dot{n}_V + 3Hn_V \simeq 3 \sum_f \frac{m_V^2 \Gamma_{V\to f\bar{f}}}{2\pi^2} T K_1\left(\frac{m_V}{T}\right), \tag{30}$$

where K_1 is the first modified Bessel Function of the 2nd kind. The decay width in the V rest frame is given by

$$\Gamma(V \to f\bar{f}) = \frac{g_{B-L}^2 N_C Q_f^2 m_V}{12\pi}\left(1+\frac{2m_f^2}{m_V^2}\right) \times \left(1-\frac{4m_f^2}{m_V^2}\right)^{1/2}, \tag{31}$$

where $N_C = 3(1)$ and $Q_f = 1/3(-1)$ for quarks(leptons).

As usual we define the yield of particle i as

$$Y_i = \frac{n_i}{s}, \tag{32}$$

where s is the entropy density

$$s = \frac{2\pi^2}{45} g_s^* T^3, \tag{33}$$

and we can assume $g_s^* \simeq g^*$. We also consider the averaged momentum approximation which amounts to assuming that f_V has the same momentum dependence as f^{eq}. Changing variable from time to temperature, the final evolution equation for Y_V reads:

$$\frac{dY_V}{dT} = -3\sum_f \frac{m_V^2 \Gamma_{V\to f\bar{f}}}{2\pi^2 Hs\left[1+\frac{1}{3}\frac{T dg_*}{g_* dT}\right]} K_1\left(\frac{m_V}{T}\right) \times \left(1-\frac{sY_V}{n_V^{eq}}\right), \tag{34}$$

where $n_V^{eq} = \frac{3}{2\pi^2} m_V^2 T K_2(m_V/T)$.

The production of N_1 is dominated by the decay $V \to N_1 N_1$. There is also the contribution via mixing with the active neutrinos but this is negligible for mixings that evade present X ray bounds. Neglecting the inverse processes, the evolution equation for n_1 is

$$\dot{n}_1 + 3Hn_1 = 2\frac{K_1(x)}{K_2(x)}\Gamma(V \to N_1 N_1) n_V, \tag{35}$$

and in terms of the yield

$$\frac{dY_{N_1}}{dT} = -\frac{2}{HT\left[1+\frac{1}{3}\frac{T dg_*}{g_* dT}\right]}\frac{K_1(x)}{K_2(x)}\Gamma(V \to N_1 N_1) Y_V, \tag{36}$$

where

$$\Gamma(V \to N_1 N_1) = \frac{g_{B-L}^2 m_V}{24\pi}\left(1-\frac{4m_{N_1}^2}{m_V^2}\right)^{3/2}. \tag{37}$$

It is straightforward to solve these equations. In Fig. 6 we show the yields of V and N as function of the inverse temperature for $m_V = 10$ MeV, $m_{N_1} = 10$ keV and $g_{B-L} = 10^{-11.4}$.

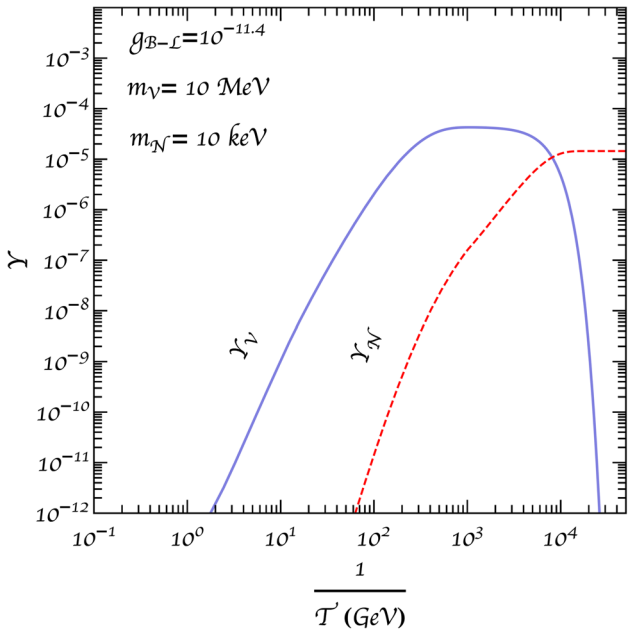

Fig. 6 V and N_1 yields as a function of the inverse temperature for $m_V = 10$ MeV and $g_{B-L} = 10^{-11.4}$

The resulting abundance of N_1 is

$$\Omega_{N_1} h^2 \equiv \frac{s_0 m_{N_1}}{\rho_c h^{-2}} Y_{N_1} \simeq 2.7 \times 10^2 Y_{N_1} \frac{m_{N_1}}{\text{keV}}, \tag{38}$$

where $s_0 = 2889.2$ cm^{-3} is the entropy today and $\rho_c = 1.0510^{-5} h^2$ GeV cm^{-3} is the critical density. The evolution of $\Omega_{N_1} h^2$ is shown in Fig. 7 for two values of m_V and a fixed value of g_{B-L}. Requiring that $\Omega_{N_1} h^2$ equals the full DM contribution of $\Omega_{DM} h^2 \simeq 0.12$ implies a relation between m_V and g_{B-L} as shown in the curves of Fig. 2. The values of g_{B-L} corresponding to the right dark matter relic abundance do not affect leptogenesis and lie far below the actual collider limits. Nevertheless some regions of the parameter space are interestingly excluded from supernova and BBN observations.

A final comment concerns the comparison of our calculation of the DM abundance and that in Ref. [67]. In this reference only the evolution of the N_1 is considered, and the collision term corresponds to the scattering process $f\bar{f} \to N_1 N_1$, where the narrow width approximation is assumed. We believe this method is only equivalent to ours when all f, $\bar{f}$ and V distributions are the equilibrium ones, but this is not the case here. In the region they can be compared our results are roughly a factor three smaller than those in [67].

3.3 Couplings

According to the previous calculation, the relic DM abundance requires a very small $B-L$ coupling. In order to

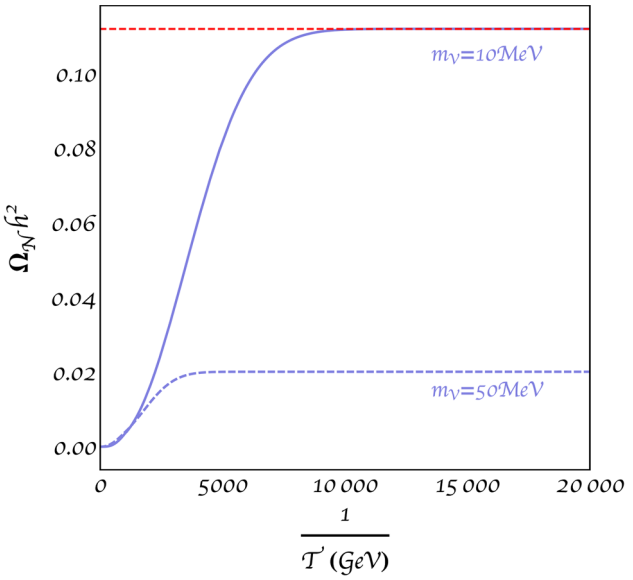

Fig. 7 The evolution of the density $\Omega_N h^2$ of the sterile neutrino N_1 in the $B-L$ model as a function of $1/T\,(GeV)$. Here we have fixed $m_{N_1} = 10$ keV, $g_{B-L} = 10^{-11.4}$, and used two different value of the boson mass: $m_V = 10, 50$ MeV. The gray line indicates the experimental value for dark matter abundance today

obtain, for example, a mass $m_V \sim 1$ MeV, the gauge coupling needed to generate DM is

$$g_{B-L} \sim 10^{-11.8}, \tag{39}$$

and therefore

$$\langle\phi\rangle \sim 2 \cdot 10^8\,\text{GeV}. \tag{40}$$

In order to get the N_1 and $N_{2,3}$ in the target range of keV and 1–100 GeV respectively, small and hierarchical h_{N_i} couplings are needed:

$$h_{N_2} \simeq h_{N_3} \sim 10^{-6} - 10^{-8}, \tag{41}$$

for the heavy sterile neutrinos involved in BO leptogenesis and

$$h_{N_1} \sim 10^{-12}, \tag{42}$$

for the dark matter candidate. Note that the required h_N's couplings are in the same ballpark as the yukawa couplings. The gauged $B - L$ model works nicely to explain neutrino masses, the baryon asymmetry and dark matter. Unfortunately it also requires a very small g_{B-L} which will be very hard to test experimentally. An alternative might be to consider a flavoured $U(1)$, for example $L_\mu - L_\tau$, that might be compatible with a larger g_{B-L}, provided the assignment of charges to the singlet states ensures that not all of them reach thermalization via the flavoured gauge interaction before t_{EW}.

4 Axion and neutrinos

As a second example we consider an extension of Eq. (1) with a scalar doublet and a scalar singlet. This model is also an extension of the invisible axion model [87] with sterile neutrinos, that was first considered in [46], providing a connection between the Peccei–Quinn (PQ) symmetry breaking scale and the seesaw scale of the neutrino masses. The model contains two scalar doublets, Φ_i, and one singlet, ϕ. A $U(1)_{PQ}$ global symmetry exists if the two Higgs doublets couple separately to the up and down quarks and leptons so that the Yukawa Lagrangian takes the form:

$$\begin{aligned}\mathcal{L} \supset & -Y_u \overline{Q}_L \Phi_1 u_R - Y_d \overline{Q}_L \Phi_2 d_R - Y \overline{L}_L \Phi_1 N \\ & - Y_l \overline{L}_L \Phi_2 l_R - \frac{h_N}{\sqrt{2}} \overline{N^c} N \phi + h.c.\end{aligned} \tag{43}$$

leading naturally to type II two-Higgs-doublet models without FCNC [88,89].

The most general scalar potential of the model compatible with a global $U(1)_{PQ}$ is the following

$$\begin{aligned}V = & \, m_1^2|\Phi_1|^2 + m_2^2|\Phi_2|^2 + m^2|\phi|^2 \\ & + \frac{\lambda_1}{2}|\Phi_1|^4 + \frac{\lambda_2}{2}|\Phi_2|^4 + \lambda_3|\Phi_1|^2|\Phi_2|^2 \\ & + \lambda_4(\Phi_1^\dagger \Phi_2)(\Phi_2^\dagger \Phi_1) \\ & + \frac{\lambda_\phi}{2}|\phi|^4 + \lambda_{1\phi}|\Phi_1|^2|\phi|^2 + \lambda_{2\phi}|\Phi_2|^2|\phi|^2 \\ & + k(\Phi_1^\dagger \Phi_2)\phi^2.\end{aligned} \tag{44}$$

The couplings in this potential can be chosen such that ϕ gets an expectation value,

$$\langle\phi\rangle = \frac{1}{\sqrt{2}} f_a, \tag{45}$$

$U(1)_{PQ}$ is then spontaneously broken and a Nambu-Goldstone boson appears, the QCD axion. Furthermore the Majorana singlets N get a mass. Expanding around the right vacuum, the field can be writen as

$$\phi = \frac{1}{\sqrt{2}}(f_a + \sigma + ia), \tag{46}$$

where σ is a massive field, while a is the axion. Therefore after symmetry breaking we obtain an interaction term between sterile neutrinos and axions

$$\mathcal{L} \supset -\frac{i h_N}{2} a \overline{N^c} N + h.c. \tag{47}$$

The breaking scale f_a must be much larger than the vacuum expectation values of the doublets, $\gg v_{1,2}$, so that the axion can evade the stringent bounds from rare meson decays and supernova cooling, which sets a stringent lower bound $f_a \geq 4 \cdot 10^8$GeV [90].

The mass of the axion is induced by the QCD anomaly in the sub-eV range:

$$m_a \simeq \frac{z^{1/2}}{1+z}\frac{m_\pi f_\pi}{\langle\phi\rangle}, \tag{48}$$

where $z = m_u/m_d$. For $f_a \geq 4 \cdot 10^8$ GeV, we have

$$m_a \leq \mathcal{O}\left(10^{-2}\right) \text{eV}. \tag{49}$$

It is well known that the invisible axion is a viable cold DM candidate, through the misalignment mechanism [87,91,92] (for recent reviews see [93,94]). The DM energy density is given by

$$\Omega_a h^2 \sim 2 \cdot 10^4 \left(\frac{f_a}{10^{16}\text{GeV}}\right)^{7/6} \langle\theta_0\rangle^2, \tag{50}$$

where θ_0 is the misalignment angle. The constraints on f_a depend on whether the breaking of the PQ symmetry happens before or after inflation; in the latter case the misalignment angle can be averaged over many patches

$$\langle\theta_0\rangle^2 \sim \frac{\pi^2}{3}, \tag{51}$$

so $\Omega_a \leq \Omega_{\text{DM}}$ implies

$$f_a \lesssim 1.2 \cdot 10^{11}\text{GeV}, \tag{52}$$

with the equality reproducing the observed cold dark matter energy density $\Omega_{\text{CDM}}h^2 \sim 0.12$. This correspond to the solid line in Fig. 8. If the PQ symmetry is broken before inflation, θ_0 is a free parameter and the value of f_a to account for DM is inversely proportional to θ_0^2.

The axion can also manifest itself as dark radiation [95], given that it is also thermally produced [96]. This population of hot axions contributes to the effective number of relativistic species, but the size of this contribution is currently well within the observational bounds [97].

In this model the VEV of the scalar singlet gives a Majorana mass to the sterile neutrinos:

$$m_N \approx h_N f_a. \tag{53}$$

So, if we want a mass in the electroweak range, $\mathcal{O}(1-10^2)$ GeV and $f_a \in [10^8, 10^{11}]$ GeV, we need the coupling h_N to be in the range:

$$h_N \in [10^{-11}, 10^{-6}]. \tag{54}$$

The hierarchy between f_a and the electroweak scale requires that some couplings in the scalar potential in Eq. (44) $(k, \lambda_{1\phi}, \lambda_{2\phi})$ are very small. Even if not very appealing theoretically, these small numbers are technically natural as already pointed out in [98], where the authors studied the same model with very heavy sterile neutrinos.

A relevant question is that of naturalness or fine-tunning of the Higgs mass in this model. In [98], this issue was studied in the context of high-scale thermal leptogenesis, and it was concluded that stability imposes relevant constraints. In particular, a relatively small $v_2 \lesssim 30$ GeV is necessary to ensure viable leptogenesis for lower $m_N = 10^5 - 10^6$GeV so that yukawa's are small enough, $y \leq 10^{-4}$, and do not induce unnaturally large corrections to the Higgs mass. In our case, the yukawa couplings, Eq. (5), are too small to give large corrections to the Higgs mass , so no additional constraint needs to be imposed on v_2. As a consequence other invisible axion models, such as the KSVZ [99,100], would also work in the context of low-scale m_N, but leads to tension with stability bounds in the high-scale version [101,102].

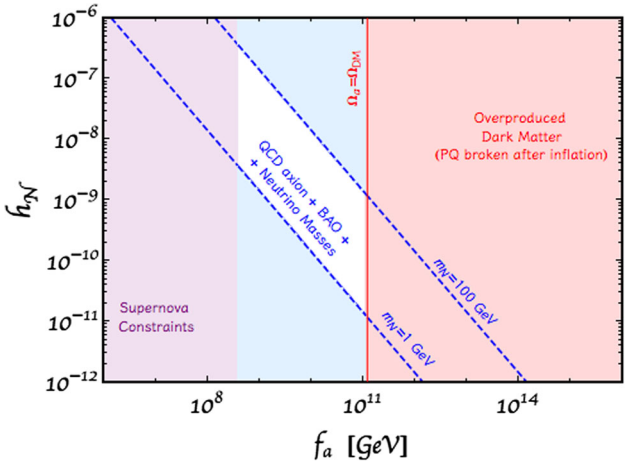

Fig. 8 The light purple region is forbidden by supernova cooling constraints (left band) and the red one by axions over closing the universe (right band). Axions can explain the DM relic density in the vertical line, if inflation happens before PQ symmetry breaking. Within the remaining parameter space, in the region between the two dashed lines successful leptogenesis via oscillations is possible

4.1 Baryon asymmetry

The possibility to generate the baryon asymmetry in this model a la Fukugita-Yanagida for very heavy neutrinos $m_N \sim f_a$ was recognized in the original proposal [46] and further elaborated in [98]. We want to point out here that for much smaller values of h_N, the BO mechanism could also work successfully.

As explained above the crucial point is whether the new interactions of the sterile states in this model are fast enough to equilibrate all the sterile neutrinos before EW phase transition. The leading order process we have to consider is the decay of the scalar into two sterile neutrinos $\sigma \to NN$, exactly as we considered in the previous section. The limit of $M_\sigma \sim f_a \geq 2 \times 10^5 - 5 \times 10^6$ GeV derived in Eq. (15) also applies here, which is safely satisfied given the supernova cooling bounds.

At second order, we must also consider the new annihilation process of sterile neutrinos to axions $NN \leftrightarrow aa$ as shown in Fig. 9. The rate of this process at high tempera-

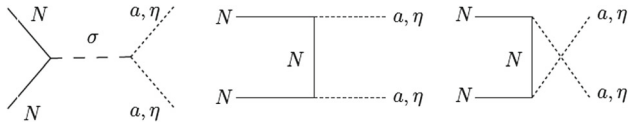

Fig. 9 Annihilations of sterile neutrinos into Majorons

tures, $T \gg m_N$, is given by

$$\Gamma_{N_a} = \frac{T^3 m_N^2}{192\pi f_a^4}. \tag{55}$$

The condition $\Gamma_{N_a}(T) < H(T)$ is satisfied for $T \leq f_a$ if

$$f_a \geq 1.2 \cdot 10^5 \left(\frac{m_N}{1\text{GeV}}\right)^{2/3} \text{GeV} \tag{56}$$

(for $m_N \in [1, 10^2]$ GeV), safely within the targeted range. Fig. 8 shows the region on the (f_a, h_N) plane for which successful baryogenesis through the BO mechanism and DM can work in this model.

Even if the necessary condition for BO leptogenesis is met for $f_a \geq 10^8$ GeV, the presence of the extra degrees of freedom, the axion, the heavy scalar and the second doublet could modify quantitatively the baryon asymmetry. For example, the presence of two scalar doublets could modify the scattering rates of the sterile neutrinos considered in the BO scenario, where the main contributions [35,50,52,103] are:

- $2 \leftrightarrow 2$ scatterings on top quarks via higgs exchange
- $2 \leftrightarrow 2$ scatterings on gauge bosons
- $1 \leftrightarrow 2$ decays or inverse decays including resumed soft-gauge interactions

Sterile neutrinos are coupled to the same Higgs doublet that also couples to the top quarks; in this case nothing changes with respect to the usual calculation, in which the reactions with top quarks are mediated by Φ_1. However, an alternative model, with a different $U(1)_{PQ}$ charge assignment, is also possible, in which the sterile neutrinos couple to ϕ_2 and not ϕ_1, as done in [98]. In this case top quark scattering does not contribute to sterile neutrino production at tree level, but the baryon asymmetry is not expected to change significantly, since the scattering rate on gauge bosons and the $1 \to 2$ processes are equally important [50,52].

The process $\sigma \to NN$ is not foreseen to be relevant for $M_\sigma \sim f_a$, since the scalar is long decoupled when the generation of the asymmetry starts, while the new process $NN \leftrightarrow aa$ is expected to be very small according to the above estimates. It could nevertheless be interesting to look for possible corners of parameter space where the differences with respect to the minimal model is not negligible since this could provide a testing ground for the axion sector of the model.

5 Majoron model

In between the two models described in 3–4, there is the possibility of having a global $U(1)$ spontaneously broken, which is not related to the strong CP problem and we call it lepton number. This is of course the well-known singlet majoron model [47,48,104]. We assume the sterile neutrinos carry lepton number, $L_N = 1$, but Majorana masses are forbidden and replaced by a yukawa interaction as in the $B - L$ model:

$$\mathcal{L} \supset -\left(\overline{L} Y N \Phi + \frac{1}{\sqrt{2}} h_N \overline{N^c} N \phi + h.c.\right) \tag{57}$$

where Φ is the standard model Higgs doublet, while ϕ is a complex scalar which carries lepton number $L_\phi = -2$. Then, the complex scalar acquires a VEV

$$\phi = \frac{f + \sigma + i\eta}{\sqrt{2}} \tag{58}$$

and the $U(1)_L$ is spontaneously broken giving rise to the right-handed Majorana mass matrix and leading to a Goldstone boson η, the majoron. Consequently the Lagrangian will induce the new scattering processes for neutrinos depicted in Fig. 9.

As usual we have to ensure that at least one sterile neutrino does not equilibrate before T_{EW} (see [105,106] for a recent discussion in the standard high-scale or resonant leptogenesis). As in the previous cases we have to consider the decay $\sigma \to N_i N_i$ and the annihilation into majorons, Fig. 9. The former gives the strongest constraint, as in Eq. (15):

$$M_\sigma \sim f \geq 2 \times 10^5 - 5 \times 10^6 \text{GeV}. \tag{59}$$

These lower bounds for $m_N = 1$ and 100 GeV are shown by the horizontal lines in Fig. 10.

5.1 Dark matter

There are two candidates in this model for dark matter that we consider in turn: the Majoron and the lightest sterile neutrino, N_1.

5.1.1 Majoron

In this model a natural candidate for dark matter is the majoron itself, but it has to acquire a mass, therefore becoming a pseudo Nambu-Goldstone boson (pNGB). One possibility is to appeal to gravitational effects [107,108]. However, the contribution to the mass from gravitational instantons is estimated to be [109–111]

$$m_\eta \sim M_P e^{-\frac{M_P}{f}}, \tag{60}$$

and therefore extremely tiny, unless f is close to the Planck scale.

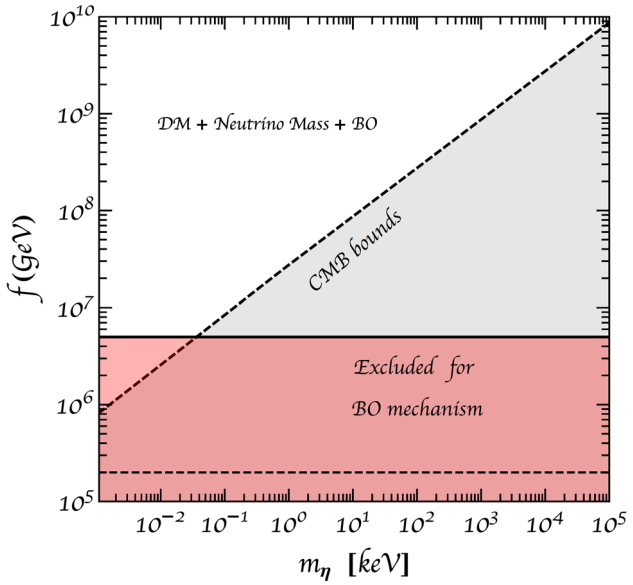

Fig. 10 Constraints in the plane $f - m_\eta$ considering the Majoron as the only dark matter component. The region in gray below the dashed line is excluded from CMB measurements [115], while the light red region below the solid (dashed) line is excluded in order not to spoil ARS for $M_N = 100$ (1) GeV

Another alternative is to consider a flavoured $U(1)_X$ and soft symmetry breaking terms in the form of yukawa couplings [112,113]. This possibility has been studied in detail in Ref. [113]. It has been shown that the majoron can be the main component of dark matter for sterile neutrino masses $m_N \geq 10^5$ GeV, while for masses in the range we are interested in ($m_N \sim 1 - -100$ GeV) neither thermal production via freeze-out nor via freeze-in works.

The possibility to produce it via vacuum misalignment, analogous to the one which produces the axion relic density has also been discussed in [113]. It was shown to give a negligible contribution compared to the thermal one, because the majoron gets a temperature dependent mass at early times. Even if the mass of the majoron is significantly smaller in our situation, with lighter m_N, we find the same result, ie. that only a small fraction of the DM can be produced via misalignmet.

No matter what the production mechanism is if the majoron constitutes the dark matter, there are constraints from the requirement that the majoron be stable on a cosmological timescale and its decay to the light neutrinos

$$\Gamma(\eta \to \nu\nu) = \frac{1}{64\pi}\frac{\sum_i m_{\nu_i}^2}{f^2} m_\eta \tag{61}$$

should not spoil the CMB anisotropy spectrum [114,115]. This gives constraints on the mass m_η and the symmetry breaking scale f, as showed in Fig.10.

As in the axion case there are additional constraints from supernova cooling [116], but they are much weaker and give an upper bound much lower than the range shown in Fig. 10. In the unconstrained region in Fig. 10, ARS leptogenesis and majoron DM could in principle work provided the mechanism to generate the majoron mass does not involve further interactions of the sterile neutrinos.

5.1.2 Sterile neutrino

We want now to consider the sterile neutrino as a dark matter candidate, a possibility already explored in [117,118] in a model with a real scalar field and therefore no Majoron. In our case the presence of the Majoron could make the sterile neutrino unstable, given that it would decay through the channel

$$\Gamma(N \to \nu\eta) = \frac{1}{32\pi}\left(\frac{m_N}{f}\right)^2 m_\nu \tag{62}$$

Thus one has to assume that the Majoron has a larger mass so that this decay is kinematically forbidden.

As in the $B-L$ case, BO leptogenesis is driven by the other two heavier neutrino states $N_{2,3}$, while N_1 can be produced through freeze-in from $\sigma \to N_1 N_1$ decay. Assuming σ is in thermal equilibrium with the bath the Boltzmann equation describing the evolution of the N_1 density:

$$\dot{n}_1 + 3Hn_1 = 2\frac{M_\sigma^2 \Gamma_{\sigma\to N_1 N_1}}{2\pi^2} T K_1\left(\frac{M_\sigma}{T}\right), \tag{63}$$

where we have neglected Pauli blocking, and the inverse processes.

Following the standard procedure we end with the contribution to the abundance:

$$\Omega_{N_1} h^2 \sim \frac{10^{27}}{g_*^{3/2}} \frac{m_{N_1}\Gamma_{\sigma\to N_1 N_1}}{M_\sigma^2}. \tag{64}$$

Using

$$\Gamma_{\sigma\to N_1 N_1} = \frac{h_N^2 M_\sigma}{16\pi}\left(1 - \frac{4m_{N_1}^2}{M_\sigma^2}\right) \sim \frac{h_N^2 M_\sigma}{16\pi}, \tag{65}$$

and requiring that $\Omega_{N_1} h^2$ matches the observed DM we find

$$h_N \sim 4.3 \cdot 10^{-13}\sqrt{\frac{m_{N_1}}{M_\sigma}}\left(\frac{g_*(m_{N_1})}{10}\right)^{3/4}. \tag{66}$$

The mass of the DM candidate is related to the coupling which regulates the freeze-in process through the VEV of ϕ

$$m_{N_1} = h_{N_1}\langle\phi\rangle, \tag{67}$$

therefore if $M_\sigma \sim \langle\phi\rangle$, the coupling needs to be

$$h_{N_1} \sim 10^{-9} - 10^{-8}, \tag{68}$$

as shown in Fig. 11.

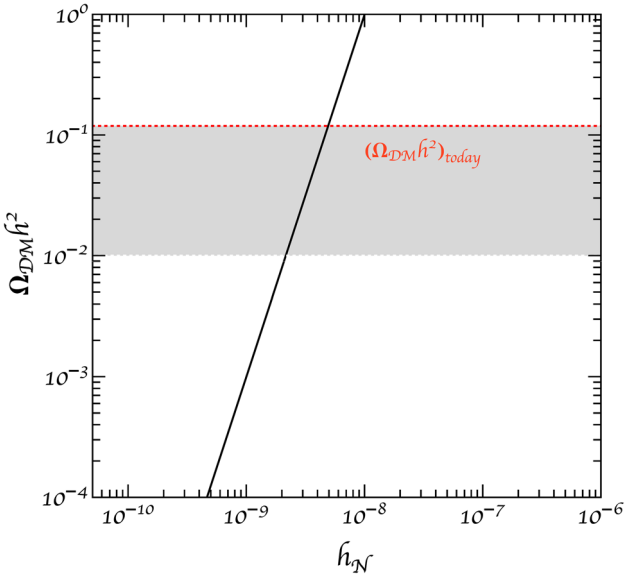

Fig. 11 Dark matter relic density as a function of the Yukawa coupling h_N of the lightest sterile neutrino. The gray region identifies $0.01 < \Omega_{DM}h^2 < 0.12$, that is to say a sterile neutrino contribution to DM density between 10 and 100%. Taking $\langle\Phi\rangle \sim$TeV, this region corresponds to $m_{N_1} \sim keV$

If m_{N_1} is the keV range so that it can satisfy cosmological and astrophysical constraints, the scale of the VEV should be

$$\langle\phi\rangle \sim \text{TeV}. \tag{69}$$

As a consequence we see that if one couples the $B-L$ scalar also to the heavier neutrinos, the interactions are too fast and the BO mechanism cannot work since the bound in Eq. (59) is not satisfied. Alternatively, if we assume Eq. (59), then

$$m_N \sim \mathcal{O}(\text{MeV}). \tag{70}$$

Such a massive neutrino would need extremely small active-sterile mixing angle (collectively labeled θ) to be sufficiently long-lived. The strongest bound from X-rays [119] give

$$\sin^2(2\theta) \lesssim \text{few} \times 10^{-6} \quad , m_N \sim \text{keV}, \tag{71}$$

while the soft gamma ray bound [120] gives

$$\sin^2(2\theta) \lesssim \text{few} \times 10^{-21}, \quad m_N \sim \text{MeV}. \tag{72}$$

In conclusion, either we consider a global symmetry with different family charges, more concretely a $(B-L)_1$, or we need to require extremely tiny yukawa coupling for the DM sterile neutrino, making this last model theoretically unappealing.

6 Conclusion

The extension of the Standard Model with three heavy majorana singlets at the weak scale can explain neutrino masses and also account for the baryon asymmetry in the Universe via the oscillation mechanism [8,9]. This scenario could be testable in future experiments. Unfortunately the simplest model cannot easily accommodate dark matter. In the νMSM [9], one of the three heavy states is in the keV range and provides a candidate for dark matter, but it requires huge lepton asymmetries that cannot be naturally achieved in the minimal setup.

In this paper we have explored three extensions of the minimal scenario that can accommodate dark matter without spoiling baryogenesis. This is non trivial because new interactions of the heavy singlets can disrupt the necessary out-of-equilibrium condition which is mandatory to generate a lepton asymmetry. We have shown that a extension of the minimal model with a $U(1)_{B-L}$ gauge interaction can achieve this goal. The two heavier majorana fermions take part in the generation of the baryon asymmetry, while the lighest one in the keV range, N_1, is the dark matter. In contrast with the νMSM the production of the dark matter is not via mixing, but it is dominated by the $B-L$ gauge boson decay. The mixing is however what controls the decay of the N_1 and can be made sufficiently small to avoid the stringent X-ray constraints. The correct DM abundance is achieved for very small $B-L$ gauge couplings, $g_{B-L} \lesssim 10^{-8}$, which are safely small not to disturb the baryon asymmetry, which remains the same as in the minimal model. Such tiny couplings are far below the reach of colliders. Supernova and BBN provide the most stringent constraints in the relevant region of parameter space, while future searches in SHIP might have a chance to touch on it.

We have also considered an extension involving an invisible axion sector with an extra scalar doublet and a complex singlet. The heavy majorana singlets get their mass from the PQ breaking scale [46]. DM is in the form of cold axions, from the misalignment mechanism and as is well known, the right relic abundance can be achieved for a large value of the PQ breaking scale, $f_a \simeq 10^{11}$GeV. We have shown that such large scale is compatible with having the heavy neutrinos in the 1–100 GeV scale, and ARS leptogenesis. Finally we have considered the singlet majoron extension of the minimal model, with a global $U(1)_{B-L}$, that contains two potential DM candidates, the majoron or the lightest heavy neutrino, N_1. Unperturbed ARS baryogenesis requires a relatively high $B-L$ breaking scale, $f \gtrsim 10^6$ GeV. Majoron DM requires exotic production scenarios, while neutrino DM works for masses around MeV, which requires extremely small mixings to make it sufficiently long-lived, or alternatively a less theoretically appealing possibity, where the scalar couples to

only one sterile neutrino, while the other two have tree level masses or couple to a different scalar with a larger VEV.

As a general rule, adding new interactions that affect the heavy Majorana singlets modifies leptogenesis in the minimal model and viable extensions that can explain DM are likely to involve the freeze-in mechanism as in the examples above.

Acknowledgements We thank M. Escudero, M. Kekic, J. López-Pavón and J. Salvado for useful discussions. We acknowledge support from national grants FPA2014-57816-P, FPA2017-85985-P and the European projects H2020-MSCA-ITN-2015//674896-ELUSIVES and H2020-MSCA-RISE-2015

Data Availability Statement This manuscript has no associated data or the data will not be deposited. [Authors' comment: We didn't use real data in this paper, which is mostly a theoretical one. The only data we analyzed were taken from other works and are shown in the constraints plots.]

A Computation of momentum averaged rates in gauged $B-L$

In this appendix we give some details on the computation of the momentum averaged rates in Eq. (24). The amplitude for $\bar{f}f \to NN$ for vanishing masses is given by

$$\sum_{spins} |\mathcal{M}|^2 = 4g_{B-L}^4 \sum_f Q_f^2 N_c \left[\frac{t^2+u^2}{s^2}\right] \equiv A\left[\frac{t^2+u^2}{s^2}\right], \tag{73}$$

while that for $VV \to NN$, in the limit $M_\sigma^2 \gg s,t \gg m_N^2, m_V^2$ is

$$\sum_{spins} |\mathcal{M}|^2 = 4g_{B-L}^4 \frac{m_N^2 s}{m_V^4}. \tag{74}$$

Defining the Bose–Einstein and Fermi–Dirac distributions

$$f_B(x) = \frac{1}{e^x - 1}, \quad f_F(x) = \frac{1}{e^x + 1}, \tag{75}$$

and the variables

$$q_\pm \equiv \frac{1}{2}(q_0 \pm |\mathbf{q}|), \tag{76}$$

where $q = p_1 + p_2$. We express all momenta in units of temperature T.

Following the procedure of Ref. [50] the rate $f\bar{f} \to NN$ can be writen as

$$R^{(1)}(k) = \frac{A}{4(2\pi)^3 k_0}\left(r_1(k) + r_2(k) + r_3(k)\right), \tag{77}$$

with

$$r_1(k) \equiv \int_{k_0}^\infty dq_+ \int_0^{k_0} dq_- f_B(q_+ + q_-) I_1(q_+, q_-), \tag{78}$$

$$r_2(k) \equiv 2\int_{k_0}^\infty dq_+ \int_0^{k_0} dq_- f_B(q_+ + q_-) \times \sum_{i=1,2} I_i(q_+, q_-) a_i[q_+, q_-, k_0] \tag{79}$$

$$r_3(k) \equiv 2\int_{k_0}^\infty dq_+ \int_0^{k_0} dq_- f_B(q_+ + q_-) \times \sum_{i=1,3} I_i(q_+, q_-) b_i[q_+, q_-, k_0] \tag{80}$$

with

$$I_n(q_+, q_-) \equiv \int_{q_-}^{q_+} x^{n-1}\left[1 - 2f_F(x)\right] dx, \tag{81}$$

and

$$\begin{aligned} a_1[q_+, q_-, k_0] &\equiv -1 + \frac{q_+(k_0 - q_-) + q_-(k_0 - q_+)}{(q_+ - q_-)^2}, \\ a_2[q_+, q_-, k_0] &\equiv \frac{q_+ + q_- - 2k_0}{(q_+ - q_-)^2}, \\ b_1[q_+, q_-, k_0] &\equiv a_1^2 + 2q_+q_- \frac{(q_+ - k_0)(q_- - k_0)}{(q_+ - q_-)^4} b_2[q_+, q_-, k_0] \\ &\equiv 2a_1[q_+, q_-, k_0]a_2[q_+, q_-, k_0] + \\ &\quad -2(q_+ + q_-)\frac{(q_+ - k_0)(q_- - k_0)}{(q_+ - q_-)^4} \\ b_3[q_+, q_-, k_0] &\equiv a_2^2 + 2\frac{(q_+ - k_0)(q_- - k_0)}{(q_+ - q_-)^4} \end{aligned} \tag{82}$$

The rate $VV \to NN$ can be written as

$$R^{(2)}(k) = \frac{A'}{(2\pi)^3 k_0}\int_{k_0}^\infty dq_+ \int_0^{k_0} dq_- (q_+ q_-) f_B(q_+ + q_-) \times I_1'(q_+, q_-), \tag{83}$$

with

$$I_1'(q_+, q_-) \equiv \int_{q_-}^{q_+} \left[1 + 2f_B(x)\right] dx. \tag{84}$$

and $A' \equiv g_{B-L}^4 \frac{m_N^2}{m_V^4}$.

The total rate is

$$R(k) = \sum_{i=1,2} R^{(i)}(k), \tag{85}$$

and the averaged rates $\gamma_V^{(0)}$ and $\gamma_V^{(1)}$ are found to be:

$$\langle \gamma_V^{(0)} \rangle = g_{B-L}^4 T$$

$$\times \left(3.2(3) \times 10^{-3} + 2.95 \times 10^{-4} \frac{m_N^2 T^2}{m_V^4}\right) \quad (86)$$

$$\langle \gamma_V^{(1)} \rangle = g_{B-L}^4 T \times \left(3.4(1) \times 10^{-4} + 3.55 \times 10^{-5} \frac{m_N^2 T^2}{m_V^4}\right). \quad (87)$$

where

$$\langle \gamma_V^{(0)} \rangle \equiv \frac{\int \frac{d^3k}{(2\pi)^3 2k_0} R[k]}{\int \frac{d^3k}{(2\pi)^3} f_F(k)} \quad (88)$$

and

$$\langle \gamma_V^{(1)} \rangle \equiv \frac{\int \frac{d^3k}{(2\pi)^3 2k_0} R[k] f_F(k)}{\int \frac{d^3k}{(2\pi)^3} f_F(k)} \quad (89)$$

References

1. P. Minkowski, $\mu \to e\gamma$ at a Rate of One Out of 10^9 Muon Decays? Phys. Lett. **67B**, 421–428 (1977). https://doi.org/10.1016/0370-2693(77)90435-X
2. M. Gell-Mann, P. Ramond, R. Slansky, Complex spinors and unified theories. Conf. Proc. C **790927**, 315–321 (1979). arXiv:1306.4669
3. T. Yanagida, Horizontal symmetry and masses of neutrinos. Conf. Proc. C **7902131**, 95–99 (1979)
4. R.N. Mohapatra, G. Senjanovic, Neutrino Mass and Spontaneous Parity Violation. Phys. Rev. Lett. **44**, 912 (1980). https://doi.org/10.1103/PhysRevLett.44.912
5. M. Fukugita, T. Yanagida, Baryogenesis without grand unification. Phys. Lett. B **174**, 45–47 (1986). https://doi.org/10.1016/0370-2693(86)91126-3
6. S. Davidson, A. Ibarra, A Lower bound on the right-handed neutrino mass from leptogenesis. Phys. Lett. B **535**, 25–32 (2002). https://doi.org/10.1016/S0370-2693(02)01735-5. arXiv:hep-ph/0202239
7. A. Abada, S. Davidson, A. Ibarra, F.X. Josse-Michaux, M. Losada, A. Riotto, Flavour matters in leptogenesis. JHEP **09**, 010 (2006). https://doi.org/10.1088/1126-6708/2006/09/010. arXiv:hep-ph/0605281
8. E.K. Akhmedov, V.A. Rubakov, AYu. Smirnov, Baryogenesis via neutrino oscillations. Phys. Rev. Lett. **81**, 1359–1362 (1998). https://doi.org/10.1103/PhysRevLett.81.1359. arXiv:hep-ph/9803255
9. T. Asaka, M. Shaposhnikov, The nuMSM, dark matter and baryon asymmetry of the universe. Phys. Lett. B **620**, 17–26 (2005). https://doi.org/10.1016/j.physletb.2005.06.020. arXiv:hep-ph/0505013
10. V.A. Kuzmin, V.A. Rubakov, M.E. Shaposhnikov, On the anomalous electroweak baryon number nonconservation in the early universe. Phys. Lett. **155B**, 36 (1985). https://doi.org/10.1016/0370-2693(85)91028-7
11. A. Ferrari, J. Collot, M.-L. Andrieux, B. Belhorma, P. de Saintignon, J.-Y. Hostachy, P. Martin, M. Wielers, Sensitivity study for new gauge bosons and right-handed Majorana neutrinos in pp collisions at s = 14-TeV. Phys. Rev. D **62**, 013001 (2000). https://doi.org/10.1103/PhysRevD.62.013001
12. M. L. Graesser, Experimental constraints on higgs boson decays to TeV-scale right-handed neutrinos. arXiv:0705.2190
13. F. del Aguila, J.A. Aguilar-Saavedra, Distinguishing seesaw models at LHC with multi-lepton signals. Nucl. Phys. B **813**, 22–90 (2009). https://doi.org/10.1016/j.nuclphysb.2008.12.029. arXiv:0808.2468
14. P.S. Bhupal Dev, R. Franceschini, R.N. Mohapatra, Bounds on TeV seesaw models from LHC higgs data. Phys. Rev. D **86**, 093010 (2012). https://doi.org/10.1103/PhysRevD.86.093010. arXiv:1207.2756
15. J.C. Helo, M. Hirsch, S. Kovalenko, Heavy neutrino searches at the LHC with displaced vertices. Phys. Rev. D **89**, 073005 (2014) [Erratum: Phys. Rev.D93,no.9,099902(2016)]. arXiv:1312.2900, https://doi.org/10.1103/PhysRevD.89.073005. https://doi.org/10.1103/PhysRevD.93.099902
16. A. Blondel, E. Graverini, N. Serra, M. Shaposhnikov, Search for heavy right handed neutrinos at the FCC-ee. Nucl. Part. Phys. Proc. **273–275**, 1883–1890 (2016). https://doi.org/10.1016/j.nuclphysbps.2015.09.304. arXiv:1411.5230
17. A. Abada, V. De Romeri, S. Monteil, J. Orloff, A.M. Teixeira, Indirect searches for sterile neutrinos at a high-luminosity Z-factory. JHEP **04**, 051 (2015). https://doi.org/10.1007/JHEP04(2015)051. arXiv:1412.6322
18. Y. Cui, B. Shuve, Probing baryogenesis with displaced vertices at the LHC. JHEP **02**, 049 (2015). https://doi.org/10.1007/JHEP02(2015)049. arXiv:1409.6729
19. S. Antusch, O. Fischer, Testing sterile neutrino extensions of the Standard Model at future lepton colliders. JHEP **05**, 053 (2015). https://doi.org/10.1007/JHEP05(2015)053. arXiv:1502.05915
20. A.M. Gago, P. Hernandez, J. Jones-Perez, M. Losada, A. Moreno Briceño, Probing the Type I seesaw mechanism with displaced vertices at the LHC. Eur. Phys. J. C **75**(10), 470 (2015). https://doi.org/10.1140/epjc/s10052-015-3693-1. arXiv:1505.05880
21. S. Antusch, E. Cazzato, O. Fischer, Displaced vertex searches for sterile neutrinos at future lepton colliders. JHEP **12**, 007 (2016). https://doi.org/10.1007/JHEP12(2016)007. arXiv:1604.02420
22. A. Caputo, P. Hernandez, M. Kekic, J. Lopez-Pavon, J. Salvado, The seesaw path to leptonic CP violation. Eur. Phys. J. C **77**(4), 258 (2017). https://doi.org/10.1140/epjc/s10052-017-4823-8. arXiv:1611.05000
23. A. Caputo, P. Hernandez, J. Lopez-Pavon, J. Salvado, The seesaw portal in testable models of neutrino masses. JHEP **06**, 112 (2017). https://doi.org/10.1007/JHEP06(2017)112. arXiv:1704.08721
24. M. Shaposhnikov, The nuMSM, leptonic asymmetries, and properties of singlet fermions. JHEP **08**, 008 (2008). https://doi.org/10.1088/1126-6708/2008/08/008. arXiv:0804.4542
25. L. Canetti, M. Drewes, M. Shaposhnikov, Matter and antimatter in the universe. New J. Phys. **14**, 095012 (2012). https://doi.org/10.1088/1367-2630/14/9/095012. arXiv:1204.4186
26. L. Canetti, M. Drewes, T. Frossard, M. Shaposhnikov, Dark matter, baryogenesis and neutrino oscillations from right handed neutrinos. Phys. Rev. D **87**, 093006 (2013). https://doi.org/10.1103/PhysRevD.87.093006. arXiv:1208.4607
27. T. Asaka, S. Eijima, H. Ishida, Kinetic equations for baryogenesis via sterile neutrino oscillation. JCAP **1202**, 021 (2012). https://doi.org/10.1088/1475-7516/2012/02/021. arXiv:1112.5565
28. B. Shuve, I. Yavin, Baryogenesis through neutrino oscillations: a unified perspective. Phys. Rev. D **89**(7), 075014 (2014). https://doi.org/10.1103/PhysRevD.89.075014. arXiv:1401.2459
29. A. Abada, G. Arcadi, V. Domcke, M. Lucente, Lepton number violation as a key to low-scale leptogenesis. JCAP **1511**(11), 041 (2015). https://doi.org/10.1088/1475-7516/2015/11/041. arXiv:1507.06215
30. P. Hernandez, M. Kekic, J. Lopez-Pavon, J. Racker, N. Rius, Leptogenesis in GeV scale seesaw models. JHEP **10**, 067 (2015). https://doi.org/10.1007/JHEP10(2015)067. arXiv:1508.03676

31. P. Hernandez, M. Kekic, J. Lopez-Pavon, J. Racker, J. Salvado, Testable Baryogenesis in Seesaw Models. JHEP **08**, 157 (2016). https://doi.org/10.1007/JHEP08(2016)157. arXiv:1606.06719
32. M. Drewes, B. Garbrecht, D. Gueter, J. Klaric, Leptogenesis from oscillations of heavy neutrinos with large mixing angles. JHEP **12**, 150 (2016). https://doi.org/10.1007/JHEP12(2016)150. arXiv:1606.06690
33. M. Drewes, B. Garbrecht, D. Gueter, J. Klaric, Testing the low scale seesaw and leptogenesis. JHEP **08**, 018 (2017). https://doi.org/10.1007/JHEP08(2017)018. arXiv:1609.09069
34. T. Hambye, D. Teresi, Higgs doublet decay as the origin of the baryon asymmetry. Phys. Rev. Lett. **117**(9), 091801 (2016). https://doi.org/10.1103/PhysRevLett.117.091801. arXiv:1606.00017
35. J. Ghiglieri, M. Laine, GeV-scale hot sterile neutrino oscillations: a derivation of evolution equations. JHEP **05**, 132 (2017). https://doi.org/10.1007/JHEP05(2017)132. arXiv:1703.06087
36. T. Asaka, S. Eijima, H. Ishida, K. Minogawa, T. Yoshii, Initial condition for baryogenesis via neutrino oscillation. arXiv:1704.02692
37. T. Hambye, D. Teresi, Baryogenesis from L-violating Higgs-doublet decay in the density-matrix formalism. Phys. Rev. D **96**(1), 015031 (2017). https://doi.org/10.1103/PhysRevD.96.015031. arXiv:1705.00016
38. A. Abada, G. Arcadi, V. Domcke, M. Lucente, Neutrino masses, leptogenesis and dark matter from small lepton number violation? JCAP **1712**(12), 024 (2017). https://doi.org/10.1088/1475-7516/2017/12/024. arXiv:1709.00415
39. J. Ghiglieri, M. Laine, GeV-scale hot sterile neutrino oscillations: a numerical solution. JHEP **02**, 078 (2018). https://doi.org/10.1007/JHEP02(2018)078. arXiv:1711.08469
40. S. Dodelson, L.M. Widrow, Sterile-neutrinos as dark matter. Phys. Rev. Lett. **72**, 17–20 (1994). https://doi.org/10.1103/PhysRevLett.72.17. arXiv:hep-ph/9303287
41. X.-D. Shi, G.M. Fuller, A New dark matter candidate: nonthermal sterile neutrinos. Phys. Rev. Lett. **82**, 2832–2835 (1999). https://doi.org/10.1103/PhysRevLett.82.2832. arXiv:astro-ph/9810076
42. K. Perez, K.C.Y. Ng, J.F. Beacom, C. Hersh, S. Horiuchi, R. Krivonos, Almost closing the ν MSM sterile neutrino dark matter window with NuSTAR. Phys. Rev. D **95**(12), 123002 (2017). https://doi.org/10.1103/PhysRevD.95.123002. arXiv:1609.00667
43. J. Baur, N. Palanque-Delabrouille, C. Yeche, A. Boyarsky, O. Ruchayskiy, É. Armengaud, J. Lesgourgues, Constraints from Ly-α forests on non-thermal dark matter including resonantly-produced sterile neutrinos. JCAP **1712**(12), 013 (2017). https://doi.org/10.1088/1475-7516/2017/12/013. arXiv:1706.03118
44. S. Baumholzer, V. Brdar, P. Schwaller, The New νMSM: radiative neutrino masses, keV-scale dark matter and viable leptogenesis with sub-TeV new physics. arXiv:1806.06864
45. R.N. Mohapatra, R.E. Marshak, Local B-L symmetry of electroweak interactions, majorana neutrinos and neutron oscillations. Phys. Rev. Lett. **44**, 1316–1319 (1980) [Erratum: Phys. Rev. Lett.44,1643(1980)]. https://doi.org/10.1103/PhysRevLett.44.1644.2. https://doi.org/10.1103/PhysRevLett.44.1316
46. P. Langacker, R.D. Peccei, T. Yanagida, Invisible axions and light neutrinos: are they connected? Mod. Phys. Lett. A **1**, 541 (1986). https://doi.org/10.1142/S0217732386000683
47. Y. Chikashige, R.N. Mohapatra, R.D. Peccei, Are there real goldstone bosons associated with broken lepton number? Phys. Lett. **98B**, 265–268 (1981). https://doi.org/10.1016/0370-2693(81)90011-3
48. J. Schechter, J.W.F. Valle, Neutrino decay and spontaneous violation of lepton number. Phys. Rev. D **25**, 774 (1982). https://doi.org/10.1103/PhysRevD.25.774
49. M. Drewes, B. Garbrecht, P. Hernandez, M. Kekic, J. Lopez-Pavon, J. Racker, N. Rius, J. Salvado, D. Teresi, A.R.S. Leptogenesis, Int. J. Mod. Phys. A **33**(05n06), 1842002 (2018). https://doi.org/10.1142/S0217751X18420022. arXiv:1711.02862
50. D. Besak, D. Bodeker, Thermal production of ultrarelativistic right-handed neutrinos: complete leading-order results. JCAP **1203**, 029 (2012). https://doi.org/10.1088/1475-7516/2012/03/029. arXiv:1202.1288
51. B. Garbrecht, F. Glowna, P. Schwaller, Scattering Rates for leptogenesis: damping of lepton flavour coherence and production of singlet neutrinos. Nucl. Phys. B **877**, 1–35 (2013). https://doi.org/10.1016/j.nuclphysb.2013.08.020. arXiv:1303.5498
52. I. Ghisoiu, M. Laine, Right-handed neutrino production rate at $T>160$ GeV. JCAP **1412**(12), 032 (2014). https://doi.org/10.1088/1475-7516/2014/12/032. arXiv:1411.1765
53. G. Bellini et al., Precision measurement of the 7Be solar neutrino interaction rate in Borexino. Phys. Rev. Lett. **107**, 141302 (2011). https://doi.org/10.1103/PhysRevLett.107.141302. arXiv:1104.1816
54. S. Chatrchyan et al., Measurement of the differential and double-differential Drell-Yan cross sections in proton-proton collisions at $\sqrt{s} = 7$ TeV. JHEP **12**, 030 (2013). https://doi.org/10.1007/JHEP12(2013)030. arXiv:1310.7291
55. J.P. Lees et al., Search for a dark photon in e^+e^- collisions at BaBar. Phys. Rev. Lett. **113**(20), 201801 (2014). https://doi.org/10.1103/PhysRevLett.113.201801. arXiv:1406.2980
56. J.P. Lees et al., Search for Invisible decays of a dark photon produced in e^+e^- collisions at BaBar. Phys. Rev. Lett. **119**(13), 131804 (2017). https://doi.org/10.1103/PhysRevLett.119.131804. arXiv:1702.03327
57. V. Khachatryan et al., Search for physics beyond the standard model in dilepton mass spectra in proton-proton collisions at $\sqrt{s} = 8$ TeV. JHEP **04**, 025 (2015). https://doi.org/10.1007/JHEP04(2015)025. arXiv:1412.6302
58. G. Aad et al., Search for high-mass dilepton resonances in pp collisions at $\sqrt{s} = 8$TeV with the ATLAS detector. Phys. Rev. D **90**(5), 052005 (2014). https://doi.org/10.1103/PhysRevD.90.052005. arXiv:1405.4123
59. A Combination of preliminary electroweak measurements and constraints on the standard model. arXiv:hep-ex/0412015
60. T. Appelquist, B.A. Dobrescu, A.R. Hopper, Nonexotic neutral gauge bosons. Phys. Rev. D **68**, 035012 (2003). https://doi.org/10.1103/PhysRevD.68.035012. arXiv:hep-ph/0212073
61. B. Batell, M. Pospelov, B. Shuve, Shedding light on neutrino masses with dark forces. JHEP **08**, 052 (2016). https://doi.org/10.1007/JHEP08(2016)052. arXiv:1604.06099
62. M. Klasen, F. Lyonnet, F.S. Queiroz, NLO+NLL collider bounds, Dirac fermion and scalar dark matter in the B-L model. Eur. Phys. J. C **77**(5), 348 (2017). https://doi.org/10.1140/epjc/s10052-017-4904-8. arXiv:1607.06468
63. P. Ilten, Y. Soreq, M. Williams, W. Xue, Serendipity in dark photon searches. JHEP **06**, 004 (2018). https://doi.org/10.1007/JHEP06(2018)004. arXiv:1801.04847
64. M. Escudero, S. J. Witte, N. Rius, The dispirited case of gauged $U(1)_{B-L}$ dark matter. arXiv:1806.02823
65. S. Alekhin et al., A facility to search for hidden particles at the CERN SPS: the SHiP physics case. Rept. Prog. Phys. **79**(12), 124201 (2016). https://doi.org/10.1088/0034-4885/79/12/124201. arXiv:1504.04855
66. D. Gorbunov, A. Makarov, I. Timiryasov, Decaying light particles in the SHiP experiment: signal rate estimates for hidden photons. Phys. Rev. D **91**(3), 035027 (2015). https://doi.org/10.1103/PhysRevD.91.035027. arXiv:1411.4007
67. K. Kaneta, Z. Kang, H.-S. Lee, Right-handed neutrino dark matter under the $B-L$ gauge interaction. JHEP **02**, 031 (2017). https://doi.org/10.1007/JHEP02(2017)031. arXiv:1606.09317

68. J.H. Chang, R. Essig, S.D. McDermott, Revisiting supernova 1987A constraints on dark photons. JHEP **01**, 107 (2017). https://doi.org/10.1007/JHEP01(2017)107. arXiv:1611.03864
69. B. Ahlgren, T. Ohlsson, S. Zhou, Comment on "Is dark matter with long-range interactions a solution to all small-scale problems of cold dark matter cosmology?". Phys. Rev. Lett. **111**(19), 199001 (2013). https://doi.org/10.1103/PhysRevLett.111.199001. arXiv:1309.0991
70. M. Williams, C.P. Burgess, A. Maharana, F. Quevedo, New constraints (and Motivations) for Abelian Gauge Bosons in the MeV-TeV mass range. JHEP **08**, 106 (2011). https://doi.org/10.1007/JHEP08(2011)106. arXiv:1103.4556
71. R. Mayle, J.R. Wilson, J.R. Ellis, K.A. Olive, D.N. Schramm, G. Steigman, Constraints on Axions from SN 1987a. Phys. Lett. B **203**, 188–196 (1988). https://doi.org/10.1016/0370-2693(88)91595-X
72. G. Raffelt, D. Seckel, Bounds on exotic particle interactions from SN 1987a. Phys. Rev. Lett. **60**, 1793 (1988). https://doi.org/10.1103/PhysRevLett.60.1793
73. M.S. Turner, Axions from SN 1987a. Phys. Rev. Lett. **60**, 1797 (1988). https://doi.org/10.1103/PhysRevLett.60.1797
74. J.D. Bjorken, R. Essig, P. Schuster, N. Toro, New fixed-target experiments to search for dark Gauge forces. Phys. Rev. D **80**, 075018 (2009). https://doi.org/10.1103/PhysRevD.80.075018. arXiv:0906.0580
75. P. Vilain et al., Measurement of differential cross-sections for muon-neutrino electron scattering. Phys. Lett. B **302**, 351–355 (1993). https://doi.org/10.1016/0370-2693(93)90408-A
76. J.D. Bjorken, S. Ecklund, W.R. Nelson, A. Abashian, C. Church, B. Lu, L.W. Mo, T.A. Nunamaker, P. Rassmann, Search for neutral metastable penetrating particles produced in the SLAC beam dump. Phys. Rev. D **38**, 3375 (1988). https://doi.org/10.1103/PhysRevD.38.3375
77. E.M. Riordan et al., A search for short lived axions in an electron beam dump experiment. Phys. Rev. Lett. **59**, 755 (1987). https://doi.org/10.1103/PhysRevLett.59.755
78. A. Bross, M. Crisler, S.H. Pordes, J. Volk, S. Errede, J. Wrbanek, A search for shortlived particles produced in an electron beam dump. Phys. Rev. Lett. **67**, 2942–2945 (1991). https://doi.org/10.1103/PhysRevLett.67.2942
79. A. Fradette, M. Pospelov, J. Pradler, A. Ritz, Cosmological constraints on very dark photons. Phys. Rev. D **90**(3), 035022 (2014). https://doi.org/10.1103/PhysRevD.90.035022. arXiv:1407.0993
80. J. Berger, K. Jedamzik, D.G.E. Walker, Cosmological constraints on decoupled dark photons and dark higgs. JCAP **1611**, 032 (2016). https://doi.org/10.1088/1475-7516/2016/11/032. arXiv:1605.07195
81. G.-Y. Huang, T. Ohlsson, S. Zhou, Observational constraints on secret neutrino interactions from big bang nucleosynthesis. Phys. Rev. D **97**(7), 075009 (2018). https://doi.org/10.1103/PhysRevD.97.075009. arXiv:1712.04792
82. J. Heeck, D. Teresi, Leptogenesis and neutral gauge bosons. Phys. Rev. D **94**(9), 095024 (2016). https://doi.org/10.1103/PhysRevD.94.095024. arXiv:1609.03594
83. H.A. Weldon, Effective Fermion masses of order gT in high temperature gauge theories with exact chiral invariance. Phys. Rev. D **26**, 2789 (1982). https://doi.org/10.1103/PhysRevD.26.2789
84. G. Sigl, G. Raffelt, General kinetic description of relativistic mixed neutrinos. Nucl. Phys. B **406**, 423–451 (1993). https://doi.org/10.1016/0550-3213(93)90175-O
85. J. McDonald, Thermally generated gauge singlet scalars as selfinteracting dark matter. Phys. Rev. Lett. **88**, 091304 (2002). https://doi.org/10.1103/PhysRevLett.88.091304. arXiv:hep-ph/0106249
86. L.J. Hall, K. Jedamzik, J. March-Russell, S.M. West, Freeze-in production of FIMP dark matter. JHEP **03**, 080 (2010). https://doi.org/10.1007/JHEP03(2010)080. arXiv:0911.1120
87. M. Dine, W. Fischler, The Not So Harmless Axion. Phys. Lett. B **120**, 137–141 (1983). https://doi.org/10.1016/0370-2693(83)90639-1
88. G.C. Branco, P.M. Ferreira, L. Lavoura, M.N. Rebelo, M. Sher, J.P. Silva, Theory and phenomenology of two-Higgs-doublet models. Phys. Rept. **516**, 1–102 (2012). https://doi.org/10.1016/j.physrep.2012.02.002. arXiv:1106.0034
89. D. Espriu, F. Mescia, A. Renau, Axion-Higgs interplay in the two Higgs-doublet model. Phys. Rev. D **92**(9), 095013 (2015). https://doi.org/10.1103/PhysRevD.92.095013. arXiv:1503.02953
90. G.G. Raffelt, Particle physics from stars. Ann. Rev. Nucl. Part. Sci. **49**, 163–216 (1999). https://doi.org/10.1146/annurev.nucl.49.1.163. arXiv:hep-ph/9903472
91. J. Preskill, M.B. Wise, F. Wilczek, Cosmology of the invisible axion. Phys. Lett. B **120**, 127–132 (1983). https://doi.org/10.1016/0370-2693(83)90637-8
92. L.F. Abbott, P. Sikivie, A cosmological bound on the invisible axion. Phys. Lett. B **120**, 133–136 (1983). https://doi.org/10.1016/0370-2693(83)90638-X
93. M. Kawasaki, K. Nakayama, Axions: theory and cosmological role. Ann. Rev. Nucl. Part. Sci. **63**, 69–95 (2013). https://doi.org/10.1146/annurev-nucl-102212-170536. arXiv:1301.1123
94. D.J.E. Marsh, Axion cosmology. Phys. Rept. **643**, 1–79 (2016). https://doi.org/10.1016/j.physrep.2016.06.005. arXiv:1510.07633
95. S. Weinberg, Goldstone Bosons as fractional cosmic neutrinos. Phys. Rev. Lett. **110**(24), 241301 (2013). https://doi.org/10.1103/PhysRevLett.110.241301. arXiv:1305.1971
96. P. Graf, F.D. Steffen, Thermal axion production in the primordial quark-gluon plasma. Phys. Rev. D **83**, 075011 (2011). https://doi.org/10.1103/PhysRevD.83.075011. arXiv:1008.4528
97. A. Salvio, A. Strumia, W. Xue, Thermal axion production. JCAP **1401**, 011 (2014). https://doi.org/10.1088/1475-7516/2014/01/011. arXiv:1310.6982
98. J.D. Clarke, R.R. Volkas, Technically natural nonsupersymmetric model of neutrino masses, baryogenesis, the strong CP problem, and dark matter. Phys. Rev. D **93**(3), 035001 (2016). https://doi.org/10.1103/PhysRevD.93.035001. [Phys. Rev.D93,035001(2016)]. arXiv:1509.07243
99. J.E. Kim, Weak interaction singlet and strong CP invariance. Phys. Rev. Lett. **43**, 103 (1979). https://doi.org/10.1103/PhysRevLett.43.103
100. M.A. Shifman, A.I. Vainshtein, V.I. Zakharov, Can confinement ensure natural CP invariance of strong interactions? Nucl. Phys. B **166**, 493–506 (1980). https://doi.org/10.1016/0550-3213(80)90209-6
101. G. Ballesteros, J. Redondo, A. Ringwald, C. Tamarit, Unifying inflation with the axion, dark matter, baryogenesis and the seesaw mechanism. Phys. Rev. Lett. **118**(7), 071802 (2017). https://doi.org/10.1103/PhysRevLett.118.071802. arXiv:1608.05414
102. G. Ballesteros, J. Redondo, A. Ringwald, C. Tamarit, Standard Model axion seesaw Higgs portal inflation. Five problems of particle physics and cosmology solved in one stroke. JCAP **1708**(08), 001 (2017). https://doi.org/10.1088/1475-7516/2017/08/001. arXiv:1610.01639
103. T. Asaka, M. Laine, M. Shaposhnikov, On the hadronic contribution to sterile neutrino production. JHEP **06**, 053 (2006). https://doi.org/10.1088/1126-6708/2006/06/053. arXiv:hep-ph/0605209
104. J.M. Cline, K. Kainulainen, K.A. Olive, Constraints on majoron models, neutrino masses and baryogenesis. Astropart. Phys. **1**, 387–398 (1993). https://doi.org/10.1016/0927-6505(93)90005-X. arXiv:hep-ph/9304229

105. P.-H. Gu, U. Sarkar, Leptogenesis bound on spontaneous symmetry breaking of global lepton number. Eur. Phys. J. C **71**, 1560 (2011). https://doi.org/10.1140/epjc/s10052-011-1560-2. arXiv:0909.5468
106. P.S.B. Dev, R.N. Mohapatra, Y. Zhang, Leptogenesis constraints on $B - L$ breaking Higgs boson in TeV scale seesaw models. JHEP **03**, 122 (2018). https://doi.org/10.1007/JHEP03(2018)122. arXiv:1711.07634
107. E.K. Akhmedov, Z.G. Berezhiani, R.N. Mohapatra, G. Senjanovic, Planck scale effects on the majoron. Phys. Lett. B **299**, 90–93 (1993). https://doi.org/10.1016/0370-2693(93)90887-N. arXiv:hep-ph/9209285
108. I.Z. Rothstein, K.S. Babu, D. Seckel, Planck scale symmetry breaking and majoron physics. Nucl. Phys. B **403**, 725–748 (1993). https://doi.org/10.1016/0550-3213(93)90368-Y. arXiv:hep-ph/9301213
109. A. Hebecker, P. Mangat, S. Theisen, L.T. Witkowski, Can gravitational instantons really constrain axion inflation? JHEP **02**, 097 (2017). https://doi.org/10.1007/JHEP02(2017)097. arXiv:1607.06814
110. R. Alonso, A. Urbano, Wormholes and masses for Goldstone bosons. arXiv:1706.07415
111. K.-M. Lee, Wormholes and goldstone bosons. Phys. Rev. Lett. **61**, 263–266 (1988). https://doi.org/10.1103/PhysRevLett.61.263
112. C.T. Hill, G.G. Ross, Models and new phenomenological implications of a class of pseudogoldstone bosons. Nucl. Phys. B **311**, 253–297 (1988). https://doi.org/10.1016/0550-3213(88)90062-4
113. M. Frigerio, T. Hambye, E. Masso, Sub-GeV dark matter as pseudo-Goldstone from the seesaw scale. Phys. Rev. X **1**, 021026 (2011). https://doi.org/10.1103/PhysRevX.1.021026. arXiv:1107.4564
114. M. Lattanzi, J.W.F. Valle, Decaying warm dark matter and neutrino masses. Phys. Rev. Lett. **99**, 121301 (2007). https://doi.org/10.1103/PhysRevLett.99.121301. arXiv:0705.2406
115. M. Lattanzi, R.A. Lineros, M. Taoso, Connecting neutrino physics with dark matter. New J. Phys. **16**(12), 125012 (2014). https://doi.org/10.1088/1367-2630/16/12/125012. arXiv:1406.0004
116. K. Choi, A. Santamaria, Majorons and supernova cooling. Phys. Rev. D **42**, 293–306 (1990). https://doi.org/10.1103/PhysRevD.42.293
117. A. Kusenko, Sterile neutrinos, dark matter, and the pulsar velocities in models with a Higgs singlet. Phys. Rev. Lett. **97**, 241301 (2006). https://doi.org/10.1103/PhysRevLett.97.241301. arXiv:hep-ph/0609081
118. K. Petraki, A. Kusenko, Dark-matter sterile neutrinos in models with a gauge singlet in the Higgs sector. Phys. Rev. D **77**, 065014 (2008). https://doi.org/10.1103/PhysRevD.77.065014. arXiv:0711.4646
119. N. Sekiya, N. Y. Yamasaki, K. Mitsuda, A Search for a keV signature of radiatively decaying dark matter with Suzaku XIS Observations of the X-ray Diffuse Background, Publ. Astron. Soc. Jap. https://doi.org/10.1093/pasj/psv081. arXiv:1504.02826
120. A. Boyarsky, D. Malyshev, A. Neronov, O. Ruchayskiy, Constraining DM properties with SPI. Mon. Not. R. Astron. Soc. **387**, 1345 (2008). https://doi.org/10.1111/j.1365-2966.2008.13003.x. arXiv:0710.4922

Detecting the stimulated decay of axions at radio frequencies

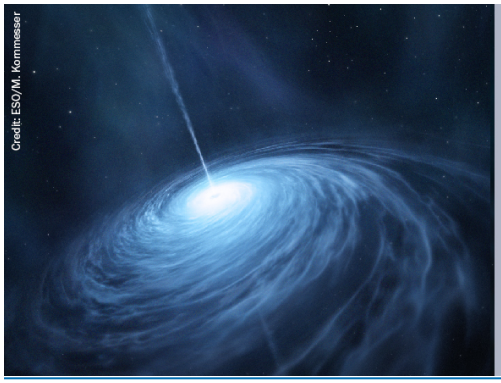

Journal of Cosmology and Astroparticle Physics
An IOP and SISSA journal

Detecting the stimulated decay of axions at radio frequencies

Andrea Caputo,[a] **Marco Regis,**[b,c] **Marco Taoso**[c] **and Samuel J. Witte**[a]

[a]Instituto de Física Corpuscular, CSIC-Universitat de Valencia, Apartado de Correos 22085, E-46071, Spain
[b]Dipartimento di Fisica, Università di Torino, via P. Giuria 1, I–10125 Torino, Italy
[c]Istituto Nazionale di Fisica Nucleare, Sezione di Torino, via P. Giuria 1, I–10125 Torino, Italy

E-mail: andrea0292@hotmail.it, regis@to.infn.it, marco.taoso@gmail.com, samuel.witte@uv.es

Received November 27, 2018
Revised January 26, 2019
Accepted March 4, 2019
Published March 14, 2019

Abstract. Assuming axion-like particles account for the entirety of the dark matter in the Universe, we study the possibility of detecting their decay into photons at radio frequencies. We discuss different astrophysical targets, such as dwarf spheroidal galaxies, the Galactic Center and halo, and galaxy clusters. The presence of an ambient radiation field leads to a stimulated enhancement of the decay rate; depending on the environment and the mass of the axion, the effect of stimulated emission may amplify the photon flux by serval orders of magnitude. For axion-photon couplings allowed by astrophysical and laboratory constraints (and possibly favored by stellar cooling), we find the signal to be within the reach of next-generation radio telescopes such as the Square Kilometer Array.

Keywords: axions, dark matter theory, dark matter detectors, dwarfs galaxies

ArXiv ePrint: 1811.08436

https://doi.org/10.1088/1475-7516/2019/03/027

JCAP03(2019)027

Contents

1 Introduction

The cumulative astrophysical and cosmological evidence for the existence of a non-baryonic, minimally interacting, cold matter component of the Universe (conventionally referred to as dark matter) is overwhelming, with current observations suggesting that dark matter resides in the form of new unknown particles. However, the exact nature of dark matter continues to evade physicists.

The most popular dark matter candidates are those naturally capable resolving additional fundamental problems at the forefront of particle physics. One such candidate is the QCD axion, which inherently appears in the Peccei-Quinn solution to the strong CP problem [1–4].[1] If the mass of the axion is $\lesssim 20\,\mathrm{eV}$, the axion is stable on cosmological timescales and can contribute substantially to the current fraction of energy density in the Universe stored in form of cold dark matter [5–8]. Astrophysical observations constrain the axion mass to reside approximately between $10^{-4}\,\mu\mathrm{eV}$ and $10^{4}\,\mu\mathrm{eV}$ [9, 10].[2] The mass range where axions can account for the entirety of the dark matter depends on the interplay between different production mechanisms (in particular, the interplay between the misalignment mechanism and the decay of topological defects) and whether the PQ symmetry (i.e. the symmetry introduced in the Peccei-Quinn solution to the strong CP problem) is broken before or after inflation (see e.g. [9, 10] for more extensive discussions). In the post-inflationary

[1] Simply put, the strong CP problem arises from the fact that the QCD θ term predicts a non-vanishing neutron electric dipole moment, while current experimental bounds constrain θ to an unnaturally small value, $\theta \lesssim 10^{-10}$.

[2] However see [11] for models where the astrophysical bounds are relaxed.

JCAP03(2019)027

PQ breaking scenario, and assuming axions are produced exclusively from the misalignment mechanism, one finds the axion mass $m_a \simeq$ few $\times$ (10) μeV [12]. As we will show, radio telescopes searching for axion decay are ideally placed to probe this mass regime.

In recent years an increasing amount of attention has shifted toward searching for axion dark matter. An important consequence of this has been the development of a diverse and complementary search program intended to probe the many unique facets of such a dark matter candidate; this program includes, but is not limited to, haloscopes [13–17], helioscopes [18–20], 5$^{\rm th}$ force experiments [21–25], light-shinning-through wall experiments [26–31], LC circuit resonators [32–34], oscillating nuclear dipole searches [35–37], axion-induced atomic transitions [38, 39], axion-induced atomic and molecular electric dipole moments [40], and indirect axion searches [41–46]. Many of these searches, although certainly not all, rely on the axion's coupling to photons; this interaction is given by the operator $\mathcal{L} = -\frac{1}{4} g_{a\gamma\gamma}\, a\, F_{\mu\nu}\tilde{F}_{\mu\nu}$, where a is the axion field, $F_{\mu\nu}$ is the electromagnetic field strength, $\tilde{F}_{\mu\nu}$ its dual, and $g_{a\gamma\gamma}$ the coupling constant. Of particular importance here is the notion that one may be able to exploit the large number density of axions in astrophysical environments to indirectly infer their existence through the detection of low-energy photons. For axion masses in the 'characteristic' dark matter window (i.e. $\mu\text{eV} \lesssim m_a \lesssim 10^2 \mu\text{eV}$), the energy of a non-relativistic axion corresponds to a photon with a frequency ranging from $\sim \mathcal{O}(100)$ MHz to $\sim \mathcal{O}(10)$ GHz; intriguingly, this lies exactly in the range of frequencies probed by radio telescopes.

There have been various attempts in recent years to use radio telescopes to detect axion dark matter, a majority of which have relied on the axion-to-photon conversion process (i.e. the so-called Primakoff effect). Recently it was shown that unless one exploits a resonant axion-photon conversion (as e.g. was done in [43–45]), the rate of axion decay into two photons will likely supersede that of axion-photon conversion in large-scale astrophysical environments [42, 46]. One of the difficulties with resonant searches is that they rely on a comprehensive understanding of highly uncertain astrophysical environments. An alternative approach with a far more limited dependence on astrophysical uncertainties, albeit at the potential cost of sensitivity, was proposed in [46]. Ref. [46] performed an exploratory study for an idealized near future radio telescope to determine whether the axion-to-two-photon decay process could potentially produce an observable signature. This work presented here is intended to serve as a comprehensive follow-up, incorporating a far more sophisticated treatment of near-future radio sensitivity and exploring a variety of astrophysical sources (including the Galactic halo, the galaxy M87 in the Virgo cluster and dwarf spheroidal galaxies). Moreover, this work presents a more detailed treatment of the stimulated emission, a mechanism which is induced by the presence of a background radiation in the medium where the axion decay occurs (see also [47–49]). At low radio frequencies, this effect enhances the expected emission by several orders of magnitude.

The coupling of the QCD axion to the photon $g_{\gamma\gamma}$ grows linearly with the axion mass and with a proportionality constant that depends on the UV completion of the axion model. Considering various types of UV completions thus defines a band in the mass-coupling plane identifying where viable QCD axions may reside (see the light green region in figure 2).[3] More generically, many extensions of the Standard Model predict light particles with similar properties to the QCD axion, but that might not be related to the strong CP problem and for which the relation between $g_{\gamma\gamma}$ and the mass could be different. These are referred to as axion-like particles (ALPs), and they appear generically in low energy-effective theories

[3] See [50] for a recent determination of the allowed region in the $g_{\gamma\gamma} - m_a$ plane for the KSVZ model [51, 52] and [53, 54] for scenarios where the range of couplings can be further extended.

JCAP03(2019)027

arising from string theory, e.g. [55–58]. It is therefore important to explore all the parameter space of ALPs, beyond the well-motivated case of the QCD axion.

The results presented here suggest that near-future surveys will be incapable of probing the parameter space of the QCD axion; however we find that the Square Kilometer Array (SKA) will be able to improve current bounds on ALPs by about one order of magnitude.

The paper is organized as follows. Section 2 outlines the origin of stimulated decay and the relevant contributions to the ambient photon background. Section 3 describes how to compute the expected signal-to-noise arising from axion decay for a generic choice of astrophysical environment and radio telescope. We present the sensitivity on the ALP-photon coupling for various astrophysical targets and telescopes in section 4. In section 5 we conclude.

2 Axion decay in a photon bath-stimulated emission

The decay of an axion with mass m_a proceeds through the chiral anomaly and produces two photons, each with a frequency $\nu = m_a/4\pi$. The lifetime of the axion can be expressed in terms of its mass and the effective axion-two-photon coupling $g_{a\gamma\gamma}$ as

$$\tau_a = \frac{64\pi}{m_a^3\, g_{a\gamma\gamma}^2}\,. \tag{2.1}$$

Evaluating the lifetime for an axion mass $m_a \sim 1\,\mu$eV and a coupling near the current upper limit, i.e. $g_{a\gamma\gamma} \sim 10^{-10}\,\mathrm{GeV}^{-1}$, one finds $\tau_a \sim 10^{32}$ years; this is perhaps the main reason why axion decay has been largely neglected in the literature. The decay rate, however, is only valid in vacuum. In reality, for the axion masses of interest this decay process takes place in an ambient radiation field, which, at radio frequencies is sourced by the combination of cosmic microwave background (CMB) radiation, synchrotron radiation, and bremsstrahlung radiation. Consequently, the photon production rate is enhanced via stimulated emission, a phenomenon due to the indistinguishability of photons and Bose-Einstein statistics. Here we review how to derive the effect in the case of a decay into two photons (for the more canonical decay into a single photon, see, e.g. [59]).

Let us denote a particular phase-space distribution with f, related to the number density of particles n by $dn = \frac{g}{(2\pi)^3}\, f(\mathbf{p})\, d^3p$, with g being the number of degrees of freedom. We consider a initial quantum state where there exist f_a axions with a particular momentum. The final state contains $f_a - 1$ axions and two photons, each with half the energy of the initial axion. The decay occurs in a medium of photons, with f_γ particles with the same momentum and polarization as the photons produced by the axion decay. Therefore, the initial state is $|f_a; f_\gamma; f_\gamma\rangle$ and the final state is $|f_a - 1; f_\gamma + 1; f_\gamma + 1\rangle$. The interaction Hamiltonian in terms of the creation and annihilation operators looks like

$$H_{\rm int} = \mathcal{M}_0^\dagger a_\gamma^\dagger a_\gamma^\dagger a_a + h.c. \tag{2.2}$$

where $\mathcal{M}_0$ is related to the spontaneous emission, as will be made clear momentarily. The matrix element associated with the probability of having a transition from initial to final state is:

$$\mathcal{M}_{i\to f} = \langle f_a - 1; f_\gamma + 1; f_\gamma + 1|H|f_a; f_\gamma; f_\gamma\rangle = \mathcal{M}_0^\dagger \sqrt{f_a}\sqrt{f_\gamma + 1}\sqrt{f_\gamma + 1}. \tag{2.3}$$

JCAP03(2019)027

where we have used the properties of ladder operators (i.e., $a|f_i\rangle = \sqrt{f_i}|f_i - 1\rangle$ and $a^\dagger|f_i\rangle = \sqrt{f_i + 1}|f_i + 1\rangle$). Squaring the matrix element, one finds

$$|\mathcal{M}_{i\to f}|^2 = |\mathcal{M}_0|^2 \, f_a \, (f_\gamma + 1)^2 \, . \tag{2.4}$$

A similar computation can be performed for the inverse process (i.e. two photons creating an axion in a medium with f_γ photons and f_a axions):

$$\mathcal{M}_{f\to i} = \langle f_a + 1; f_\gamma - 1; f_\gamma - 1|H|f_a; f_\gamma; f_\gamma\rangle \to |\mathcal{M}_{f\to i}|^2 = |\mathcal{M}_0|^2 \, f_\gamma^2 \, (f_a + 1) \, . \tag{2.5}$$

The variation of the number of axions is just the difference between production (described by eq. (2.5), which is the term usually identified as the "absorption" term) and decay of axions (given by eq. (2.4), i.e., the emission term):

$$|\mathcal{M}_{f\to i}|^2 - |\mathcal{M}_{i\to f}|^2 = -|\mathcal{M}_0|^2 \, (f_a + 2 f_a \, f_\gamma - f_\gamma^2) \tag{2.6}$$

The last three terms in the right-hand side of eq. (2.6) describe the spontaneous decay, stimulated decay, and inverse decay, respectively. Note that the term $\propto f_a \, f_\gamma^2$ cancels out between decay and production. For all environments considered in this work $f_a \gg f_\gamma$, so the inverse decay can be neglected.

The axion decay rate can then be obtained integrating the matrix element over all the momenta (and imposing energy-momentum conservation), leading to the well-known Boltzmann Equation (see e.g. [60]):

$$\begin{aligned}
\dot{n}_a &= -\int d\Pi_a d\Pi_\gamma d\Pi_\gamma (2\pi)^4 \, \delta^4(p_a - p_\gamma - p_\gamma) \, |\mathcal{M}_0|^2 \, [f_a \, (f_\gamma + 1)(f_\gamma + 1) + (f_a + 1) \, f_\gamma \, f_\gamma] \\
&= -\int d\Pi_a d\Pi_\gamma d\Pi_\gamma (2\pi)^4 \, \delta^4(p_a - p_\gamma - p_\gamma) \, |\mathcal{M}_0|^2 \, [f_a \, (1 + 2 \, f_\gamma) - f_\gamma^2] \\
&\simeq -n_a \, \Gamma_a \, (1 + 2 \, f_\gamma) \, ,
\end{aligned} \tag{2.7}$$

where $d\Pi_i = g_i/(2\pi)^3 d^3p/(2\,E)$ and in the last line we used the definition of the decay rate $\Gamma_a = \int d\Pi_\gamma d\Pi_\gamma (2\pi)^4 \, \delta^4(p_a - p_\gamma - p_\gamma) \, |\mathcal{M}_0|^2/(2\, m_a)$.

It should be clear from eq. (2.7) that the effect of stimulated emission can be incorporated by simply multiplying the rate of spontaneous emission by a factor $2\, f_\gamma$. The photon occupation number f_γ can be obtained from the associated differential energy density of the ambient radiation using $\rho_i(E_i) \, dE_i = d\Pi_i \, 2 \, E_i^2 \, f_i$ which leads to:

$$f_\gamma = \frac{\pi^2 \rho_\gamma}{E_\gamma^3} . \tag{2.8}$$

In figure 1, we show the stimulated emission factor arising from the CMB (black), Galactic diffuse emission (red), and the extragalactic radio background (green), as a function of the axion mass. Figure 1 shows that for an axion mass $m_a \sim 1\,\mu$eV, the stimulated decay produces an enhancement by a factor $\gtrsim 10^5$, regardless of the astrophysical environment.

3 Radio sensitivity

In the following sections we outline the procedure for computing the expected radio emission from, and the detectability of, axion decay for various astrophysical targets and telescopes.

JCAP03(2019)027

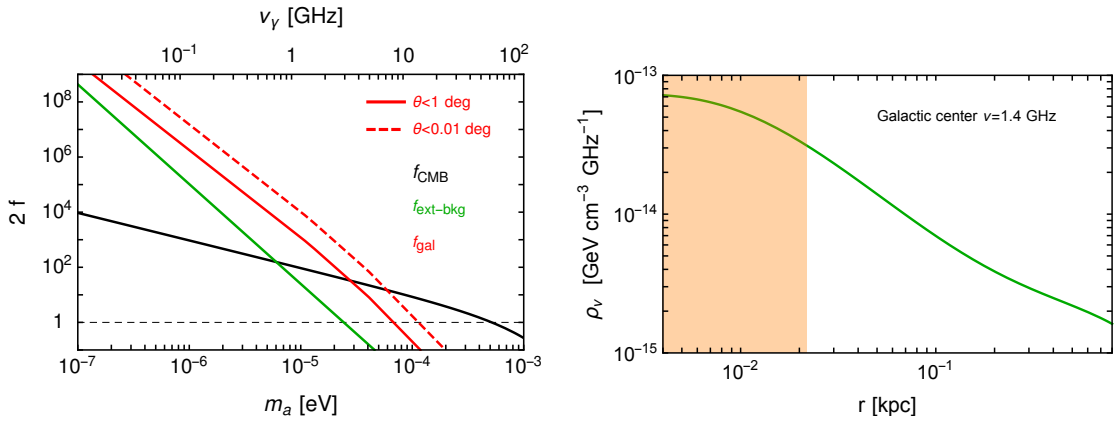

Figure 1. Left: stimulated emission factor ($2\,f_\gamma$) broken down in terms of contributions from the CMB, the extragalactic radio background, and Galactic diffuse emission. The Galactic contribution is averaged in a region of angular radius of 1 and 0.01 degrees about the Galactic center, see eq. (4.8). Right: differential photon energy density at $\nu = 1.4$ GHz as a function of the distance from the Galactic Center.

Before beginning, we comment on a number of subtle, but important features of the expected signal. First, the signal is expected to be rather diffuse, at least when compared with the beam of typical radio telescopes. For such a diffuse emission, a relatively large beam is desired in order to enhance the signal-to-noise. This can be easily achieved by single-dish telescopes. On the other hand, their collecting area (and thus the sensitivity) is typically much smaller than that of interferometers (that, in addition, have a smaller synthesized beam). Moreover, larger beams also imply larger foregrounds and larger confusion from background sources. Since it is not obvious *a priori* whether single-dish telescopes or radio interferometers will perform better, we consider results for both observing modes.

In the near future, one of the most powerful radio telescopes available will be the SKA. We consider here a total of five different configurations for SKA [61]. Phase one of SKA-Mid (labeled here as 'SKA1-Mid') will be built and operational as early as 2022. We also consider a configuration of SKA-Mid consistent with the proposed upgrade (labeled here as 'SKA2-Mid'), which has a slightly wider frequency band, 10 times more telescopes, and includes phase array feed (PAF) technology.[4] The analysis below allows both telescopes to operate in either single-dish or interferometric modes. The SKA collaboration has also planned the construction of a low frequency array, which is assumed here to operate solely in the interferometric configuration (note that the synthesized beam increases at small frequencies, and thus the potential tradeoff between interferometric and single-dish observations is reduced significantly). In the coming years, the radio community will begin a significant experimental effort to map large scales at frequencies below 1 GHz in connection to the study of cosmological hydrogen (redshifted 21 cm line). Data collected in these surveys can also be used to search for the signal discussed here. As a reference telescope of this class, we consider the inteferometer HIRAX [62]. Other planned surveys that can be used to this aim involve, among others, the APERTIF, BINGO, CHIME, FAST and Tianlai telescopes (see [63] for a review of forthcoming experiments).

[4] A PAF consists of an array of receivers that are off-set in the focal plane of the dish and therefore see slightly different parts of the sky. Combining multiple simultaneous beams, an antenna equipped with PAF provides a much larger field-of-view.

JCAP03(2019)027

	SKA1-Mid	SKA2-Mid	SKA-Low	HIRAX
Freq. [GHz]	0.35–14	0.35–30	0.05–0.35	0.4–0.8
$N_{\rm PAF}$	1	36	1	1
$N_{\rm tele}$	200	2000	911	1024
D [m]	15	15	35	6
$\theta_{\rm sinth}$ [$'$]	3.6–0.09	3.6–0.04	25.2–3.6	10–5
$T_{\rm rcvr}$ [K]	20	20	40	50

Table 1. Telescope performances and configurations considered in this work. For the case of SKA1-Mid and SKA2-Mid, we consider the array working both in interferometric and single-dish modes.

Details of the performances for HIRAX and for the various configurations of SKA considered in this work are summarized in table 1.

The axion signal is expected to appear as a narrow spectral line, broadened by the axion velocity dispersion. For targets in ordinary galaxies, the expected velocity dispersion is $\sim 10^{-3}\,c$, while for dwarf galaxies may be as small as a few km/s (i.e., a few times $10^{-5}\,c$). An experiment hoping to resolve the spectral features of the line would therefore typically require, respectively, $\sim 10^3$ and $\sim 10^5$ frequency channels. This is in full compliance with SKA capabilities, and while the current HIRAX design includes only 1024 channels, there exists however a foreseen possibility to up-channelizing data to a spectral resolution of 1.5 km/s.

3.1 Expected flux

The flux density, i.e. the power per unit area per unit frequency, from the spontaneous and stimulated decay of an axion is given by

$$S_{\rm decay} = \frac{\Gamma_a}{4\pi\Delta\nu}\int d\Omega\, d\ell\, \rho_a(\ell,\Omega)\, e^{-\tau(m_a,\ell,\Omega)}\, \left[1+2f_\gamma(\ell,\Omega,m_a)\right]\,, \tag{3.1}$$

where m_a is the axion mass, $\Gamma_a = \tau_a^{-1}$ is the spontaneous decay rate of axions (given by the inverse of eq. (2.1)), $\rho_a(\ell,\Omega)$ is the axion mass density, $\Delta\nu$ is the width of the axion line, $f_\gamma(\ell,\Omega,m_a)$ is the ambient photon occupation evaluated at an energy $E_\gamma = m_a/2$, and τ is the optical depth. The integral in eq. (3.1) should be performed over the solid angle covered by the radio telescope and the line of sight between the source and the location of Earth.

Eq. (3.1) describes an isotropic emission. On the other hand, if the ambient radiation field is anisotropic, then the stimulated axion-decay emission will follow the direction of the ambient radiation (since the photon emitted from stimulated axion-decay is produced in the same quantum state as the ambient photon sourcing the stimulated emission). As it will be clearer in the following, we either consider radiation field that are isotropic up to very good approximation (such as CMB and extragalactic background) or model the ambient photons at the source location by exactly taking only the measured continuum emission, namely, only the photons directed towards us. In other words, we consider photons with the right direction to induce a stimulated emission directed towards our location and therefore our estimate are not affected by possible anisotropies in the considered ambient fields.

JCAP03(2019)027

It is conventional in radio astronomy to work with effective temperatures rather than flux densities. The observed antenna temperature in a single radio telescope is given by

$$T_{\rm ant} = \frac{A_{\rm eff}\ \langle S \rangle}{2k_b}\,, \tag{3.2}$$

where $A_{\rm eff}$ is the effective area of the telescope, which we set to be $A_{\rm eff} = \eta\, A_{\rm coll}$ where $A_{\rm coll}$ is the physical collecting area of the telescope and η is the efficiency (assumed to be 0.8 for SKA [61] and 0.6 for HIRAX [62]), and $\langle S \rangle$ is the bandwidth-averaged flux density. Throughout this work we take the bandwidth to be equal to that width of the axion line, i.e. $\Delta B = \Delta\nu = \nu_a\, \sigma/c$, where ν_a is the central frequency of the line and σ the velocity dispersion of the dark matter particles.

3.2 Telescope sensitivities

The minimum (rms) observable temperature for a single telescope and one polarization is given by

$$T_{\rm min} = \frac{T_{\rm sys}}{\sqrt{\Delta B\, t_{\rm obs}}}\,, \tag{3.3}$$

where $t_{\rm obs}$ is the observation time (set to be equal to 100 hours throught this work), ΔB is the bandwidth, and the system temperature $T_{\rm sys}$ is given by $T_{\rm sys} = T_{\rm rcvr} + T_{\rm sky}$. $T_{\rm rcvr}$ is the noise of the receiver, while $T_{\rm sky}(\ell, b)$ is the "sky noise" in the direction of observation. In the case of dSph galaxies, we extracted the temperature $T_{\rm sky}$ at the dSph position from the Haslam map [64] at 408 MHz and rescaled to other frequencies with a spectral index of -2.55. In the cases of the Galactic center and M87, we considered the temperature derived by the same observations we used to describe the radiation field in the context of computing the stimulated emission, see below. Finally, in the case of the Galactic halo, we adopt a sky-average value $T_{\rm sky} \simeq 60\,(\lambda/{\rm m})^{2.55}\,{\rm K}$ [61], since we are considering a very large fraction of the sky.

Transitioning from eq. (3.2) and eq. (3.3) to observable signal-to-noise of a telescope or an array depends inherently the mode of observation, i.e. interferometric or single-dish observation. The field of view (FoV) can be computed similarly in the two cases, while angular resolution and sensitivity have to be treated separately.

3.3 Field of view

The angle corresponding to the full-width at half maximum (FWHM) of the primary beam is given by

$$\theta_{\rm pb} \simeq 1.22\,\frac{\lambda}{D} \simeq 0.7^\circ \left(\frac{1\,{\rm GHz}}{\nu}\right)\left(\frac{15\,{\rm m}}{D}\right)\,, \tag{3.4}$$

where λ and ν are the wavelength and frequency of observation, and D is the diameter of the dish/station. Here, we consider the primary beam area to be $\Omega_{\rm pb} = 2\pi\,(1 - \cos(\theta_{\rm pb}/2))$. In the cases of SKA1-Mid, SKA-Low and HIRAX, the FoV is set by the primary beam, i.e. ${\rm FoV} = \Omega_{\rm pb}$.

The FoV can be however enlarged by equipping the interferometer with PAF technology, which makes ${\rm FoV} = N_{\rm PAF}\,\Omega_{\rm pb}$, with $N_{\rm PAF}$ expected to be $\gtrsim 36$ for next generation radio telescopes [61]. This is the picture we consider for SKA2-Mid and in this case the signal-to-noise ratio becomes

$$\left(\frac{S}{N}\right)^{\rm PAF} = \sqrt{\sum_{i=1}^{N_{\rm PAF}} \left(\frac{S}{N}\right)^2_{b_i}} \tag{3.5}$$

JCAP03(2019)027

where $(S/N)_{b_i}$ is the signal-to-noise in the beam i and there are $N_{\rm PAF}$ beams in the FoV. For a spatially uniform emission, the increase of the FoV due to PAF would lead to an increase of the signal-to-noise by a factor of ten.

3.4 Single-dish angular resolution and sensitivity

For single-dish telescopes, the angular resolution is set by eq. (3.4). The latter defines the integration angle to be used in eq. (3.1), which leads (through eq. (3.2)) to a certain $T_{\rm ant}^{\rm pb}$. The signal-to-noise ratio for a single telescope and one polarization is simply given by the ratio between eq. (3.2) and eq. (3.3):

$$\left(\frac{S}{N}\right)_{sd,\rm single} = \frac{T_{\rm ant}^{\rm pb}}{T_{\rm min}} \,. \tag{3.6}$$

Clearly the actual temperature measured by the telescope will not just include the emission associated to axion decay, but also a number of other Galactic or extragalactic radio sources. We assume to be able to remove the continuum ("smooth") radiation, since the telescope considered in this work have a large number of frequency channels that can be used to constrain the spectrum. For a discussion about foreground removal, see, e.g., [65, 66]. On top of that, if the continuum emission is also spatially smooth, like in the direction of dSphs (since they are not expected to source a significant continuum emission, see, e.g., [67]), the foreground does not even enter interferometric observations which are blind to large scales. Therefore, the case of interferometric observations of dSph can be considered the most solid scenario for what concerns foreground removal.

The presence of spectral lines would instead constitute an irreducible background (in particular, if the width is comparable to the width of the axion line). However, there are only a very limited number of radio lines in the frequency range of interest. The only potentially problematic spectral line is the redshifted 21-cm line, which is relatively bright at low redshifts. The observed frequency scales as $\nu_{\rm obs} = \nu_{em}/(1+z)$ and the emission stays significant up to approximately $z \lesssim 5$. Therefore, it affects the possible detection of axions with masses between about 2–12 μeV. This range is however already strongly constrained by haloscopes except for a narrow window around 3–4 μeV (see figure 2). To study potential technical ways to remove such a background (exploiting e.g. different line width and morphology of the axion signal) is beyond the goal of this paper.

Considering an array with $N_{\rm tele}$ telescopes observing in single-dish mode, the signal-to-noise is given by

$$\left(\frac{S}{N}\right)_{sd,\rm array} = \sqrt{N_{\rm tele}\, n_{\rm pol}} \left(\frac{S}{N}\right)_{\rm single} = \sqrt{N_{\rm tele}\, n_{\rm pol}}\, \frac{T_{\rm ant}^{\rm pb}}{T_{\rm min}} \,, \tag{3.7}$$

where $n_{\rm pol}$ is the number of polarizations (we set $n_{\rm pol} = 2$). Finally, for an array equipped with PAF the signal-to noise is simply

$$\left(\frac{S}{N}\right)_{sd,\rm array}^{\rm PAF} = \sqrt{N_{\rm tele}\, n_{\rm pol}} \sqrt{\sum_{b=1}^{N_{\rm PAF}} \left(\frac{T_{\rm ant}^{b}}{T_{\rm min}}\right)^2} \,, \tag{3.8}$$

where $T_{\rm ant}^{b}$ is the antenna temperature in the beam b.

JCAP03(2019)027

3.5 Angular resolution and sensitivity of interferometers

In a radio interferometer, the angular resolution is set by the longest baseline $b_{\rm max}$, i.e. $\theta_{\rm res} \simeq 1.22\,\lambda/b_{\rm max}$, while the largest scale that can be imaged is set by the shortest baseline $b_{\rm min}$, i.e. $\theta_{\rm max} \simeq 1.22\,\lambda/b_{\rm min}$. The actual synthesized beam and largest observable scale depends also on observational details, such as the coverage in the visibility plane. The emissions discussed here have a typical size $\lesssim \theta_{\rm max}$ for all telescopes, so it is reasonable to assume that there is no flux lost by the interferometric observations, except possibly for high frequencies and extended targets (cases for which we will consider single-dish observations, see section 4). The synthesized beam is determined by considering an "average" baseline, leading to the values of $\theta_{\rm sinth}$ detailed in table 1. The signal in each "pixel" is the integral of eq. (3.1) over the synthesized beam, which provides $T^{\rm sb}_{\rm ant}$ (again through eq. (3.2)).

Considering an array with $N_{\rm tele}$ telescopes operating in an interferometric mode, there are $N_{\rm tele}(N_{\rm tele}-1)/2$ independent baselines, the signal-to-noise given by

$$\left(\frac{S}{N}\right)_{if,{\rm array}} = \sqrt{\frac{1}{2}N_{\rm tele}(N_{\rm tele}-1)\,n_{\rm pol}}\sqrt{\sum_{\rm pix=1}^{N_{\rm pix}}\left(\frac{T^{\rm pix}_{\rm ant}}{T_{\rm min}}\right)^2}\,, \tag{3.9}$$

where $N_{\rm pix}$ is the number of synthesized beams contained in the area of the primary beam. For a spatially uniform emission, the signal-to-noise is increased by a factor $\sqrt{N_{\rm pix}}$ in the limit that the synthesized beam is equal to the primary beam.

To compute $\left(\frac{S}{N}\right)^{\rm PAF}_{if,{\rm array}}$, one can again apply eq. (3.5).

3.6 Radiation fields for stimulated emission

As discussed in section 2, the presence of a non-negligible photon background with the same energy as that produced in the axion decay implies a stimulated enhancement of the axion decay rate; this effect manifests in terms of a non-zero contribution to f_γ in eq. (3.1). In general, f_γ will be a linear combination over the sources which contribute to the photon bath. At radio frequencies, this includes, but is not limited to,[5] photons from the cosmic microwave background (CMB), diffuse emission from within the galaxy under consideration, and the radio background from extragalactic sources, i.e. we assume

$$f_\gamma(\ell,\Omega,m_a) \simeq f_{\gamma,{\rm CMB}}(m_a) + f_{\gamma,{\rm gal}}(\ell,\Omega,m_a) + f_{\gamma,{\rm ext-bkg}}(m_a)\,, \tag{3.10}$$

where the spatial dependence of f_γ appears exclusively in the contribution from galactic emission, while $f_{\gamma,{\rm CMB}}$ and $f_{\gamma,{\rm ext-bkg}}$ are (at first approximation) isotropic.

The photon occupation from a blackbody spectrum is given by

$$f_{\gamma,bb} = \frac{1}{e^x-1} \qquad x \equiv \frac{E_\gamma}{k_b T} \tag{3.11}$$

where k_b is Boltzmann's constant and T is the blackbody temperature. Eq. (3.11) can be used to incorporate the contribution to f_γ from the CMB, taking $T = 2.725\,{\rm K}$.

For the galactic diffuse and the extragalactic contributions we use eq. (2.8), namely, we derive the stimulated enhancement factor from the measured radio intensity. The extragalactic radio background has been measured [68, 69] to have a frequency-dependent temperature

[5] It is worthwhile to note that at high-frequencies, free-free emission in hot and high-density environments may become the dominant contribution to f_γ. This contribution is neglected in this work.

JCAP03(2019)027

given by

$$T_{\rm ext-bkg}(\nu) \simeq 1.19 \left(\frac{\rm GHz}{\nu}\right)^{2.62} \ {\rm K}\,. \tag{3.12}$$

The contribution to f_γ from galactic diffuse emission will be instead specified for each target (Galactic center, M87, Galactic halo) in the next section. Its spatial dependence is computed from the angular profile of the measured radio flux.

4 Results

Below we present the projected sensitivity contours in the ALP parameter space for different astrophysical targets. For the SKA-Mid, we considered the telescope operating both in single-dish and interferometric modes. These two configurations lead to similar results for the Galactic center and dwarf spheroidal galaxies and we quote only the sensitivities from single-dish observations. This is because in the high-frequency end, the largest scale that can be imaged by the interferometer becomes comparable/smaller than the size of the source, so there might be some loss of flux (that we are not including in the modeling), which does not happen in the case of single-dish observations. At lower frequencies, observational beams become larger, and SKA-Low and HIRAX do not face above issue. For M87 instead, SKA-Mid operating in interferometric mode provides significantly better sensitivities, therefore we show the results only for this configuration. Given the distance from us and the large stimulated emission factor in the central region of the galaxy, the emission from M87 is more compact than in the case of the Galactic center and dwarf spheroidal galaxies. This explains why the interferometric mode, which has a better rms sensitivity and a smaller smaller synthesized beam, is favored with respect to the single-dish mode.

4.1 Dwarf galaxies

As a first target we consider dwarf spheroidal galaxies, refining the analysis performed in [46]. Dwarf spheroidal galaxies offer large dark matter densities, a low velocity dispersion and their angular size is within the field of view of the radio telescopes that we are considering. These properties make them prime targets for searches of radio emissions produced by the decay of axions. The signal, as shown in eq. (3.1), depends on the integral of the dark matter density distribution in the region of observation, the so-called D-factor $D(\theta)$:

$$D(\theta) = \int d\Omega\, dl\, \rho_a(l, \Omega), \tag{4.1}$$

with θ the angular distance from the center of the the dwarf galaxy. A significant effort is ongoing to reconstruct the D-factors from stellar kinematical observations, see for example [71–76]. Here we make use of the publicly available data in [72, 73], which provide the median values of the D-factors and their uncertainty intervals for several dwarf galaxies. In particular we focus on Reticulum II, which is one of the most promising dwarf galaxies that can be observed by radio telescopes located in the southern hemisphere, like SKA and HIRAX. Similar D-factors have been reported also for other observable (by southern located telescopes) dwarf spheroidal galaxies, both classical (e.g. Sculpture) and ultrafaint (e.g. Coma).

The dark matter velocity dispersion is estimated from the measured stellar velocity dispersion which we take to be $\sigma \simeq 4$ km s^{-1}, see [73]. The uncertainty on σ affects the

JCAP03(2019)027

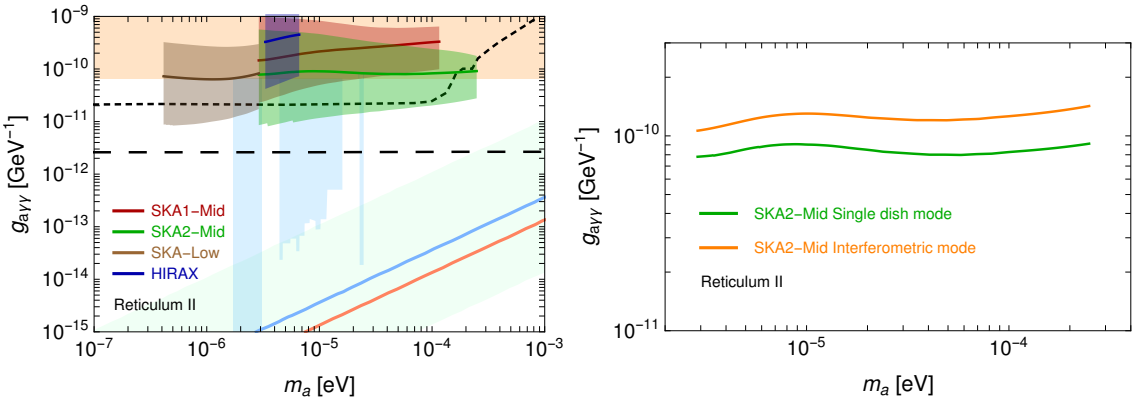

Figure 2. Left panel: projected sensitivities for the Reticulum II dwarf galaxy. Results are displayed alongside current bounds from haloscopes (light blue) [14–17] and helioscopes (orange) [18], projected bounds from ALPS-II [70] (black, short dashed) and IAXO [19, 20] (black, long dashed), and benchmark QCD axion models (light green band, blue line, orange line) [50]. The width of the expected exclusion contours reflect the astrophysical uncertainty in the dSph environment. Right panel: comparison between the sensitivites of interferometric and single-dish observations for the Reticulum II dwarf galaxy, considering the SKA2-Mid configuration.

results mildly, since the sensitivity on $g_{a\gamma\gamma}$ scales as $\sigma^{-1/4}$. For the stimulated emission, we include only the contributions from the CMB and the extragalactic radiation, neglecting any (currently undetected, and likely subdominant) radio emission produced inside the dwarf galaxy.

We show our results in the left panel of figure 2. The bands refer to the 95% credibility interval on the D-factor provided in [73]. Under the stated assumptions future radio telescopes might be able to probe a currently unexplored region of the parameter space, corresponding to $g_{a\gamma\gamma} \gtrsim 10^{-11}\,\mathrm{GeV}^{-1}$.

In figure 2 (right), we compare the results of single-dish versus inteferometric observing modes for the SKA2-Mid configuration. As clear from the plot, the difference is limited. For what said in section 3.4, this also shows that the main conclusion of this paper should be not affected by the removal of the continuum emission.

The sensitivity reported in this work differs by about three orders of magnitude (about a factor of 30 in the axion-photon coupling) with respect to [46]. That work applied the SKA interferometric sensitivity as if the source were point-like rather than extended as instead we consider in eq. (3.9). Moreover, they considered an optimistic SKA collecting area which is not currently foreseen in the future SKA design (i.e., $A_{\rm eff}/T_{\rm sys} = 10^5 \mathrm{m}^2/\mathrm{K}$ at high-frequency, about one order of magnitude larger than our SKA-2 case).

4.2 Galactic center

Due to the close proximity and high dark matter column density, the Galactic center is typically among the most promising targets for indirect dark matter searches. Additionally, the presence of a large synchrotron background is expected to lead to a significant enhancement of the decay rate of axions. We describe the details and caveats of this calculation below.

The distribution of dark matter in the Galactic center, and in particular the inner slope of the density profile, remains largely unknown. N-body simulations of collisionless cold dark matter predict density profiles well-modeled by a Navarro-Frenk-White (NFW) profile [77],

JCAP03(2019)027

in which $\rho(r) \propto r^{-1}$ at small radii. However, mechanisms have been proposed which can either flatten or steepen the distribution to produce a core or cusp. In an attempt to account for this source of uncertainty, we present sensitivity studies for three distinct profiles, one 'reference' distribution, and two profiles intended to characterize the relative extremes. The reference distribution that we consider is the NFW profile:

$$\rho(r) = \frac{\rho_s}{\left(\frac{r}{r_s}\right)\left(1+\frac{r}{r_s}\right)^2}\,, \tag{4.2}$$

where we take a scale radius $r_s = 24.42\,\mathrm{kpc}$ [78] and ρ_s is normalized in order to obtain a density at the Earth's location ($r_\odot = 8.3\,\mathrm{kpc}$) $\rho(r_\odot) = 0.3\,\mathrm{GeV/cm^3}$. For the more optimistic scenario we consider a cuspy distribution, given by a generalized NFW profile

$$\rho(r) = \frac{\rho_s}{\left(\frac{r}{r_s}\right)^\gamma\left(1+\frac{r}{r_s}\right)^{3-\gamma}}\,, \tag{4.3}$$

with r_s and ρ_s defined as before, and an inner slope γ taken to be 1.3. To model the cored dark matter density profile we adopt the so-called Burkert profile, given by

$$\rho(r) = \frac{\rho_s}{\left(1+\frac{r}{r_{sb}}\right)\left(1+\frac{r}{r_{sb}}\right)^2}\,, \tag{4.4}$$

where $r_{sb} = 12.67\,\mathrm{kpc}$ [78], and as before the scale density is set to provide the reference local density $\rho(r_\odot)$.

The velocity dispersion of dark matter, characterizing the width of the decay line, is taken to be $\sigma = 200\,\mathrm{km/s}$. To estimate the Galactic contribution to f_γ in eq. (3.10) the morphology of the radio diffuse emission should be taken into account. Here, we attempt to infer the value and spatial dependence of $f_{\gamma,\mathrm{gal}}$ from the measurements of the radio flux in the Galactic center region presented in [79]. Specifically, we analyze the radial profile at $\nu_* = 1.415$ GHz derived by averaging the emission in elliptical annuli (with aspect ratio of two-to-one), located around the Galactic center. To simplify the analysis, we assume that the flux observed in [79], extending up to an angular scale of one degree along the semi-major axis, can be mapped onto a spherically symmetric region, i.e. a circle rather than elliptic annuli, of equivalent area. The observed flux at Earth from a spherically symmetric emissivity $j(r)$ is given by

$$I(\theta) = \frac{1}{4\pi}\int ds\, j(\hat{r}(\theta, s, r_\odot))\,, \tag{4.5}$$

where the line-of-sight coordinate s is related to the radial distance from the Galactic center $\hat{r} = \sqrt{s^2 + r_\odot^2 - 2\,s\,r_\odot\cos(\theta)}$ and θ is the aperture angle from the line-of-sight and the Galactic center direction. For the small angles θ under consideration, one can perform an Abel transform to infer the value of $j(r)$ from the value of $I(\theta)$ provided in [79]. Then, once the emissivity profile has been obtained, one can compute the differential photon density (at the frequency ν_*) as a function of the distance r from the Galactic center:

$$\rho_\nu(r) = \frac{1}{4\pi}\int ds\, d\Omega\, j(\hat{r}(\theta, s, r))\,. \tag{4.6}$$

The resulting distribution is shown in the right panel of figure 1. The intensity profile $I(\theta)$ in [79] flattens at small values of θ, an effect due to the finite angular resolution ($539''$) of

JCAP03(2019)027

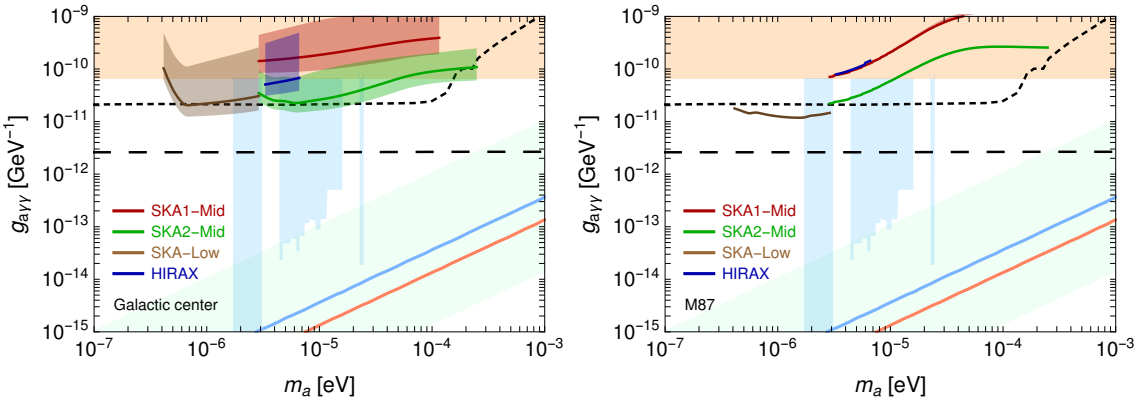

Figure 3. Same as figure 2 but for Galactic center (left) and M87 (right).

the observations. In figure 1, the corresponding range of Galactic distances r is shaded: in that region the $\rho_\nu(r)$ distribution is likely to be steeper than reported, but we conservatively choose not to extrapolate it. The $\rho_\nu(r)$ is instead extrapolated as r^{-2} at large distances, beyond the range covered by the observations. We checked that our results do not depend on the specific prescription adopted. Finally, it is then straightforward to obtain the photon occupation number $f_{\gamma,\mathrm{gal}}(r,\nu)$ from the density distribution $\rho_\nu(r)$. The frequency dependence of the occupation number can be obtained from the observed spectral shape of the emission. From table 1 of [79] we obtain:

$$f_{\gamma,\mathrm{gal}}(r,\nu) = f_{\gamma,\mathrm{gal}}(r)\Big|_{\nu=\nu_*} \times \begin{cases} (\nu/\nu_*)^{-3.173} & \nu < \nu_* \\ (\nu/\nu_*)^{-3.582} & \nu_* \leq \nu \leq 4.85\,\mathrm{GHz} \\ 0.49 \times (\nu/\nu_*)^{-4.14} & \nu > 4.85\,\mathrm{GHz} \end{cases} . \tag{4.7}$$

The contribution of $f_{\gamma,\mathrm{gal}}$ to the stimulated emission is presented in the left panel of figure 1. We show the average value in a region of 1 and 0.01 degrees around the Galactic center, defined as:

$$\bar{f}_{\gamma,\mathrm{gal}} = \frac{\int d\Omega\, d\ell\, \rho_a(\ell,\Omega)\, f_\gamma(\ell,\Omega,m_a)}{\int d\Omega\, d\ell\, \rho_a(\ell,\Omega)} \tag{4.8}$$

The Galactic contribution dominates over the CMB and extragalactic ones in a large range of frequencies.

The free-free self absorption becomes relevant only at frequencies $\nu \lesssim 10 - 20$ MHz for observations of targets located above the Galactic plane, as dwarf galaxies, and so can be neglected for our purposes. Instead, the emission of sources located at low Galactic latitudes is significantly absorbed already at $\nu \lesssim 200\,\mathrm{MHz}$, because of the large column density of electrons lying in the Galactic plane. We need to incorporate this effect in our analysis of the Galactic center. We compute the optical depth τ in eq. (3.1) using [80] and setting a kinetic temperature of 5000 K and an emission measure $EM = 10^4\,\mathrm{cm}^{-6}\,\mathrm{pc}$. The impact of absorption in our results, presented in the left panel of figure 3, can be easily recognized: the sensitivity quickly degrades moving towards low frequencies. Overall, the sensitivity reach that we obtain is similar to the one found in section 4.1 for dwarf spheroidal galaxies.

JCAP03(2019)027

4.3 M87

Given its position in the sky, mass, and distance, the Virgo cluster is likely to be among the most promising galaxy clusters in the search for axion decay. The massive elliptical galaxy M87 lying at its center accounts for a significant fraction of the Virgo mass ($\simeq 5-10\%$), and it is a bright radio emitter. An intra-cluster large scale radio halo is much fainter [81]. We checked that M87 provides stronger constraints on ALP parameter space than the Virgo intra-cluster medium. This is because the former hosts a large density of radio photons, leading to a large stimulated emission. In the following we show results only for M87.

To obtain the contribution to the stimulated emission from the diffuse radiation in M87, $f_{\gamma,\rm gal}(r,\nu)$ in eq. (3.10), we proceed as follows. The total power radiated by M87 from 10 MHz up to 150 GHz is $L_\gamma = 9.6\times10^{41}$ erg/s, and it is predominantly produced within $r_p = 40$ kpc of the center of the galaxy [82]. The photon energy density ρ can be estimated simply as $\rho = \frac{L_\gamma\, r_p}{V\, c}$ with $V = \frac{4}{3}\pi r_p^3$. Then, using a spectral dependence of the flux $\propto \nu^{-1}$ [82], one can infer the photon energy density, and thus the occupation number $f_{\gamma,\rm gal}(r,\nu)$, at any frequency. For simplicity we consider a constant photon distribution inside r_p, with an average value estimated as explained above, and an abrupt depletion of the photon density outside this region.

The dark matter density distribution is modeled using the results of [83], where the mass density has been inferred by jointly analyzing the dynamics of stars, globular clusters, and satellites. In particular, we consider two density distributions, the NFW profile and a cored profile (cgNW in [83]). Finally we caution that we do not attempt to model any absorption inside M87. On the other hand, this can have an impact on both the derived energy density of background photons and the estimated axion-induced flux, with the two effects expected to be of similar size.

The sensitivities are shown in figure 3 (right). The changes due to the different choice of dark matter density profile are modest. The two adopted profiles differ little at the distances corresponding to the angular scales under examination.

4.4 Wide field surveys

One of the primary goals of HIRAX is to observe the large-scale structure of the Universe through the 21 cm emission line produced by the neutral hydrogen, the so-called hydrogen intensity mapping. For this purpose HIRAX has been designed to measure a large fraction of the sky (1.5×10^4 squared degrees) with a fairly large integrated time (10^4 hours) [62]. We investigate whether the same observational campaign can be used to search for radio lines produced by the decay of axions inside the Galactic halo. We estimate the sensitivity of HIRAX, approximating the region of observation with a circle centered at the Galactic center and spanning an equal area (i.e. 1.5×10^4 squared degrees). The signal is computed assuming the NFW density profile in section 4.2 and a velocity dispersion $\sigma \simeq 200$ km/s. To model the stimulated emission, in eq. (3.10) we incorporate the sum of the Galactic and extragalactic contribution using $T_{\rm sky}$ described in section 3.2 as a measure of the total radio flux.

We find that the reach is at the level of the region already excluded by haloscopes, namely $g_{a\gamma\gamma} \simeq 8.6-17\times10^{-11}\,\text{GeV}^{-1}$ in the mass range $m_a \simeq 3.3-6.7\,\mu$eV. We have obtained similar sensitivities for the CHIME telescope [84], which will perform a complementary survey of the northern sky.

These estimates, although involving several approximations (namely the patch of the sky which will actually be observed, and the modeling of $f_{\gamma,\rm gal}(r,\nu)$), are enough to conclude

JCAP03(2019)027

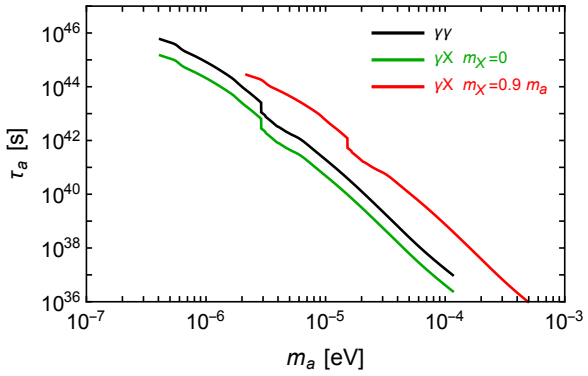

Figure 4. Projected sensitivity from figures 2 and 3, translated into constraints on the ALP lifetime as a function of the ALP mass. We show the cases of decays into two photons (black) and into a photon plus a state X, massless (green) or with $m_X = 0.9\, m_a$ (red).

that the strategies considered in the previous sections, i.e. observations of the Galactic center, dwarf galaxies and galaxy clusters, are more promising to look for the decay of axions.

The cumulative line emission from all dark matter halos at all redshifts forms a nearly isotropic emission with a continuum spectrum. We find the cosmological emission to be $\lesssim 10^{-4}$ of the measured extragalactic background (for couplings in the allowed range). Since this collection of lines determines a contribution with no prominent spatial or spectral features, it can be very complicated to identify. A potentially interesting way to overcome this issue is given by line-intensity mapping [85]. We postpose a dedicated analysis of this approach to future work.

4.5 Discussion

The main goal of this work was to study the observability of the two-photon decay of ALPs, with the QCD axion used as a very well-motivated benchmark. More generally, our results apply to any scenario in which a light dark matter candidate (with mass in the range $0.1 - 100\,\mu$eV) has a monochromatic decay to one or two photons. For instance, one could extend the ALP model that we have analyzed, supplementing the Lagrangian by a term $a\, F^{\mu\nu} \tilde{F}'_{\mu\nu}$, where $\tilde{F}'_{\mu\nu}$ is the dual of a new field strength tensor arising from a dark U(1) gauge symmetry [86–90]. Here, if the mass of the dark photon is less than the mass of the axion, the axion decay will proceed via $a \to \gamma\gamma'$ (this model has beed studied e.g. in [91–94]).

For sake of generality, in figure 4 we present our sensitivities in terms of the ALP lifetime; these results can then be easily recast for alternatively models. The sensitivity curve is plotted as a function of the ALP mass. For the decay into two photons, we show the best sensitivity from figures 2 and 3. For the decay into a photon plus a lighter state X, we recast the sensitivity using the relation $E_\gamma = \frac{m_a}{2}\left(1 - \frac{m_X^2}{m_a^2}\right)$ and we show two cases: $m_X = 0$ and $m_X = 0.9\, m_a$. Remarkably, figure 4 shows that it may be possible to probe lifetimes as large as 10^{46} seconds.

JCAP03(2019)027

5 Conclusions

In this work we studied the radio emission arising from axion decays in various types of nearby astrophysical structures. We have presented projected sensitivities for targets with the best observational prospects, including the Galactic center, the ReticulumII dwarf galaxy, M87, and the Galactic halo. We have found that for ALPs with masses below meV, the stimulated decay arising from the presence of ambient photons results in a large enhancement of the decay rate — potentially up to eight orders of magnitude for axion masses $\sim \mu$eV and in environments with large radio emission like the Galactic Center.

Once the axion mass and the coupling to photons are fixed, the main uncertainty comes from the dark matter distribution in the structure under consideration. Indeed, the effect of stimulated emission can be well determined since the distribution of ambient photons can be confidently derived from continuum radio measurements. This is different from the possible signal coming from photon-axion conversion in strong magnetic fields around stars, which is potentially more promising but suffers of larger uncertainties associated with the poorly known astrophysics (namely the structure of the magnetic field and the plasma density).

We have showed that with near-future radio observations by SKA, it will be possible to increase sensitivity to the ALP-photon coupling by nearly one order of magnitude. Interestingly, it has been shown that in this range of parameter space, axions provide a viable solution to a non-standard cooling mechanism identified in various stellar systems [95]. If forthcoming axion search experiments, such as ALPS-II and IAXO, find a signal consistent with axion dark matter in the $10^{-7} - 10^{-3}$ eV mass range, the technique proposed here might become the standard route to understand the properties of dark matter, such as e.g. its spatial distribution and clustering in cosmological structures.

Acknowledgments

We thank S. Camera, J. Fonseca, N. Fornengo, P. Serpico and M. Viel. MR acknowledges support by "Deciphering the high-energy sky via cross correlation" funded by Accordo Attuativo ASI-INAF n. 2017-14-H.0 and by the "Departments of Excellence 2018-2022" Grant awarded by the Italian Ministry of Education, University and Research (MIUR) (L. 232/2016). MR and MT acknowledge support from the project "Theoretical Astroparticle Physics (TAsP)" funded by the INFN. AC and SW acknowledge support from the European projects H2020-MSCAITN-2015//674896-ELUSIVES and H2020-MSCA-RISE2015.

References

[1] R.D. Peccei and H.R. Quinn, *CP Conservation in the Presence of Instantons*, *Phys. Rev. Lett.* **38** (1977) 1440 [INSPIRE].

[2] R.D. Peccei and H.R. Quinn, *Constraints Imposed by CP Conservation in the Presence of Instantons*, *Phys. Rev.* **D 16** (1977) 1791 [INSPIRE].

[3] S. Weinberg, *A New Light Boson?*, *Phys. Rev. Lett.* **40** (1978) 223 [INSPIRE].

[4] F. Wilczek, *Problem of Strong P and T Invariance in the Presence of Instantons*, *Phys. Rev. Lett.* **40** (1978) 279 [INSPIRE].

[5] J. Preskill, M.B. Wise and F. Wilczek, *Cosmology of the Invisible Axion*, *Phys. Lett.* **B 120** (1983) 127 [INSPIRE].

[6] M. Dine and W. Fischler, *The Not So Harmless Axion*, *Phys. Lett.* **B 120** (1983) 137 [INSPIRE].

JCAP03(2019)027

[7] L.F. Abbott and P. Sikivie, *A Cosmological Bound on the Invisible Axion*, *Phys. Lett.* **B 120** (1983) 133 [INSPIRE].

[8] R.L. Davis, *Cosmic Axions from Cosmic Strings*, *Phys. Lett.* **B 180** (1986) 225 [INSPIRE].

[9] D.J.E. Marsh, *Axions and ALPs: a very short introduction*, in *Proceedings of 13th Patras Workshop on Axions, WIMPs and WISPs, (PATRAS 2017)*, Thessaloniki Greece (2017), pg. 59 [arXiv:1712.03018] [INSPIRE].

[10] I.G. Irastorza and J. Redondo, *New experimental approaches in the search for axion-like particles*, *Prog. Part. Nucl. Phys.* **102** (2018) 89 [arXiv:1801.08127] [INSPIRE].

[11] L. Di Luzio, F. Mescia, E. Nardi, P. Panci and R. Ziegler, *Astrophobic Axions*, *Phys. Rev. Lett.* **120** (2018) 261803 [arXiv:1712.04940] [INSPIRE].

[12] S. Borsányi et al., *Calculation of the axion mass based on high-temperature lattice quantum chromodynamics*, *Nature* **539** (2016) 69 [arXiv:1606.07494] [INSPIRE].

[13] C. Hagmann, P. Sikivie, N.S. Sullivan and D.B. Tanner, *Results from a search for cosmic axions*, *Phys. Rev.* **D 42** (1990) 1297 [INSPIRE].

[14] ADMX collaboration, *Results from a high sensitivity search for cosmic axions*, *Phys. Rev. Lett.* **80** (1998) 2043 [astro-ph/9801286] [INSPIRE].

[15] ADMX collaboration, *Large scale microwave cavity search for dark matter axions*, *Phys. Rev.* **D 64** (2001) 092003 [INSPIRE].

[16] ADMX collaboration, *A Search for Invisible Axion Dark Matter with the Axion Dark Matter Experiment*, *Phys. Rev. Lett.* **120** (2018) 151301 [arXiv:1804.05750] [INSPIRE].

[17] HAYSTAC collaboration, *Results from phase 1 of the HAYSTAC microwave cavity axion experiment*, *Phys. Rev.* **D 97** (2018) 092001 [arXiv:1803.03690] [INSPIRE].

[18] CAST collaboration, *New CAST Limit on the Axion-Photon Interaction*, *Nature Phys.* **13** (2017) 584 [arXiv:1705.02290] [INSPIRE].

[19] I. Irastorza et al., *The International Axion Observatory IAXO*, Letter of Intent to the CERN SPS committee (2013).

[20] E. Armengaud et al., *Conceptual Design of the International Axion Observatory (IAXO)*, 2014 *JINST* **9** T05002 [arXiv:1401.3233] [INSPIRE].

[21] G. Vasilakis, J.M. Brown, T.W. Kornack and M.V. Romalis, *Limits on new long range nuclear spin-dependent forces set with a K – He-3 co-magnetometer*, *Phys. Rev. Lett.* **103** (2009) 261801 [arXiv:0809.4700] [INSPIRE].

[22] G. Raffelt, *Limits on a CP-violating scalar axion-nucleon interaction*, *Phys. Rev.* **D 86** (2012) 015001 [arXiv:1205.1776] [INSPIRE].

[23] B.R. Heckel, W.A. Terrano and E.G. Adelberger, *Limits on Exotic Long-Range Spin-Spin Interactions of Electrons*, *Phys. Rev. Lett.* **111** (2013) 151802 [INSPIRE].

[24] W.A. Terrano, E.G. Adelberger, J.G. Lee and B.R. Heckel, *Short-range spin-dependent interactions of electrons: a probe for exotic pseudo-Goldstone bosons*, *Phys. Rev. Lett.* **115** (2015) 201801 [arXiv:1508.02463] [INSPIRE].

[25] ARIADNE collaboration, *Progress on the ARIADNE axion experiment*, *Springer Proc. Phys.* **211** (2018) 151 [arXiv:1710.05413] [INSPIRE].

[26] R. Cameron et al., *Search for nearly massless, weakly coupled particles by optical techniques*, *Phys. Rev.* **D 47** (1993) 3707 [INSPIRE].

[27] C. Robilliard et al., *No light shining through a wall*, *Phys. Rev. Lett.* **99** (2007) 190403 [arXiv:0707.1296] [INSPIRE].

JCAP03(2019)027

[28] GammeV (T-969) collaboration, *Search for axion-like particles using a variable baseline photon regeneration technique*, *Phys. Rev. Lett.* **100** (2008) 080402 [arXiv:0710.3783] [INSPIRE].

[29] A. Afanasev et al., *New Experimental limit on Optical Photon Coupling to Neutral, Scalar Bosons*, *Phys. Rev. Lett.* **101** (2008) 120401 [arXiv:0806.2631] [INSPIRE].

[30] K. Ehret et al., *New ALPS Results on Hidden-Sector Lightweights*, *Phys. Lett.* **B 689** (2010) 149 [arXiv:1004.1313] [INSPIRE].

[31] OSQAR collaboration, *New exclusion limits on scalar and pseudoscalar axionlike particles from light shining through a wall*, *Phys. Rev.* **D 92** (2015) 092002 [arXiv:1506.08082] [INSPIRE].

[32] P. Sikivie, N. Sullivan and D.B. Tanner, *Proposal for Axion Dark Matter Detection Using an LC Circuit*, *Phys. Rev. Lett.* **112** (2014) 131301 [arXiv:1310.8545] [INSPIRE].

[33] Y. Kahn, B.R. Safdi and J. Thaler, *Broadband and Resonant Approaches to Axion Dark Matter Detection*, *Phys. Rev. Lett.* **117** (2016) 141801 [arXiv:1602.01086] [INSPIRE].

[34] M. Silva-Feaver et al., *Design Overview of DM Radio Pathfinder Experiment*, *IEEE Trans. Appl. Supercond.* **27** (2017) 1400204 [arXiv:1610.09344] [INSPIRE].

[35] P.W. Graham and S. Rajendran, *Axion Dark Matter Detection with Cold Molecules*, *Phys. Rev.* **D 84** (2011) 055013 [arXiv:1101.2691] [INSPIRE].

[36] D. Budker, P.W. Graham, M. Ledbetter, S. Rajendran and A. Sushkov, *Proposal for a Cosmic Axion Spin Precession Experiment (CASPEr)*, *Phys. Rev.* **X 4** (2014) 021030 [arXiv:1306.6089] [INSPIRE].

[37] R. Barbieri et al., *Searching for galactic axions through magnetized media: the QUAX proposal*, *Phys. Dark Univ.* **15** (2017) 135 [arXiv:1606.02201] [INSPIRE].

[38] P. Sikivie, *Axion Dark Matter Detection using Atomic Transitions*, *Phys. Rev. Lett.* **113** (2014) 201301 [arXiv:1409.2806] [INSPIRE].

[39] V.V. Flambaum, H.B. Tran Tan, I.B. Samsonov, Y.V. Stadnik and D. Budker, *Resonant detection and production of axions with atoms*, *Int. J. Mod. Phys.* **A 33** (2018) 1844030 [INSPIRE].

[40] Y.V. Stadnik, V.A. Dzuba and V.V. Flambaum, *Improved Limits on Axionlike-Particle-Mediated P , T -Violating Interactions between Electrons and Nucleons from Electric Dipole Moments of Atoms and Molecules*, *Phys. Rev. Lett.* **120** (2018) 013202 [arXiv:1708.00486] [INSPIRE].

[41] K. Kelley and P.J. Quinn, *A Radio Astronomy Search for Cold Dark Matter Axions*, *Astrophys. J.* **845** (2017) L4 [arXiv:1708.01399] [INSPIRE].

[42] G. Sigl, *Astrophysical Haloscopes*, *Phys. Rev.* **D 96** (2017) 103014 [arXiv:1708.08908] [INSPIRE].

[43] F.P. Huang, K. Kadota, T. Sekiguchi and H. Tashiro, *Radio telescope search for the resonant conversion of cold dark matter axions from the magnetized astrophysical sources*, *Phys. Rev.* **D 97** (2018) 123001 [arXiv:1803.08230] [INSPIRE].

[44] A. Hook, Y. Kahn, B.R. Safdi and Z. Sun, *Radio Signals from Axion Dark Matter Conversion in Neutron Star Magnetospheres*, *Phys. Rev. Lett.* **121** (2018) 241102 [arXiv:1804.03145] [INSPIRE].

[45] B.R. Safdi, Z. Sun and A.Y. Chen, *Detecting Axion Dark Matter with Radio Lines from Neutron Star Populations*, arXiv:1811.01020 [INSPIRE].

[46] A. Caputo, C.P. Garay and S.J. Witte, *Looking for axion dark matter in dwarf spheroidal galaxies*, *Phys. Rev.* **D 98** (2018) 083024 [arXiv:1805.08780] [INSPIRE].

JCAP03(2019)027

[47] J.G. Rosa and T.W. Kephart, *Stimulated Axion Decay in Superradiant Clouds around Primordial Black Holes*, *Phys. Rev. Lett.* **120** (2018) 231102 [arXiv:1709.06581] [INSPIRE].

[48] I.I. Tkachev, *An Axionic Laser in the Center of a Galaxy?*, *Phys. Lett.* **B 191** (1987) 41 [INSPIRE].

[49] T.W. Kephart and T.J. Weiler, *Stimulated radiation from axion cluster evolution*, *Phys. Rev.* **D 52** (1995) 3226 [INSPIRE].

[50] L. Di Luzio, F. Mescia and E. Nardi, *Redefining the Axion Window*, *Phys. Rev. Lett.* **118** (2017) 031801 [arXiv:1610.07593] [INSPIRE].

[51] A.R. Zhitnitsky, *On Possible Suppression of the Axion Hadron Interactions* (in Russian), *Sov. J. Nucl. Phys.* **31** (1980) 260 [INSPIRE].

[52] M. Dine, W. Fischler and M. Srednicki, *A Simple Solution to the Strong CP Problem with a Harmless Axion*, *Phys. Lett.* **B 104** (1981) 199 [INSPIRE].

[53] P. Agrawal, J. Fan, M. Reece and L.-T. Wang, *Experimental Targets for Photon Couplings of the QCD Axion*, *JHEP* **02** (2018) 006 [arXiv:1709.06085] [INSPIRE].

[54] M. Farina, D. Pappadopulo, F. Rompineve and A. Tesi, *The photo-philic QCD axion*, *JHEP* **01** (2017) 095 [arXiv:1611.09855] [INSPIRE].

[55] E. Witten, *Some Properties of $O(32)$ Superstrings*, *Phys. Lett.* **B 149** (1984) 351 [INSPIRE].

[56] P. Svrček and E. Witten, *Axions In String Theory*, *JHEP* **06** (2006) 051 [hep-th/0605206] [INSPIRE].

[57] A. Arvanitaki, S. Dimopoulos, S. Dubovsky, N. Kaloper and J. March-Russell, *String Axiverse*, *Phys. Rev.* **D 81** (2010) 123530 [arXiv:0905.4720] [INSPIRE].

[58] M. Cicoli, *Axion-like Particles from String Compactifications*, in *Proceedings of 9th Patras Workshop on Axions, WIMPs and WISPs (AXION-WIMP 2013)*, Mainz Germany (2013), pg. 235 [arXiv:1309.6988] [INSPIRE].

[59] M.D. Schwartz, *Quantum Field Theory and the Standard Model*, Cambridge University Press, Cambridge U.K. (2014).

[60] E.W. Kolb and M.S. Turner, *The Early Universe*, *Front. Phys.* **69** (1990) 1 [INSPIRE].

[61] SKA Whitepaper, https://www.skatelescope.org/wp-content/uploads/2014/03/SKA-TEL-SKO-0000308_SKA1_System_Baseline_v2_DescriptionRev01-part-1-signed.pdf.

[62] L.B. Newburgh et al., *HIRAX: A Probe of Dark Energy and Radio Transients*, *Proc. SPIE Int. Soc. Opt. Eng.* **9906** (2016) 99065X [arXiv:1607.02059] [INSPIRE].

[63] P. Bull, P.G. Ferreira, P. Patel and M.G. Santos, *Late-time cosmology with 21 cm intensity mapping experiments*, *Astrophys. J.* **803** (2015) 21 [arXiv:1405.1452] [INSPIRE].

[64] C.G.T. Haslam, C.J. Salter, H. Stoffel and W.E. Wilson, *A 408 MHz all-sky continuum survey. II. The atlas of contour maps*, *Astron. Astrophys. Suppl. Ser.* **47** (1982) 1.

[65] M.G. Santos et al., *Cosmology with a SKA HI intensity mapping survey*, arXiv:1501.03989 [INSPIRE].

[66] A. Liu and M. Tegmark, *How well can we measure and understand foregrounds with 21 cm experiments?*, *Mon. Not. Roy. Astron. Soc.* **419** (2012) 3491 [arXiv:1106.0007] [INSPIRE].

[67] M. Regis, L. Richter, S. Colafrancesco, S. Profumo, W.J.G. de Blok and M. Massardi, *Local Group dSph radio survey with ATCA – II. Non-thermal diffuse emission*, *Mon. Not. Roy. Astron. Soc.* **448** (2015) 3747 [arXiv:1407.5482] [INSPIRE].

[68] D.J. Fixsen et al., *ARCADE 2 Measurement of the Extra-Galactic Sky Temperature at 3–90 GHz*, *Astrophys. J.* **734** (2011) 5 [arXiv:0901.0555] [INSPIRE].

JCAP03(2019)027

[69] N. Fornengo, R.A. Lineros, M. Regis and M. Taoso, *The isotropic radio background revisited*, *JCAP* **04** (2014) 008 [arXiv:1402.2218] [INSPIRE].

[70] R. Bähre et al., *Any light particle search II —Technical Design Report*, 2013 *JINST* **8** T09001 [arXiv:1302.5647] [INSPIRE].

[71] A. Geringer-Sameth, S.M. Koushiappas and M. Walker, *Dwarf galaxy annihilation and decay emission profiles for dark matter experiments*, *Astrophys. J.* **801** (2015) 74 [arXiv:1408.0002] [INSPIRE].

[72] V. Bonnivard et al., *Dark matter annihilation and decay profiles for the Reticulum II dwarf spheroidal galaxy*, *Astrophys. J.* **808** (2015) L36 [arXiv:1504.03309] [INSPIRE].

[73] V. Bonnivard et al., *Dark matter annihilation and decay in dwarf spheroidal galaxies: The classical and ultrafaint dSphs*, *Mon. Not. Roy. Astron. Soc.* **453** (2015) 849 [arXiv:1504.02048] [INSPIRE].

[74] K. Hayashi, K. Ichikawa, S. Matsumoto, M. Ibe, M.N. Ishigaki and H. Sugai, *Dark matter annihilation and decay from non-spherical dark halos in galactic dwarf satellites*, *Mon. Not. Roy. Astron. Soc.* **461** (2016) 2914 [arXiv:1603.08046] [INSPIRE].

[75] J.L. Sanders, N.W. Evans, A. Geringer-Sameth and W. Dehnen, *Indirect Dark Matter Detection for Flattened Dwarf Galaxies*, *Phys. Rev.* **D 94** (2016) 063521 [arXiv:1604.05493] [INSPIRE].

[76] N.W. Evans, J.L. Sanders and A. Geringer-Sameth, *Simple J-Factors and D-Factors for Indirect Dark Matter Detection*, *Phys. Rev.* **D 93** (2016) 103512 [arXiv:1604.05599] [INSPIRE].

[77] J.F. Navarro, C.S. Frenk and S.D.M. White, *The Structure of cold dark matter halos*, *Astrophys. J.* **462** (1996) 563 [astro-ph/9508025] [INSPIRE].

[78] M. Cirelli et al., *PPPC 4 DM ID: A Poor Particle Physicist Cookbook for Dark Matter Indirect Detection*, *JCAP* **03** (2011) 051 [*Erratum ibid.* **1210** (2012) E01] [arXiv:1012.4515] [INSPIRE].

[79] F. Yusef-Zadeh et al., *Interacting Cosmic Rays with Molecular Clouds: A Bremsstrahlung Origin of Diffuse High Energy Emission from the Inner 2deg by 1deg of the Galactic Center*, *Astrophys. J.* **762** (2013) 33 [arXiv:1206.6882] [INSPIRE].

[80] P.C. Gregory and E.R. Seaquist, *The nature of Cygnus X-3 radio outbursts from an analysis of radiofrequency spectra*, *Astrophys. J.* **194** (1974) 715.

[81] B. Vollmer, W. Reich and R. Wielebinski, *Detection of a radio halo in the Virgo cluster*, *Astron. Astrophys.* **423** (2004) 57 [astro-ph/0404124] [INSPIRE].

[82] F.N. Owen, J.a. Eilek and N.E. Kassim, *M87 at 90cm: a different picture*, *Astrophys. J.* **543** (2000) 611 [astro-ph/0006150] [INSPIRE].

[83] L.J. Oldham and M.W. Auger, *Galaxy structure from multiple tracers–ii. m87 from parsec to megaparsec scales*, *Mon. Not. Roy. Astron. Soc.* **457** (2016) 421.

[84] L.B. Newburgh et al., *Calibrating CHIME, A New Radio Interferometer to Probe Dark Energy*, *Proc. SPIE Int. Soc. Opt. Eng.* **9145** (2014) 4V [arXiv:1406.2267] [INSPIRE].

[85] C. Creque-Sarbinowski and M. Kamionkowski, *Searching for Decaying and Annihilating Dark Matter with Line Intensity Mapping*, *Phys. Rev.* **D 98** (2018) 063524 [arXiv:1806.11119] [INSPIRE].

[86] P. Ilten, Y. Soreq, M. Williams and W. Xue, *Serendipity in dark photon searches*, *JHEP* **06** (2018) 004 [arXiv:1801.04847] [INSPIRE].

[87] BaBar collaboration, *Search for a Dark Photon in e^+e^- Collisions at BaBar*, *Phys. Rev. Lett.* **113** (2014) 201801 [arXiv:1406.2980] [INSPIRE].

[88] M. Bauer, P. Foldenauer and J. Jaeckel, *Hunting All the Hidden Photons*, *JHEP* **07** (2018) 094 [arXiv:1803.05466] [INSPIRE].

JCAP03(2019)027

[89] M. Endo, K. Hamaguchi and G. Mishima, *Constraints on Hidden Photon Models from Electron g-2 and Hydrogen Spectroscopy*, *Phys. Rev.* **D 86** (2012) 095029 [arXiv:1209.2558] [INSPIRE].

[90] J. Kozaczuk, *Dark Photons from Nuclear Transitions*, *Phys. Rev.* **D 97** (2018) 015014 [arXiv:1708.06349] [INSPIRE].

[91] K. Kaneta, H.-S. Lee and S. Yun, *Portal Connecting Dark Photons and Axions*, *Phys. Rev. Lett.* **118** (2017) 101802 [arXiv:1611.01466] [INSPIRE].

[92] K. Kohri, T. Moroi and K. Nakayama, *Can decaying particle explain cosmic infrared background excess?*, *Phys. Lett.* **B 772** (2017) 628 [arXiv:1706.04921] [INSPIRE].

[93] R. Daido, F. Takahashi and N. Yokozaki, *Enhanced axion–photon coupling in GUT with hidden photon*, *Phys. Lett.* **B 780** (2018) 538 [arXiv:1801.10344] [INSPIRE].

[94] O.E. Kalashev, A. Kusenko and E. Vitagliano, *Cosmic infrared background excess from axionlike particles and implications for multimessenger observations of blazars*, *Phys. Rev.* **D 99** (2019) 023002 [arXiv:1808.05613] [INSPIRE].

[95] M. Giannotti, I. Irastorza, J. Redondo and A. Ringwald, *Cool WISPs for stellar cooling excesses*, *JCAP* **05** (2016) 057 [arXiv:1512.08108] [INSPIRE].

JCAP03(2019)027

Journal of Cosmology and
Astroparticle Physics

SISSA

Searching for sterile neutrino with X-ray intensity mapping

Journal of Cosmology and Astroparticle Physics
An IOP and SISSA journal

Searching for sterile neutrino with X-ray intensity mapping

Andrea Caputo,[a] **Marco Regis**[b,c] **and Marco Taoso**[c]

[a]Instituto de Física Corpuscular, CSIC-Universitat de Valencia,
Apartado de Correos 22085, E-46071, Spain
[b]Dipartimento di Fisica, Università di Torino,
via P. Giuria 1, I–10125 Torino, Italy
[c]Istituto Nazionale di Fisica Nucleare, Sezione di Torino,
via P. Giuria 1, I–10125 Torino, Italy

E-mail: andrea.caputo@uv.es, regis.mrc@gmail.com, marco.taoso@to.infn.it

Received December 1, 2019
Revised February 5, 2020
Accepted February 18, 2020
Published March 2, 2020

Abstract. The cosmological X-ray emission associated to the possible radiative decay of sterile neutrinos is composed by a collection of lines at different energies. For a given mass, each line corresponds to a given redshift. In this work, we cross correlate such line emission with catalogs of galaxies tracing the dark matter distribution at different redshifts. We derive observational prospects by correlating the X-ray sky that will be probed by the eROSITA and Athena missions with current and near future photometric and spectroscopic galaxy surveys. A relevant and unexplored fraction of the parameter space of sterile neutrinos can be probed by this technique.

Keywords: X-ray telescopes, dark matter experiments, dark matter theory, power spectrum

ArXiv ePrint: 1911.09120

JCAP03(2020)001

 https://doi.org/10.1088/1475-7516/2020/03/001

Contents

JCAP03(2020)001

1 Introduction

Unveiling the nature of dark matter (DM) is one of the most intriguing goals of fundamental physics nowadays. In fact, despite the compelling astrophysical and cosmological evidences, still we do not know what DM is made of. The most popular DM candidates are those connected to additional problems faced by the Standard Model (SM) of particle physics.

An example is the sterile neutrino. This particle is a singlet under the SM gauge group and arises in scenarios of active neutrino mass generation, notably the see-saw mechanism [1, 2]. The mass of the sterile neutrino can span a very large range, from the GUT scale [3–7] down to eV [8–10]. In particular, a sterile neutrino with a mass around the keV scale has attracted a lot of interest since it constitutes a viable and appealing DM candidate (see, e.g., the νMSM model [11] for a concrete implementation and refs. [12–14] for reviews).

A keV sterile neutrino mixes with ordinary active neutrinos and can be produced in the early Universe through oscillations (Dodelson-Widrow mechanism) [15], resonantly enhanced oscillations in presence of a primordial lepton asymmetry (Shi-Fuller mechanism) [16], through the decay of heavy particles [17–26] or obtain the correct DM abundance via dilution of a thermal sterile neutrino component through entropy production [27–30].[1]

As a basic requirement in order to be the DM, sterile neutrinos need to be cold enough to be confined inside galaxies. Fermions obey the Pauli exclusion principle and in a system with N fermions, the minimum momentum is therefore $p \sim N^{1/3}h/R$, where h is the Planck constant and R the size of the fermionic system. Analyzing the DM phase-space distribution of galaxies one can deduce a lower limit on the mass of a fermionic DM candidate, the so-called Tremaine-Gunn-type bound [33]. Additional and stronger constraints on the coldness of DM can be obtained from the number of collapsed structures (like counts of the Milky Way satellites) and measurements of the matter power spectrum at small scales, in particular

[1] See [31, 32] for the production of sterile neutrinos in non-standard cosmologies.

through the Lyman-alpha forest method. The corresponding bounds on the sterile neutrino mass depend on the production mechanism. We refer to refs. [12–14] for more details and discussions on the uncertainties affecting these astrophysical constraints.

Sterile neutrinos decay into SM particles via the mixing with the active neutrinos, the main process being $\nu_s \to \nu\nu\nu$. An additional channel is the radiative decay $\nu_s \to \nu\gamma$, occurring with a rate [34, 35]:

$$\Gamma_S \equiv \Gamma_{\nu_s \to \nu\gamma} \sim (7.2\ 10^{29}\mathrm{s})^{-1} \left(\frac{\sin^2(2\theta)}{10^{-8}}\right) \left(\frac{m_S}{1\,\mathrm{keV}}\right)^5 , \tag{1.1}$$

where θ is the mixing angle between active and sterile neutrinos, and m_S is the mass of the latter.

Therefore, a smoking gun signature for sterile neutrino DM would be to detect a monoenergetic X-ray signal from the above process. Constraints on the sterile-active neutrino mixing have been set from the non-observation of such decay line from different targets, including dwarf spheroidal galaxies, clusters of galaxies, the Milky Way and the X-ray background (again see, e.g., reviews in refs. [12–14] and references therein). Interestingly enough, the detection of an unidentified line at energy $E \simeq 3.5\,\mathrm{keV}$ was reported recently in different astrophysical environments, including galaxy clusters, with both stacked [36] and individual [36, 37] spectra, the Andromeda galaxy [37] and the Galactic Center [38, 39]. It has been suggested that this observational finding may be a signature of the decay of a sterile-neutrino DM. Several works have been trying to test the presence of such excess, finding controversial results (see, e.g., ref. [40] and the review in ref. [12]). Future data and new analyses are therefore necessary to reach a conclusive answer.

In this work we entertain the possibility to detect the sterile neutrino decay signal produced in cosmic structures. This cumulative emission is the superposition of all the X-ray lines produced in DM halos and redshifted by the expansion of the Universe. In order to exploit the correlation between the energy of the line and the redshift of the corresponding halos, we cross correlate the X-ray extragalactic emission with catalogs of galaxies, tracing the DM distribution at different redshifts. We derive prospects for the eROSITA mission [41], currently in operation, expanding over the study conducted in ref. [42]. A significant improvement in the sensitivity will be provided by the next-generation X-ray telescope Athena [43]. We compute forecasts for its operations, and considering, on the galaxy catalog side, current and near future spectroscopic and photometric surveys. In particular, Athena will allow to perform high-resolution spectroscopy thanks to the X-IFU instrument. The combination with spectroscopic galaxy catalogs will provide a framework where to fully perform a line intensity mapping analysis. Indeed, the Athena X-IFU detector will be able to resolve the narrow line induced by sterile neutrino decay and will provide a good rejection of backgrounds, given by continuum spectra and other emission lines at different energies, from the vast number of cross energy-redshift bins where the DM signal is absent.

The role of line intensity mapping for DM searches has been highlighted also in ref. [44].

The paper is organized as follows. Section 2 describes the formalism used to compute the cross-correlation signal. In section 3 we describe the experimental configurations considered in the derivation of the projected bounds. The statistical analysis and results are presented in section 4. Details on the astrophysical models are in the appendix. In section 5 we conclude.

JCAP03(2020)001

2 Models

The monopole of the intensity associated to X-ray emission $I_{\rm X}$ can be described by means of an integral of the window function $W_{\rm X}$ as

$$I_{\rm X}(E) = \int_0^\infty d\chi \; W_{\rm X}(E,z)\,, \tag{2.1}$$

where E is the observed X-ray energy, and $\chi(z)$ is the comoving distance to redshift z, obeying, in a flat Universe, $c\,{\rm d}z/{\rm d}\chi = H(z)$ with $H(z)$ being the Hubble rate. It is clear that $W_{\rm X}$ (also called weight function) provides the fraction of intensity emitted in a given redshift slice.

We will consider four extragalactic emitters of X-rays: Active Galactic Nuclei (AGN), galaxies, clusters of galaxies, and DM in the form of sterile neutrinos.

In the case of X-ray emission coming from the decay of sterile neutrinos DM, the window function takes the form

$$W_{X_S}(E,z) = \frac{\Omega_{\rm DM}\rho_c}{4\pi}\frac{\Gamma_S}{m_S(1+z)}\frac{1}{\sqrt{2\pi}\sigma_E}\exp\left[-\frac{(E-\frac{m_S}{2(1+z)})^2}{2\sigma_E^2}\right]\,, \tag{2.2}$$

where the Gaussian function provides the broadening of the emission line (centered at $E = \frac{m_S}{2(1+z)}$) due to the spectral resolution σ_E of the X-ray telescope. We neglect the velocity dispersion of sterile neutrinos in halos, since it is always smaller than the experimental energy resolution considered (as we will comment in the following).

Throughout the paper, we consider the sterile neutrino to be the only DM component in the Universe, thus having a relic density set by $\Omega_{\rm DM}\rho_c$. We take the value of cosmological parameters from ref. [45].

For AGN and galaxies, $W_{\rm X}$ reads:

$$W_{\rm X_a}(E,z) = \frac{1}{\chi(z)^2}\int_{L_{\rm min}}^{L_{\rm max}(F_{\rm sens},z)} {\rm d}L\,\frac{dF}{dE}(L,z)\,\phi(L,z)\,, \tag{2.3}$$

where F is the flux provided by a source with rest-frame luminosity L at redshift z, ϕ is the X-ray luminosity function, namely, the number of X-ray sources per unit volume and unit luminosity, and the maximum luminosity $L_{\rm max}$ of an unresolved source is dictated by the sensitivity flux $F_{\rm sens}$, providing the minimum detectable flux. Details concerning the models adopted for ϕ are given in the appendix.

Clusters of galaxies can emit X-rays by means of bremsstrahlung radiation of their gas. We assume the minimum mass of a cluster to be $M_{500} = 10^{14}\,{\rm M}_\odot$, which is also approximately the same value one obtains from the temperature-mass relation [47] by requiring to have a sizable emission above 1 keV (i.e., in the energy range we are considering). We checked that all clusters above this mass will be under the detection reach of eROSITA and Athena, and are therefore masked in our analysis, see details in appendix.

Note that by masking all halos above $10^{14}\,{\rm M}_\odot$, we will be masking as well the possible contribution of sterile neutrino decay from such massive halos. In our computation, we thus set the maximum halo mass to be $M_{500} = 10^{14}\,{\rm M}_\odot$ in the computation of the DM signal. In order to retain instead such DM contribution, one could include clusters and treat them as a background component, as done in ref. [42]. This approach would increase the DM signal but at the cost of highly increasing the noise of the measurement.

JCAP03(2020)001

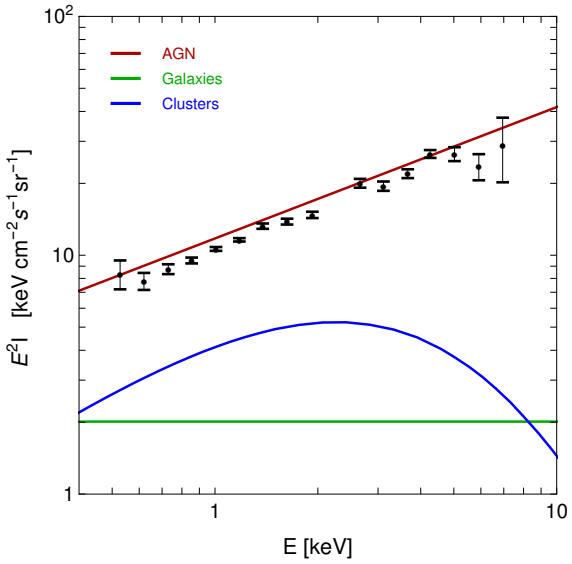

Figure 1. Total X-ray intensity produced by AGN, galaxies and clusters (i.e., the sum of resolved and unresolved sources). Data points show the total extragalactic X-ray background measured by Chandra [46].

The intensity provided by the astrophysical emitters is reported in figure 1, where we compare the predictions of the adopted models with the measurement of ref. [46].

In our modeling of the background we do not include emission lines. They can be given by several atomic processes, but the exact strength, size, dependence on the type of astrophysical object, and redshift scaling are typically quite unknown (for an example, see the debate on the interpretation of the 3.5 keV line [48]). For sufficiently large energy bins, these lines are not expected to significantly alter our estimate of the background, and therefore of the covariance entering the computation of the projected bounds (but see comments below on the Athena X-IFU case). On the other hand, in the case of detection of a line feature, clearly, there will be some degeneracy between the interpretation in terms of sterile neutrino decay and an atomic line. However, since the latter is associated to astrophysical processes, it typically has quite different redshift behaviour and width with respect to the DM-induced line. These two handles can help in disentangling between the two cases.

For what concerns the description of the catalogs of galaxies, the window function is simply provided by the redshift distribution of the objects, dN_g/dz. More precisely, $W_g(z) = H(z)/c\, dN_g/dz$ such that $\int \mathrm{d}\chi W_g(\chi) = 1$ for a redshift distribution dN_g/dz normalized to unity. The form of dN_g/dz for the different catalogs adopted in our work is shown in the left panel of figure 2.

On the right panel of figure 2 we show the window function of DM, for an example mass of 7.2 keV and in a few different energy bins. Note that they correspond to a given redshift bins. Therefore the cross correlation of a given energy bin selects a specific redshift slice in the galaxy distribution, something which is not true for the astrophysical sources (having a continuum energy spectrum) and is a key point of the line intensity mapping strategy.

The angular power spectrum (APS) of the cross correlation between a map of X-rays in the ath energy bin and a catalog of galaxies in the rth redshift bin can be computed as:

$$C_\ell^{ar} = \int_{\Delta z_r} \mathrm{d}z \int_{\Delta E_a} \mathrm{d}E \, \frac{c}{H(z)} \frac{W_\mathrm{X}(E,z) W_\mathrm{g}(z)}{\chi(z)^2} P_\mathrm{X,g}\left[k = \frac{\ell}{\chi(z)}, z\right], \tag{2.4}$$

JCAP03(2020)001

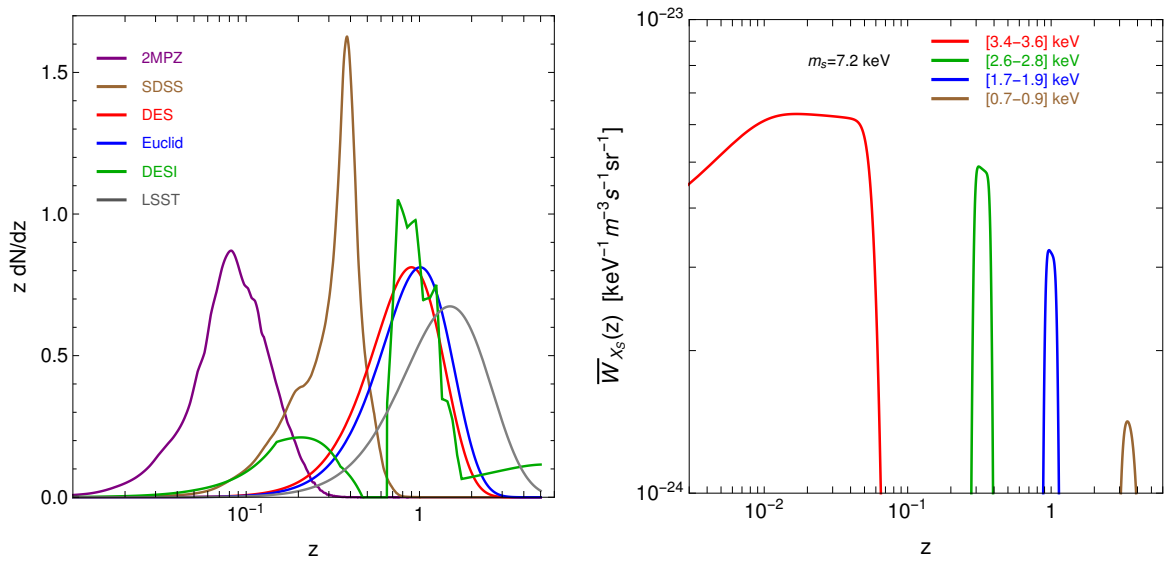

Figure 2. Left: window functions of the catalogs of galaxies considered in the analysis. All the window functions are normalized to unit, $\int dz\, dN_g/dz = 1$. Right: average window function of sterile neutrino in different energy bins, i.e., $\bar{W}_{X_S}(z) \equiv 1/\Delta E \int_{\Delta E} dE\, W_{X_S}(E,z)$. In this example, the DM mass is 7.2 keV and $\sin^2(2\theta) = 3.4 \times 10^{-11}$.

where $P_{\rm X,g}$ is the three-dimensional cross power spectrum between a given X-ray population and a given galaxy catalog. It is a function of both redshift and modulus of the physical wavenumber k. In the Limber approximation [49], k and the angular multipole ℓ are linked by $k = \ell/\chi(z)$. This approximation is valid for $\ell \gg 1$, i.e., in the range considered in the present work.

In the case of X-ray auto correlation (relevant to compute the covariance of the cross correlation), the expression of the APS reduces to:

$$C_\ell^{ab} = \int \mathrm{d}z \int_{\Delta E_a} \mathrm{d}E \int_{\Delta E_b} \mathrm{d}E' \, \frac{c}{H(z)} \frac{W_{\rm X}(E,z) W_{\rm X}(E',z)}{\chi(z)^2} P_{\rm X}\left[k = \frac{\ell}{\chi(z)}, z\right]. \tag{2.5}$$

We will compute the 3D power spectrum using the halo model formalism (for a review, see, e.g., ref. [50]), where the power spectrum is described in terms of the sum of the one-halo (P^{1h}) and two-halo (P^{2h}) components. Their generic expression is given by (see, e.g., ref. [51]):

$$\begin{aligned} P_{ij}^{1h}(k) &= \int dM \, \frac{dn}{dM} \hat{f}_i^*(k|M)\, \hat{f}_j(k|M) \\ P_{ij}^{2h}(k) &= \left[\int dM \, \frac{dn}{dM} b_i(M) \hat{f}_i^*(k|M)\right] \left[\int dM \, \frac{dn}{dM} b_j(M) \hat{f}_j(k|M)\right] P^{\rm lin}(k) \end{aligned} \tag{2.6}$$

where M is the halo mass, dn/dM is the halo mass function, $\hat{f}$ is the Fourier transforms of the field under consideration, b is the bias of the source with respect to matter and $P^{\rm lin}$ is the linear matter power spectrum. The expressions for the various cases considered in our work are detailed in the appendix.

Let us note here that we will be considering the power spectrum of cold DM, even though the sterile neutrino can be a warm DM candidate. The deviation of its power spectrum from

JCAP03(2020)001

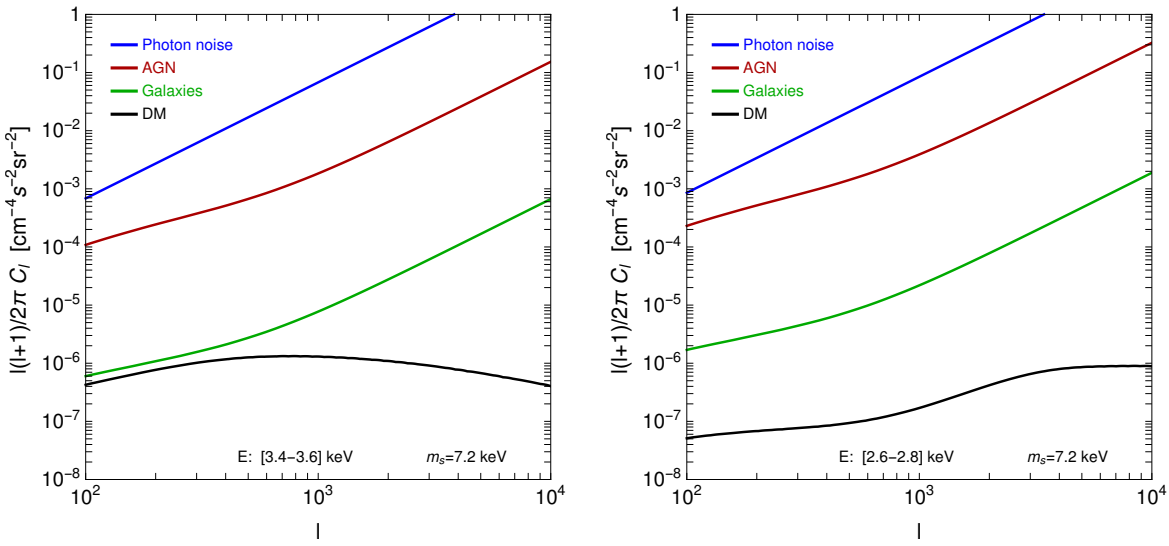

Figure 3. Auto-correlation APS of the different X-ray extragalactic emitters as predicted for eROSITA. The DM mass and $\sin^2(2\theta)$ are as in figure 2. Left and right plots show different energy bins, $[3.4, 3.6]$ and $[2.6, 2.8]$ keV, respectively. The blue line shows the photon noise, described in section 4.

a pure cold DM power spectrum strongly depends on its production mechanism. On the other hand, luckily, this does not impact our results, since the signal we are considering is mostly produced in massive halos, where differences between cold and warm scenarios are negligible (see also ref. [42]).

Examples of the auto- and cross-APS are shown in figures 3–6. In figure 3 and figure 5, we consider the eROSITA experimental setup (described in the following), a sterile neutrino with mass $m_S = 7.2\,\text{keV}$, and two energy bins $[3.4, 3.6]$ and $[2.6, 2.8]\,\text{keV}$. For the cross-correlation plots we select the redshift bins providing the DM signal ($[0, 0.059]$ for cross correlation with the $[3.4, 3.6]\,\text{keV}$ energy bin, and $[0.29, 0.38]$ for the $[2.6, 2.8]\,\text{keV}$ energy bin) and consequently the two catalogs whose galaxy distribution is peaked in such bins, that are, respectively, 2MPZ and SDSS. For the same DM mass, in figure 4 and figure 6 we show the auto- and cross-APS as predicted for Athena. We cross correlate the X-ray signals with the Euclid survey of galaxies. We select a low redshifit bin $[0, 0.1]$ and one closer to the peak of the galaxy distribution, $[0.6, 0.7]$. The energy bins are those providing the DM signal, i.e. $[3.27 - 3.6]\,\text{keV}$ and $[2.12 - 2.25]\,\text{keV}$.

Note that, while the auto correlation is largely dominated by AGN (and photon noise), the DM signal becomes important in the cross correlation, especially at low redshift. This highlights the importance of a tomographic approach involving DM tracers at different redshift in order to distentangle the DM cosmological X-ray emission from astrophysical contributions.

3 Experiments

The eROSITA instrument, in orbit since July 2019, is going to perform a deep survey of the entire sky in the $0.3 - 10\,\text{keV}$ energy range, with unprecedented angular and energy resolution. It is therefore ideally placed to search for the cosmological DM signal described

JCAP03(2020)001

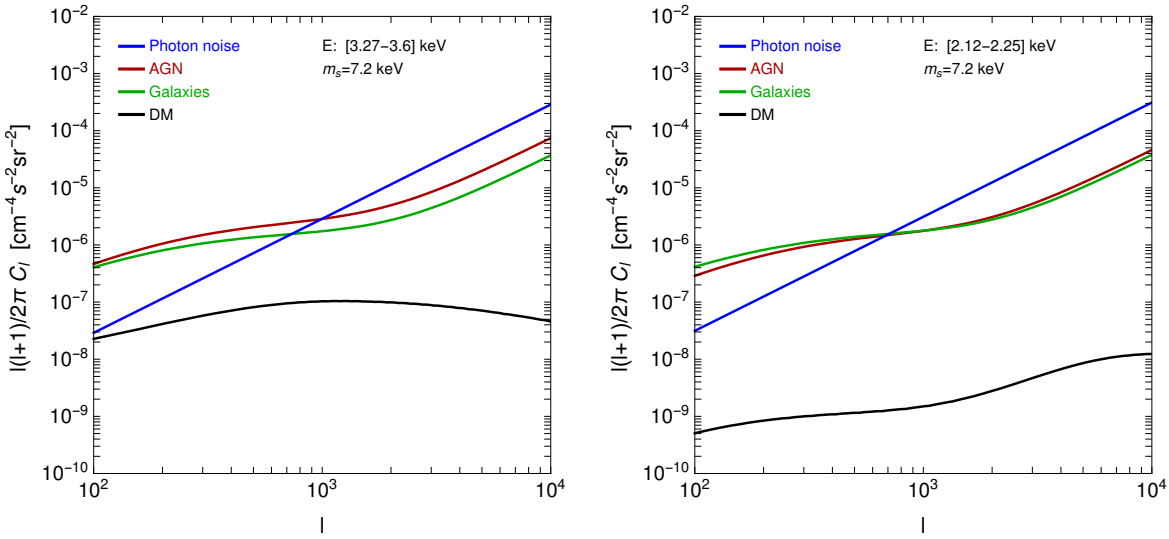

Figure 4. Auto-correlation APS of the different X-ray extragalactic emitters as predicted for Athena WFI. The DM mass is 7.2 keV and $\sin^2(2\theta) = 1.5 \times 10^{-12}$. Left and right plots show different energy bins, $[3.27, 3.6]$ and $[2.12, 2.25]$ keV, respectively. The blue line shows the photon noise, described in section 4.

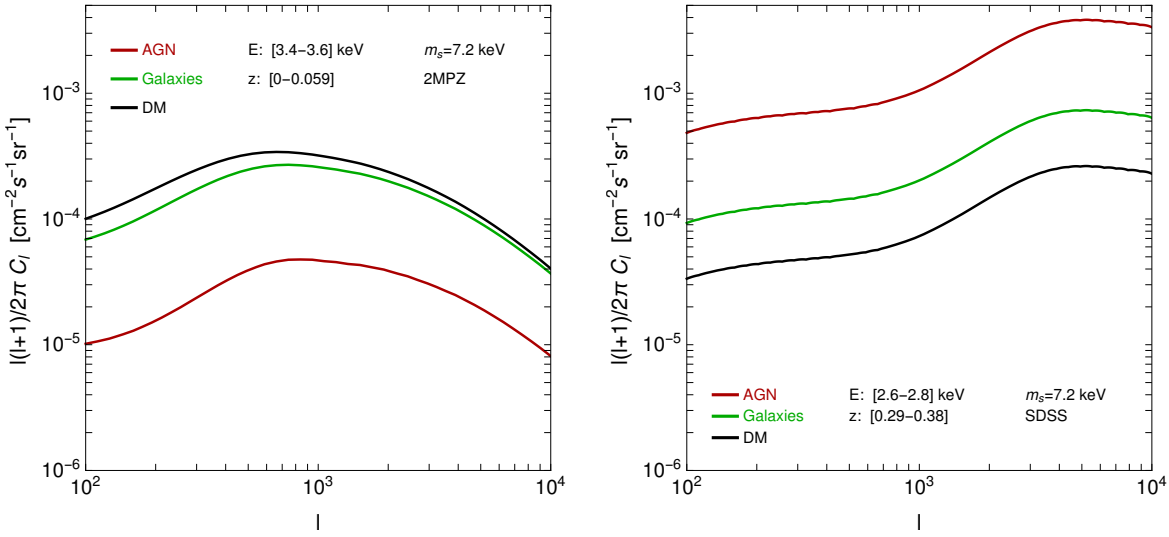

Figure 5. Same as in figure 3 but for the cross-correlation APS. The corresponding redshift bins are selected from the relation $z = m_S/(2\,E) - 1$.

in the previous section. In table 1 we summarize its performances for those parameters more relevant to our analysis. The energy-dependent effective area and spectral resolution are taken from refs. [41, 52, 53]. We consider an observational time of four years, corresponding to the duration of the all-sky survey program. For our sensitivity forecasts we focus on a fraction of sky $f_{\rm sky}^X = 0.8$, after masking the Galactic plane and resolved sources. As explained in section 4, we need to model the total intensity received by instrument, which is the sum of the extragalactic emission in eq. (2.1), the Galactic contribution and the instrumental

JCAP03(2020)001

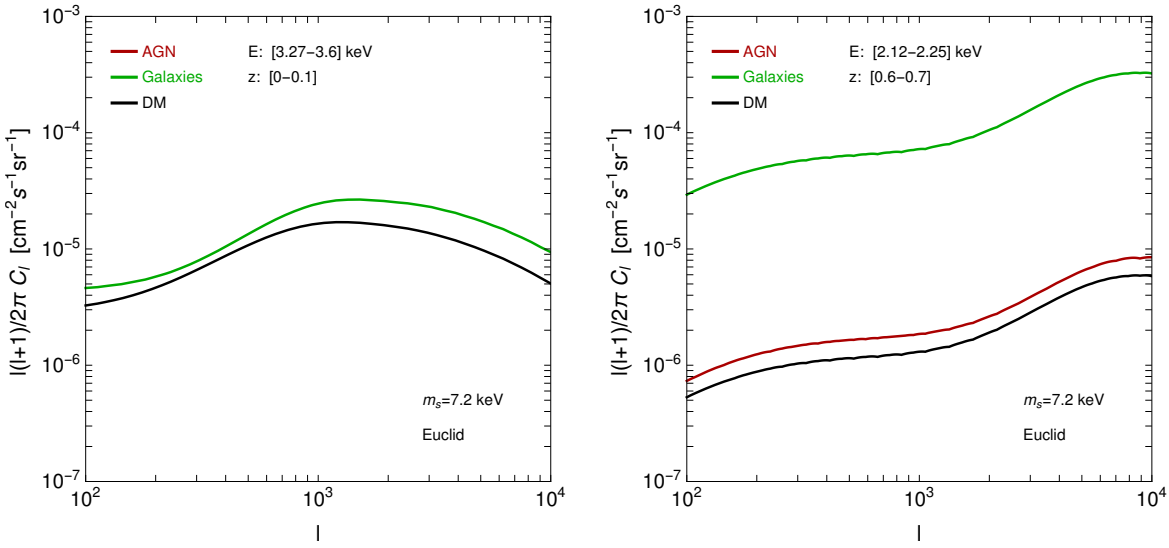

Figure 6. Same as in figure 4 but for the cross-correlation APS. The corresponding redshift bins are selected from the relation $z = m_S/(2\,E) - 1$.

	eROSITA	Athena WFI	Athena X-IFU
Energy range [keV]	0.3–10	0.1–12	0.3–12
$A_{\rm eff}$ at 3 keV [m^2]	0.03	0.79	0.68
$\Omega_{\rm FoV}$ [deg^2]	0.66	0.69	0.014
HEW [arcsec]	28	5	5
Spectral resolution (FWHM) at 7 keV [eV]	138	138	2.5
$F_{\rm sens}$ [erg cm^{-2} s^{-1}]	1.1×10^{-14}	2.4×10^{-17}	2.4×10^{-17}
Particle bkg [counts keV^{-1} s^{-1} sr^{-1}]	1.2×10^3	1.2×10^3	5.8×10^3

Table 1. Key performances of the three X-rays instruments considered in the analysis. The rows report the energy range, the effective area at 3 keV, the field of view, the angular resolution (Half Energy Width), the energy resolution (at 7 keV), the source sensitivity in the 0.5–2 keV band (considering observations in survey mode for eROSITA, while 450 ks exposure in the Athena cases) and the rate of particle background.

background. The Galactic foreground, modeled as in section 4.2 of ref. [41], is relevant only at energies $\lesssim 1$ keV. The particle background is generated by the interactions of particles, mostly protons and secondary electrons, with the instrument. The expected rate is 1151 counts keV^{-1} s^{-1} sr^{-1} [41].

The Athena X-ray observatory is planned to be launched in early 2030s. The experiment will host two instruments, the Wide Field Imager (WFI) and the X-ray Integral Field Unit (X-IFU). The performances of the instruments, taken from ref. [43], are summarized in table 1.

JCAP03(2020)001

	2MPZ	SDSS	DES	DESI	Euclid	LSST
# of galaxies	6.7×10^5	1.5×10^7	2×10^8	3.5×10^7	2×10^9	3.6×10^9
Sky coverage	0.66	0.26	0.12	0.34	0.36	0.49
z-range	0–0.08	0.08–0.8	0.08–2	0–2	0–2	0–3
# of z-bins	1	4	6	132*	7	8
Reference	[57]	[58]	[59]	[60]	[61]	[62]

* The number of z-bins quoted for DESI is in the case of cross correlation with Athena data, see text for the case of eROSITA.

Table 2. Properties of the galaxy catalogs considered in this work. First line reports the total number of objects in the catalog, second line is the fraction of sky covered by the survey (after masking), third and fourth lines show the redshift range and number of bins we considered in our analysis for each catalog.

Athena WFI will have a field of view similar to eROSITA, with a dramatically improved effective area (taken from ref. [54]). Athena X-IFU will deliver in-depth spectroscopic observations, thanks to a superior spectral resolution (2.5 eV for $E < 7\,\mathrm{keV}$ and $E/\Delta E = 2800$ for $E > 7\,\mathrm{keV}$, see ref. [55]), but over a more limited field of view.

For the sake of definiteness, we consider the average exposure for each field observed by Athena to be 450 ks. Taking a total observing time of 5 years, corresponding to the integrated nominal mission lifetime, this leads to a number of observed fields of $5\mathrm{yr}/450\mathrm{ks} \simeq 350$. The sky coverage is thus computed as $f_{\rm sky}^{X} = 350\,\Omega_{\rm FOV}$, resulting to $f_{\rm sky}^{\rm WFI} = 5.9 \times 10^{-3}$ and $f_{\rm sky}^{\rm X-IFU} = 1.2 \times 10^{-4}$.

The rate of particle background is obtained following ref. [56].

In order to maximize the cross-correlation signal, we selected the deepest and widest, in terms of number of objects and sky coverage, surveys of galaxies at mid-low redshift of the near past/future. Photometric surveys have the advantage of detecting a larger number of galaxies, while spectroscopic surveys are superior in the search for a spectral line. We consider both cases.

Concerning available data, we selected 2MPZ [57] at low-z and SDSS [58] at mid-z. At the time of writing, the largest photometric survey is DES [59], which has completed data-taking and is finalizing the data-reduction. The spectroscopic survey DESI [60] just started observations and will have a timeline similar to eROSITA. In a few years, two wide-field surveys, Euclid [61] and LSST [62], will reach the milestone of observing billions of galaxies, thanks to their deep sensitivity (35 gal/arcmin^2 and 50 gal/arcmin^2, respectively). They are expected to complete observations before/around the launch of Athena satellite.

In table 2, we list the catalogs considered in our analysis and report the relevant properties entering the computation of the cross-correlation signal and covariance matrix. The redshift distribution of the galaxies in each catalog is shown in figure 2.

4 Results

In section 2, we depicted how to compute the auto- and cross-correlation APS, and in section 3 we summarized the experimental quantities needed for their estimates. Now we describe how bounds on the sterile neutrino properties are derived from such forecasts and we discuss our findings.

JCAP03(2020)001

In order to define a statistical significance, we need first to introduce the covariance matrix associated to the cross-correlation APS. In the Gaussian approximation, it can be written as:

$$\Gamma_{ar\ell,br'\ell'} = \frac{\delta^{\rm K}_{\ell\ell'}}{(2\ell+1)\Delta\ell f_{\rm sky}}\left[C^{ar}_{\ell}C^{br'}_{\ell'} + \left(C^{ab}_{\ell}+C^{ab}_{\mathcal{N}}\delta^{\rm K}_{ab}\right)\left(C^{rr'}_{\ell'}+C^{rr'}_{\mathcal{N}}\right)\delta^{\rm K}_{rr'}\right], \tag{4.1}$$

where again a and b label energy bins of X-ray measurements, and r and r' label redshift bins in the catalogs. The analysis is performed over 40 multipole bins in the ℓ-range $[10^2, 10^4]$, with even logarithmic spacing. The size of the bins is pretty large, and this further justifies the Gaussian approximation of the covariance.

The auto- and cross-correlation APS entering in eq. (4.1) are described in section 2. The photon noise term is given by $C^a_{\mathcal{N}} = 4\pi f^X_{\rm sky} W_\ell^{-2}\langle I^a_X\rangle^2/N^a_X$, where $\langle I^a_X\rangle$ is the sky-averaged X-ray intensity observed by the telescope in the ath energy bin and given by the sum of the extragalactic contributions computed from eq. (2.1) plus the Galactic emission plus the particle background, with the latter two described in section 3; the number of observed photons is $N^a_X = \langle I^a_X\, A^a_{\rm eff}\rangle\, t_{\rm obs}\,\Omega_{\rm FoV}$; W_ℓ is the beam window function whose effect is however negligible at $\ell < 10^4$ given the angular resolution (HEW) reported in table 1. The shot noise term for galaxies is given by $C^r_{\mathcal{N}} = 4\pi f^g_{\rm sky}/N^r_g$, where the number of galaxies in the rth redshift bin is computed from the distribution shown in figure 2. Here we neglect the beam window function since again the typical angular resolution is significantly smaller the smallest scale considered in our analysis.

The fraction of sky in eq. (4.1) is taken to be the smallest between X-ray and galaxy surveys, i.e., $f_{\rm sky} = \min[f^X_{\rm sky}, f^g_{\rm sky}]$. In the case of eROSITA, the galaxy surveys have a smaller sky coverage, while we have the opposite picture in the case of Athena.

The upper limits on the sterile neutrino parameter space are derived at 95% C.L. by requiring $\chi^2 = 2.71$ with the estimator assumed to follow a χ^2 distribution with one dof (i.e., $\sin^2(2\theta)$ for a given m_S) defined as:

$$\chi^2 = \sum_{a,b,\ell} C^{ar}_{\ell,S}\Gamma^{-1}_{ar\ell,br'\ell}C^{br'}_{\ell,S}\,. \tag{4.2}$$

There are two things to note. First, only the cross-correlation term involving sterile neutrinos is present in the signal part of eq. (4.2). This is because we assume to be able to extract the background associated to X-ray emitting AGN and galaxies to a good precision, and so we neglect model uncertainties in the astrophysical components. This assumption is well justified in the case of spectroscopic surveys, where there is a huge number of cross energy-redshift terms not entering in the signal of eq. (4.2), and that can be used to fit a continuum term. In the case of photometric surveys, it has instead to be checked with data at hands whether this assumption is fully valid. As stated in the Introduction, this is the reason why a spectroscopic approach that fully exploits the line intensity mapping can be considered more robust. The second crucial point to note in eq. (4.2) is that the sum does not run over the redshift bins. This is because for a given energy bin we select the corresponding redshift bin from the relation $z = m_S/(2\,E) - 1$. As already mentioned above, the DM signal in the other redshift bins is predicted to be null.

The contamination from emission lines deserves a separate discussion. The emission from the Galaxy or from the instrument only affects the covariance estimate (i.e., it is not correlated with extragalactic surveys). In the case of eROSITA and Athena WFI this occurs at a negligible level (for the energy range of interest), due to the smearing associated to the

JCAP03(2020)001

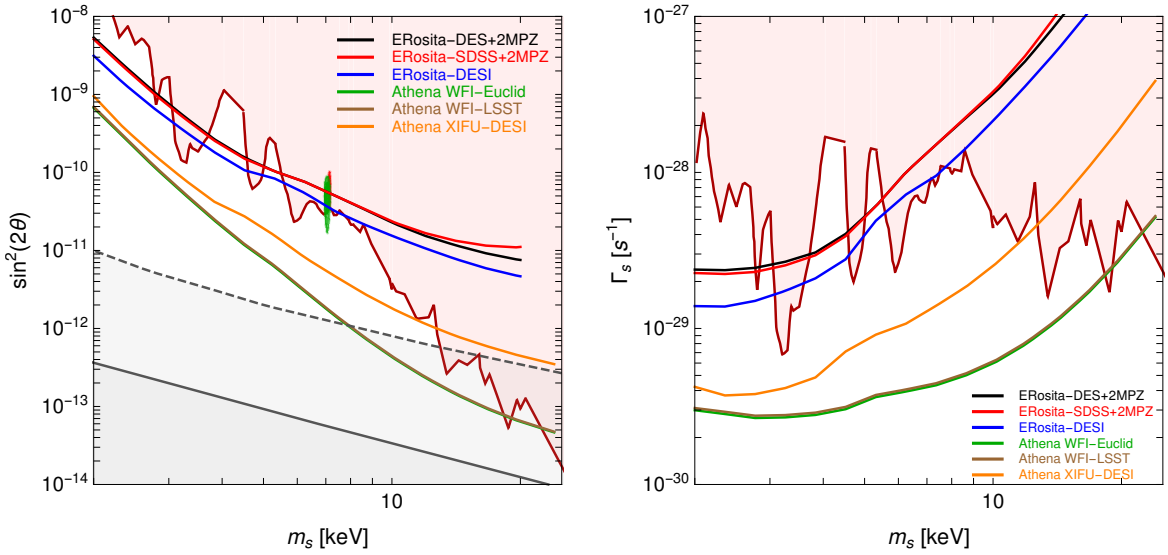

Figure 7. Projected 95% C.L. bounds for the different cross-correlation analyses. The left plot presents the results in the sterile neutrino m_S vs $\sin^2(2\theta)$ plane. The light red region is excluded by current X-ray observations [13, 63]. The red and green contours are the 2-σ regions for the 3.55 keV line excess respectively from the MOS stacked clusters [36] and M31 [37]. For the case of resonant production, the solid (dashed) gray line shows where sterile neutrino accounts for all the DM for a lepton asymmetry $L = 7 \cdot 10^{-5}$ ($L = 2.5 \cdot 10^{-3}$, the maximum value allowed by BBN [64]). Below these lines sterile neutrino is a subdominant DM component (for these choices of L and considering resonant production only). The right plot presents the projected bounds and current X-ray constraints in the plane DM decay rate versus DM mass.

energy resolution, included in the model we are adopting [41]. For Athena X-IFU, these lines can be sizable in a handful of energy bins. However, they can be just removed from the analysis without compromising the sensitivity.

On the other hand, emission lines from extragalactic sources can be more degenerate with the sterile neutrino signal, if occurring at the same energy, and can have a larger impact on the error estimate (in particular in the case of Athena X-IFU). The degeneracy might be broken looking at the different properties of two lines, as mentioned in section 2, but still the sensitivity on a few DM masses can be affected and the final exclusion bound would result to be more jagged than our "smooth" projected curve, which is intended to show the attainable level with a good cleaning of line contamination.

Results obtained with the assumptions and procedure outlined above are shown in figure 7, which reports the 95% C.L. bounds in the plane $\sin^2(2\theta)$ versus m_S.

4.1 eROSITA

We analyze the cross-correlation of the X-ray sky from eROSITA (which recently started its operation, as mentioned in section 3) with past/ongoing experiments. In particular, the red, black and blue lines in figure 7 show the bounds from the cross correlation with SDSS+2MPZ, DES+2MPZ, and DESI, respectively. In the case of photometric surveys, we take 2MPZ as the catalog of reference at low-z considering a bin $z = [0, 0.08]$, and four (six) additional bins at $z > 0.08$ referring to SDSS (DES) data. Despite DES observes a significantly larger number of galaxies than SDSS, it covers a smaller portion of the sky (see table 2), and the

JCAP03(2020)001

associated bounds come out to be comparable. In other words, DES has a lower noise term but higher cosmic variance contribution with respect to SDSS. This means to have a lower $C_{\mathcal{N}}$ but also lower $f_{\rm sky}$ in eq. (4.1) with the two effects (accidentally) compensating each other in the computation of the bound.

It is interesting to note that the case of cross correlation with the DESI catalog is more constraining than SDSS despite having similar number of galaxies and sky coverage. This is because in the search for a line, clearly, the closer the size of the energy/redshift bin is with respect to the line width the higher is the signal to noise ratio. On the other hand, the increase in sensitivity is not dramatic because the spectral resolution of eROSITA prevents to have very narrow bins. Namely their size ranges from $E/\sigma_{\rm FWHM} = 59$ to $E/\sigma_{\rm FWHM} = 6$ for $E = 10\,{\rm keV}$ and $E = 0.3\,{\rm keV}$ respectively.

In figure 7, we show also the preferred regions for the possible excess found in a few X-ray observations and interpreted as a potential signature of sterile neutrino. The regions are taken from refs. [36, 37]. Note that with the technique proposed in this paper, it will be possible to test this interpretation with the data acquired by eROSITA in the forthcoming years.

4.2 Athena WFI and X-IFU

In the epoch of Athena observations, the data from the surveys of DESI, Euclid, and LSST will be available. We show the corresponding bounds on the sterile neutrino properties from the cross-correlation analysis with orange, green, and brown lines, respectively.

The cases of photometric surveys (Euclid and LSST) cross correlated with Athena WFI provide an improvement of more than one order of magnitude with respect to the case of eROSITA cross correlated with DES. This is due to improvements on both sides: larger $f_{\rm sky}$ and number of galaxies on the catalog side, and improved effective area of Athena versus eROSITA. In particular the latter allows to significantly reduce the photon noise term $C^a_{\mathcal{N}}$ in eq. (4.1), overcoming the reduction in the sky coverage of ATHENA with respect to eROSITA. The derived bound has the capability to close the allowed window for a resonantly produced sterile neutrino parameter for $m_S > 7\,{\rm keV}$ (and lepton asymmetry of $L \lesssim 7 \cdot 10^{-5}$). Despite the number of galaxies in LSST is larger with respect to Euclid, the bounds are similar. This is because those galaxies are added at high redshift, where the contribution of the signal to the χ^2 is very small.

Athena X-IFU is potentially a game-changer, in the sense that its superior spectral resolution makes the line intensity mapping fully attainable. On the other hand, the reduced $\Omega_{\rm FoV}$ with respect to the WFI detector (fifty times smaller, see table 1), leads to a reduced sky coverage (for the same flux sensitivity). In order to compensate for this, we should consider (around) fifty times more redshift bins than in the WFI case. This is in principle possible at high X-ray energy. On the other hand, such a thinner binning would bring us to consider a full 3D correlation instead of the 2D case analysed throughout the paper, in order to include effects like redshift space distorsion. We leave this improvement for future developments, while here we set the spectral resolution of the correlation DESI-Athena X-IFU to $R = 120$ (corresponding to $\Delta z \sim 40$ Mpc), which also corresponds to the X-IFU resolution at low energy. In this way, the DM velocity dispersion in halos can be safely neglected. Note that this bound, contrary to the photometric case, does not benefit from an improvement on the galaxy survey side since we consider DESI as for the eROSITA bound (whilst we move from DES to Euclid/LSST in the photometric case). A future spectroscopic survey with enhanced sensitivity will clearly tighten the constraint. Dedicated deep observations in the main Athena X-IFU fields are foreseeable, also given the limited field of view of the

JCAP03(2020)001

instrument. It is also worth to stress again that the prospects for background subtraction are much more favourable in the case of the spectroscopic sample than in the photometric case, and consequently the forecast can be considered more robust in the former case.

Before concluding, we would like to mention that the strategy here proposed for the Athena telescope could be undertaken, on a shorter timescale, by the X-ray Imaging and Spectroscopy Mission (XRISM) [65], expected to launch in 2022. XRISM has a reduced effective area with respect to Athena (by a factor of 45 at 1 keV, reducing to a factor of 6 at 7 keV and less at higher energies) but it can be able to improve the bounds derived in the eROSITA case for large sterile neutrino masses.

5 Conclusions

We have studied the X-ray signal produced by the $\nu_s \to \nu\,\gamma$ decay of sterile neutrino DM in cosmological structures. For a given energy, such monochromatic signal is associated to a certain redshift slice. Exploiting this property, we have investigated the cross correlation of the X-ray emission with catalogues of galaxies in the corresponding redshift range.

We have performed such line intensity mapping analysis for the eROSITA and Athena X-ray telescopes, and considering current and near future photometric and spectroscopic galaxy surveys. Our main results are summarized in figure 7.

eROSITA, which is currently in operation, will be able to slightly improve existing bounds and test the DM interpretation of the 3.55 keV line excess. Thanks to the improved effective area, Athena WFI will test a much larger and unexplored region of the parameter space. Finally, the line intensity mapping technique can be fully exploited combining the superior spectral resolution of Athena X-IFU with spectroscopic surveys, like DESI. The limited field of view of the X-IFU leads to sensitivities slightly worse than in the case of the WFI. On the other hand, X-IFU spectroscopic observations can allow a more robust identification and characterization of the DM cosmological line.

Summarizing, we found that, in the near future, X-ray line intensity mapping can become a suitable technique to search for a sterile neutrino decay signal, complementary to observations of individual targets [66].

Acknowledgments

We thank E. Branchini for insightful comments. MR acknowledges support by "Deciphering the high-energy sky via cross correlation" funded by the agreement ASI-INAF n. 2017-14-H.0, by the "Departments of Excellence 2018 – 2022" Grant awarded by MIUR (L. 232/2016), and by the research grant "From Darklight to Dark Matter: understanding the galaxy/matter connection to measure the Universe" No. 20179P3PKJ funded by MIUR. MT acknowledge support from the INFN grant LINDARK and the research grant 'The Dark Universe: A Synergic Multimessenger Approach' No. 2017X7X85K funded by MIUR. MR and MT acknowledge support from the project "Theoretical Astroparticle Physics (TAsP)" funded by the INFN. A.C. is supported by "Generalitat Valenciana" (Spain) through the "plan GenT" program (CIDEGENT/2018/019), by grants FPA2014-57816-P, PROMETEOII/2014/050 and SEV-2014-0398, as well as by the EU projects H2020-MSCA-RISE-2015 and H2020-MSCA-ITN- 2015//674896-ELUSIVES.

JCAP03(2020)001

A X-ray emission from clusters

The X-ray cluster emission is due to bremsstrahlung radiation. The associated window function W_{X_c} is given by (see also ref. [42])

$$W_{X_c}(E,z) = \frac{k_{\rm ff}\exp\left(-\frac{E\,(1+z)}{k_{\rm B}T_{\rm gas}(M)}\right)}{4\pi\,\sqrt{k_{\rm B}T_{\rm gas}(M)}\,E\,(1+z)}\int dM\frac{dn}{dM}\int dV\rho^2_{\rm gas}(r|M)\,. \tag{A.1}$$

To easy the physical interpretation, we can decompose it as $W_{X_c} = W^0_{X_c}\,\langle\delta^2_{\rm gas}\rangle$ with $W^0_{X_c}$ being defined as

$$W^0_{X_c}(E,z) = \frac{k_{\rm ff}\ (\Omega_b\,\rho_c)^2}{4\pi\,\sqrt{k_{\rm B}T^0_{\rm gas}}\,E\,(1+z)}\exp\left(-\frac{E\,(1+z)}{k_{\rm B}T^0_{\rm gas}}\right), \tag{A.2}$$

where $T^0_{\rm gas}$ is a reference temperature that can be arbitrarily chosen, and $k_{\rm ff} = \frac{32\pi e^6}{3m_ec^2}\left(\frac{2\pi}{3k_{\rm B}m_e}\right)^{1/2}(4\pi\epsilon_0)^{-3}g_{\rm ff}$, where $g_{\rm ff}=1.1$ is the Gaunt factor for the free-free emission.

The term $\langle\delta^2_{\rm gas}\rangle$ involves mass-dependent quantities:

$$\langle\delta^2_{\rm gas}\rangle = \left(\frac{1}{\Omega_{\rm b}\ \rho_{\rm c}}\right)^2\int dM\frac{dn}{dM}\,f(T|M)\int dV\rho^2_{\rm gas}(r|M)\,, \tag{A.3}$$

where the function $f(T|M)$ is

$$f(T|M) = \sqrt{\frac{T^0_{\rm gas}}{T_{\rm gas}(M)}}\exp\left(\frac{E\,(1+z)}{k_{\rm B}T^0_{\rm gas}} - \frac{E\,(1+z)}{k_{\rm B}T_{\rm gas}(M)}\right). \tag{A.4}$$

$\rho_{\rm gas}$ and $T_{\rm gas}$ are the ICM density and temperature, respectively. To describe them, we consider state-of-the-art models. More precisely, the shape of the ICM density $g(R/R_{500})$ is taken from eq. 7 in ref. [67] with values of the parameters from the best-fit in their table 3. The overall normalization is set through $M_{\rm gas,500} = f_{\rm gas,500}\,M_{500} = \int dV\rho_0\,g(R/R_{500})$, considering $f_{\rm gas,500} = 0.131$ [68]. For the temperature-mass relation we adopt a power-law

$$T_{\rm gas}(M_{500}) = T_0\left(\frac{M_{500}\,E(z)}{M_0}\right)^{\alpha}, \tag{A.5}$$

setting the parameters of the relation from ref. [47]: $\alpha = 0.6$, $T_0 = 1\,{\rm keV}$ and $M_0 = 10^{13.57}h_{70}^{-1}M_\odot$.

In figure 8, we show the predicted X-ray flux as a function of the cluster mass and for different redshift. All clusters with mass $M_{500} > 10^{14}\,M_\odot$ are expected to be within the reach of eROSITA and Athena. This means they can be masked and for this reason they are not included in our analysis of the correlation of the unresolved X-ray background.

B X-ray luminosity function of AGN and galaxies

The X-ray luminosity function of AGN is taken from the model of ref. [69], calibrated on X-ray Chandra observations:

$$\phi = K(z)\left[\left(\frac{L}{L_*(z)}\right)^{\gamma_1} + \left(\frac{L}{L_*(z)}\right)^{\gamma_2}\right], \tag{B.1}$$

JCAP03(2020)001

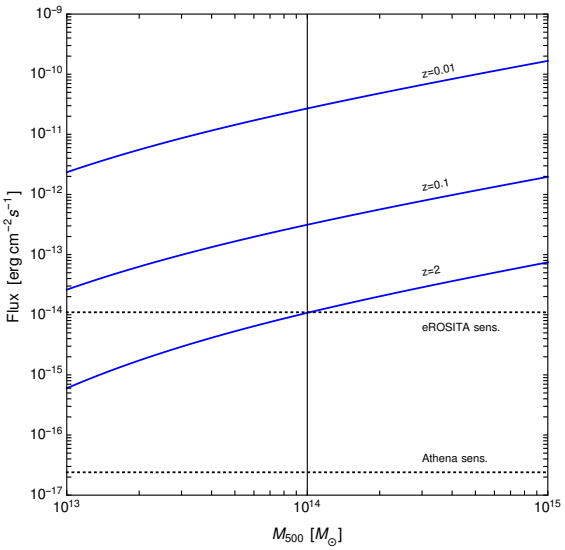

Figure 8. X-ray flux from a cluster in the [0.5–2] keV band as a function of its mass and for three redshifts. We show also the source sensitivities of eROSITA and Athena telescopes.

with $\gamma_1 = 0.62$, $\gamma_2 = 3.01$ and $K(z) = 10^{-4.53-0.19\,(1+z)}$. The characteristic luminosity is

$$L_*(z) = L_0 \left[\left(\frac{1+z_c}{1+z} \right)^{p_1} + \left(\frac{1+z_c}{1+z} \right)^{p_2} \right]^{-1} , \tag{B.2}$$

with $p_1 = 6.36$, $p_2 = -0.24$, $z_c = 0.75$ and $L_0 = 10^{44.77}$ erg s^{-1}. The spectral energy distribution is taken to be a power-law with spectral index of 1.45, the best-fit value in ref. [46].

Concerning the galaxies, we adopt the model of ref. [70]:

$$\phi = \phi_* \left(\frac{L}{L_*} \right)^{1-\alpha} \exp \left[-\frac{1}{2\sigma^2} \log_{10}^2 \left(1 + \frac{L}{L_*} \right) \right] , \tag{B.3}$$

with $\alpha = 1.43$, $\sigma = 0.72$, $\phi_* = 10^{-2.23}$ Mpc^{-3} and $L_* = 10^{39.74} \left(\frac{1+z}{1.25}\right)^{1.9}$ erg s^{-1}. As for AGN, we consider a power-law spectral energy distribution, in this case with spectral index of 2 [71].

C Three-dimensional power spectra

In eq. (2.6), we described the general formalism used to estimate the 3D power spectra entering in our analysis. In order to apply them to each specific case, we need to specify the functions $\hat{f}$ (Fourier transforms of the field) and b (bias of the source with respect to matter).

The case of auto correlation of X-rays from decaying DM (labeled with δ) is given by

$$\begin{aligned} P^{1h}_{\delta,\delta}(k,z) &= \int_{M_{\rm min}}^{M_{\rm max}} dM \, \frac{dn}{dM} \tilde{v}_\delta(k|M)^2 \\ P^{2h}_{\delta,\delta}(k,z) &= \left[\int_{M_{\rm min}}^{M_{\rm max}} dM \, \frac{dn}{dM} b_h(M) \, \tilde{v}_\delta(k|M) \right]^2 P^{\rm lin}(k) \, , \end{aligned} \tag{C.1}$$

JCAP03(2020)001

where $\tilde{v}_\delta(k|M)$ is the Fourier transform of $\rho_h(\boldsymbol{x}|M)/\bar{\rho}_{DM}$, with ρ_h being the DM halo profile, for which we assume the NFW shape [72] with halo concentration from ref. [73]. The bias of halos b_h with respect to matter is taken from ref. [74], as well as the halo mass function dn/dM. This estimate agrees very well with the non-linear matter power spectrum derived from N-body numerical simulations [51, 75]. Let us remind that we are taking $M_{\rm max} = 10^{14}\,M_\odot$, due to the masking of galaxy clusters. For definiteness, we set $M_{\rm min} = 10^6\,M_\odot$.

We consider AGNs and galaxies (labeled with a) as point-like sources, since their average size is smaller (or at most comparable) to the angular scales we analyze. Under this assumption, the 1-halo term is a Poissonian contribution (i.e., independent on k) which reads:

$$P^{1h}_{a,a}(z) = \int_{\mathcal{L}_{\rm min}(z)}^{\mathcal{L}_{\rm max}(z)} d\mathcal{L}\ \Phi_a(\mathcal{L},z)\left(\frac{\mathcal{L}}{\langle f_a\rangle}\right)^2 \tag{C.2}$$

with $\langle f_a\rangle = \int d\mathcal{L}\,\Phi_a\,\mathcal{L}$. This term is taken to be zero when cross correlating X-rays from AGNs with X-rays from galaxies. The 2-halo term can be computed as $P^{2h}_{a,a'}(k,z) = \langle b_a(z)\rangle\,\langle b_{a'}(z)\rangle\,P^{2h}_{\delta,\delta}(k,z)$. We take the average bias $\langle b_a(z)\rangle$ from ref. [42].

The power spectrum of cross correlation between X-rays from decaying DM and astrophysical sources is modeled through $P_{\delta,a}(k,z) = \langle b_a(z)\rangle P_{\delta,\delta}(k,z)$. This is exact for what concerns the 2-halo term, while just an approximation for the 1-halo component. We use this approximate description since the latter is just a highly subdominant contribution entering the covariance estimate.

In order to evaluate the correlation of galaxy catalogs with X-ray emitters, and since we adopt the halo model approach for the structure clustering, we need to describe how galaxies populate halos.[2] To this aim, we employ the halo occupation distribution (HOD) formalism that provides the number of galaxies of a certain catalogue residing in a halo of mass M at redshift z and their spatial distribution. We follow the approach described, e.g., in ref. [76], where the HOD is parameterized by distinguishing the contributions of central and satellite galaxies, $N_g = N_{\rm cen} + N_{\rm sat}$. The details of the HOD model for the 2MPZ and SDSS catalogs are provided in refs. [77] and [78]. For the on-going/future surveys DES, DESI and Euclid, we assume the same HOD as for SDSS. We expect this to be a good approximation, and small deviations from this reference model would have a negligible impact on our results.

For the catalog auto correlation, we refer the reader to e.g. ref. [50], while the power spectrum of cross correlation between decaying DM and a catalog of galaxies (labeled with g) can be written as:

$$\begin{aligned} P^{1h}_{g,\delta}(k,z) &= \int_{M_{\rm min}}^{M^\delta_{\rm max}} dM\ \frac{dn}{dM}\frac{\langle N_g\rangle}{\bar{n}_g}\tilde{v}_g(k|M)\tilde{v}_\delta(k|M) \\ P^{2h}_{g,\delta}(k,z) &= \left[\int_{M_{\rm min}}^{M^g_{\rm max}} dM\,\frac{dn}{dM}b_h(M)\frac{\langle N_g\rangle}{\bar{n}_g}\tilde{v}_g(k|M)\right] \\ &\quad\times\left[\int_{M_{\rm min}}^{M^\delta_{\rm max}} dM\,\frac{dn}{dM}b_h(M)\,\tilde{v}_\delta(k|M)\right] P^{\rm lin}(k)\,, \end{aligned} \tag{C.3}$$

where the notation emphasises that the maximum mass considered for the X-ray signal is different (smaller) than for galaxy catalogs.

[2] A different approach is to directly describe the galaxy clustering with an effective bias term, as done in ref. [42].

JCAP03(2020)001

The product $\langle N_g \rangle \tilde{v}_g(k|m)$ is the Fourier transform of $\langle N_{\rm cen}(M) \rangle \delta^3(\boldsymbol{x}) + \langle N_{\rm sat}(M) \rangle \rho_h(\boldsymbol{x}|M)/M$. The average number of galaxies at a given redshift is given by $\bar{n}_g(z) = \int dM \, dn/dM \, \langle N_g \rangle$.

The power spectrum of cross correlation between X-rays from astrophysical sources (AGN and galaxies) and galaxy catalogs is approximated with $P_{g,a}(k,z) = \langle b_a(z) \rangle P_{g,\delta}(k,z)$, following the same reasoning discussed above for the case of $P_{\delta,a}$.

References

[1] P. Minkowski, *$\mu \to e\gamma$ at a Rate of One Out of 10^9 Muon Decays?*, *Phys. Lett.* **67B** (1977) 421 [INSPIRE].

[2] R.N. Mohapatra and G. Senjanović, *Neutrino Mass and Spontaneous Parity Nonconservation*, *Phys. Rev. Lett.* **44** (1980) 912 [INSPIRE].

[3] M. Fukugita and T. Yanagida, *Baryogenesis Without Grand Unification*, *Phys. Lett.* **B 174** (1986) 45 [INSPIRE].

[4] B. Brahmachari and R.N. Mohapatra, *Grand unification of the sterile neutrino*, *Phys. Lett.* **B 437** (1998) 100 [hep-ph/9805429] [INSPIRE].

[5] H. Fritzsch and P. Minkowski, *Unified Interactions of Leptons and Hadrons*, *Annals Phys.* **93** (1975) 193 [INSPIRE].

[6] S. Nandi and U. Sarkar, *A Solution to the Neutrino Mass Problem in Superstring E6 Theory*, *Phys. Rev. Lett.* **56** (1986) 564 [INSPIRE].

[7] R.N. Mohapatra and J.W.F. Valle, *Neutrino Mass and Baryon Number Nonconservation in Superstring Models*, *Phys. Rev.* **D 34** (1986) 1642 [INSPIRE].

[8] A. Diaz, C.A. Argüelles, G.H. Collin, J.M. Conrad and M.H. Shaevitz, *Where Are We With Light Sterile Neutrinos?*, arXiv:1906.00045 [INSPIRE].

[9] M. Dentler et al., *Updated Global Analysis of Neutrino Oscillations in the Presence of eV-Scale Sterile Neutrinos*, *JHEP* **08** (2018) 010 [arXiv:1803.10661] [INSPIRE].

[10] J. Kopp, M. Maltoni and T. Schwetz, *Are There Sterile Neutrinos at the eV Scale?*, *Phys. Rev. Lett.* **107** (2011) 091801 [arXiv:1103.4570] [INSPIRE].

[11] T. Asaka, S. Blanchet and M. Shaposhnikov, *The nuMSM, dark matter and neutrino masses*, *Phys. Lett.* **B 631** (2005) 151 [hep-ph/0503065] [INSPIRE].

[12] M. Drewes et al., *A White Paper on keV Sterile Neutrino Dark Matter*, *JCAP* **01** (2017) 025 [arXiv:1602.04816] [INSPIRE].

[13] K.N. Abazajian, *Sterile neutrinos in cosmology*, *Phys. Rept.* **711–712** (2017) 1 [arXiv:1705.01837] [INSPIRE].

[14] A. Boyarsky, M. Drewes, T. Lasserre, S. Mertens and O. Ruchayskiy, *Sterile Neutrino Dark Matter*, *Prog. Part. Nucl. Phys.* **104** (2019) 1 [arXiv:1807.07938] [INSPIRE].

[15] S. Dodelson and L.M. Widrow, *Sterile-neutrinos as dark matter*, *Phys. Rev. Lett.* **72** (1994) 17 [hep-ph/9303287] [INSPIRE].

[16] X.-D. Shi and G.M. Fuller, *A new dark matter candidate: Nonthermal sterile neutrinos*, *Phys. Rev. Lett.* **82** (1999) 2832 [astro-ph/9810076] [INSPIRE].

[17] A. Kusenko, *Sterile neutrinos, dark matter and the pulsar velocities in models with a Higgs singlet*, *Phys. Rev. Lett.* **97** (2006) 241301 [hep-ph/0609081] [INSPIRE].

[18] K. Petraki and A. Kusenko, *Dark-matter sterile neutrinos in models with a gauge singlet in the Higgs sector*, *Phys. Rev.* **D 77** (2008) 065014 [arXiv:0711.4646] [INSPIRE].

JCAP03(2020)001

[19] S. Khalil and O. Seto, *Sterile neutrino dark matter in B-L extension of the standard model and galactic 511 keV line*, *JCAP* **10** (2008) 024 [arXiv:0804.0336] [INSPIRE].

[20] A. Merle, V. Niro and D. Schmidt, *New Production Mechanism for keV Sterile Neutrino Dark Matter by Decays of Frozen-In Scalars*, *JCAP* **03** (2014) 028 [arXiv:1306.3996] [INSPIRE].

[21] B. Shuve and I. Yavin, *Dark matter progenitor: Light vector boson decay into sterile neutrinos*, *Phys. Rev.* **D 89** (2014) 113004 [arXiv:1403.2727] [INSPIRE].

[22] A. Abada, G. Arcadi and M. Lucente, *Dark Matter in the minimal Inverse Seesaw mechanism*, *JCAP* **10** (2014) 001 [arXiv:1406.6556] [INSPIRE].

[23] J. König, A. Merle and M. Totzauer, *keV Sterile Neutrino Dark Matter from Singlet Scalar Decays: The Most General Case*, *JCAP* **11** (2016) 038 [arXiv:1609.01289] [INSPIRE].

[24] A. Merle and M. Totzauer, *keV Sterile Neutrino Dark Matter from Singlet Scalar Decays: Basic Concepts and Subtle Features*, *JCAP* **06** (2015) 011 [arXiv:1502.01011] [INSPIRE].

[25] A. Caputo, P. Hernández and N. Rius, *Leptogenesis from oscillations and dark matter*, *Eur. Phys. J.* **C 79** (2019) 574 [arXiv:1807.03309] [INSPIRE].

[26] K. Kaneta, Z. Kang and H.-S. Lee, *Right-handed neutrino dark matter under the $B-L$ gauge interaction*, *JHEP* **02** (2017) 031 [arXiv:1606.09317] [INSPIRE].

[27] T. Asaka, M. Shaposhnikov and A. Kusenko, *Opening a new window for warm dark matter*, *Phys. Lett.* **B 638** (2006) 401 [hep-ph/0602150] [INSPIRE].

[28] F. Bezrukov, H. Hettmansperger and M. Lindner, *keV sterile neutrino Dark Matter in gauge extensions of the Standard Model*, *Phys. Rev.* **D 81** (2010) 085032 [arXiv:0912.4415] [INSPIRE].

[29] M. Nemevšek, G. Senjanović and Y. Zhang, *Warm Dark Matter in Low Scale Left-Right Theory*, *JCAP* **07** (2012) 006 [arXiv:1205.0844] [INSPIRE].

[30] A.V. Patwardhan, G.M. Fuller, C.T. Kishimoto and A. Kusenko, *Diluted equilibrium sterile neutrino dark matter*, *Phys. Rev.* **D 92** (2015) 103509 [arXiv:1507.01977] [INSPIRE].

[31] G.B. Gelmini, P. Lu and V. Takhistov, *Cosmological Dependence of Resonantly Produced Sterile Neutrinos*, arXiv:1911.03398 [INSPIRE].

[32] G.B. Gelmini, P. Lu and V. Takhistov, *Cosmological Dependence of Non-resonantly Produced Sterile Neutrinos*, *JCAP* **12** (2019) 047 [arXiv:1909.13328] [INSPIRE].

[33] S. Tremaine and J.E. Gunn, *Dynamical Role of Light Neutral Leptons in Cosmology*, *Phys. Rev. Lett.* **42** (1979) 407 [INSPIRE].

[34] B.W. Lee and R.E. Shrock, *Natural Suppression of Symmetry Violation in Gauge Theories: Muon-Lepton and Electron Lepton Number Nonconservation*, *Phys. Rev.* **D 16** (1977) 1444 [INSPIRE].

[35] P.B. Pal and L. Wolfenstein, *Radiative Decays of Massive Neutrinos*, *Phys. Rev.* **D 25** (1982) 766 [INSPIRE].

[36] E. Bulbul, M. Markevitch, A. Foster, R.K. Smith, M. Loewenstein and S.W. Randall, *Detection of An Unidentified Emission Line in the Stacked X-ray spectrum of Galaxy Clusters*, *Astrophys. J.* **789** (2014) 13 [arXiv:1402.2301] [INSPIRE].

[37] A. Boyarsky, O. Ruchayskiy, D. Iakubovskyi and J. Franse, *Unidentified Line in X-Ray Spectra of the Andromeda Galaxy and Perseus Galaxy Cluster*, *Phys. Rev. Lett.* **113** (2014) 251301 [arXiv:1402.4119] [INSPIRE].

[38] A. Boyarsky, J. Franse, D. Iakubovskyi and O. Ruchayskiy, *Checking the Dark Matter Origin of a 3.53 keV Line with the Milky Way Center*, *Phys. Rev. Lett.* **115** (2015) 161301 [arXiv:1408.2503] [INSPIRE].

JCAP03(2020)001

[39] S. Riemer-Sørensen, *Constraints on the presence of a 3.5 keV dark matter emission line from Chandra observations of the Galactic centre*, *Astron. Astrophys.* **590** (2016) A71 [arXiv:1405.7943] [INSPIRE].

[40] C. Dessert, N.L. Rodd and B.R. Safdi, *Evidence against the decaying dark matter interpretation of the 3.5 keV line from blank sky observations*, arXiv:1812.06976 [INSPIRE].

[41] EROSITA collaboration, *eROSITA Science Book: Mapping the Structure of the Energetic Universe*, arXiv:1209.3114 [INSPIRE].

[42] F. Zandanel, C. Weniger and S. Ando, *The role of the eROSITA all-sky survey in searches for sterile neutrino dark matter*, *JCAP* **09** (2015) 060 [arXiv:1505.07829] [INSPIRE].

[43] K. Nandra et al., *The Hot and Energetic Universe: A White Paper presenting the science theme motivating the Athena+ mission*, arXiv:1306.2307 [INSPIRE].

[44] C. Creque-Sarbinowski and M. Kamionkowski, *Searching for Decaying and Annihilating Dark Matter with Line Intensity Mapping*, *Phys. Rev.* **D 98** (2018) 063524 [arXiv:1806.11119] [INSPIRE].

[45] PLANCK collaboration, *Planck 2018 results. VI. Cosmological parameters*, arXiv:1807.06209 [INSPIRE].

[46] N. Cappelluti et al., *The Chandra COSMOS legacy survey: Energy Spectrum of the Cosmic X-ray Background and constraints on undetected populations*, *Astrophys. J.* **837** (2017) 19 [arXiv:1702.01660] [INSPIRE].

[47] M. Lieu et al., *The XXL Survey IV. Mass-temperature relation of the bright cluster sample*, *Astron. Astrophys.* **592** (2016) A4 [arXiv:1512.03857] [INSPIRE].

[48] E. Bulbul, M. Markevitch, A.R. Foster, R.K. Smith, M. Loewenstein and S.W. Randall, *Comment on "Dark matter searches going bananas: the contribution of Potassium (and Chlorine) to the 3.5 keV line"*, arXiv:1409.4143 [INSPIRE].

[49] D.N. Limber, *The Analysis of Counts of the Extragalactic Nebulae in Terms of a Fluctuating Density Field*, *Astrophys. J.* **117** (1953) 134.

[50] A. Cooray and R.K. Sheth, *Halo Models of Large Scale Structure*, *Phys. Rept.* **372** (2002) 1 [astro-ph/0206508] [INSPIRE].

[51] N. Fornengo and M. Regis, *Particle dark matter searches in the anisotropic sky*, *Front. Phys.* **2** (2014) 6 [arXiv:1312.4835].

[52] eROSITA, https://www.mpe.mpg.de/455799/instrument.

[53] A.Merloni, https://www.cosmos.esa.int/documents/332006/1402684/AMerloni_t.pdf.

[54] D. Barret et al., *Athena+: The first Deep Universe X-ray Observatory*, 2013, arXiv:1310.3814 [INSPIRE].

[55] X-IFU, http://x-ifu.irap.omp.eu/the-x-ifu-in-a-nutshell/.

[56] S. Lotti et al., *In-orbit background of X-ray microcalorimeters and its effects on observations*, *Astron. Astrophys.* **569** (2014) A54 [arXiv:1410.3373] [INSPIRE].

[57] M. Bilicki, T.H. Jarrett, J.A. Peacock, M.E. Cluver and L. Steward, *2MASS Photometric Redshift catalog: a comprehensive three-dimensional census of the whole sky*, arXiv:1311.5246 [INSPIRE].

[58] R. Beck, L. Dobos, T. Budavári, A.S. Szalay and I. Csabai, *Photometric redshifts for the SDSS Data Release 12*, *Mon. Not. Roy. Astron. Soc.* **460** (2016) 1371 [arXiv:1603.09708].

[59] DES collaboration, *The dark energy survey*, astro-ph/0510346 [INSPIRE].

[60] DESI collaboration, *The DESI Experiment Part I: Science, Targeting and Survey Design*, arXiv:1611.00036 [INSPIRE].

JCAP03(2020)001

[61] EUCLID collaboration, *Euclid Definition Study Report*, arXiv:1110.3193 [INSPIRE].

[62] LSST SCIENCE and LSST PROJECT collaborations, *LSST Science Book, Version 2.0*, arXiv:0912.0201 [INSPIRE].

[63] B.M. Roach et al., *NuSTAR Tests of Sterile-Neutrino Dark Matter: New Galactic Bulge Observations and Combined Impact*, arXiv:1908.09037 [INSPIRE].

[64] A. Boyarsky, O. Ruchayskiy and M. Shaposhnikov, *The Role of sterile neutrinos in cosmology and astrophysics*, *Ann. Rev. Nucl. Part. Sci.* **59** (2009) 191 [arXiv:0901.0011].

[65] M. Tashiro et al., *Concept of the X-ray Astronomy Recovery Mission*, in *Proceedings of the SPIE*, vol. 10699 of *Society of Photo-Optical Instrumentation Engineers (SPIE) Conference Series*, July 2018, p. 1069922, DOI.

[66] A. Neronov and D. Malyshev, *Toward a full test of the νMSM sterile neutrino dark matter model with Athena*, *Phys. Rev.* **D 93** (2016) 063518 [arXiv:1509.02758] [INSPIRE].

[67] V. Ghirardini et al., *Universal thermodynamic properties of the intracluster medium over two decades in radius in the X-COP sample*, *Astron. Astrophys.* **621** (2019) A41 [arXiv:1805.00042] [INSPIRE].

[68] D. Eckert et al., *Non-thermal pressure support in X-COP galaxy clusters*, *Astron. Astrophys.* **621** (2019) A40 [arXiv:1805.00034] [INSPIRE].

[69] J. Aird et al., *The evolution of the hard X-ray luminosity function of AGN*, *Mon. Not. Roy. Astron. Soc.* **401** (2010) 2531 [arXiv:0910.1141].

[70] A. Ptak, B. Mobasher, A. Hornschemeier, F. Bauer and C. Norman, *X-Ray Luminosity Functions of Normal Galaxies in the Great Observatories Origins Deep Survey*, *Astrophys. J.* **667** (2007) 826.

[71] M. Young et al., *Variability Selected Low-Luminosity Active Galactic Nuclei in the 4 Ms Chandra Deep Field-South*, *Astrophys. J.* **748** (2012) 124 [arXiv:1201.4391] [INSPIRE].

[72] J.F. Navarro, C.S. Frenk and S.D.M. White, *A universal density profile from hierarchical clustering*, *Astrophys. J.* **490** (1997) 493 [astro-ph/9611107] [INSPIRE].

[73] F. Prada, A.A. Klypin, A.J. Cuesta, J.E. Betancort-Rijo and J. Primack, *Halo concentrations in the standard LCDM cosmology*, *Mon. Not. Roy. Astron. Soc.* **428** (2012) 3018 [arXiv:1104.5130].

[74] R.K. Sheth and G. Tormen, *Large scale bias and the peak background split*, *Mon. Not. Roy. Astron. Soc.* **308** (1999) 119 [astro-ph/9901122] [INSPIRE].

[75] R. Takahashi, M. Sato, T. Nishimichi, A. Taruya and M. Oguri, *Revising the Halofit Model for the Nonlinear Matter Power Spectrum*, *Astrophys. J.* **761** (2012) 152 [arXiv:1208.2701] [INSPIRE].

[76] Z. Zheng et al., *Theoretical models of the halo occupation distribution: Separating central and satellite galaxies*, *Astrophys. J.* **633** (2005) 791 [astro-ph/0408564] [INSPIRE].

[77] S. Ammazzalorso, N. Fornengo, S. Horiuchi and M. Regis, *Characterizing the local gamma-ray Universe via angular cross-correlations*, *Phys. Rev.* **D 98** (2018) 103007 [arXiv:1808.09225] [INSPIRE].

[78] A. Cuoco, J.-Q. Xia, M. Regis, E. Branchini, N. Fornengo and M. Viel, *Dark Matter Searches in the Gamma-ray Extragalactic Background via Cross-correlations With Galaxy Catalogs*, *Astrophys. J. Suppl.* **221** (2015) 29 [arXiv:1506.01030] [INSPIRE].

JCAP03(2020)001

JHEP

Published for SISSA by Springer

Received: March 31, 2020
Accepted: June 15, 2020
Published: June 30, 2020

Minimal flavor violation in the see-saw portal

Daniele Barducci,[a] **Enrico Bertuzzo,**[b] **Andrea Caputo**[c] **and Pilar Hernandez**[c]

[a] *Dipartimento di Fisica Università degli Studi di Roma La Sapienza and INFN Sezione di Roma, Piazzale Aldo Moro 5, 00185, Roma, Italy*

[b] *Instituto de Fisica, Universidade de Sao Paulo, C.P. 66.318, 05315-970 Sao Paulo, Brazil*

[c] *Institut de Física Corpuscular — CSIC/Universitat de València, Parc Científic de Paterna, Paterna, Spain*

E-mail: daniele.barducci@roma1.infn.it, bertuzzo@if.usp.br, andrea.caputo@uv.es, pilar.hernandez@ific.uv.es

Abstract: We consider an extension of the Standard Model with two singlet leptons, with masses in the electroweak range, that induce neutrino masses via the see-saw mechanism, plus a generic new physics sector at a higher scale, Λ. We apply the minimal flavor violation (MFV) principle to the corresponding Effective Field Theory (νSMEFT) valid at energy scales $E \ll \Lambda$. We identify the irreducible sources of lepton flavor and lepton number violation at the renormalizable level, and apply the MFV ansätz to derive the scaling of the Wilson coefficients of the νSMEFT operators up to dimension six. We highlight the most important phenomenological consequences of this hypothesis in the rates for exotic Higgs decays, the decay length of the heavy neutrinos, and their production modes at present and future colliders. We also comment on possible astrophysical implications.

Keywords: Neutrino Physics, Beyond Standard Model, CP violation

ArXiv ePrint: 2003.08391

https://doi.org/10.1007/JHEP06(2020)185

JHEP06(2020)185

Contents

JHEP06(2020)185

1 Introduction

The observed pattern of neutrino masses and oscillations parameters [1] calls for the existence of new physics (NP) beyond the Standard Model (SM). One of the simplest solution is to extend the SM with the right-handed (RH) chiral counterparts of the left-handed SM neutrinos, with which the new states can have Yukawa type interactions at the renormalizable level. Being electroweak (EW) singlets, the RH neutrinos N_R (also dubbed sterile neutrinos) can have Majorana masses and provide a mechanism that explains the lightness of the observed neutrinos in terms of a large hierarchy between the EW scale v and

the Majorana mass scale. This is the essence of the see-saw mechanism [2–5] which is parametrically expressed by the well-known relation

$$m_{\nu_L} \propto \frac{y^2\, v^2}{M_{N_R}}\,, \tag{1.1}$$

where y and M_{N_R} are the Yukawa coupling and the Majorana mass term for the RH neutrinos respectively. In its original realization the mechanism assumes M_{N_R} at around the Grand Unification Scale while the Yukawa coupling y is an $\mathcal{O}(1)$ parameter. Low scale see-saw models, with RH neutrino masses at the EW scale, have recently received more attention. They can in fact explain the matter-antimatter asymmetry of the Universe via neutrino oscillations [6, 7], without introducing a severe fine tuning of the Higgs mass [8]. More interestingly they can also be tested for in beam dump experiments and at colliders, see e.g. [9–21], possibly giving rise to spectacular signals such as displaced vertices.

The presence of additional NP states at a scale $\Lambda \gg v, M_{N_R}$ can modify the phenomenological predictions of the see-saw model. At low energy these effects can be generically parametrized by an effective field theory (EFT) that contains a tower of higher dimensional operators $\mathcal{O}^d/\Lambda^{d-4}$ with dimension $d > 4$, that can induce new production and decay modes for the RH neutrinos, as well as new exotic Higgs decays [10, 21–26]. Sizable effects clearly arise only if Λ is not too much higher than the EW scale. However, as it is well known, higher dimensional operators with a generic flavor structure, and suppressed by a scale $\Lambda \sim \mathcal{O}(1-10)\,\text{TeV}$, are grossly excluded by a variety of searches for flavor changing neutral currents (FCNC) and lepton number violating (LNV) decays. For example the dimension six operator $(\bar{L}\sigma_{\mu\nu}e_R)HB^{\mu\nu}/\Lambda^2$ induces at tree level the transition $\mu \to e\gamma$ for which the constraint from the MEG experiment [27] sets $\Lambda \gtrsim 6\times 10^4\,\text{TeV}$ [28].

The Minimal Flavor Violation (MFV) paradigm [29, 30] provides a suppression for these processes derived from a symmetry principle. Briefly, it states that all flavor and charge-parity violating interactions in the EFT should be linked to the ones of the renormalizable Lagrangian. In practice, for the case of the quark sector of the SM this mechanism is implemented by promoting the Yukawa matrices to spurion fields with well-defined transformation properties under the flavor group in such a way that the full Lagrangian, including the non-renormalizable interactions, has the same global symmetry as the kinetic term [30]. In the lepton sector however the still unknown mechanism that gives mass to the light neutrinos adds model-dependent spurions. For example, in the minimal see-saw model considered in this work, the leptonic spurions include the neutrino Yukawa coupling and the Majorana mass matrix for the RH neutrinos, M_{N_R}, which generally also acts as a source of lepton number breaking. Leptonic MFV in the context of the SMEFT has been first analyzed in [31–36], where the authors have identified the conditions under which one can expect measurable rates for LFV low-energy processes induced by higher dimensional operators. The main conclusion is that one needs a large separation between the scale of lepton number violation (LNV), for example M_{N_R}, and the scale of the higher dimensional operators that induce LFV processes, i.e. $M_{N_R} \gg \Lambda$. In this work we are instead interested in RH neutrinos at the EW scale, i.e. $M_{N_R} \ll \Lambda$. The higher dimensional operators must therefore be built including also the RH neutrino fields, and it is precisely their phe-

JHEP06(2020)185

nomenology that we want to understand. In this sense our approach is then complementary to the one of [31, 34].

The SMEFT extended to include the RH neutrino fields, that we will refer to as νSMEFT, has been constructed up to $d = 7$ in [10, 22–24, 37]. The smallness of neutrino masses are not compatible with large LFV effects from higher dimensional operators, unless the couplings of the higher dimensional operators are strongly hierarchical. For the $d = 5$ operators, such a hierarchy has been shown to arise with the imposition of the MFV ansätz [22], as well as in the presence of an approximate $\mathrm{U}(1)_L$ lepton number symmetry [20].

In this paper we systematically study the implications of the MFV ansätz on the scaling of the Wilson coefficients of all $d = 5$ and $d = 6$ operators involving RH neutrinos and SM fields, including quark bilinears. Particularly interesting for phenomenology is the scenario where the textures of the neutrino spurions imply strong deviations from the naive see-saw scaling of eq. (1.1) [34, 38], allowing for observable LFV effects compatible with the measured values of the light neutrino masses. We discuss in this context the implications of MFV for the phenomenology of the RH neutrino states at present and future colliders. In particular, we study when prompt or displaced signatures can be expected from their decay, a property which is essential for experimental search strategies. We also qualitatively discuss the sensitivity of present and future experiments to the new physics scale Λ via RH neutrino searches, stressing the impact of the MFV ansätz. Finally, we also briefly comment on astrophysical constraints, which are relevant when RH neutrinos masses lie in the keV to MeV range.

The paper is organized as follows. In section 2 we fix our notation and discuss the global symmetries of the SM extended with an arbitrary number of RH neutrinos. In section 3 we review the MFV ansätz and parametrize the various source of flavor breaking by "composed spurion" fields, while in section 4 we establish a connection between the masses of the active neutrinos and the higher dimensional operators that modify their mass spectrum. Section 5 and section 6 discuss the scaling of the Wilson coefficients of the $d = 5$ and $d = 6$ operators under the MFV paradigm, while in section 7 we briefly highlight the more relevant phenomenological consequences. We then conclude in section 8.

2 Setting the stage

We will work with the νSMEFT which is described by the following Lagrangian

$$\begin{aligned}\mathcal{L}_{\nu\mathrm{SMEFT}} \simeq \mathcal{L}_{\mathrm{kin}} - \bar{Q}Y_d H d_R - \bar{Q}Y_u \tilde{H} u_R - \bar{L}Y_e H e_R - \bar{L}Y_\nu \tilde{H} N_R - \frac{1}{2}\bar{N}_R^c M_N N_R + \mathrm{h.c.} \\ + \frac{1}{\Lambda}\mathcal{L}_5 + \frac{1}{\Lambda^2}\mathcal{L}_6 + \dots \end{aligned} \tag{2.1}$$

where $N_R^c = C\bar{N}_R^T$, $C = i\gamma^0\gamma^2$, $\tilde{H} = i\sigma_2 H^*$. In eq. (2.1) the terms in the first line describe the SM Lagrangian extended with renormalizable operators involving RH singlet fermions, while the terms $\mathcal{L}_{d>4}$ contain all the possible higher dimensional operators built out with

JHEP06(2020)185

the SM field content plus the RH neutrinos. In our analysis we will work up to dimension six, for which a complete list of operators can be found in [10, 22–24, 37, 39].[1]

Once the Yukawa interactions and the Majorana mass are switched off, the renormalizable part of the Lagrangian of eq. (2.1) has a global symmetry

$$\begin{aligned}\mathcal{G} &= \mathrm{U}(3)_L \times \mathrm{U}(3)_e \times \mathrm{U}(\mathcal{N})_N \times \mathrm{U}(3)_q \times \mathrm{U}(3)_u \times \mathrm{U}(3)_d = \\ &= \mathrm{SU}(3)^5 \times \mathrm{U}(1)^5 \times \mathrm{SU}(\mathcal{N})_N \times \mathrm{U}(1)_N\end{aligned} \tag{2.2}$$

where $\mathcal{N}$ is the number of RH neutrinos. We can rearrange the six U(1) factors in different ways. One possible choice is to define as usual three factors to be the (global) hypercharge, baryon and lepton number. The three remaining factors can be chosen to be a Peccei-Quinn (PQ) like symmetry acting on d_R and e_R, a phase acting on e_R only (see e.g. [30]) and an extra phase acting on the RH neutrinos. We choose to assign the same lepton number to all the RH neutrinos. There is however freedom in this choice. For example in the case $\mathcal{N} = 2$ an interesting possibility would be to assign opposite charges to the two RH neutrinos as in the inverse see-saw model. We leave the discussion of this possibility for future work. Under these assumptions, let us analyze the group factors in more detail, focusing on the various sources of the breaking of the U(1) symmetries.

Yukawa terms. Baryon and lepton number, together with the global version of the hypercharge, are respected by the Yukawa terms $Y_{u,d,e,\nu}$. The PQ symmetry $\mathrm{U}(1)_{\mathrm{PQ}}$ is broken by Y_d and Y_e, while $\mathrm{U}(1)_e$ is broken by Y_e. Notice that the PQ symmetry plays an important role in flavor dynamics models with more than one Higgs doublet, since in that case it is possibile to assign a PQ charge to one of the two Higgs doublets, making then the Yukawa terms invariant under this symmetry [30]. Finally, $\mathrm{U}(1)_N$ is broken by the neutrino Yukawa term.

Majorana mass. The Majorana mass term breaks both $\mathrm{U}(1)_L$ and $\mathrm{U}(1)_N$.

With this said, we now focus on the flavor subgroup in the leptonic sector,

$$\mathcal{G}_L = \mathrm{SU}(3)_L \times \mathrm{SU}(3)_e \times \mathrm{SU}(\mathcal{N})_N \times \mathrm{U}(1)_\ell \times \mathrm{U}(1)_e \times \mathrm{U}(1)_N\,, \tag{2.3}$$

and classify fields and spurions in terms of their transformations properties. From the field transformations

$$L \to e^{i\alpha_\ell}\, V_L L, \qquad e_R \to e^{i\alpha_\ell}\, V_e e_R, \qquad N_R \to e^{i\alpha_\ell}\, V_N N_R, \tag{2.4}$$

where the V_i matrices are unitary matrices belonging to $\mathrm{SU}(3)_i$ and where we show only the lepton number transformation of parameter α_ℓ, the spurion transformations that leave the renormalizable part of the Lagrangian of eq. (2.1) invariant read

$$Y_e \to V_L Y_e V_e^\dagger, \quad Y_\nu \to V_L Y_\nu V_N^\dagger, \quad M_N \to e^{-2i\alpha_\ell}\, V_N^* M_N V_N^\dagger\,. \tag{2.5}$$

[1] Ref. [37] provides also a list of dimension seven operators involving RH neutrino fields. The first list of $d = 6$ operators including RH fields appeared in ref. [23], but as pointed out in [37] some of these were redundant.

JHEP06(2020)185

	$SU(3)_L$	$SU(3)_e$	$SU(\mathcal{N})_N$	$U(1)_\ell$	$U(1)_e$	$U(1)_N$
L	**3**	**1**	**1**	+1	0	0
e_R	**1**	**3**	**1**	+1	+1	0
N_R	**1**	**1**	$\mathcal{N}$	+1	0	+1
M_N	**1**	**1**	$\overline{\mathbf{S}}$	−2	0	−2
Y_e	**3**	$\overline{\mathbf{3}}$	**1**	0	−1	0
Y_ν	**3**	**1**	$\overline{\mathcal{N}}$	0	0	−1

Table 1. Global charges of fields and spurions in the lepton sector.

The Majorana mass matrix spurion M_N transforms under $SU(\mathcal{N})_N$ as $\overline{\mathbf{S}}$, where $\mathbf{S}$ is the symmetric representation that can be constructed out of two fundamentals. For instance, $\overline{\mathbf{S}} = \mathbf{3}$ when $\mathcal{N} = 2$, or $\overline{\mathbf{S}} = \overline{\mathbf{6}}$ when $\mathcal{N} = 3$. All together, the charge assignments under $\mathcal{G}_L$ are reported in table 1. A similar analysis can be performed for the quark sector. The analysis in this sector has been studied in detail and we refer the reader to ref. [30] for a comprehensive discussion.

Without loss of generality we can now use the transformation of eq. (2.4) to go from eq. (2.1) to a basis in which both Y_e and M_N are diagonal matrices with non negative entries. In the same way we can also choose to go in a basis where Y_d is diagonal with non negative entries and $Y_u = V_{\rm CKM}^\dagger m_u/v$, where m_u is the diagonal matrix containing the physical up type quark masses and $V_{\rm CKM}$ is the Cabibbo-Kobayashi-Maskawa matrix with $u_L = V_{\rm CKM} u_L^{\rm mass}$.

Note that we can decouple the sources of $SU(\mathcal{N})_N$ and lepton number breaking by assuming that the Majorana mass matrix is proportional to the identity in flavor space as discussed in [31]. This reduces the flavor group from $SU(\mathcal{N})_N$ to $SO(\mathcal{N})_N$ thus making V_N a real orthogonal matrix.

3 Spurion parametrization

In the MFV paradigm the flavor structure of the non renormalizable operators contained in $\mathcal{L}_{d>4}$ are to be built out of the irreducible sources of flavor breaking of the renormalizable Lagrangian in such a way that they are invariant under the full global symmetry group. Applied to the quark sector this implies that higher dimensional operators should be built out with SM fields and the Y_u and Y_d spurion fields [30].

The same paradigm applied to the lepton sector features a richer structure, due to the Majorana mass term that in general controls both the breaking of the flavor and of the lepton number symmetries, while the two Yukawa matrices, Y_e and Y_ν, act as a source of lepton flavor violation only [31]. We will impose the MFV hypothesis in the lepton sector by requiring that all the sources of lepton number and lepton flavor breaking of the $d > 4$ operators are dictated by M_N, Y_e and Y_ν. To this end we now analyze in more detail the flavor breaking spurions reported in table 1. To consider only dimensionless quantities, we

JHEP06(2020)185

define the diagonal matrix

$$\epsilon_L \equiv \frac{M_N}{\Lambda}\,, \tag{3.1}$$

with the transformation properties of eq. (2.5). In terms of ϵ_L, the mass term of the RH neutrinos amounts to $\Lambda\,\bar{N}_R^c\,\epsilon_L\,N_R$. In the $\epsilon_L \to 0$ limit we recover the $\mathrm{U}(1)_\ell$ symmetry, i.e. it is technically natural to take ϵ_L small. Note that the choice of eq. (3.1) connects with Λ also the scale of lepton number breaking, which is due at the renormalizable level to the Majorana mass term M_N. Also, as already mentioned, when the sources of lepton flavor and lepton number breaking are decoupled, this spurion will be proportional to the identity matrix in flavor space. The transformation under $\mathrm{SU}(\mathcal{N})_N$ becomes trivial, and ϵ_L is now a spurion controlling the breaking of lepton number only.

In order to determine the scaling of operators with $d = 5$ and $d = 6$, it is convenient to define some objects with well defined transformation properties under the flavor groups built out combining the fundamental spurions of the quark and the lepton sector, $Y_{u,d,e,\nu}$ and ϵ_L. The first useful class is made up by objects that transform as bifundamental under *the same* SU(3) flavor group. They are

$$\begin{aligned}
&\mathcal{S}_{LL^\dagger} \to V_L\,\mathcal{S}_{LL^\dagger}\,V_L^\dagger\,, && \mathcal{S}_{NN^\dagger} \to V_N\,\mathcal{S}_{NN^\dagger}\,V_N^\dagger\,,\\
&\mathcal{S}_{ee^\dagger} \to V_e\,\mathcal{S}_{ee^\dagger}\,V_e^\dagger\,, && \mathcal{S}_{qq^\dagger} \to V_q\,\mathcal{S}_{qq^\dagger}\,V_q^\dagger\,,\\
&\mathcal{S}_{uu^\dagger} \to V_u\,\mathcal{S}_{uu^\dagger}\,V_u^\dagger\,, && \mathcal{S}_{dd^\dagger} \to V_d\,\mathcal{S}_{dd^\dagger}\,V_d^\dagger\,.
\end{aligned} \tag{3.2}$$

We will also need objects transforming as bifundamental under *different* SU(3) flavor groups. They read

$$\begin{aligned}
&\mathcal{S}_{\nu} \to V_L\,\mathcal{S}_{\nu}\,V_N^\dagger\,, && \mathcal{S}_{\nu^\dagger} \to V_N\,\mathcal{S}_{\nu^\dagger}\,V_L^\dagger\,,\\
&\mathcal{S}_{e} \to V_L\,\mathcal{S}_{e}\,V_e^\dagger\,, && \mathcal{S}_{e^\dagger} \to V_e\,\mathcal{S}_{e^\dagger}\,V_L^\dagger\,,\\
&\mathcal{S}_{u} \to V_q\,\mathcal{S}_{u}\,V_u^\dagger\,, && \mathcal{S}_{u^\dagger} \to V_u\,\mathcal{S}_{u^\dagger}\,V_q^\dagger\,,\\
&\mathcal{S}_{d} \to V_q\,\mathcal{S}_{d}\,V_d^\dagger\,, && \mathcal{S}_{d^\dagger} \to V_d\,\mathcal{S}_{d^\dagger}\,V_q^\dagger\,.
\end{aligned} \tag{3.3}$$

Finally, we introduce the objects that are responsible for the breaking of the lepton number symmetry. They transform as

$$\mathcal{S}_{L^*L^\dagger} \to e^{-2i\alpha_L} V_L^*\,\mathcal{S}_{L^*L^\dagger}\,V_L^\dagger\,, \qquad \mathcal{S}_{N^*N^\dagger} \to e^{-2i\alpha_L} V_N^*\,\mathcal{S}_{N^*N^\dagger}\,V_N^\dagger\,. \tag{3.4}$$

We now want to write these objects in terms of the spurions in table 1. To this end, we define a general polynomial $\mathcal{F}_{\langle x,y\rangle}$ of two non commuting variables x, y as

$$\mathcal{F}_{\langle x,y\rangle} = \sum_{i=0}^{\infty} p_{i,\langle x,y\rangle}\,, \tag{3.5}$$

where $p_{i,\langle x,y\rangle}$ indicates the sum of all possibile monomial factors, each with a generic complex coefficients, with total exponent i, taking into account that in general $[x, y] \neq 0$. For example we have

$$\begin{aligned}
p_{0,\langle x,y\rangle} &= a_0\\
p_{1,\langle x,y\rangle} &= a_{1_{(1)}} x + a_{1_{(2)}} y\\
p_{2,\langle x,y\rangle} &= a_{2_{(1)}} x^2 + a_{2_{(2)}} y^2 + a_{2_{(3)}} xy + a_{2_{(4)}} yx\,.
\end{aligned} \tag{3.6}$$

JHEP06(2020)185

The generalization to a polynomial of more than two variables is straightforward. In the case of a polynomial of one variable only, the expansion simply amounts to the usual $\mathcal{F}_{\langle x\rangle} = \sum a_n x^n$. The objects in eq. (3.2) that transform as bifundamental under the same SU(3) factor can thus be written in a compact way as

$$\begin{aligned}
\mathcal{S}_{LL^\dagger} &= \mathcal{F}_{\langle Y_\nu Y_\nu^\dagger, Y_e Y_e^\dagger\rangle}\,, & \mathcal{S}_{qq^\dagger} &= \mathcal{F}_{\langle Y_u Y_u^\dagger, Y_d Y_d^\dagger\rangle}\,,\\
\mathcal{S}_{ee^\dagger} &= \mathcal{F}_{\langle Y_e^\dagger \mathcal{G}_{\langle Y_e^\dagger Y_e, Y_\nu Y_\nu^\dagger\rangle} Y_e\rangle}\,, & \mathcal{S}_{dd^\dagger} &= \mathcal{F}_{\langle Y_d^\dagger \mathcal{G}_{\langle Y_d^\dagger Y_d, Y_u Y_u^\dagger\rangle} Y_d\rangle}\,,\\
\mathcal{S}_{NN^\dagger} &= \mathcal{F}_{\langle Y_\nu^\dagger Y_\nu, \epsilon_L^* \epsilon_L, Y_\nu^\dagger \mathcal{G}_{\langle Y_\nu Y_\nu^\dagger, Y_e Y_e^\dagger\rangle} Y_\nu\rangle}\,, & \mathcal{S}_{uu^\dagger} &= \mathcal{F}_{\langle Y_u^\dagger Y_u, Y_u^\dagger \mathcal{G}_{\langle Y_d Y_d^\dagger, Y_u Y_u^\dagger\rangle} Y_u\rangle}\,,
\end{aligned} \tag{3.7}$$

where $\mathcal{G}$ is defined in the same way as $\mathcal{F}$ of eq. (3.5) with in general different coefficients. Note that the expansion of all these terms starts with a term proportional to the identity in flavor space. Moving on to the objects in eq. (3.3) that transform as bifundamental under different SU(3) flavor groups, they can be written as

$$\begin{aligned}
\mathcal{S}_\nu &= \mathcal{S}_{LL^\dagger} Y_\nu\,, & \mathcal{S}_{\nu^\dagger} &= Y_\nu^\dagger \mathcal{S}_{LL^\dagger}\,,\\
\mathcal{S}_e &= \mathcal{S}_{LL^\dagger} Y_e\,, & \mathcal{S}_{e^\dagger} &= Y_e^\dagger \mathcal{S}_{LL^\dagger}\,,\\
\mathcal{S}_u &= \mathcal{S}_{qq^\dagger} Y_u\,, & \mathcal{S}_{u^\dagger} &= Y_u^\dagger \mathcal{S}_{qq^\dagger}\,,\\
\mathcal{S}_d &= \mathcal{S}_{qq^\dagger} Y_d\,, & \mathcal{S}_{d^\dagger} &= Y_d^\dagger \mathcal{S}_{qq^\dagger}\,,
\end{aligned} \tag{3.8}$$

where now the expansion of each of the terms above starts with a term which is proportional to the respective Yukawa matrix. Here above we have used the definitions of eq. (3.7) to keep track in a synthetic way of objects with defined transformation rules. In general the spurions that multiply the Yukawa matrices in eq. (3.8) do not have the same expansion coefficients, $a_{i_{(j)}}$, as those in eq. (3.7).

Finally, the expansion of the objects that explicitly break lepton number, eq. (3.4), reads

$$\mathcal{S}_{L^*L^\dagger} = \mathcal{S}^*_{LL^\dagger}\, Y_\nu^*\, \epsilon_L\, Y_\nu^\dagger\, \mathcal{S}_{LL^\dagger}\,, \qquad \mathcal{S}_{N^*N^\dagger} = \mathcal{S}^*_{NN^\dagger} \epsilon_L \mathcal{S}_{NN^\dagger}\ . \tag{3.9}$$

In what follows we will write everything in terms of these "composed spurions" and we will expand them at leading order in the Y_ν and Y_e matrices. While we will have to find a connection with the observed values of neutrino masses and mixing parameters to determine the order of magnitude of the elements of Y_ν, we can already determine the numerical size of the terms involving Y_e. Since we work in the basis in which Y_e is diagonal with non negative entries, we have[2]

$$Y_e = \lambda_e^{\rm diag} \simeq \begin{pmatrix} 3\times 10^{-6} & 0 & 0\\ 0 & 6\times 10^{-4} & 0\\ 0 & 0 & 10^{-2}\end{pmatrix}. \tag{3.10}$$

Analogously, in the down-quark sector we have

$$Y_d = \lambda_d^{\rm diag} \simeq \begin{pmatrix} 3\times 10^{-5} & 0 & 0\\ 0 & 6\times 10^{-4} & 0\\ 0 & 0 & 2\times 10^{-2}\end{pmatrix}, \tag{3.11}$$

[2]We work with $\langle H\rangle = 174\,\text{GeV}$.

JHEP06(2020)185

	Operator	Scaling	Loop generated
$\mathcal{O}^5_{NH}$	$\bar{N}^c_R N_R H^\dagger H$	$[\mathcal{S}_{N^* N^\dagger}]_S/2$	✗
$\mathcal{O}^5_{NB}$	$\bar{N}^c_R \sigma^{\mu\nu} N_R B_{\mu\nu}$	$[\mathcal{S}_{N^* N^\dagger}]_A$	✓
$\mathcal{O}^5_{W}$	$(\bar{L}^c \epsilon H)(L \epsilon H)$	$[\mathcal{S}_{L^* L^\dagger}]_S/2$	✗

Table 2. Dimension five operators constructed with the SM and the RH neutrino fields. We also show the scaling of their Wilson coefficients in terms of the spurions of eq. (3.7) and eq. (3.9), and whether they are generated at one loop in a general UV completion. The additional factor of 1/2 is conventional and allows to simplify the mass matrix in eq. (4.1).

while in the up-quark sector we obtain

$$Y_u = V^\dagger_{CKM} \lambda_u^{\text{diag}} \simeq \begin{pmatrix} 10^{-5} & -2\times 10^{-3} & 8\times 10^{-3} \\ 3\times 10^{-6} & 7\times 10^{-3} & 4\times 10^{-2} \\ 5\times 10^{-8} & 3\times 10^{-4} & 0.99 \end{pmatrix} . \tag{3.12}$$

An implicit assumption we are making in eq. (3.7), eq. (3.8) and eq. (3.9) is that we can stop the polynomial expansion to some finite order in the spurion insertions. While this is clearly true for the spurions involving the charged lepton and quark Yukawa couplings, this requirement might not be satisfied for the terms involving Y_ν. One needs to check that bilinears constructed out of them like $Y_\nu Y_\nu^\dagger$ have entries typically smaller than 1. This condition turns out to be satisfied for the range of RH neutrino masses we are interested in, and we will comment more on this in section 4.

We now use the formal definition of the spurions to determine the scaling of the Wilson coefficients of the higher dimensional operators. They are summarized in table 2 for the $d = 5$ operators and in table 3 for the $d = 6$ operators. For the $d = 6$ case we only show the operators that contain one or more RH neutrino fields, while for $d = 5$ we also show the Weinberg operator [40], due to its connection with the generation of neutrino masses. In table 3 the $\times$ symbol denotes the direct product between the two composite spurions. The flavor indices are contracted within the brackets. When more than one contraction of flavor indices is possible, we show only the less suppressed spurion combination.[3] In both tables we indicate with the subscripts S and A the symmetric and antisymmetric flavor combinations. This comes from the fact that the operators $\mathcal{O}^5_{NH}$ and $\mathcal{O}^5_{NB}$ are symmetric and antisymmetric in the $\mathcal{N}$ flavor indices respectively. The same applies to the O^6_{4N} operator. The latter also violates lepton number by four units and identically vanishes when all the four RH neutrinos are identical. In table 2 and table 3 we also indicate whether the operators are expected to arise at tree level or at loop level in a generic ultraviolet (UV) completion as discussed in refs. [41, 42]. This will add an additional

[3]For instance, in the case of the $\mathcal{O}^6_{Ne}$ operator, we have an additional flavor combination in which the flavor index of $\bar{N}_R$ is contracted with the flavor index of e_R via a $\mathcal{S}^\dagger_\nu \mathcal{S}_e$ spurion (and the conjugate for the other flavor indices). This contribution is suppressed with respect to the one we show in table 3.

JHEP06(2020)185

Operators involving the Higgs boson			
	Operator	Scaling	Loop generated
$\mathcal{O}^6_{LNH}$	$(\bar{L}\tilde{H}N_R)(H^\dagger H) + \text{h.c.}$	$\mathcal{S}_\nu$	✗
$\mathcal{O}^6_{LNB}$	$(\bar{L}\sigma^{\mu\nu}N_R)B_{\mu\nu}\tilde{H} + \text{h.c.}$	$\mathcal{S}_\nu$	✓
$\mathcal{O}^6_{LNW}$	$(\bar{L}\sigma^{\mu\nu}N_R)\sigma^a W^a_{\mu\nu}\tilde{H} + \text{h.c.}$	$\mathcal{S}_\nu$	✓
$\mathcal{O}^6_{NH}$	$(\bar{N}_R\gamma^\mu N_R)(H^\dagger i\overleftrightarrow{D}_\mu H)$	$\mathcal{S}_{NN^\dagger}$	✗
$\mathcal{O}^6_{NeH}$	$(\bar{N}_R\gamma^\mu e_R)(\tilde{H}^\dagger i\overleftrightarrow{D}_\mu H) + \text{h.c.}$	$\mathcal{S}_{\nu^\dagger}\mathcal{S}_e$	✗
Operators unsuppressed by MFV			
	Operator	Scaling	Loop generated
$\mathcal{O}^6_{Ne}$	$(\bar{N}_R\gamma^\mu N_R)(\bar{e}_R\gamma_\mu e_R)$	$\mathcal{S}_{NN^\dagger} \times \mathcal{S}_{ee^\dagger}$	✗
$\mathcal{O}^6_{Nu}$	$(\bar{N}_R\gamma^\mu N_R)(\bar{u}_R\gamma_\mu u_R)$	$\mathcal{S}_{NN^\dagger} \times \mathcal{S}_{uu^\dagger}$	✗
$\mathcal{O}^6_{Nd}$	$(\bar{N}_R\gamma^\mu N_R)(\bar{d}_R\gamma_\mu d_R)$	$\mathcal{S}_{NN^\dagger} \times \mathcal{S}_{dd^\dagger}$	✗
$\mathcal{O}^6_{Nq}$	$(\bar{N}_R\gamma^\mu N_R)(\bar{q}_L\gamma_\mu q_L)$	$\mathcal{S}_{NN^\dagger} \times \mathcal{S}_{qq^\dagger}$	✗
$\mathcal{O}^6_{NL}$	$(\bar{N}_R\gamma^\mu N_R)(\bar{L}_L\gamma_\mu L_L)$	$\mathcal{S}_{NN^\dagger} \times \mathcal{S}_{LL^\dagger}$	✗
$\mathcal{O}^6_{NN}$	$(\bar{N}_R\gamma^\mu N_R)(\bar{N}_R\gamma_\mu N_R)$	$\mathcal{S}_{NN^\dagger} \times \mathcal{S}_{NN^\dagger}$	✗
Other operators suppressed by MFV			
	Operator	Scaling	Loop generated
$\mathcal{O}^6_{4N}$	$(\bar{N}^c_R N_R)(\bar{N}^c_R N_R) + \text{h.c.}$	$[\mathcal{S}_{N^*N^\dagger} \times \mathcal{S}_{N^*N^\dagger}]_S$	✗
$\mathcal{O}^6_{Nedu}$	$(\bar{N}_R\gamma^\mu e_R)(\bar{d}_R\gamma_\mu u_R)$	$\mathcal{S}_{\nu^\dagger}\mathcal{S}_e \times \mathcal{S}_{d^\dagger}\mathcal{S}_u$	✗
$\mathcal{O}^6_{NLqu}$	$(\bar{N}_R L)(\bar{q}_L u_R) + \text{h.c.}$	$\mathcal{S}_{\nu^\dagger} \times \mathcal{S}_u$	✗
$\mathcal{O}^6_{LNqd}$	$(\bar{L}N_R)\varepsilon(\bar{q}_L d_R) + \text{h.c.}$	$\mathcal{S}_\nu \times \mathcal{S}_d$	✗
$\mathcal{O}^6_{LdqN}$	$(\bar{L}d_R)\varepsilon(\bar{q}_L N_R) + \text{h.c.}$	$\mathcal{S}_\nu \times \mathcal{S}_d$	✗
$\mathcal{O}^6_{LNLe}$	$(\bar{L}N_R)\varepsilon(\bar{L}e_R) + \text{h.c.}$	$\mathcal{S}_\nu \times \mathcal{S}_e$	✗
L and B violating four fermions operators			
$\mathcal{O}^6_{uddN}$	$(\bar{u}^c_R d_R \bar{d}^c_R)N_R + \text{h.c.}$	✗	✗
$\mathcal{O}^6_{qqdN}$	$(\bar{q}^c_L \varepsilon q_L \bar{d}^c_R)N_R + \text{h.c.}$	✗	✗

Table 3. Dimension six operators involving a RH neutrino N_R [37]. We also show the scaling of the Wilson coefficients in terms of the spurions of eq. (3.7), eq. (3.8) and eq. (3.9), and if they are generated at one loop in a general UV completion. The classification is useful in the discussion of the phenomenological implications of MFV, see sections 6 and 7.

suppression factors $\propto (4\pi)^{-2}$ to the corresponding spurion and it will be important when discussing the phenomenological implications of these operators. Note that we cannot write the L and B number violating operators in table 3 in terms of the spurions introduced so far, since an additional source of B number violation would be needed, see section 6.4.

JHEP06(2020)185

4 Connection with the neutrino mass matrix

After electroweak symmetry breaking (EWSB) the operators $\mathcal{O}^5_{NH}$ and $\mathcal{O}^6_{LNH}$ contribute to the neutrino mass matrix. In this section we study these corrections assuming the MFV ansätz. For definitiveness, we work with $\mathcal{N} = 2$ RH neutrinos, i.e. the minimal number of states with which is possible to generate the observed pattern of neutrino masses and mixings in the limit $\Lambda \to \infty$. By defining $n = (\nu_L, N^c_R)$ the mass Lagrangian $\mathcal{L}_{\rm mass} = -1/2\, \bar{n}^c\, \mathcal{M}\, n + \text{h.c.}$ can be written in terms of the following mass matrix

$$\mathcal{M} = \begin{pmatrix} -[\mathcal{S}^*_{L^*L^\dagger}]_S \frac{v^2}{\Lambda} & Y_\nu v - \mathcal{S}_\nu \frac{v^3}{\Lambda^2} \\ Y_\nu^T v - \mathcal{S}_\nu^T \frac{v^3}{\Lambda^2} & \tilde{M} \end{pmatrix} , \tag{4.1}$$

where we have defined

$$\tilde{M} = M_N - [\mathcal{S}_{N^*N^\dagger}]_S \frac{v^2}{\Lambda} = \left(\epsilon_L - [\mathcal{S}_{N^*N^\dagger}]_S \frac{v^2}{\Lambda^2} \right) \Lambda \ . \tag{4.2}$$

The $\nu_L - \nu_L$ block in eq. (4.1) is generated by the Weinberg operator $\mathcal{O}^5_W$. The $\nu_L - N_R$ block receives a $d = 4$ contribution from the $\bar{L}\tilde{H}N_R$ operator, as well as a $d = 6$ contribution from the operator $\mathcal{O}^6_{LHN}$. The RH neutrino mass matrix $\tilde{M}$ has a $d = 4$ contribution, from M_N, and a $d = 5$ contribution from the operator $\mathcal{O}^5_{NH}$. The former dominates in the MFV ansätz, as can be easily derived from eq. (3.1) and (3.9)

$$M_N = \epsilon_L \Lambda \gg \epsilon_L \Lambda \frac{v^2}{\Lambda^2} \propto [S_{N^*N^\dagger}]_S \frac{v^2}{\Lambda} \ . \tag{4.3}$$

In order to compute the neutrino masses we diagonalize the matrix in eq. (4.1) to first order in the active-sterile mixing, i.e. assuming $Y_\nu v \ll M_N$ (a condition that, as we will see, will be always verified in the allowed region of parameter space). We get

$$m_\nu \simeq [\mathcal{S}^*_{L^*L^\dagger}]_S \frac{v^2}{\Lambda} + v^2 \left(Y_\nu - \mathcal{S}_\nu \frac{v^2}{\Lambda^2} \right) \tilde{M}^{-1} \left(Y_\nu^T - \mathcal{S}_\nu^T \frac{v^2}{\Lambda^2} \right) , \tag{4.4}$$

where we redefined the phase of the LH neutrino fields to change the sign of the neutrino mass matrix m_ν. Although not conventional, this choice allows to simplify the following equations. With our assumption the matrix $\tilde{M}$ can be inverted perturbatively in powers of v/Λ. We obtain

$$\tilde{M}^{-1} \simeq \frac{1}{M_N} + \frac{1}{M_N} [\mathcal{S}_{N^*N^\dagger}]_S \frac{1}{M_N} \frac{v^2}{\Lambda} \ . \tag{4.5}$$

By considering again eq. (3.9) (i.e. $[\mathcal{S}_{N^*N^\dagger}]_S = c\, \epsilon_L + \dots$), we can write this quantity as

$$\tilde{M}^{-1} = \frac{1}{M_N} \left(1 + c \frac{v^2}{\Lambda^2} \right) \ . \tag{4.6}$$

Using this expression in eq. (4.4) and taking $\mathcal{S}_\nu = b Y_\nu$ as it follows from eq. (3.9), we obtain an expression for the neutrino masses as an expansion in v/Λ:

$$m_\nu \simeq [\mathcal{S}^*_{L^*L^\dagger}]_S \frac{v^2}{\Lambda} + v^2 Y_\nu \frac{1}{M_N} Y_\nu^T \left(1 + (c - b) \frac{v^2}{\Lambda^2} \right) + \dots \ . \tag{4.7}$$

JHEP06(2020)185

We will now use the leading expression of the Weinberg operator computed according to eq. (3.9), i.e. $[\mathcal{S}^*_{L^*L^\dagger}]_S = aY_\nu \epsilon_L Y_\nu^T + \ldots$, to write the neutrino mass matrix as

$$m_\nu \simeq v^2\, Y_\nu \frac{\left(1+(c-b)\frac{v^2}{\Lambda^2}\right)\mathbb{1} + a\,\epsilon_L^2}{M_N} Y_\nu^T = U^* m_\nu^{(d)} U^\dagger \ . \tag{4.8}$$

In the last expression we have introduced the Pontecorvo-Maki-Nakagawa-Sakata (PMNS) matrix U [43, 44], and the matrix $m_\nu^{(d)}$ is diagonal with non negative entries. In the following, we will fix the phases of the PMNS matrix to zero and the mixing angles to their latest fit [1], unless otherwise specified. Using eq. (4.8) we can write

$$Y_\nu \simeq \frac{1}{v} U^* \sqrt{\mu}\, \frac{\sqrt{M_N}}{\sqrt{\left(1+(c-b)\frac{v^2}{\Lambda^2}\right)\mathbb{1} + a\epsilon_L^2}} \,, \tag{4.9}$$

where $\sqrt{\mu}$ is a 3×2 matrix satisfying $\sqrt{\mu}\sqrt{\mu}^T = m_\nu^{(d)}$. This allows us to write a compact expressions for the various matrices involved. The most general form this matrix can take in the case of normal (NH) and inverted hierarchy (IH) is

$$\sqrt{\mu_{\rm NH}} = \begin{pmatrix} 0 & 0 \\ -\sin z\sqrt{m_2} & \pm\cos z\sqrt{m_2} \\ \cos z\sqrt{m_3} & \pm\sin z\sqrt{m_3} \end{pmatrix} , \qquad \sqrt{\mu_{\rm IH}} = \begin{pmatrix} -\sin z\sqrt{m_1} & \pm\cos z\sqrt{m_1} \\ \cos z\sqrt{m_2} & \pm\sin z\sqrt{m_2} \\ 0 & 0 \end{pmatrix} , \tag{4.10}$$

where m_i are the physical neutrino masses for the two hierarchies.[4] In the expressions above the angle z can be taken complex. This is the so-called Casas-Ibarra parametrization [45], which can be written as

$$\sqrt{\mu_{\rm NH}} = \begin{pmatrix} 0 & 0 \\ 0 & \sqrt{m_2} \\ \sqrt{m_3} & 0 \end{pmatrix} \mathcal{R} \equiv \sqrt{m_{\rm NH}}\mathcal{R} \,, \qquad \sqrt{\mu_{\rm IH}} = \begin{pmatrix} 0 & \sqrt{m_1} \\ \sqrt{m_2} & 0 \\ 0 & 0 \end{pmatrix} \mathcal{R} \equiv \sqrt{m_{\rm IH}}\mathcal{R} \,, \tag{4.11}$$

where $\mathcal{R}$ is a generic complex 2×2 matrix satisfying $\mathcal{R}\mathcal{R}^T = \mathbb{1}$

$$\mathcal{R} = \begin{pmatrix} \cos z & \pm\sin z \\ -\sin z & \pm\cos z \end{pmatrix} \ . \tag{4.12}$$

This form includes matrices with $\det\mathcal{R} = 1$ (proper rotations, to which the $+$ sign applies) and matrices with $\det\mathcal{R} = -1$ (to which the $-$ sign applies). A similar expression can be written in the inverted hierarchy case. Overall, for both hierarchies we write

$$Y_\nu \simeq \frac{1}{v} U^* \sqrt{m}\,\mathcal{R}\, \frac{\sqrt{M_N}}{\sqrt{\left(1+(c-b)\frac{v^2}{\Lambda^2}\right)\mathbb{1} + a\epsilon_L^2}} \,, \tag{4.13}$$

[4] We remind that with two RH neutrinos in the NH case $m_{\nu_3} > m_{\nu_2}$ and $m_{\nu_1} = 0$ while in the IH case $m_{\nu_2} > m_{\nu_1}$ and $m_{\nu_3} = 0$. For the NH case we take $m_{\nu_2} = 8.6\times 10^{-3}\,$eV and $m_{\nu_3} = 4.9\times 10^{-2}\,$eV while for the IH we take $m_{\nu_1} = 5.0\times 10^{-2}\,$eV and $m_{\nu_2} = 5.1\times 10^{-2}\,$eV.

JHEP06(2020)185

where $\sqrt{m}$ is any of the two matrices defined in eq. (4.11). The active sterile neutrino mixing thus reads

$$\begin{aligned}\theta_{\nu N} &\simeq -v\left(Y_\nu - \mathcal{S}_\nu \frac{v^2}{\Lambda^2}\right)\frac{1}{\tilde{M}} + 2\,a\,\frac{v^2}{\Lambda}[\mathcal{S}^*_{L^*L^\dagger}]_S\left(Y_\nu - \mathcal{S}_\nu\frac{v^2}{\Lambda^2}\right)v\,\frac{1}{\tilde{M}^2} \\ &\simeq -v\,Y_\nu\,\frac{1}{M_N}\left[\left(1+(2c-b)\frac{v^2}{\Lambda^2}\right)\mathbb{1} - 2\,a\,\frac{v^2}{\Lambda^2}M_N^2 Y_\nu^T Y_\nu \frac{1}{M_N^2} + \dots\right] \\ &\simeq -U^*\sqrt{m}\mathcal{R}\frac{1}{\sqrt{M_N}} + \dots\ .\end{aligned} \tag{4.14}$$

In the limit of *real* orthogonal $\mathcal{R}$ matrix it is easy to estimate the order of magnitude of the entries of Y_ν. Taking U and $\mathcal{R}$ with generic $\mathcal{O}(1)$ entries and degenerate masses for the RH neutrinos, $M_{N_1} = M_{N_2} = M_{N_{1,2}}$, we conclude that for both hierarchies the entries of Y_ν scale as shown in eq. (1.1),

$$Y_\nu \sim \frac{\sqrt{M_{N_{1,2}} m_\nu}}{v} \sim 4\times 10^{-8}\left(\frac{M_{N_{1,2}}}{1\,\text{GeV}}\right)^{1/2}\ . \tag{4.15}$$

For the numerical estimate we have assumed NH and $m_\nu = m_{\nu_3}$, but the expression is valid also for IH apart from small numerical factors. We have neglected corrections proportional to $(v/\Lambda)^2$ or ϵ_L^2. This naive estimate can be challenged by turning on the imaginary part of the z angle of the $\mathcal{R}$ matrix. Writing $z = \alpha + i\gamma$ and taking the $\gamma \gg 1$ limit, we obtain

$$\mathcal{R} \simeq \frac{e^{\gamma - i\alpha}}{2}\begin{pmatrix} 1 & \pm i \\ -i & \pm 1\end{pmatrix}\ . \tag{4.16}$$

We see that the imaginary part of the angle z can break the naive see-saw scaling, and we thus need to modify eq. (4.15). The correct estimate in the $\gamma \gg 1$ limit is

$$Y_\nu \sim 2\times 10^{-8}\, e^{\gamma - i\alpha}\left(\frac{M_{N_{1,2}}}{1\,\text{GeV}}\right)^{1/2}\ . \tag{4.17}$$

The active-sterile mixing clearly has the same enhancement behavior and its entries read

$$\theta_{i,\alpha} \equiv (\theta_{\nu N})_{i\alpha} \sim 7.2\times 10^{-6}\, e^{\gamma - i\alpha}\left(\frac{1\,\text{GeV}}{M_{N_{1,2}}}\right)^{1/2}\ . \tag{4.18}$$

In the previous expression $\alpha = 1,\, 2$, $i = e, \mu, \tau$ and we show only the lowest order in v/Λ and ϵ_L. Higher orders can be easily taken into account, but for the range of masses we are interested in, and taking $\Lambda \gtrsim 1\,\text{TeV}$, such corrections are at most of order 1% and we will neglect them.

The mixing angles are constrained by a variety of experimental searches and large value of γ are ruled out. Using the bounds on $\theta_i = \sum_{\alpha=1,2}|\theta_{i,\alpha}|^2$, with $i = e, \mu, \tau$, reported in [46–48] we show in figure 1 the allowed region in the $M_N - \gamma$ plane, assuming degenerate masses for N_1 and N_2 and neglecting the small Λ dependence. For concreteness we show only the most stringent bound, coming from θ_μ. The bound applies for both hierarchies.[5]

[5]Strictly speaking, in the case of IH the most stringent bound for masses below 70 GeV is the one coming from θ_e. Numerically however the bound is only slightly more stringent than the θ_μ one. For simplicity we therefore only show the latter.

JHEP06(2020)185

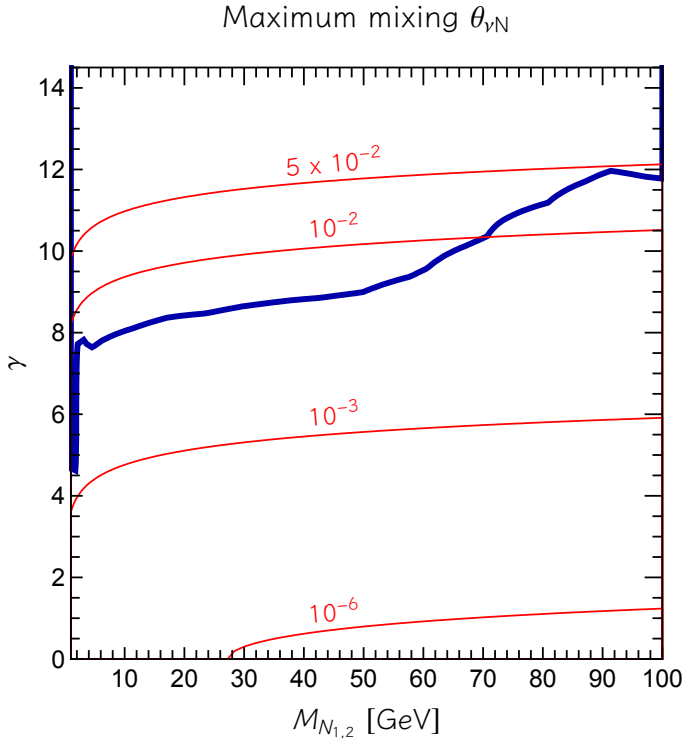

Figure 1. Constraints on the mixing angles $\theta_i = \sum_{\alpha=1,2} |\theta_{i,\alpha}|^2$ in the $M_N - \gamma$ plane, where the masses of the RH neutrinos are taken degenerate with a value $M_{N_{1,2}}$. The region above the colored thick line is excluded by the bounds on active-sterile mixing angles [46–48]. We show only the most restrictive bound for NH hierarchy, i.e. the one coming from the θ_μ. The red thin lines show the corresponding maximum value of the active-sterile mixing angle computed according to eq. (4.14).

For $M_{N_{1,2}} = (1 \div 100)\,\text{GeV}$ we see that values of γ up to ~ 8 are allowed by existing constraints. We also show the maximum value of the active-sterile mixing matrix computed according to eq. (4.14). As we can see, for low values $\gamma \sim 1 \div 2$ the maximum mixing is of order 10^{-6}, and it increases until a maximum value of 5% for $\gamma \simeq 12$ and $M_{N_{1,2}} \simeq (80 \div 100)\,\text{GeV}$. These values leave us safely within the range of the perturbative diagonalization performed to derive eq. (4.1). These values for the $\theta_{\nu N}$ matrix will be important in the spurion discussion in section 5 and section 6.

With this information we can go back to a point already raised in section 3. Implicit in the definitions of eq. (3.2), eq. (3.3) and eq. (3.4) is the fact that we can expand in Y_ν, so schematically one requires $Y_\nu^{ij} \lesssim 1$. For this to be true we need

$$e^\gamma \lesssim 0.5 \times 10^8 \left(\frac{1\,\text{GeV}}{M_{N_{1,2}}}\right)^{1/2} . \tag{4.19}$$

This gives $\gamma \lesssim 15\,(17)$ for $M_{N_{1,2}} = 1\ (100)\,\text{GeV}$. We conclude that whenever the experimental bounds on the active-sterile mixing are satisfied the expansion holds and we can keep only the lowest order terms in the spurion expansions.

JHEP06(2020)185

5 Hierarchies between the composed spurions: d=5 operators

We now use the parametrization of section 3 and the constraints of section 4 to express the composed spurions of eq. (3.2), eq. (3.3) and eq. (3.4) in terms of fundamental spurions. The aim is to understand their order of magnitude and the relative importance of the Wilson coefficients of the $d = 5$ operators.

5.1 Operator $\mathcal{O}^5_{NH}$

The $\mathcal{O}^5_{NH}$ operator has a Wilson coefficient proportional to the symmetric part of the $\mathcal{S}_{N^*N^\dagger}$ spurion. Working at the next-to-leading order in Y_ν or ϵ_L, we have

$$\mathcal{S}_{N^*N^\dagger} = a_0\,\epsilon_L + a_1 Y_\nu^T Y_\nu^* \epsilon_L + a_2 \epsilon_L Y_\nu^\dagger Y_\nu + a_3 \epsilon_L \epsilon_L^* \epsilon_L + \dots\,, \tag{5.1}$$

where the coefficients a_i are of order unity and, as already pointed out, the entries of the bilinears built from Y_ν are somewhat smaller than unity. The relevant combination for the $\mathcal{O}^5_{NH}$ operator is the flavor symmetric, and we thus have

$$\begin{aligned}[\mathcal{S}_{N^*N^\dagger}]_S &\simeq (a_0 + a_3 \epsilon_L \epsilon_L^*)\,\epsilon_L + \frac{a_1+a_2}{2}\left(Y_\nu^T Y_\nu^* \epsilon_L + \epsilon_L Y_\nu^\dagger Y_\nu\right) \\ &\simeq a_0 \frac{M_N}{\Lambda} + a_3 \frac{M_N^3}{\Lambda^3} + \frac{a_1+a_2}{2\,v^2\,\Lambda}\left(M_N^{1/2}\mathcal{R}^T \tilde{m}_\nu \mathcal{R}^* M_N^{3/2} + M_N^{3/2}\mathcal{R}^\dagger \tilde{m}_\nu \mathcal{R} M_N^{1/2}\right),\end{aligned} \tag{5.2}$$

where we have defined $\tilde{m}_\nu \equiv \sqrt{m}^T \sqrt{m}$. In the expression for Y_ν we kept only the leading terms in v/Λ and ϵ_L. For both normal and inverted hierarchy this matrix reads

$$\tilde{m}_\nu = \begin{pmatrix} m_{\text{heavy}} & 0 \\ 0 & m_{\text{light}} \end{pmatrix}, \tag{5.3}$$

where $m_{\text{heavy}} = m_3(m_2)$ and $m_{\text{light}} = m_2(m_1)$ in the normal (inverted) case. Using this expression in eq. (5.2) together with eq. (4.12) we obtain

$$\begin{aligned}[\mathcal{S}_{N^*N^\dagger}]_S \simeq \frac{M_N}{\Lambda}&\left[a_0 + \frac{a_1+a_2}{v^2} M_N \left(\bar{m}\cosh(2\gamma)\mathbb{1} + \Delta m \cos(2\alpha)\sigma_3\right) + a_3 \frac{M_N^2}{\Lambda^2}\right] \\ &\pm \frac{(a_1+a_2)\sqrt{M_1 M_2}}{v^2\,\Lambda}\left(\bar{M}\,\Delta m \sin(2\alpha) - i\Delta M\,\bar{m}\sinh(2\gamma)\right)\sigma_1\,,\end{aligned} \tag{5.4}$$

where σ_1 and σ_3 are the Pauli matrices. To simplify the equation we have defined $\bar{m} = (m_{\text{light}} + m_{\text{heavy}})/2$ and $\Delta m = (m_{\text{heavy}} - m_{\text{light}})/2$ for the light neutrinos, $\bar{M} = (M_1 + M_2)/2$ and $\Delta M = (M_2 - M_1)/2$ for the RH neutrinos. As expected, we see that the terms in eq. (5.2) arising from the neutrino Yukawa matrix are suppressed by the mass scale of the neutrinos $\bar{m}$ or their mass difference Δm. As a consequence, only the terms exponentially enhanced by the imaginary part of the z rotation angle in the $\mathcal{R}$ matrix, see eq. (4.12), can be important when $\gamma \gg 1$. By taking the limit of degenerate RH neutrino masses $\Delta M \to 0$ we obtain

$$[\mathcal{S}_{N^*N^\dagger}]_S^{NH} \simeq \frac{\bar{M}}{\Lambda}\left(a_0 + a_3\frac{\bar{M}^2}{\Lambda^2} + 10^{-13}\,(a_1+a_2)\cosh(2\gamma)\frac{\bar{M}}{100\,\text{GeV}}\right)\times \mathbb{1}\,, \tag{5.5}$$

JHEP06(2020)185

where we have neglected entries suppressed by the neutrino mass scale or mass difference not proportional to an hyperbolic function of γ. The same expression is valid for both hierarchies apart from $\mathcal{O}(1)$ factors. In the case of non degenerate RH neutrino mass there will be an off-diagonal exponentially enhanced term proportional to σ_1. Note that the term proportional to the Yukawa coupling grows with $\bar{M}$ and γ. Considering the experimentally allowed region in figure 1, we see that for $\bar{M} \simeq 100\,\text{GeV}$ and $\gamma \simeq 12$ this term can be at most an order 10^{-3} correction to the leading contribution for both hierarchies. Importantly, and as already noticed in [22], the operator $\mathcal{O}^5_{NH}$ is not suppressed by a Yukawa at leading order, although it turns out to be suppressed by ϵ_L also in the $M_N \sim \mathbb{1}$ limit in which the $\text{SU}(2)_N$ factor in $\mathcal{G}_L$ reduces to $\text{SO}(2)_N$.

5.2 Operator $\mathcal{O}^5_{NB}$

Moving to the $\mathcal{O}^5_{NB}$ operator, the relevant contribution is now the antisymmetric one, which reads

$$\begin{aligned}[\mathcal{S}_{N^*N^\dagger}]_A &\simeq \frac{a_1 - a_2}{2}\left(Y_\nu^T Y_\nu^* \epsilon_L - \epsilon_L Y_\nu^\dagger Y_\nu\right) \\ &\simeq \frac{a_1 - a_2}{2\,v^2\,\Lambda}\left(M_N^{1/2}\mathcal{R}^T \tilde{m}_\nu \mathcal{R}^* M_N^{3/2} - M_N^{3/2}\mathcal{R}^\dagger \tilde{m}_\nu \mathcal{R} M_N^{1/2}\right)\,.\end{aligned} \tag{5.6}$$

Again, we keep only terms at the smallest order in v/Λ and ϵ_L. Using the expression for $\tilde{m}_\nu$ of eq. (5.3) together with eq. (4.12) we obtain the simple expression

$$[\mathcal{S}_{N^*N^\dagger}]_A \simeq \pm\frac{(a_1 - a_2)\sqrt{M_1 M_2}}{v^2\,\Lambda}\left[\bar{m}\,\bar{M}\sinh(2\gamma) + i\Delta m\,\Delta M \sin(2\alpha)\right]\sigma_2\,, \tag{5.7}$$

where σ_2 is the second Pauli matrix. Note that in the $\text{SU}(2)_N \to \text{SO}(2)$ limit the second term vanishes, and we are left with a dependence on γ only. In this limit we obtain

$$[\mathcal{S}_{N^*N^\dagger}]_A \simeq \pm\,10^{-13}(a_1 - a_2)\,\sinh(2\gamma)\left(\frac{\bar{M}}{\Lambda}\right)\frac{\bar{M}}{100\,\text{GeV}} \times \sigma_2\,, \tag{5.8}$$

where the same expression is valid for both hierarchies, apart from $\mathcal{O}(1)$ numerical factors, and the high suppression due to the active neutrino mass scale is evident. We conclude that RH neutrinos production processes mediated by the $\mathcal{O}^5_{NB}$ operator, such as $pp \to \gamma, Z \to N_1 N_2$, turn out the be completely irrelevant if MFV is imposed, while heavy to light decay as e.g., $N_2 \to N_1\gamma, N_1 Z$ will have a highly suppressed partial width.

5.3 Operator $\mathcal{O}^5_W$

The Weinberg operator carries the spurion $[\mathcal{S}_{L^*L^\dagger}]_S$, which starts its expansion as

$$[\mathcal{S}_{L^*L^\dagger}]_S \simeq Y_\nu^*\,\epsilon_L\,Y_\nu^\dagger + \cdots \simeq \frac{1}{v^2}U\sqrt{m}\mathcal{R}^*\frac{M_N^2}{\Lambda\sqrt{\mathbb{1} + a\epsilon_L^2}}\mathcal{R}^\dagger\sqrt{m}U^T\,. \tag{5.9}$$

In the limit of degenerate RH neutrino masses the Casas-Ibarra matrix disappears from the expression. For non-degenerate RH neutrinos, however, there is a residual γ dependence

JHEP06(2020)185

that could make this term large. The potentially large term can be easily isolated by writing $M_N = \bar{M}\mathbb{1} - \Delta M \sigma_3$. To leading order in v/Λ and ϵ_L we obtain

$$[\mathcal{S}_{L^* L^\dagger}]_S \simeq \frac{\bar{M}^2 + \Delta M^2}{v^2\,\Lambda} m_\nu - \frac{2\Delta M\,\bar{M}}{v^2\,\Lambda} U^* \sqrt{m}\mathcal{R}\sigma_3\mathcal{R}^T\sqrt{m}^T U^\dagger \ . \tag{5.10}$$

Interestingly, the spurion of the Weinberg operator is not simply proportional to the light neutrino masses for non-degenerate heavy neutrinos. This in a explicit demonstration that there can be lepton number breaking effects that the neutrino mass is not sensitive to at tree level, as well known in the so-called extended see-saw scenarios [49]. Indeed, the second term in eq. (5.10) enhanced by γ gets cancelled against the second term in eq. (4.7) in the neutrino mass matrix, but could be parametrically much larger than the latter if γ and ΔM are large enough. On the contrary, for $\Delta M = 0$ and large γ , one can show that there is effectively an approximate lepton number symmetry (that assigns opposite lepton number charges to the two N_R fields), which suppresses the neutrino mass and any other lepton number breaking effect, but this not the case for non-degenerate neutrinos.

6 Hierarchies between the composed spurions: d=6 operators

We now analyze the scaling of the Wilson coefficients of the $d = 6$ operators. Unlike what we did in section 5, for these operators we find more convenient to organize the discussion in terms of the spurions. We follow the classification outlined in table 3. We start from the operators involving the Higgs field because they will be the most relevant for the phenomenological considerations of section 7. Inspecting table 3 we immediately see that we can classify them in three categories: (i) operators that scale like $\mathcal{S}_\nu$,namely $\mathcal{O}^6_{LHN}$, $\mathcal{O}^6_{LNB}$ and $\mathcal{O}^6_{LNW}$, (ii) operators that scale like $\mathcal{S}_{NN^\dagger}$, namely $\mathcal{O}^6_{NH}$, and (iii) operators that scale like $\mathcal{S}_{\nu^\dagger}\mathcal{S}_e$, namely $\mathcal{O}^6_{NeH}$. We will then comment on the scaling of the other spurions.

6.1 Spurion $\mathcal{S}_\nu$

Let us start with the spurion $\mathcal{S}_\nu$. From eq. (3.8) we can write it as

$$\mathcal{S}_\nu = a_0 Y_\nu + a_1 Y_\nu Y_\nu^\dagger Y_\nu + a_2 Y_e Y_e^\dagger Y_\nu + \dots \tag{6.1}$$

We will now show that $\mathcal{S}_\nu \simeq Y_\nu$ apart from corrections at most of order $\mathcal{O}(10^{-3})$. To see this it is easier to rewrite eq. (6.1) in terms of the mixing angle matrix $\theta_{\nu N}$ of eq. (4.14). We obtain

$$\mathcal{S}_\nu = \left[a_0 + a_1\,\frac{\theta_{\nu N} M_N^2 \theta_{\nu N}^\dagger}{v^2} + a_2\,\lambda_e^2\right] Y_\nu + \dots \ . \tag{6.2}$$

Remembering now that in the experimentally allowed region of figure 1 the entries of the $\theta_{\nu N}$ matrix are at most of order 5%, we conclude that we can write

$$\mathcal{S}_\nu \lesssim \left[a_0 + a_1 \times 10^{-3}\left(\frac{M_{N_{1,2}}}{100\,\text{GeV}}\right)^2 + a_2 \times 10^{-4}\right] Y_\nu + \dots \tag{6.3}$$

JHEP06(2020)185

as claimed above. In what follows we will always take $\mathcal{S}_\nu \simeq Y_\nu$. To obtain an approximate expression for Y_ν (and therefore for the spurion $\mathcal{S}_\nu$) we write it in the limit of degenerate light and heavy neutrinos masses. The light neutrino mass scale will be denoted by m, and the RH neutrino mass scale with M. To simplify further the expressions, we will take the limit $\theta_{13} \to 0$ and $\theta_{12} \to \pi/4$ in the PMNS matrix. In the case of normal hierarchy we obtain

$$Y_\nu^{(\mathrm{NH})} \simeq \cosh(\gamma - i\alpha)\frac{\sqrt{m\,M}}{v}\begin{pmatrix} -\frac{i}{\sqrt{2}} & \pm\frac{1}{\sqrt{2}} \\ -i\,\tilde{c}_{23} & \pm\tilde{c}_{23} \\ i\,\tilde{s}_{23} & \mp\tilde{s}_{23} \end{pmatrix}, \tag{6.4}$$

where we have defined $\tilde{c}_{23} \equiv c_{23}/\sqrt{2} + i s_{23}$ and $\tilde{s}_{23} = s_{23}/\sqrt{2} - i c_{23}$ in terms of $s_{23} = \sin\theta_{23}$ and $c_{23} = \cos\theta_{23}$, with θ_{23} the atmospheric angle of the PMNS matrix. In the case of inverted hierarchy we instead obtain

$$Y_\nu^{(\mathrm{IH})} \simeq \cosh(\gamma - i\alpha)\frac{\sqrt{m\,M}}{v}\,e^{-i\pi/4}\begin{pmatrix} 1 & \pm i \\ i\,c_{23} & \mp c_{23} \\ -i\,s_{23} & \pm s_{23} \end{pmatrix}. \tag{6.5}$$

6.2 Spurion $\mathcal{S}_{NN^\dagger}$

We now analyze the spurion $\mathcal{S}_{NN^\dagger}$, which appears in the operator $\mathcal{O}^6_{NH}$. At leading order this spurion can be expanded as

$$\begin{aligned} \mathcal{S}_{NN^\dagger} &\simeq a_0\mathbb{1} + a_1\epsilon_L^*\epsilon_L + a_2 Y_\nu^\dagger Y_\nu + \dots \\ &\simeq a_0\mathbb{1} + a_1\frac{M_N^2}{\Lambda^2} + \frac{a_2}{v^2}M_N^{1/2}\mathcal{R}^\dagger\tilde{m}_\nu\mathcal{R}M_N^{1/2} + \dots \\ &\simeq a_0\mathbb{1} + a_1\frac{M_N^2}{\Lambda^2} + \frac{M_N}{v^2}\Big(\bar{m}\cosh(2\gamma)\mathbb{1} + \Delta m\cos(2\alpha)\sigma_3\Big) \\ &\quad \pm \frac{\sqrt{M_1 M_2}}{v^2}\Big(\Delta m\sin(2\alpha)\sigma_1 - \bar{m}\sinh(2\gamma)\sigma_2\Big) \;\simeq \mathbb{1}\left(a_0 + a_1\frac{M_N^2}{\Lambda^2}\right). \end{aligned} \tag{6.6}$$

where we omit to write terms of order $O(10^{-15}) \times \cosh(2\gamma)$ which are always negligible for any allowed value of the angle γ.

6.3 Spurion $\mathcal{S}_{\nu^\dagger}\mathcal{S}_e$

We now move on to the spurion combination $\mathcal{S}_{\nu^\dagger}\mathcal{S}_e$ appearing in the scaling of the operator $\mathcal{O}^6_{NeH}$. As shown in section 6.1, the dominant term in the expansion of the spurion $\mathcal{S}_\nu$ is given by Y_ν. At the same time, it is clear from eqs. (3.10) and (3.8) that the dominant term in the expansion of $\mathcal{S}_e$ is given by Y_e.[6] Putting all together we conclude that

$$\mathcal{S}_{\nu^\dagger}\mathcal{S}_e \simeq a_0\, Y_\nu^\dagger\, Y_e + \dots \tag{6.7}$$

Given the small entries in the diagonal λ_e matrix, eq. (3.10), we see that the entries of $\mathcal{S}_{\nu^\dagger}\mathcal{S}_e$ are suppressed with respect to Y_ν, Eq (4.13). The minimal suppression, by a factor of order 10^{-2}, involves the charged leptons of the third generation.

[6] As for the case of the spurion $\mathcal{S}_{NN^\dagger}$ in section 6.2, the dominant term in the expansion of the spurion $\mathcal{S}_{LL^\dagger}$ appearing in eq. (3.8) is the one proportional to the identity.

JHEP06(2020)185

6.4 Additional spurions

Using the results presented above it is immediate to compute the leading terms in the expansion of the Wilson coefficients of the remaining operators in table 3. More specifically, the dominant term for all the unsuppressed operators is proportional to the identity

$$\mathcal{S}_{XX^\dagger} \simeq \mathcal{O}(1), \quad X = e, u, d, q, L, N. \tag{6.8}$$

The remaining suppressed operators in table 3 scale as

$$\begin{gathered}
[\mathcal{S}_{N^*N^\dagger} \times \mathcal{S}_{N^*N^\dagger}]_S \simeq \left(\frac{M_N}{\Lambda}\right) \times \left(\frac{M_N}{\Lambda}\right), \quad \mathcal{S}_{\nu^\dagger}\mathcal{S}_e \times \mathcal{S}_{d^\dagger}\mathcal{S}_u \simeq \left(Y_\nu^\dagger Y_e\right) \times \left(Y_d^\dagger Y_u\right), \\
\mathcal{S}_{\nu^\dagger} \times \mathcal{S}_u \simeq \left(Y_\nu^\dagger\right) \times (Y_u), \qquad \mathcal{S}_\nu \times \mathcal{S}_d \simeq (Y_\nu) \times (Y_d),
\end{gathered} \tag{6.9}$$

and

$$\mathcal{S}_\nu \times \mathcal{S}_e \simeq (Y_\nu) \times (Y_e) \ . \tag{6.10}$$

Finally, the Wilson coefficient of the operators that violate both B and L number cannot be written solely in terms of the spurions we have introduced. Additional sources of baryon and lepton number violation are needed.[7]

7 Phenomenological implications

We have seen that MFV ansätz implies very different sizes for the coefficients of the effective operators reported in table 3, and this has important consequences for present and future collider searches of RH neutrinos in the $[1 \div 100]$ GeV range, as well as on their interpretation in terms of a given model structure. The main result of the analysis in the previous section is that operators with two RH neutrinos that preserve lepton number, that is $\mathcal{O}^6_{NX}$ with $X = e, u, d, q, L, H$, are the only ones that involve interactions with the SM particles and that can have coefficients of $\mathcal{O}(1)$ under the MFV hypothesis.[8] These are therefore the interactions that could compete with the active-sterile mixing effects to enhance the production of RH neutrinos at colliders, that would necessarily then be produced in pairs. There is a different operator that contains two RH neutrinos, $\mathcal{O}^5_{NH}$. This breaks lepton number and has then an ϵ_L but no suppression in the Yukawa couplings. On the other hand, all operators that contain a single RH neutrino, and therefore could contribute to their decay, are suppressed by at least one power of Y_ν, i.e. they have the same parametric dependence of the active-sterile mixing $\theta_{\nu N}$. In this section we will comment on how the MFV hypothesis influences searches in present and future colliders. A detailed analysis of their reach is beyond the scope of this paper and is left for future work [50]. In table 4 we summed up the scaling of the relevant spurions, which can be used to easily estimate the suppression under the MFV ansätz of any phenomenological search of interest.

[7] As an example, we can consider the operator $\mathcal{O}^6_{uddN}$. This can be obtained at tree level introducing a Yukawa term like

$$\mathcal{L} = \lambda_\phi \bar{d}^c_R d_R \tilde{\phi} + \lambda'_\phi \bar{u}^c_R N_R \tilde{\phi}^\dagger \,, \tag{6.11}$$

with $\tilde{\phi}$ a new scalar field with quantum numbers $(\mathbf{3}, \mathbf{1})_{-2/3}$ under the SM gauge group. Integrating out $\tilde{\phi}$ at tree level one produces the operator $\mathcal{O}^6_{uddN}$, with the Yukawa couplings λ_ϕ and λ'_ϕ acting as new spurion sources of baryon number violation.

[8] This feature was also previously pointed out in ref. [35].

JHEP06(2020)185

Spurion	Leading term
$[\mathcal{S}_{N^*N^\dagger}]_S$	ϵ_L
$[\mathcal{S}_{N^*N^\dagger}]_A$	$Y_\nu^T Y_\nu^* \epsilon_L - \epsilon_L Y_\nu^\dagger Y_\nu$
$[\mathcal{S}_{L^*L^\dagger}]_S$	$Y_\nu^* \epsilon_L Y_\nu^\dagger$
S_X	Y_X
$S_{XX^\dagger}$	$\mathbb{1}$

Table 4. Leading scaling of the spurions analyzed in section 5 and section 6, where $X = e, u, d, q, L, N$. All terms have generic $\mathcal{O}(1)$ factors that we do not write explicitly.

7.1 Exotic Higgs decay

The dimension five $\mathcal{O}_{NH}^5$ operator gives rise to the exotic decay of the SM Higgs into a pair of right handed neutrinos. In ref. [21] the authors investigated the reach of the Large Hadron Collider (LHC) to this interaction, ignoring the effect that dimension six operators could have on their decay lengths. The decay was assumed to be mediated by mixing and resulted in displaced decays, which was an essential feature of the search strategy. Moreover, as long as the decay length in the laboratory frame $L \sim \theta_{\nu N}^2 M_N^6$ is in the ballpark range for displaced vertices searches at LHC, the bound was found to be essentially independent of the RH neutrino mass (clearly in the kinematic region wherethe Higgs decay channel is open). In the most favorable scenario a bound of $\Lambda \gtrsim 160\,\text{TeV}$ was estimated for $300\,\text{fb}^{-1}$ of integrated luminosity at LHC 13TeV.

Under the MFV hypothesis, the Wilson coefficient of this operator has an extra ϵ_L suppression. This weakens the limit on Λ, and introduces a stronger dependence on the RH neutrino mass M_N. We obtain

$$\Lambda \gtrsim 4\,\text{TeV}\sqrt{\frac{\bar{M}}{100\,\text{GeV}}}\,. \tag{7.1}$$

It is crucial that the production channel through the decay of the SM Higgs boson is not suppressed by any Yukawa insertion, as already foreseen in [22]. Any such suppression would reduce the efficiency of the production mechanism for N_R, making it similar to that via mixing and beyond reach of LHC. We stress that even in the limit of degenerate RH neutrino masses the $\mathcal{O}_{NH}^5$ operator still violates lepton number. The MFV assumption then requires its Wilson coefficient to have the same ϵ_L suppression considered above. This implies that also in this case the bounds on the scale Λ are reduced to eq. (7.1).

On the other hand, the unsuppressed operators of dimension six, $\mathcal{O}_{NX}^6$, could potentially provide a more efficient production mechanism, as long as $\epsilon_L < \frac{v}{\Lambda}$, as we discuss in the following.

7.2 Pair production of RH neutrinos at future lepton facilities

We first consider the future International Linear Collider (ILC) operating at a center of mass energy of $\sqrt{s} = 500\,\text{GeV}$. In ref. [19] the authors estimated the reach on the

JHEP06(2020)185

combination $|\theta_e|^2 = \sum_{\alpha=1,2} |\theta_{e,\alpha}|^2$ to be or order 4×10^{-9} for $M_N \simeq 50\,\text{GeV}$.[9] This limit is obtained by assuming singly produced RH neutrinos through an s-channel Z or t-channel W and with a total integrated luminosity of $5\,\text{ab}^{-1}$. For this value of the mixing angle the $e^+e^- \to \nu N$ cross-section is $\sigma \simeq 8 \times 10^{-4}\,\text{fb}$ [19]. On the other hand the dimension-six operator $\mathcal{O}_{NL}$ gives a cross-section [51]

$$\sigma_{\mathcal{O}_{NL}} \simeq |\mathcal{S}_{NN^\dagger}\mathcal{S}_{LL^\dagger}|^2 \frac{s\beta}{64\pi^2\Lambda^4}\left(1+\frac{\beta^2}{3}\right), \tag{7.2}$$

where $\beta = \sqrt{1-4M_N^2/s}$. If the RH neutrinos are long-lived,[10] this operator gives rise to a signature with a pair of displaced vertices, probably easy to be identified in the clean environment of a leptonic machine. By making the simplified, and perhaps conservative, assumption that the experimental sensitivity on the $e^+e^- \to NN$ process is the same as the one for the $e^+e^- \to \nu N$ process, i.e. that we can exclude a cross-section of $\sigma_{\mathcal{O}_{LN}} \sim 8 \times 10^{-4}\,\text{fb}$, we estimate that the ILC could test a scale up to $\Lambda \sim 22\,\text{TeV}$, thus surpassing the reach that one could obtain at the LHC from exotics Higgs decay via the $d = 5$ operator.

7.3 Searches at FCC-eh and FCC-hh

It is interesting to note that $d = 6$ operators built out with quarks bilinear could potentially give observable effects at future electron-proton (FCC-eh) and proton-proton (FCC-hh) facilities [52], see e.g. [23, 53]. For what concerns FCC-eh, operators as $\mathcal{O}^6_{NLqu}$ could be tested in processes as $pe \to Nq$, where q represent any left- or right-handed quark. As pointed out in section 6.4, all these operators suffer from a double Yukawa insertion, one related to the neutrino sector and one to the quark sector, ending up being highly suppressed. We thus expect that they will hardly be testable at this facility. On the other hand FCC-hh could improve significantly the bounds to the unsuppressed operator $\mathcal{O}^6_{Nq}$ through, e.g., monojet processes $pp \to jN_RN_R$. Such a process was considered in [53] for the case of the LHC. In [53], a search of one lepton and missing transverse energy $u\bar{d} \to l_i^+ N_R$ was proposed to constrain the operator $\mathcal{O}^6_{NLqu}$, which however is Yukawa suppressed in the MFV hypothesis and therefore not competitive.

7.4 Prompt and displaced decays

A crucial consequence of the MFV ansätz regards the lifetime of the RH neutrino states. In the absence of higher dimensional operators, they decay through the mixing with the active neutrinos. The partial rate for N_2 to decay in the first generation of SM leptons can be approximated as [55]

$$\Gamma_\theta \simeq 10^{-2}\,\text{GeV}\left(\frac{M_{N_2}}{100\,\text{GeV}}\right)^5 |\theta_{e,2}|^2\,. \tag{7.3}$$

As we saw in figure 1, the active-sterile mixing angle depends on both the RH neutrino masses and γ. For small γ one obtains a proper decay length $c\tau > 0.1\,\text{cm}$ for all values

[9] At energies well above the Z pole the dominant contribution to the cross-section arises from the exchange of a t-channel W, hence the dependence of the results on θ_{ν_e} only.

[10] For $|\theta_{eN}|^2 \sim 4 \times 10^{-9}$ and $M_N \sim 30\,\text{GeV}$ we get a decay length via mixing of $\simeq 5\,\text{cm}$ in the laboratory frame.

JHEP06(2020)185

$M_{N_{1,2}} = [1 \div 100]\,\text{GeV}$. In particular, for $M_{N_2} \lesssim 90\,\text{GeV}$, $c\tau > 1\,\text{m}$, and most RH neutrinos decay outside the detector, while for larger masses $0.1\,\text{cm} < c\tau < 1\,\text{m}$, and the decay is mostly displaced. As γ increases, the interval in which the decay is likely to be displaced grows towards smaller RH neutrino masses, until we reach $\gamma \simeq 4$. For this value of γ a window at large masses in which the decay is prompt opens up. For $\gamma \gtrsim 8$ (i.e. for $M_{N_{1,2}} \gtrsim 10\,\text{GeV}$), all RH neutrinos in the target mass range decay promptly.

Higher dimensional operators that induce new decay modes for the RH neutrinos can drastically modify this behavior. At $d = 5$, the $\mathcal{O}^5_{NB}$ operator gives rise, if kinematically allowed, to the additional decay $N_2 \to N_1\gamma$ with an estimated rate[11]

$$\Gamma_{\mathcal{O}^5_{NB}} \sim \frac{1}{4\pi}\frac{1}{(16\pi^2)^2}\frac{M^3_{N_2}}{\Lambda^2}\,|[\mathcal{S}_{N^*N^\dagger}]_A|^2 \ . \tag{7.4}$$

where one should consider only the relevant entry of the spurion matrix and where we have also included the expected loop suppression factor as indicated in table 2. The coefficient $|[S_{N^*N^\dagger}]_A|^2$ is generally of $\mathcal{O}(1)$ under general assumptions, while the imposition of MFV implies the strong suppression $|[S_{N^*N^\dagger}]_A|^2 \propto \mathcal{O}(Y_\nu^2\epsilon_L)^2$, as shown in eq. (5.6). At $d = 6$, the operator $\mathcal{O}^6_{LNB}$ (which is also loop-suppressed, see table 3) allows for the decay $N_2 \to \nu_e\gamma$ with a rate that we estimate to be

$$\Gamma_{\mathcal{O}^6_{LNB}} \sim \frac{1}{4\pi}\frac{1}{(16\pi^2)^2}\frac{v^2}{\Lambda^4}M^3_{N_2}|\mathcal{S}_\nu|^2. \tag{7.5}$$

Again, the entries of the spurions are generally $\mathcal{O}(1)$ while MFV implies $|\mathcal{S}_\nu|^2 \propto \mathcal{O}(Y_\nu^2)$.

In general, the decay rates induced by higher dimensional operators can easily dominate over the decay rate induced by mixing [26], provided that the Wilson coefficients are $\mathcal{O}(1)$ and Λ/v is not too large. The MFV hypothesis implies an additional suppression in the Wilson coefficients that results in the hierarchy $\Gamma_{\mathcal{O}^5_{NB}}, \Gamma_{\mathcal{O}^6_{LNB}} \ll \Gamma_\theta$, so that under MFV the dominant decay channel is via active-sterile mixing. This is illustrated in figure 2, where we show $c\tau$ as a function of the RH neutrino mass for two extreme scenarios with widely different values of the active-sterile mixing, $\theta_{\nu N}$. On the left panel we assume that the mixing is as large as possible, i.e. $\gamma = \gamma_{\text{max}}$ compatible with present constraints (note that the upper limit discussed before depends on the RH neutrino mass). On the right panel we take $\gamma = 0$. We compare the result assuming MFV, solid blue line, where the dominant decay arises via active-sterile mixing, with the ones with general $\mathcal{O}(1)$ Wilson coefficients for different values of $\Lambda = 1, 10$ and $10^4\,\text{TeV}$. The horizontal band shows the values of $c\tau$ corresponding to displaced decays observable at LHC.

As mentioned above, if the MFV ansätz is imposed the mixing always dominates over the higher dimensional operators and drives the decay. In this case the usual sterile neutrino searches [17, 19–21] are not affected by the presence of higher dimensional operators, and the $c\tau$ does not depend on Λ. On the other hand, if MFV is not imposed, and Λ is not too large, the higher dimensional operators dominate the decay in a large region of the parameter space, making $c\tau$ depend strongly on Λ.

[11] For simplicity, we neglect phase space suppression in this decay mode.

JHEP06(2020)185

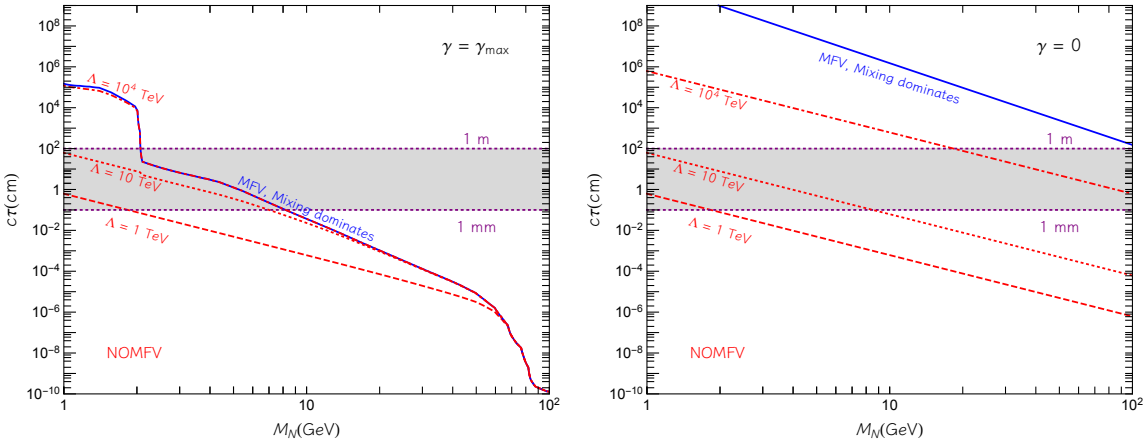

Figure 2. Proper decay length $c\tau$ of the sterile neutrinos as a function of the mass scale $M_{N_{1,2}}$ for different choices of parameters: $\gamma = \gamma_{\max}$ and $\alpha = 0$ (left) and $\gamma = 0$ and $\alpha = \pi/4$ (right). The red lines show the results without assuming MFV for three different values of the new physics scale: $\Lambda = 1\,\text{TeV}$ (dashed line), $\Lambda = 10\,\text{TeV}$ (dotted line) and $\Lambda = 10^4\,\text{TeV}$ (dot-dashed line). The blue lines are instead drawn assuming MFV, with the decay rate driven by the mixing. In the gray region the decay will produce a detectable displaced vertex at the LHC [54].

For the largest possible values of the mixings, $\gamma = \gamma_{\max}$, left panel, we see that the range of masses for which displaced decays are expected is between $[2 \div 10]\,\text{GeV}$ if MFV is assumed, while for larger masses prompt decays will occur. This region shifts to lower masses as Λ decreases in the absence of MFV. For smaller mixings $\gamma \sim 0$, right panel, decay via mixing always leads to average decay lengths much longer than the LHC detector sizes. However the situation changes dramatically with the presence of higher dimensional operators if no MFV is assumed: even for values of Λ as large as $\Lambda \simeq 10^4\,\text{TeV}$, the average decay length could correspond to displaced decays for the largest mass range and even prompt decay for smaller Λ. The effects of the higher dimensional operators only become negligible for scales of order $\Lambda \gtrsim 10^6\,\text{TeV}$.

Summing up, we have illustrated the two effects that modify the pattern of the RH neutrino decays when more than one RH neutrino is added to the SM in the mass range $[1 \div 10^2]\,\text{GeV}$, and higher dimensional operators are also considered. The first one is the active-sterile neutrino mixing. While for small mixing, $\gamma \simeq 0$, the decay length is always outside the detector, for the largest values of γ the decay can be displaced or even prompt. The situation is further modified when higher dimensional operators are considered. If we do not assume any symmetry principle, the additional channels opened up by $d = 5$ and $d = 6$ operators drive the decay length to smaller values. If MFV is imposed, the effect of the higher dimensional operators is negligible, and the decay is always dominated by the active-sterile mixing. Collider searches of displaced decays of RH neutrinos can thus be very useful to identify an underlying flavor structure of the theory.

JHEP06(2020)185

7.5 Astrophysics

We now briefly comment on the implications of the MFV ansätz for astrophysical studies, relevant for slightly lower neutrino masses than those considered in the previous sections [56–62]. The basic idea is that RH neutrinos in this mass range can modify stellar evolution, in particular non-degenerate stars and supernovae, for neutrino masses $M_{N_{1,2}} \lesssim 10\,\text{MeV}$.

As first discussed in [24], in the mass region $M_\nu \ll 10\,\text{keV}$, the $d = 5$ dipole moment operator $\mathcal{O}^5_{NB}$ will produce a dominant decay $\gamma \to N_R N_R$ of a plasmon into two sterile neutrinos, resulting in the limit $\Lambda \gtrsim 4 \times 10^6\,\text{TeV}$. The same reasoning can be applied to supernovae bounds. The relevant mass range in this case is $10\,\text{keV} \lesssim M_{N_{1,2}} \lesssim 30\,\text{MeV}$, for which a new cooling process $\gamma + \nu \to N_R$ can occur, implying the lower limit [24]

$$\Lambda \gtrsim 4 \times 10^6 \sqrt{\frac{m_\nu}{M_{N_{1,2}}}}\ \text{TeV}\ . \tag{7.6}$$

These results assume $\mathcal{O}(1)$ Wilson couplings. Instead, if the MFV hypothesis is assumed, the relevant operators are suppressed by the light neutrino mass and, as a result, no meaningful constrain on the scale Λ can be derived from these astrophysical observables.

8 Conclusions

The evidence for non zero neutrino masses and mixings requires extending the SM with additional degrees of freedom. One of the simplest possibilities is to add to the SM particle content two or more RH neutrinos. Active neutrino masses compatible with experimental measurements are generated by an interplay of the Yukawa coupling between the active and sterile neutrinos and the Majorana mass term for the new RH states via the see-saw relation. Motivated by considerations related to naturalness and the observation of a large baryon asymmetry in the Universe, we focused on RH neutrino masses between $[1 \div 100]\,\text{GeV}$, *i.e.* in a mass range relevant for present and future collider searches. In this mass range and in the absence of other new physics, the RH neutrinos can be produced via mixing with the active neutrino states in charged and neutral current processes or Higgs decays. Also the decay of these particles is in this case driven by mixing via charged currents. The presence of additional new physics states at a scale $\Lambda \gg v, M_{N_{1,2}}$ can modify the phenomenology of the RH neutrinos, which therefore become a new portal, *the see-saw portal*. Such modifications can be parametrized at low energies as an effective field theory with higher dimensional operators $\mathcal{O}^{4+d}/\Lambda^d$ with $d > 4$, that include both the SM fields and two RH singlets. This effective theory has been subject of various studies before [10, 22–24, 37].

In this work we have considered the implications of the MFV principle [31–36] in this theory. We have presented the dependence of the Wilson coefficients of the $d = 5$ and $d = 6$ operators involving RH neutrino fields on the flavor spurions parametrizing lepton flavor and lepton number breaking effects in the renormalizable Lagrangian, highlighting which ones are suppressed by the tiny active neutrino masses and which are not. Particular attention has been devoted to the most accessible parameter space that corresponds to

JHEP06(2020)185

large active-sterile mixing. We have then discussed the most important phenomenological consequences relevant for present and future collider experiments, particularly the aspects related to production rate and decay properties of the RH neutrinos, since the most sensitive searches are based on displaced decay patterns. In particular we have found that the imposition of the MFV ansätz can strongly modify previous estimates of the decay length of the RH neutrinos induced by $d = 5$ and $d = 6$ operators. In particular, our main result is that the imposition of the MFV hypothesis implies that the decay of the RH neutrinos is always dominated by mixing. On the other hand, we have found that pair production can have strongly enhanced production rates at colliders with respect to the single production mediated by mixing, even if MFV is assumed, via $d = 6$ operators of the form $\bar{N}_R \gamma^\mu N_R \bar{X} \gamma_\mu X$, with $X = Q, L, u, d, e$. Sensitivity of future colliders, such as FCC-ee, -eh and -hh, to Λ will significanlty improve present LHC bounds. Finally, we have also shown the consequences of MFV in astrophysical searches, and found that they become non-competitive under this hypothesis.

Acknowledgments

DB thanks the Galileo Galilei Institute for theoretical physics for hospitality while part of this work was carried out. EB was supported by Fundação de Amparo à Pesquisa (FAPESP), under contract 2015/25884-4. AC acknowledges support from the Generalitat Valenciana (GVA) through the GenT program (CIDEGENT/2018/019). Furthermore AC and PH acknowledge support from the GVA project PROMETEO/2019/083, as well as the national grant FPA2017-85985-P, and the European projects H2020-MSCA-ITN-2015//674896-ELUSIVES and 690575-InvisiblesPlus-H2020-MSCA- RISE-2015.

References

[1] Particle Data Group collaboration, *Review of Particle Physics*, *Phys. Rev. D* **98** (2018) 030001 [INSPIRE].

[2] P. Minkowski, $\mu \to e\gamma$ *at a Rate of One Out of* 10^9 *Muon Decays?*, *Phys. Lett. B* **67** (1977) 421 [INSPIRE].

[3] R.N. Mohapatra and G. Senjanović, *Neutrino Mass and Spontaneous Parity Nonconservation*, *Phys. Rev. Lett.* **44** (1980) 912 [INSPIRE].

[4] T. Yanagida, *Horizontal gauge symmetry and masses of neutrinos*, *Conf. Proc. C* **7902131** (1979) 95 [INSPIRE].

[5] M. Gell-Mann, P. Ramond and R. Slansky, *Complex Spinors and Unified Theories*, arXiv:1306.4669 [INSPIRE].

[6] E.K. Akhmedov, V.A. Rubakov and A. Smirnov, *Baryogenesis via neutrino oscillations*, *Phys. Rev. Lett.* **81** (1998) 1359 [hep-ph/9803255] [INSPIRE].

JHEP06(2020)185

[7] T. Asaka and M. Shaposhnikov, *The νMSM, dark matter and baryon asymmetry of the universe*, *Phys. Lett. B* **620** (2005) 17 [hep-ph/0505013] [INSPIRE].

[8] F. Vissani, *Do experiments suggest a hierarchy problem?*, *Phys. Rev. D* **57** (1998) 7027 [hep-ph/9709409] [INSPIRE].

[9] A. Ferrari et al., *Sensitivity study for new gauge bosons and right-handed Majorana neutrinos in pp collisions at s = 14-TeV*, *Phys. Rev. D* **62** (2000) 013001 [INSPIRE].

[10] M.L. Graesser, *Experimental Constraints on Higgs Boson Decays to TeV-scale Right-Handed Neutrinos*, arXiv:0705.2190 [INSPIRE].

[11] F. del Aguila and J.A. Aguilar-Saavedra, *Distinguishing seesaw models at LHC with multi-lepton signals*, *Nucl. Phys. B* **813** (2009) 22 [arXiv:0808.2468] [INSPIRE].

[12] P.S. Bhupal Dev, R. Franceschini and R.N. Mohapatra, *Bounds on TeV Seesaw Models from LHC Higgs Data*, *Phys. Rev. D* **86** (2012) 093010 [arXiv:1207.2756] [INSPIRE].

[13] J.C. Helo, M. Hirsch and S. Kovalenko, *Heavy neutrino searches at the LHC with displaced vertices*, *Phys. Rev. D* **89** (2014) 073005 [*Erratum ibid.* **93** (2016) 099902] [arXiv:1312.2900] [INSPIRE].

[14] FCC-EE STUDY TEAM collaboration, *Search for Heavy Right Handed Neutrinos at the FCC-ee*, *Nucl. Part. Phys. Proc.* **273-275** (2016) 1883 [arXiv:1411.5230] [INSPIRE].

[15] A. Abada, V. De Romeri, S. Monteil, J. Orloff and A.M. Teixeira, *Indirect searches for sterile neutrinos at a high-luminosity Z-factory*, *JHEP* **04** (2015) 051 [arXiv:1412.6322] [INSPIRE].

[16] Y. Cui and B. Shuve, *Probing Baryogenesis with Displaced Vertices at the LHC*, *JHEP* **02** (2015) 049 [arXiv:1409.6729] [INSPIRE].

[17] S. Antusch and O. Fischer, *Testing sterile neutrino extensions of the Standard Model at future lepton colliders*, *JHEP* **05** (2015) 053 [arXiv:1502.05915] [INSPIRE].

[18] A.M. Gago, P. Hernández, J. Jones-Pérez, M. Losada and A. Moreno Briceño, *Probing the Type I Seesaw Mechanism with Displaced Vertices at the LHC*, *Eur. Phys. J. C* **75** (2015) 470 [arXiv:1505.05880] [INSPIRE].

[19] S. Antusch, E. Cazzato and O. Fischer, *Displaced vertex searches for sterile neutrinos at future lepton colliders*, *JHEP* **12** (2016) 007 [arXiv:1604.02420] [INSPIRE].

[20] A. Caputo, P. Hernández, M. Kekic, J. López-Pavón and J. Salvado, *The seesaw path to leptonic CP-violation*, *Eur. Phys. J. C* **77** (2017) 258 [arXiv:1611.05000] [INSPIRE].

[21] A. Caputo, P. Hernández, J. Lopez-Pavon and J. Salvado, *The seesaw portal in testable models of neutrino masses*, *JHEP* **06** (2017) 112 [arXiv:1704.08721] [INSPIRE].

[22] M.L. Graesser, *Broadening the Higgs boson with right-handed neutrinos and a higher dimension operator at the electroweak scale*, *Phys. Rev. D* **76** (2007) 075006 [arXiv:0704.0438] [INSPIRE].

[23] F. del Aguila, S. Bar-Shalom, A. Soni and J. Wudka, *Heavy Majorana Neutrinos in the Effective Lagrangian Description: Application to Hadron Colliders*, *Phys. Lett. B* **670** (2009) 399 [arXiv:0806.0876] [INSPIRE].

[24] A. Aparici, K. Kim, A. Santamaria and J. Wudka, *Right-handed neutrino magnetic moments*, *Phys. Rev. D* **80** (2009) 013010 [arXiv:0904.3244] [INSPIRE].

[25] C.-X. Yue, Y.-C. Guo and Z.-H. Zhao, *Majorana neutrino signals at Belle-II and ILC*, *Nucl. Phys. B* **925** (2017) 186 [arXiv:1710.06144] [INSPIRE].

JHEP06(2020)185

[26] J.M. Butterworth, M. Chala, C. Englert, M. Spannowsky and A. Titov, *Higgs phenomenology as a probe of sterile neutrinos*, *Phys. Rev. D* **100** (2019) 115019 [arXiv:1909.04665] [INSPIRE].

[27] MEG collaboration, *Search for the lepton flavour violating decay $\mu^+ \to e^+\gamma$ with the full dataset of the MEG experiment*, *Eur. Phys. J. C* **76** (2016) 434 [arXiv:1605.05081] [INSPIRE].

[28] G.M. Pruna and A. Signer, *The $\mu \to e\gamma$ decay in a systematic effective field theory approach with dimension 6 operators*, *JHEP* **10** (2014) 014 [arXiv:1408.3565] [INSPIRE].

[29] R. Chivukula and H. Georgi, *Composite Technicolor Standard Model*, *Phys. Lett. B* **188** (1987) 99 [INSPIRE].

[30] G. D'Ambrosio, G.F. Giudice, G. Isidori and A. Strumia, *Minimal flavor violation: An Effective field theory approach*, *Nucl. Phys. B* **645** (2002) 155 [hep-ph/0207036] [INSPIRE].

[31] V. Cirigliano, B. Grinstein, G. Isidori and M.B. Wise, *Minimal flavor violation in the lepton sector*, *Nucl. Phys. B* **728** (2005) 121 [hep-ph/0507001] [INSPIRE].

[32] S. Davidson and F. Palorini, *Various definitions of Minimal Flavour Violation for Leptons*, *Phys. Lett. B* **642** (2006) 72 [hep-ph/0607329] [INSPIRE].

[33] G.C. Branco, A.J. Buras, S. Jager, S. Uhlig and A. Weiler, *Another look at minimal lepton flavour violation, $l_i \to l_{j\gamma}$, leptogenesis and the ratio M_ν/Λ_{LFV}*, *JHEP* **09** (2007) 004 [hep-ph/0609067] [INSPIRE].

[34] M.B. Gavela, T. Hambye, D. Hernandez and P. Hernández, *Minimal Flavour Seesaw Models*, *JHEP* **09** (2009) 038 [arXiv:0906.1461] [INSPIRE].

[35] R. Alonso, G. Isidori, L. Merlo, L.A. Muñoz and E. Nardi, *Minimal flavour violation extensions of the seesaw*, *JHEP* **06** (2011) 037 [arXiv:1103.5461] [INSPIRE].

[36] D.N. Dinh, L. Merlo, S.T. Petcov and R. Vega-Álvarez, *Revisiting Minimal Lepton Flavour Violation in the Light of Leptonic CP-violation*, *JHEP* **07** (2017) 089 [arXiv:1705.09284] [INSPIRE].

[37] Y. Liao and X.-D. Ma, *Operators up to Dimension Seven in Standard Model Effective Field Theory Extended with Sterile Neutrinos*, *Phys. Rev. D* **96** (2017) 015012 [arXiv:1612.04527] [INSPIRE].

[38] J. Kersten and A.Y. Smirnov, *Right-Handed Neutrinos at CERN LHC and the Mechanism of Neutrino Mass Generation*, *Phys. Rev. D* **76** (2007) 073005 [arXiv:0705.3221] [INSPIRE].

[39] B. Grzadkowski, M. Iskrzynski, M. Misiak and J. Rosiek, *Dimension-Six Terms in the Standard Model Lagrangian*, *JHEP* **10** (2010) 085 [arXiv:1008.4884] [INSPIRE].

[40] S. Weinberg, *Baryon and Lepton Nonconserving Processes*, *Phys. Rev. Lett.* **43** (1979) 1566 [INSPIRE].

[41] W. Buchmüller and D. Wyler, *Effective Lagrangian Analysis of New Interactions and Flavor Conservation*, *Nucl. Phys. B* **268** (1986) 621 [INSPIRE].

[42] N. Craig, M. Jiang, Y.-Y. Li and D. Sutherland, *Loops and Trees in Generic EFTs*, arXiv:2001.00017 [INSPIRE].

[43] B. Pontecorvo, *Inverse beta processes and nonconservation of lepton charge*, *Sov. Phys. JETP* **7** (1958) 172 [*Zh. Eksp. Teor. Fiz.* **34** (1957) 247] [INSPIRE].

JHEP06(2020)185

[44] Z. Maki, M. Nakagawa and S. Sakata, *Remarks on the unified model of elementary particles*, *Prog. Theor. Phys.* **28** (1962) 870 [INSPIRE].

[45] J.A. Casas and A. Ibarra, *Oscillating neutrinos and $\mu \to e, \gamma$*, *Nucl. Phys. B* **618** (2001) 171 [hep-ph/0103065] [INSPIRE].

[46] BELLE collaboration, *Search for heavy neutrinos at Belle*, *Phys. Rev. D* **87** (2013) 071102 [*Erratum ibid.* **95** (2017) 099903] [arXiv:1301.1105] [INSPIRE].

[47] LHCb collaboration, *Search for massive long-lived particles decaying semileptonically in the LHCb detector*, *Eur. Phys. J. C* **77** (2017) 224 [arXiv:1612.00945] [INSPIRE].

[48] DELPHI collaboration, *Search for neutral heavy leptons produced in Z decays*, *Z. Phys. C* **74** (1997) 57 [*Erratum ibid.* **75** (1997) 580] [INSPIRE].

[49] J. Lopez-Pavon, S. Pascoli and C.-f. Wong, *Can heavy neutrinos dominate neutrinoless double beta decay?*, *Phys. Rev. D* **87** (2013) 093007 [arXiv:1209.5342] [INSPIRE].

[50] E.B.D. Barducci and A. Caputo, in progress.

[51] J. Peressutti, I. Romero and O.A. Sampayo, *Majorana Neutrinos Production at NLC in an Effective Approach*, *Phys. Rev. D* **84** (2011) 113002 [arXiv:1110.0959] [INSPIRE].

[52] FCC collaboration, *FCC Physics Opportunities*: Future Circular Collider Conceptual Design Report Volume 1, *Eur. Phys. J. C* **79** (2019) 474 [INSPIRE].

[53] J. Alcaide, S. Banerjee, M. Chala and A. Titov, *Probes of the Standard Model effective field theory extended with a right-handed neutrino*, *JHEP* **08** (2019) 031 [arXiv:1905.11375] [INSPIRE].

[54] ATLAS collaboration, *Search for long-lived, heavy particles in final states with a muon and multi-track displaced vertex in proton-proton collisions at $\sqrt{s} = 7$ TeV with the ATLAS detector*, *Phys. Lett. B* **719** (2013) 280 [arXiv:1210.7451] [INSPIRE].

[55] A. Atre, T. Han, S. Pascoli and B. Zhang, *The Search for Heavy Majorana Neutrinos*, *JHEP* **05** (2009) 030 [arXiv:0901.3589] [INSPIRE].

[56] G. Raffelt and D. Seckel, *Bounds on Exotic Particle Interactions from SN 1987a*, *Phys. Rev. Lett.* **60** (1988) 1793 [INSPIRE].

[57] G. Raffelt and A. Weiss, *Nonstandard neutrino interactions and the evolution of red giants*, *Astron. Astrophys.* **264** (1992) 536 [INSPIRE].

[58] G.G. Raffelt, *Stars as laboratories for fundamental physics*, University of Chicago Press, Chicago U.S.A. (1996).

[59] G.G. Raffelt, *Limits on neutrino electromagnetic properties: An update*, *Phys. Rept.* **320** (1999) 319 [INSPIRE].

[60] M. Haft, G. Raffelt and A. Weiss, *Standard and nonstandard plasma neutrino emission revisited*, *Astrophys. J.* **425** (1994) 222 [*Erratum ibid.* **438** (1995) 1017] [astro-ph/9309014] [INSPIRE].

[61] V. Castellani and S. Degl'Innocenti, *Stellar evolution as a probe of neutrino properties*, *Astrophys. J.* **402** (1993) 574 [INSPIRE].

[62] A. Heger, A. Friedland, M. Giannotti and V. Cirigliano, *The Impact of Neutrino Magnetic Moments on the Evolution of Massive Stars*, *Astrophys. J.* **696** (2009) 608 [arXiv:0809.4703] [INSPIRE].

JHEP06(2020)185